



<https://theses.gla.ac.uk/>

Theses Digitisation:

<https://www.gla.ac.uk/myglasgow/research/enlighten/theses/digitisation/>

This is a digitised version of the original print thesis.

Copyright and moral rights for this work are retained by the author

A copy can be downloaded for personal non-commercial research or study,  
without prior permission or charge

This work cannot be reproduced or quoted extensively from without first  
obtaining permission in writing from the author

The content must not be changed in any way or sold commercially in any  
format or medium without the formal permission of the author

When referring to this work, full bibliographic details including the author,  
title, awarding institution and date of the thesis must be given

Enlighten: Theses

<https://theses.gla.ac.uk/>  
[research-enlighten@glasgow.ac.uk](mailto:research-enlighten@glasgow.ac.uk)

**A NUMERICAL AND EXPERIMENTAL STUDY  
OF  
THE DEVELOPMENT OF SEMI-ELLIPTICAL FATIGUE CRACKS  
BY DEFECT COALESCENCE**

**By  
Brian Robert Twaddle**

**Submitted to the University of Glasgow  
for the degree of  
Master of Science**

**June 1991**

**© B. R. Twaddle 1991**

ProQuest Number: 10987061

All rights reserved

INFORMATION TO ALL USERS

The quality of this reproduction is dependent upon the quality of the copy submitted.

In the unlikely event that the author did not send a complete manuscript and there are missing pages, these will be noted. Also, if material had to be removed, a note will indicate the deletion.



ProQuest 10987061

Published by ProQuest LLC (2018). Copyright of the Dissertation is held by the Author.

All rights reserved.

This work is protected against unauthorized copying under Title 17, United States Code  
Microform Edition © ProQuest LLC.

ProQuest LLC.  
789 East Eisenhower Parkway  
P.O. Box 1346  
Ann Arbor, MI 48106 – 1346

## ABSTRACT

Fatigue failure of large fabricated structures can occur through the propagation of several small defects which either pre-exist in the structure as a result of the fabrication process or which initiate under the action of cyclic loading. The propagation of these small defects results in the coalescence of several small defects to form a dominant fatigue crack which then propagates to cause failure. In welded components such as the tubular joints of offshore jacket structures the dominant crack is often a semi-elliptical surface crack at the toe of the fillet weld. Existing methodologies offer simplistic approaches to predict the behaviour of adjacent surface defects. In general fracture mechanics offers a rational approach for the assessment of such problems.

This work utilised numerical and experimental techniques to investigate the coalescence of co-linear surface defects by fatigue crack growth to form single semi-elliptical crack shapes. A numerical study of defect interaction utilising the line spring model was supported by experimental observations. In addition a numerical evaluation of the stress intensity factor distribution around the crack periphery immediately after the coalescence of two defects was conducted utilising the line spring model and a universal weight function approach.

The line spring model analysis showed that the interaction between adjacent colinear defects was a second order effect and would have little effect on component life, this was supported by the experimental observations. In addition existing defect assessment methodologies were shown to be at best unrealistic in their approach to defect interaction and generally over-conservative for the cases considered here. Both the numerical investigations and the experimental data indicated that a significant magnification of the stress intensity factor occurs at the re-entrant sector of the coalesced crack immediately the defects coalesce. This magnification results in a rapid propagation of this sector to form a single semi-elliptical crack. Based on this analysis and the supporting experimental observations it was concluded that this behaviour was of sufficiently short duration that it could be omitted for the purpose of life prediction calculations.

In conclusion it was proposed that co-linear defects growing by fatigue should be considered as individual defects up until the point where the defects meet at the adjacent tips, at this point the defects should be re-characterised as a single crack with depth equal to that of the deepest defect and surface length equal to the combined length of the two defects.

# **CONTENTS**

Abstract

1. Introduction

2. Fracture Mechanics

2.1 Introduction

2.2 Linear Elastic Fracture Mechanics

2.2.1 The stress at a crack tip

2.2.2 The plastic zone

3. Determination of Stress Intensity Factors

3.1 Introduction

3.2 Analytical Methods

3.3 Numerical Techniques

3.4 Finite Element Methods

3.4.1 Overview

3.4.2 Direct Methods

3.4.3 Indirect Methods

3.4.3.1 Strain Energy Release Rate

3.4.3.2 Virtual Crack Extension

3.4.3.3 Contour Integration

3.4.3.4 Special Elements

3.4.4 Other Finite Element Methods

3.5 Experimental Methods

3.6 Other Methods

3.6.1 Weight Functions

3.6.2 Simple Estimation Procedures

4. Three Dimensional Crack Problems

4.1 Introduction

4.2 Embedded Defect Solution

4.3 Analysis of Semi-Elliptical Surface Cracks

4.3.1 Overview

4.3.2 Finite Element Solutions

4.3.3 Line Springs

4.3.4 Weight Functions Applied to Surface Cracks

## 5. Fatigue and Fatigue Crack Growth

- 5.1 Introduction
- 5.2 Fatigue Mechanisms in Metals
- 5.3 Crack Growth Models
- 5.4 Factors Affecting Fatigue Crack Propagation
  - 5.4.1 Environment
  - 5.4.2 Mean Stress Effects
  - 5.4.3 Sequence Effects
- 5.5 Fatigue of Surface Cracks
  - 5.5.1 Code Approaches
  - 5.5.2 Literature

## 6. Multiple Defect Behaviour

- 6.1 Introduction
- 6.2 Recommended Practice
  - 6.2.1 British Standards PD6493
  - 6.2.2 ASME XI
  - 6.2.3 CEGB R6
- 6.3 Interaction Between fully Penetrating Cracks
- 6.4 Interaction Between Colinear Surface Cracks
- 6.5 Fatigue of Multiple Surface Cracks

## 7. A Numerical Study of the Interaction Between Colinear Semi-elliptical Defects.

- 7.1 Introduction
- 7.2 Geometries Considered
- 7.3 Assumptions and Boundary Conditions
- 7.4 Load Cases
- 7.5 Results
  - 7.5.1 Aspect ratio equals 0.2
  - 7.5.2 Aspect ratio equals 0.4
  - 7.5.3 Aspect ratio equals 0.6
- 7.6 Discussion
  - 7.6.1 Validation of the Lines Spring Solution
  - 7.6.2 Defect Interaction
  - 7.6.3 Comparison With Existing Procedures
- 7.7 Conclusions for Chapter 7.

## 8. An Experimental Study of Defect Coalescence

- 8.1 Introduction
- 8.2 Experimental Procedure

### 8.3 Results

### 8.4 Analysis and Discussion

#### 8.4.1 General Observations from Fracture Surfaces

#### 8.4.2 Analysis of Crack Growth Behaviour

#### 8.4.3 Comparison with Existing Procedures

#### 8.4.4 An Alternative Prediction

### 8.5 Conclusions for Chapter 8

## 9. A Numerical Study of the Stress Intensity Factor Distribution Around A Crack Immediately After Coalescence

### 9.1 Introduction

### 9.2 Numerical Models

#### 9.2.1 Line Spring Model

#### 9.2.2 Universal Weight Function Model

### 9.3 Results

### 9.4 Discussion

### 9.5 Conclusions for Chapter 9

## 10. Discussion and Conclusions

### 10.1 Defect Interaction

### 10.2 Significance with Respect to Existing Procedures

### 10.3 The Coalescence Process

### 10.4 Overall Conclusions of This Work

## Acknowledgements

## References

## **1. INTRODUCTION**

It has been accepted for some time that large fabricated structures often fail due to the presence of cracks. Such cracks are often the result of small defects introduced to the structure during the fabrication process although they can initiate during the lifetime of the structure. Once this 'initiation' phase has occurred these small defects can propagate under the action of cyclic loads on the structure due to the environment or operating practice for the plant. It is known that crack like flaws can cause catastrophic failure of components and structures on attaining some critical size determined by factors such as material properties, loading, and geometry. This behaviour merits attention in order that rules can be developed which will enable the designer to guarantee the integrity of the structure over the envisaged operational life. In the case of nuclear power plant or offshore platforms the design life of the structure may be of the order of twenty to thirty years and hence predictive tools must enable extrapolation of data obtainable from short term laboratory tests.

There is however a dilemma in formulating such rules. The behaviour to be predicted is complex and as such simplifications are required in formulating the models. Such simplifications must ensure a conservative estimate of the lifetime if failure is to be avoided. If however the derived criteria are excessively conservative then unnecessary expense may be incurred by premature shutdown of plant which is capable of safe operation for several more years.

In recent years several design and assessment methodologies for structures subject to cyclic loading have evolved. Generally these can be grouped under two categories;

- i) those which use an empirical 'S-N' or Wohler approach and
- ii) those based on a Fracture Mechanics approach.

These techniques have been discussed more fully in Chapter 5, but in essence the S-N approach is empirical with suitable correction factors

applied to account for geometry, mean load and other significant factors whereas the fracture mechanics approach attempts to model the behaviour of a specific crack, allowing geometry and other influences to be considered in a more physically meaningful way. While the fracture mechanics approach is more versatile in its applicability it requires a certain amount of expertise to formulate the solution, further in order to apply the criterion a crack must be analysed and since at the design stage a crack size is not available some difficulty can be found. For these reasons the S-N approach is more widely adopted at the design stage particularly since designers generally do not have a great knowledge of fracture mechanics principles. The fracture mechanics methodologies are more generally used in the assessment of defects found during the service life of the structure. In this case the crack size and location are known and a more accurate assessment can be made. To facilitate this several methodologies have evolved such as the ASME XI, CEGB R6 and British Standards PD 6493 recommended routes. These methods are principally concerned with the prediction of unstable extension of a crack to cause failure. Each methodology makes some recommendation as to how existing defects should be postulated to grow under the action of cyclic loading to reach the critical size, further both the ASME and BS routes give guidelines on how adjacent defects should be taken to coalesce. Both methodologies assume that the defects will coalesce at some critical separation. No justification is given for this assumption and it must be assumed that this guideline was based on engineering judgement in order to maintain conservatism in the case of multiple defects.

The purpose of this work was to examine the coalescence of shallow surface defects to form larger cracks in order to establish whether the assumptions of existing guidelines are reasonable and, if possible, to indicate practicable improvements to these techniques. The work reviews current methodologies and reports the results of a numerical and experimental examination of the problem.

## CHAPTER 2

### FRACTURE MECHANICS

#### **3. Introduction**

The purpose of fracture mechanics is to predict the failure of a structure containing known cracks. In achieving this three preliminary procedures are required. Primarily the stress system in the defective area of the structure must be determined, this would normally be accomplished by conventional stress analysis of the uncracked body by means of numerical or analytical techniques. In addition non-destructive examination of the component or structure may be necessary to determine the size, location and orientation of the cracks to be examined and finally the determination of the pertinent material properties required by the assessment techniques. The first of these procedures is complex and must account for all operational and fault loading conditions including cyclic loads such as startup-shutdown cycles, wave loadings, pressure and thermal cycles; environmental influences, and both 'normal' fault or extreme operating conditions and the most extreme fault conditions possible for the structure. This information together with the starting crack sizes are then used as the input to the fracture mechanics analysis. Within this analysis cracks can be assessed to determine whether they will cause fracture under the postulated conditions and, further whether they will grow towards some critical size during the operating life of the plant or structure under the action of cyclic loadings and/or corrosive environments. The behaviour of the cracks will depend on the material properties and in particular the ability of the material to sustain loads in the presence of cracks, the 'toughness' of the material. Broadly the behaviour of cracked bodies can be split into two categories. Brittle where fracture occurs under generally elastic conditions by rapid, unstable propagation of sharp cracks. Conversely ductile crack propagation is accompanied by extensive plastic deformation, normally leading to crack tip blunting and some stable propagation or tearing behaviour prior to instability. Consequently two fracture mechanics analysis disciplines have developed to enable the assessment of cracked bodies under each category : Linear Elastic Fracture

Mechanics ( LEFM ) for brittle behaviour and elastic Plastic Fracture Mechanics (EPFM) or Post Yield Fracture Mechanics (PYFM) for the more ductile materials. LEFM has been considered in some detail here, however non-linear fracture mechanics was not utilised in this work and has therefore not been considered in this review. The reader is referred to standard texts for a discussion of this behaviour.

## **2.2 Linear Elastic Fracture Mechanics (LEFM)**

The basis of LEFM is generally recognised as the work of Griffith [1,2] in 1921-24. Griffith considered an infinite plate of unit thickness with a central transverse crack of length  $2a$  loaded remotely by either a fixed displacement, fixed grip loading, or a uniform load, Figure 2.1. Griffith showed that when the total energy of the system is decreased by the crack extension then propagation is energetically favourable and unstable extension of the crack will occur. By considering an energy balance between the loss of potential energy,  $U$ , of the plate due to a small change in the crack half length,  $da$ , and the energy required to create the new crack surface area ( $=4\gamma da$  :  $\gamma$  = surface energy per unit area for the plate) Griffith predicted a fracture stress of :

$$\sigma_f = \left( \frac{4\gamma E}{\pi a} \right)^{1/2} \quad \text{for plane stress} \quad (1)$$

$$\sigma_f = \left( \frac{4\gamma E}{(1-\nu^2)\pi a} \right)^{1/2} \quad \text{for plane strain}$$

Where  $\nu$  is Poisson's ratio and  $E$  is Young's modulus. Irwin and Orowan [3,4] later modified the Griffith criterion after observing that even in brittle materials, such as glass, the main energy absorbing process was plastic flow at a small region at the crack tip. However the Griffith equation can still be used if the  $4\gamma$  term is interpreted as the total potential energy release rate of the system including the plastic work at the crack tip. This is usually denoted

$G_c$  and termed the critical strain energy release rate. It should however be noted that the resulting term stills shows a dependence on an  $a^{-1/2}$  term. This dependence is the basis of modern LEFM approaches and is the most important result of Griffith's findings.

### 2.2.1 The Stress at a Crack Tip.

The faces of a crack can be considered to move relative to each other in one of three different ways, Figure 2.2. Stresses acting normal to the crack faces give rise to the opening mode or mode I loading. In-plane shear stress gives rise to a sliding mode normally termed mode II loading. Out-of-plane shear stresses lead to a tearing mode known as mode III loading. Superposition of these three modes enables the general load case to be fully described. Mode I is considered to be the most important since in practice cracks are generally found to propagate and fail under mode I conditions.

Westergaard [5] used a complex variable formulation of the Airy stress function  $\phi$  to solve two dimensional boundary value problems. This method is generally referred to as Westergaard stress functions and has been used to solve two dimensional problems in cracked structures. Under mode I loading the stresses at the tip of an elastic crack in an infinite body can be shown to be :

$$\sigma_x = \frac{K_I}{\sqrt{2\pi r}} \cos\left(\frac{\theta}{2}\right) \left(1 - \sin\left(\frac{\theta}{2}\right) \sin\left(\frac{3\theta}{2}\right)\right) + \sigma_{ox} + \dots$$

$$\sigma_y = \frac{K_I}{\sqrt{2\pi r}} \cos\left(\frac{\theta}{2}\right) \left(1 + \sin\left(\frac{\theta}{2}\right) \sin\left(\frac{3\theta}{2}\right)\right) + \dots$$

$$\sigma_{xy} = \frac{K_I}{\sqrt{2\pi r}} \sin\left(\frac{\theta}{2}\right) \cos\left(\frac{\theta}{2}\right) \cos\left(\frac{3\theta}{2}\right) + \dots$$

(2)

$$\sigma_z = 0 \text{ plane stress}$$

$$\sigma_z = \nu(\sigma_x + \sigma_y) \text{ plane strain}$$

where '+...' represents further higher order terms which are normally neglected for small  $r$ . The co-ordinate system used to describe the stress field is shown in Figure 2.3.  $K_I$  is the mode I stress intensity factor. Clearly if  $K_I$  is known then the stress system at the crack tip is fully defined irrespective of the geometry of the body in which the crack is contained. Similar solutions can be derived for the displacements in the vicinity of the crack tip and indeed for the stresses and displacements at a crack tip under the action of mode II and mode III loadings. The stresses at the crack tip may be generalised as :

$$\sigma_{ij} = \frac{K_I}{\sqrt{2\pi r}} f_{ij}(\theta) \quad (3)$$

where  $f_{ij}(\theta)$  are known dimensionless functions of  $\theta$ .  $K_I$  must have the dimensions 'stress $\sqrt{\text{length}}$ '. Since the only stress defined in the problem is the remote stress  $\sigma$  and the only available length is that of the crack, 'a', then the stress intensity factor must take the form :

$$K_I = \alpha \sigma \sqrt{a} \quad (4)$$

The dimensionless parameter  $\alpha$  is dependent on the geometry and the nature of the remote boundary conditions. In the case of the Griffith problem of an infinite elastic plate with an embedded crack of length  $2a$   $\alpha$  equals  $\sqrt{\pi}$ . It is conventional that this  $\sqrt{\pi}$  factor is taken out of  $\alpha$  and that 'a' is equivalent to the crack length when there is only one crack tip and half the crack length when two crack tips are present ie. for embedded cracks. Hence the general equation for K is:

$$K_I = \alpha \sigma \sqrt{\pi a} \quad (5)$$

$\alpha$  has been calculated for many standard geometries and is tabulated in various compendia [6,7]. Methodologies for calculating stress intensity

factors for non standard geometries include finite element techniques and weight functions, these techniques will be discussed in some detail later.

Given that  $K$  characterises the stresses at the crack tip it is reasonable to expect that the fracture stress may be related to some critical value of  $K$ ,  $K_C$ , which is a material characteristic. In fact re-arranging (5):

$$\sigma_f = \frac{K_C}{\alpha\sqrt{\pi a}} \quad (6)$$

and comparing with the Griffith equations in (1) with the Irwin-Orowan modification of  $G_C$  leads to :

$$K_C = EG_C \text{ for plane stress} \quad (7)$$

$$K_C = EG_C/(1-\nu^2) \text{ for plane strain}$$

Hence although  $K$  has been developed as a parameter which characterises the stress system at a crack tip, it can also be related to the energetics of the fracture process.

Under mode I conditions it is found that the critical value of  $K$  is dependent on the thickness of the specimen. This thickness effect is demonstrated in Figure 2.4. As the thickness is increased  $K_C$  tends towards a lower limit. This is the plane strain condition and this lower limit to  $K_C$  is termed  $K_{Ic}$  the plane strain fracture toughness and is a material property. Hence for a linear elastic body if the calculated  $K$  at a crack tip exceeds  $K_{Ic}$  for the material then the crack will be predicted to propagate.

### 2.2.2 The Plastic Zone - Limitations of LEFM

The argument so far has used the term LEFM without precise definition. Clearly equation(s) (2) predict an infinite stress at the crack tip. This is not possible in metallic materials because plasticity will occur when the stress

exceeds the yield stress, consequently a plastic zone develops at the crack tip, Figure 2.5. This contradicts the term linear elastic, however as long as the size of the plastic zone remains small compared to the crack size and specimen dimensions LEFM is considered valid, the so called small scale yielding condition. An initial estimate of the plastic zone size ahead of the crack ( $\theta = 0$ ) in plane stress can be made by substituting  $\sigma_{ys}$  for  $\sigma_y$  in equation (2) giving :

$$r_p^* = \frac{K_I^2}{2\pi\sigma_{ys}^2} \quad (8)$$

In reality the plastic zone size must be greater than this to allow the load represented by the shaded area in Figure 2.5 to be carried, hence the plastic zone may be represented schematically by Figure 2.5b. Irwin [8,9] argued that the occurrence of plasticity at the crack tip causes the crack to behave as if it were physically longer. The argument is that due to the plastic deformation the displacements in the elastic body will be larger and the stiffness will be lower than for the purely elastic case and hence that the plate behaves as if there was a larger crack present. It was then proposed that the actual crack size,  $a$ , should be increased to  $a+\Delta a$  for fracture mechanics calculations where  $\Delta a$  is a plasticity correction for the crack size. Several expressions for  $\Delta a$  have been proposed since Irwin's work including the Dugdale model [10], and similar models proposed by Barenblatt [11] and Duffy et al [12]. However it has already been stated that in order for LEFM to be valid the plastic zone must be small and hence it is arguable whether such corrections are required.

In order to gain a better representation of the plastic zone size including the variation of the extent of plasticity with respect to  $\theta$  a suitable yield criterion must be used. This is normally either the Tresca or the Von Mises yield criterion. The crack tip stress fields (2) can be recast in terms of the principal stress components as :

$$\sigma_1 = \frac{K_I}{\sqrt{2\pi r}} \cos\left(\frac{\theta}{2}\right) \left(1 + \sin\left(\frac{\theta}{2}\right)\right)$$

$$\sigma_2 = \frac{K_I}{\sqrt{2\pi r}} \cos\left(\frac{\theta}{2}\right) \left(1 - \sin\left(\frac{\theta}{2}\right)\right)$$

(9)

$$\sigma_3 = 0 \text{ Plane stress or}$$

$$\sigma_3 = 2\nu \frac{K_I}{\sqrt{2\pi r}} \cos\left(\frac{\theta}{2}\right) \text{ Plane strain}$$

The plastic zone boundary can then be calculated as a function of  $\theta$  by substituting (4) into the appropriate yield function. If the Mises yield function is used this results in :

$$r_p = \frac{K^2}{4\pi\sigma_{ys}^2} \left[ \frac{3}{2} \sin^2(\theta) + (1-2\nu)^2 (1 + \cos(\theta)) \right] \text{ for plane strain and}$$

(11)

$$r_p = \frac{K^2}{4\pi\sigma_{ys}^2} \left[ 1 + \frac{3}{2} \sin^2(\theta) + \cos(\theta) \right] \text{ for plane stress}$$

If the Tresca yield criterion is assumed :

$$r_p = \frac{K^2}{2\pi\sigma_{ys}^2} \left[ \cos\left(\frac{\theta}{2}\right) \left(1 + \frac{3}{2} \sin\left(\frac{\theta}{2}\right)\right) \right]^2 \text{ for plane stress}$$

(12)

and the larger of :

$$r_p = \frac{K^2}{2\pi\sigma_y^2} \cos^2\left(\frac{\theta}{2}\right) \left[1 - 2\nu + \sin\left(\frac{\theta}{2}\right)\right]^2$$

or

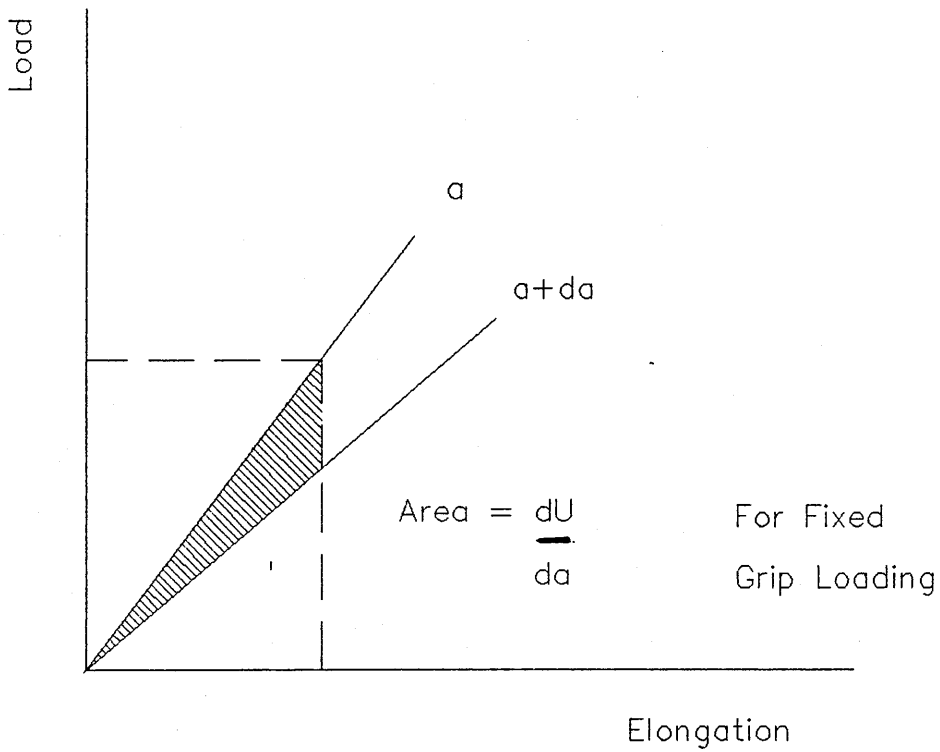
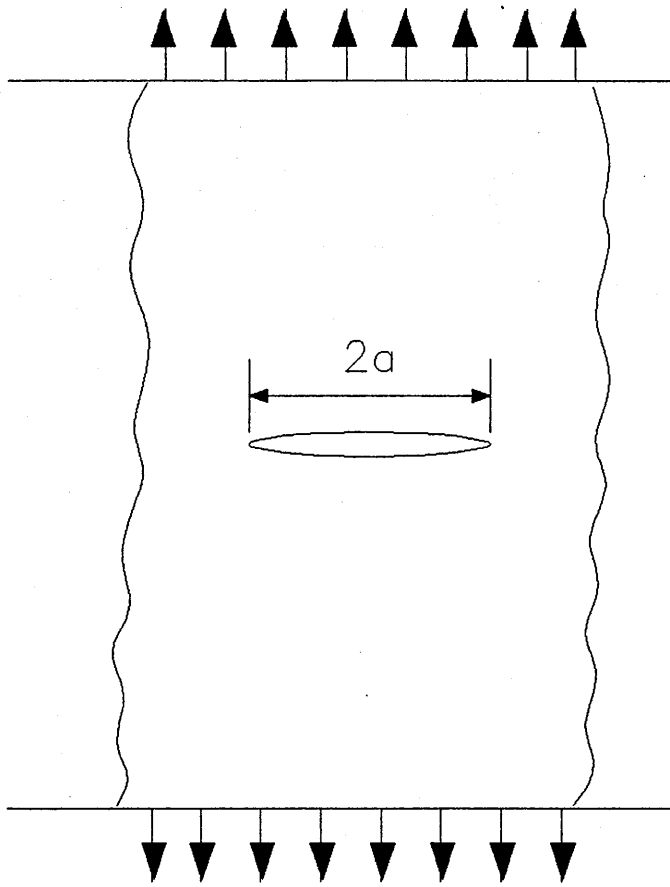
$$r_p = \frac{K^2}{2\pi\sigma_y^2} \cos^2\left(\frac{\theta}{2}\right)$$

for Plane strain

The resulting plastic zone size is therefore slightly different according to which yield criterion is adopted as shown in Figure 2.6. The plastic zones calculated using Tresca are slightly larger than the equivalent Von Mises ones. Similar analysis can be performed for mode II and III plastic zone shapes.

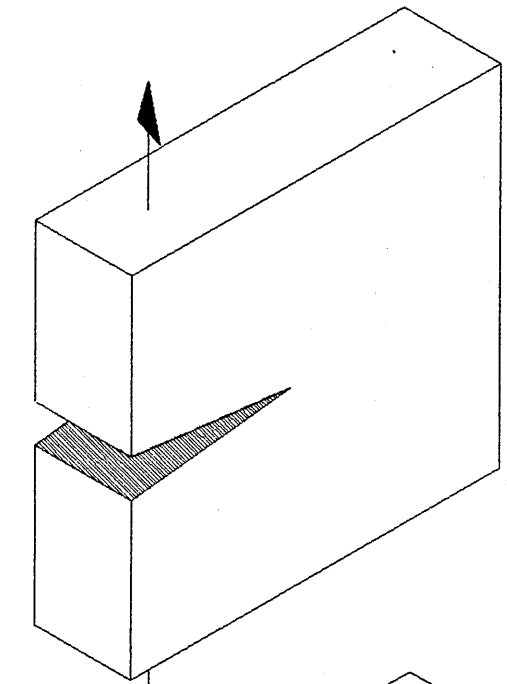
In calculating the plastic zone shapes shown in Figure 2.6 the same error has been made as in deriving equation (8), that is by limiting the stress to the yield stress the extra load from the plastic zone must be redistributed somewhere outside the calculated elastic boundary thus increasing the plastic zone size. Further neither equilibrium or compatibility have been satisfied in the calculation of the plastic zone size. Correction of this error requires more complex analysis and has been attempted by several authors [13,14] and more recently [15,16]. Verification of the analysis by experimental methods is difficult since elastic and plastic strains cannot easily be distinguished, if at all. Several workers [eg 17,18] have attempted to measure plastic zone shapes using surface techniques such as replication, photoelasticity and Moire fringes with varying degrees of success. Hahn and Rosenfield used an etching technique [19,20,21] to avoid these difficulties and concluded that none of the theoretical approaches gave an accurate estimate of the plastic zone size, particularly directly ahead of the crack, ie. at  $\theta = 0$ . Broek [22] used a technique based on the diffusion of incident light to show that the plastic zone shape in plane stress most closely resembles that predicted by Tuba [15].

States of plane stress and plane strain are limiting cases. In reality plane strain conditions may apply at the centre of a cross section but at the free surfaces of the plate  $\sigma_z = \sigma_3 = 0$ , and hence plane stress conditions apply. Consequently the plastic zone size must increase from the centre of the plate outwards, Figure 2.7. The extent of the plane stress region is dependent on the specimen thickness. As the size of the plastic zone approaches the plate thickness then a state of plane stress can develop. However if the plastic zone is small when compared to the plate thickness then deformation in the  $\epsilon_z$  direction is constrained by the surrounding elastic material and consequently the plastic zone size is restricted leading to significantly higher stress levels in the plane strain condition. This behaviour can be used to explain the thickness dependence of  $K_{IC}$ , Figure 2.4,[23].

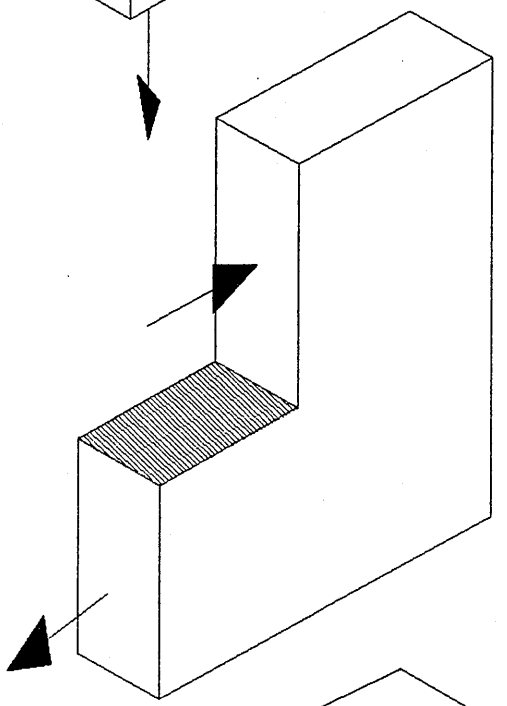


Griffith Criterion

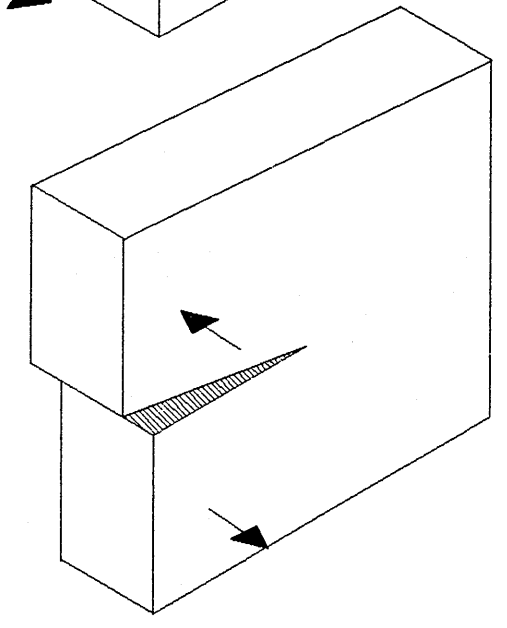
Figure 2.1



Mode I



Mode II



Mode III

Figure 2.2

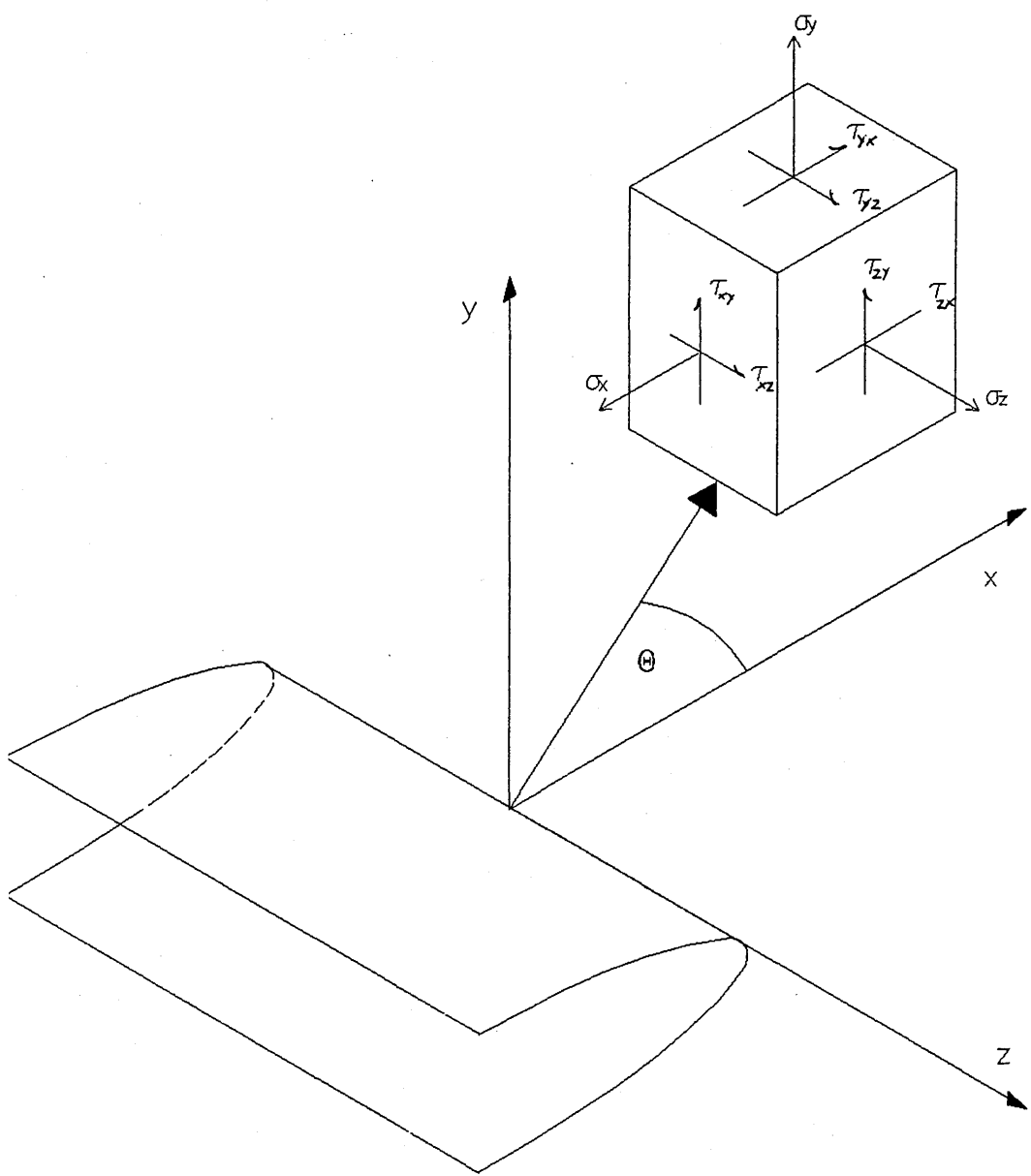
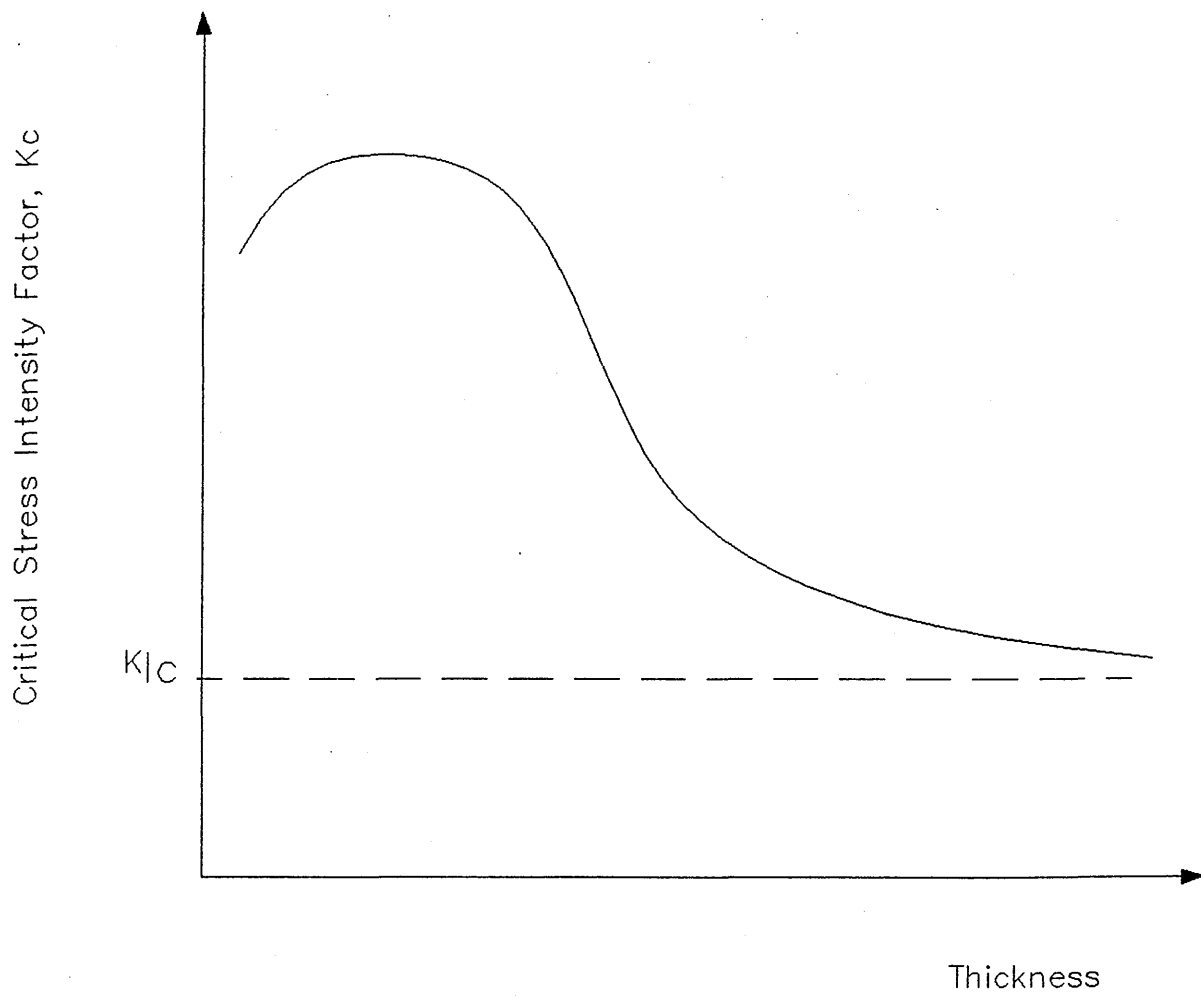


Figure 2.3



Effect of Thickness on the  
Critical Stress Intensity Factor  
Under Mode I Loading

Figure 2.4

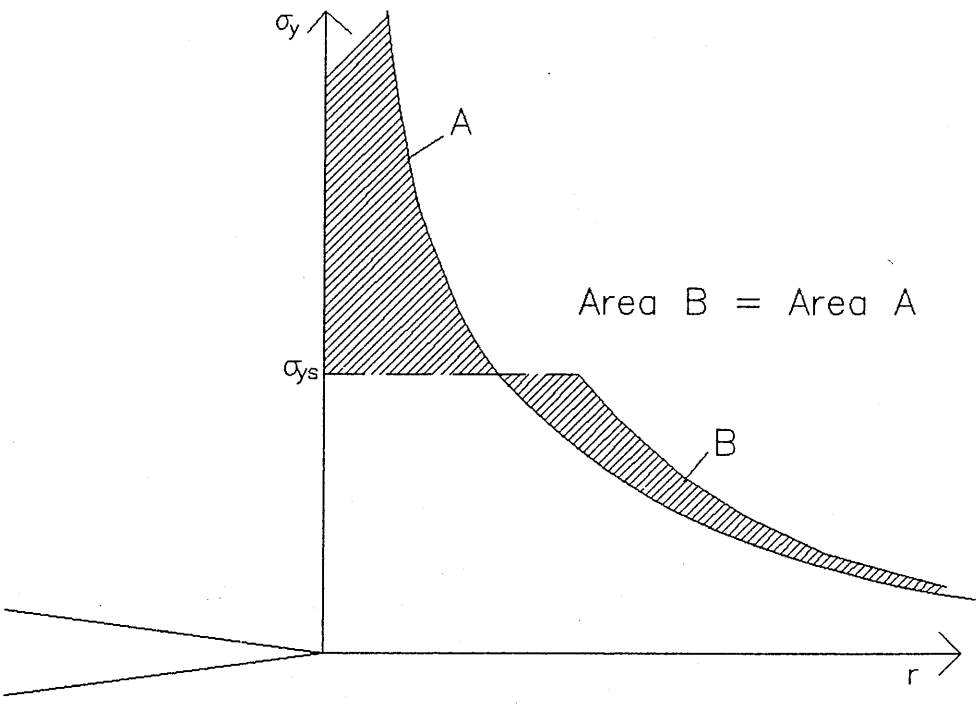
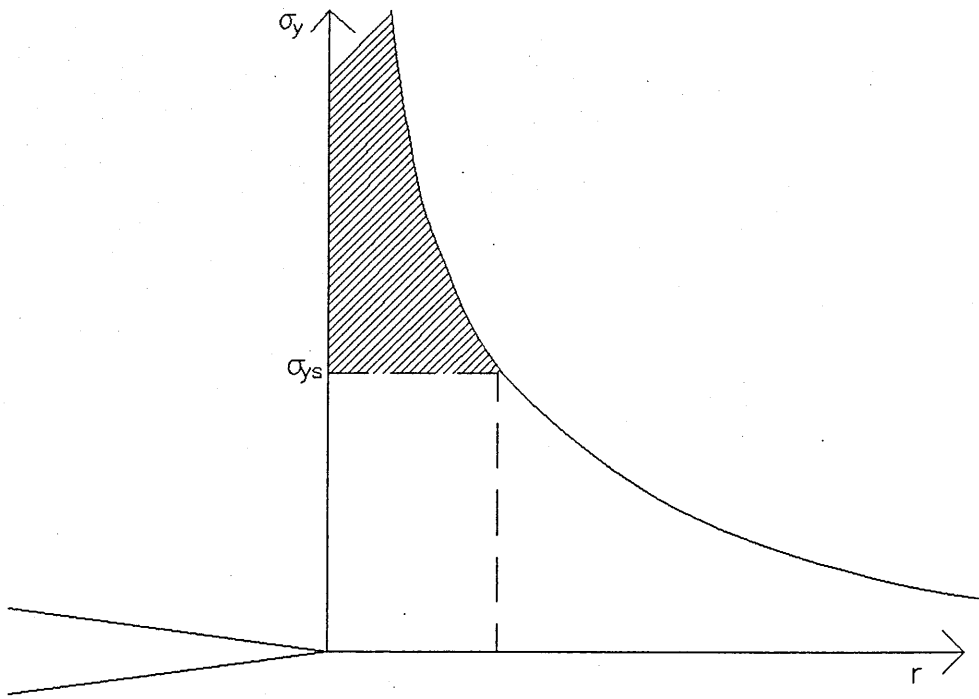
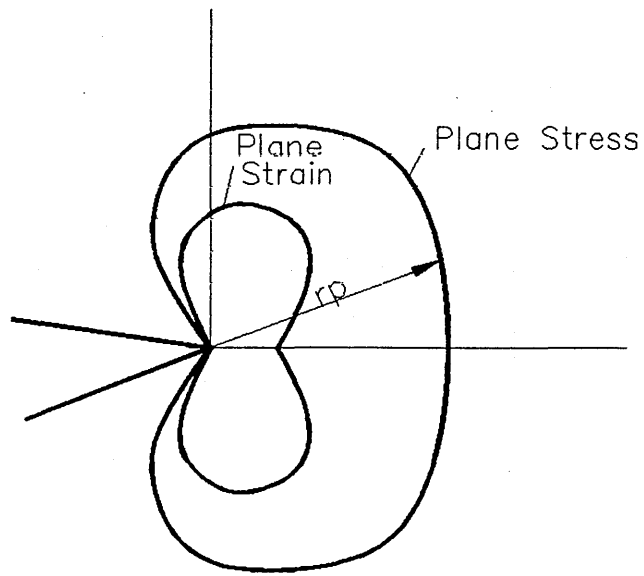
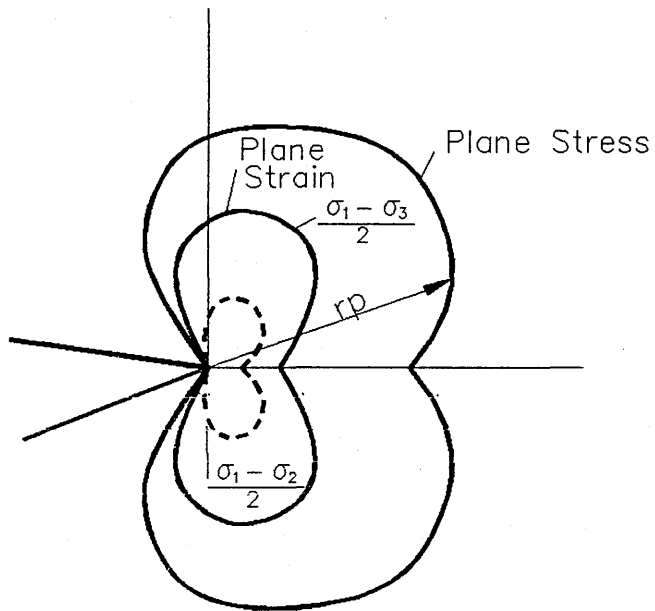


Figure 2.5



a) Mises Yield Criteria



a) Tresca Yield Criteria

Figure 2.6

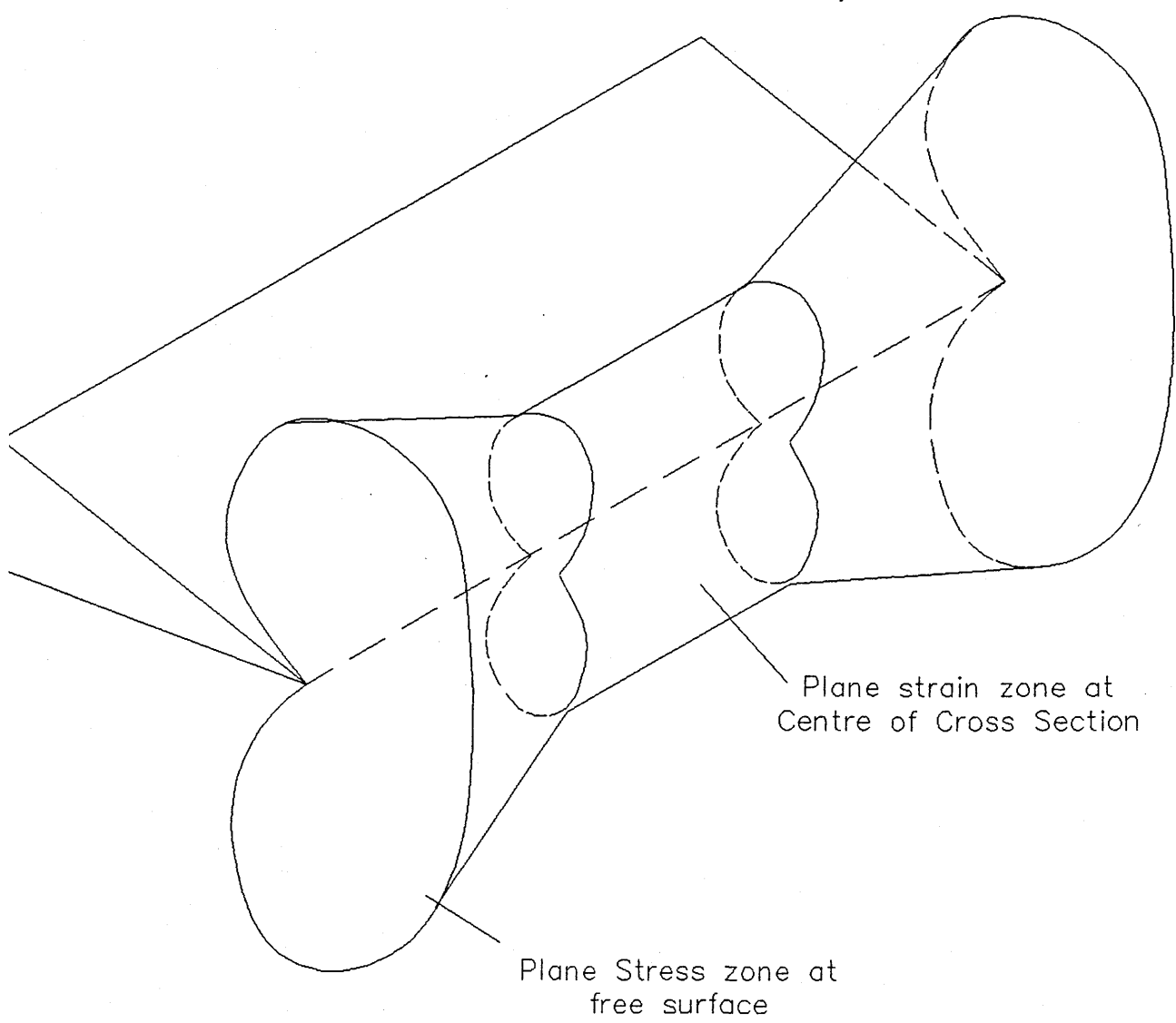


Figure 2.7

## CHAPTER 3

### DETERMINATION OF STRESS INTENSITY FACTORS

#### 3.1 Introduction

The applicability of LEFM hinges on the determination of the stress intensity factor for a specific crack in a particular component geometry. Having evaluated the appropriate stress intensity factor assessments of residual strength, crack growth rate and fitness for purpose can be made using crack growth models and measured material fracture toughness values. Such assessments form the basis of repair/no repair decisions for defects found in service and remnant life estimates for operating plant.

It has already been shown that the stress intensity factor can be generalised as :

$$K_I = \alpha \sigma \sqrt{\pi a} \quad (5)$$

where  $\alpha$  accounts for geometrical factors. The applied stress,  $\sigma$ , and the crack length,  $a$ , can be determined by conventional stress analysis and inspection techniques respectively ( at the design stage the crack length,  $a$ , will be defined ), hence the evaluation of the stress intensity factor reduces to the determination of the appropriate calibration constant ( $\alpha$ ). For standard crack geometries several compendia are available [6,7,24,25] which give  $\alpha$  in graphical or tabular form as a function of normalised crack length,  $a/W$ , where  $W$  is some characteristic length. Unfortunately 'real' components seldom look like any of the standard geometries and hence the stress intensity factor has to be evaluated using suitable techniques.

Many methods have been developed for the evaluation of stress intensity

factors, and it is beyond the scope of this thesis to describe each in detail. This section has therefore been limited to an overview of the techniques available with a more detailed description being given only to the techniques which have been utilised in this work. For a more detailed coverage the reader is referred to standard texts such as those by Cartwright and Rooke [26], Sih [27] and parts I and II of Tada [24]. Broadly the available techniques can be split into three categories; analytical, numerical and experimental. Each of these categories has been considered separately.

### 3.2 Analytical Methods

Analytical methods for the calculation of stress intensity factors form the base from which fracture mechanics developed as it was these which led to the fundamental equations for crack tip stress and strain fields (2). However since analytical techniques attempt to solve the boundary conditions exactly their range of applicability is limited to relatively simple 2-D cases such as infinite plates.

In general the analytical solutions endeavour to find an Airy stress function,  $\phi$ , to solve the problem under consideration. The stresses can then be given by:

$$\sigma_{xx} = \frac{\partial^2 \phi}{\partial y^2} \quad \sigma_{yy} = \frac{\partial^2 \phi}{\partial x^2} \quad \sigma_{xy} = \frac{\partial^2 \phi}{\partial x \partial y} \quad (13)$$

which automatically satisfy both the compatibility and equilibrium conditions since the Airy function satisfies the biharmonic condition :

$$\nabla^2(\nabla^2 \phi) \quad (14)$$

The precise form of  $\phi$  is determined by the imposed boundary conditions.

For mode I problems Westergaard[5] proposed a complex formulation of  $\phi$  :

$$\phi_I = \text{Re}[Z_I] + y \text{Im}[Z_I] \quad (15)$$

where

$$Z(z) = \text{Re}Z + i\text{Im}Z \quad \text{with} \quad z = x + iy \quad (16)$$

$Z_I$  is the Westergaard stress function and :

$$dZ_I/dz = Z_I \quad dZ_I/dz = Z_I \quad \text{and} \quad dZ_I/dz = Z_I' \quad (17)$$

Combining (13) and (17) gives:

$$\sigma_x = \text{Re}Z_I - y\text{Im}Z_I' \quad (18)$$

$$\sigma_y = \text{Re}Z_I + y\text{Im}Z_I' \quad (19)$$

$$\tau_{xy} = -y\text{Re}Z_I' \quad (20)$$

The stress intensity factor in terms of the Westergaard stress function for a crack tip situated at  $z = a$  becomes :

$$K_I = \sqrt{2\pi} \lim_{x \rightarrow a} \{\sqrt{(z-a)}Z_I\} \quad (21)$$

The simplest configuration considered by Westergaard was that of a crack in an infinite sheet subject to uniform biaxial tension ( $\sigma$ ) at infinity. For this situation Westergaard used the stress function :

$$Z_I = \frac{\sigma z}{\sqrt{(z^2 - a^2)}} \quad (22)$$

This technique was used to derive the equations for the stress field at a crack tip (2). However a non-singular term in the  $\sigma_x$  equation was added later after an oversight in the Westergaard analysis was discovered by Sih [28] and Eftis and Liebowitz [29], the additional term has no effect on the singular terms. The Westergaard analysis has been applied to several other crack problems by various workers [eg. 30,31,32].

Other forms of complex stress function have been proposed. One that has received much attention is the solution of Muskhelishvili [33] since it enables conformal mapping of cracks to holes. This method is discussed in detail by Sih [34] and was used for example by Erdogan [35] to analyse cracks in infinite sheets loaded by point forces and moments. Other analytical techniques which have been utilised in the analysis of cracked bodies include methods based on dislocation models [36,37], Greens functions [38,39], Integral transforms [40] and a method which uses the stress concentration results of Neuber [41] to obtain theoretical expressions for stress intensity factors [42].

### **3.3 Numerical Techniques**

With the advent of large computers it became possible to use numerical procedures to calculate approximate values of stress intensity factors. Initially these methods were developed as numerical solution procedures of the analytical functions described above. In particular the complex stress functions of Muskhelishvili [33] and Williams [43] have been used in the boundary collocation and conformal mapping techniques. The boundary collocation method expands the stress function as a power series in normalised distance from the crack tip. A set of simultaneous equations is formed and the coefficients of the power series derived to satisfy the boundary conditions. Gross, Strawley and Brown [44,45] used this method to solve a variety of problems including the determination of size correction factors for fracture toughness specimens and by Isida [46] to solve the problem of a crack approaching a hole. Conformal mapping was used by Bowie [47] to treat the problem of cracks emanating from holes. The technique involves deriving accurate polynomial approximations to the mapping function which transforms the cracked domain into a circular region. This reduces the solution of the stress functions in the transformed area to the solution of a system of finite equations. A combination of the boundary collocation and conformal mapping techniques, the so called mapping collocation procedure, was used by Bowie and Neal [48] in the analysis of an orthotropic plate. Other techniques available include the solution of singular

integral equations as used by Cruse [49] in the analysis of three dimensional crack profiles and the body force method [50].

### **3.4 Finite Element Methods**

#### **3.4.1 Overview**

The finite element method is now widely used in structural analysis and the theory is well documented [51]. Briefly the technique involves the discretisation of the structure into small elements. Within each element the shape, number of nodes and form of the displacement variation are assumed according to the element formulation. From this information a complete set of equations is formulated for the structure which allows stresses, strains and displacements to be calculated for a given load system (e.g. thermal, mechanical or centrifugal loading on the structure). Generally the smaller the elements used in the discretisation the more accurate the solution. Conversely the more elements the more expensive the analysis in terms of computing resources. The number of elements used to describe a model is then a compromise between accuracy and cost. This situation can be improved by using graded mesh (element) sizes ie. a fine mesh is used in the regions of particular interest such as areas local to stress concentrations and a coarse mesh is used where stresses are low or uniform.

The evaluation of stress intensity factors using the finite element method has been reviewed by Gallagher [52], Jerram and Hellen [53], and Rice and Tracey [54]. Three types of solution were identified; first and most obvious were the so called direct methods which determine the stress intensity factor from the calculated stress and strain fields, secondly the indirect methods which utilise some form of numerical differentiation to calculate related quantities such as energy release rates or compliance, and finally methods which use specially formulated crack tip elements to model the displacements at the crack tip. Each category has been considered briefly here with more detailed attention paid to the most widely used techniques

and the techniques relevant to this work.

### **3.4.2 Direct Methods**

By performing a conventional finite element analysis it is possible to calculate the stresses and displacements at the node points in the vicinity of the crack tip. Substitution of these values into the equations for the stress and strain fields at the crack tip (3) together with the co-ordinates of the node gives values of  $K_I$ . Since the Westergaard equations are normally represented by only the singular terms it is necessary to extrapolate back to the crack tip, Figure 3.1. It has generally been reported [55] that the displacement method gives better results than the stress method. This would be expected since the primary variables in the finite element method are the nodal displacements with the stresses being calculated by some extrapolation procedure. The direct method has been used to derive stress intensity factors by several authors [55 - 59] with varying degrees of accuracy depending on element formulations and mesh refinement. Chan et al [55] investigated the effect of mesh size and the comparative accuracy of each technique. The nature of both methods requires several nodes within the immediate vicinity of the crack tip at any given  $\theta$  in order to allow accurate extrapolation. This necessitates a large number of elements and hence makes even simple models very expensive in terms of computer resources.

### **3.4.3 Indirect Methods**

The advantage of using indirect methods to evaluate stress intensity factors is that exact modelling of the singular stress and displacement fields at the crack tip is not critical. It is therefore possible to derive sufficiently accurate values using relatively coarse meshes and conventional elements. Several indirect methods are now in common use and it is outwith the scope of this work to describe all the available techniques in detail. For this reason only the most common methods and those relevant to this work are discussed here. Other techniques are mentioned with references for completeness.

### 3.4.3.1 Strain Energy Release Rate

It has already been shown that the stress intensity factor can be related to the elastic energy of the cracked body through equation (7). Where  $G$ , the strain energy release rate, can be defined as :

$$G = \frac{\partial U}{\partial a} \quad (23)$$

and  $U$  is the elastic energy stored in the cracked body. Hence performing several finite element analyses for different crack lengths and numerical differentiation of the elastic strain energy stored with respect to crack length allows the calculation of  $G$  and subsequently the stress intensity factor  $K$ . This method has the disadvantage that several finite element runs are required. Encouraging results have however been demonstrated by several workers. Watwood [60] used the method to analyse a centre cracked panel of finite size with a reported difference of the order of 2 percent compared to Isida's [61] mapping solution. Swanson [62] used the method in the analysis of radially cracked cylinders subject to internal pressure. Other workers [63-65] have demonstrated the accuracy of the method by comparison with other techniques.

### 3.4.3.2 The Virtual Crack Extension Method

A variation on the strain energy release rate described above is the virtual crack extension technique. While the method is similar to the above technique it economises on computation by considering only small (virtual) crack extensions, Figure 3.2, while maintaining a constant load and recalculating only the change in the stiffness matrix due to the elements local to the crack tip. Two formulations of the virtual crack extension technique have been proposed; Parks [66] proposed a method based on the stiffness derivative local to the crack tip and used this in conjunction with contour integration to evaluate stress intensity factors; Hellen [67,68] used a property of Gaussian elimination called a front solution [69] to evaluate local energy

changes and hence to calculate stress intensity factors. These techniques are now widely implemented in finite element codes such as ABAQUS [70] and BERSAFE [71].

### 3.4.3.3 Contour Integration

An alternative method for direct evaluation of the strain energy release rate is based on contour integration of the form :

$$J = \int_{\Gamma} (W dx_2 - T_i \frac{du_i}{dx_i}) ds \quad (24)$$

This integral was originally formulated by Eshelby [72] and independently formulated for crack problems by Rice [73] and Cherepanov [74] and is normally termed the J-integral. In the above equation  $W$  is the strain energy density,  $T_i$  are the applied tractions,  $u_i$  are displacements and  $x_i$  are cartesian coordinates normally taken with the origin at the crack tip.  $\Gamma$  is a contour which begins on one crack face and ends on the other crack face,  $ds$  is an element of the path  $\Gamma$  Figure 3.3. Path independence can be demonstrated by reference to Figure 3.3b. Here a closed path is shown which does not include the crack tip consisting of four segments such that,

$$\Gamma = \Gamma_1 + \Gamma_2 + \Gamma_3 + \Gamma_4$$

By compatibility  $J=0$  over  $\Gamma$ , if the stress and displacement gradients are continuous. Further along contours  $\Gamma_2$  and  $\Gamma_4$  the tractions,  $T_i$ , are zero and by definition  $dx_2=0$ . The contributions of  $\Gamma_2$  and  $\Gamma_4$  to  $J$  must therefore vanish. Since  $\Gamma_1$  and  $\Gamma_3$  are in opposite sense then it can be concluded that since the value of  $J$  integrated over the two paths must be identical to zero then the value of  $J$  for each path must be equal in magnitude. Since these paths were chosen in a random manner the path independence of the  $J$  integral has been demonstrated. If  $\Gamma$  is allowed to shrink towards a small

contour round the crack tip such that the radius,  $r$ , of the contour tends towards zero the second term of (24) vanishes and  $J$  becomes :

$$J = \int_{\Gamma} W dx_2 = G \quad (25)$$

Therefore  $J$  represents the total energy stored at the crack tip. Due to the path independence of  $J$  demonstrated above this can be evaluated from a zone remote from the crack tip and therefore remote from the singularity. Once more this enables the stress intensity factor to be calculated without excessive mesh refinement at the crack tip.

The J-integral is now a widely utilised method for the evaluation of energy release rates and stress intensity factors and has been included as a facility in many of the commercial finite element packages suitable for fracture mechanics applications. Evaluation of the integral can be done at the post processing stage of the analysis allowing any chosen number of contours to be used without the need for repeat stress and strain analysis. Several authors [55,58,75] have used the method and shown favourable comparisons with other techniques, particularly the displacement substitution method.

In certain circumstances the path independence of  $J$  is lost. This can occur due to the presence of secondary strains, for axisymmetric problems or in non-homogeneous environments. A generalised form of  $J$ ,  $J^*$  has been proposed by Blackburn [76] to overcome these problems. Other authors have proposed alternative path independent integrals for the evaluation of stress intensity factors [77-80].

#### **3.4.3.4 Special Elements**

In conventional finite element formulations the displacement variation is fitted by a polynomial approximation, however it has already been shown, equation (2), that the displacements local to a crack tip vary as  $\sqrt{r}$ , where  $r$  is the distance from the crack tip. It then follows that the nature of conventional elements is not suitable for modelling crack tip stress and strain fields and

therefore large numbers of small elements are required to give adequate representation of crack tip conditions. This situation can be improved by the use of elements whose displacement variations are forced to include a  $\sqrt{r}$  term local to the crack tip. Such elements are termed special or singular elements. Several special elements have been proposed including [81-85] and it is not intended to review these elements here. For a comprehensive review of special crack tip elements the reader is referred to [86,87]. Generally the elements include the crack tip at a specified node and model the displacement variation radially from this node. More recently Henshell and Shaw [88] and Barsoum [89] showed, independently, that the  $\sqrt{r}$  displacement function can be achieved in quadratic isoparametric elements by moving the midside nodes to the quarter position nearest the crack tip, Figure 3.4. This holds for both triangular and quadrilateral elements in both two and three dimensions, provided that in the three dimensional case only nodal movements normal to the crack plane are made. This technique has the advantage that special element formulations are not required. While this methodology is generally attractive in the case of complex three dimensional problems considerable effort may be required to ensure the midside nodes are correctly positioned. Commercial finite element packages such as ABAQUS [90] have incorporated this methodology.

#### **3.4.4 Other Finite Element Methods**

Other numerical methods for the determination of linear elastic fracture mechanics parameters include crack closure work and compliance techniques. The compliance technique is based on the same principle as the experimental method described in the following section with the only difference being that the compliance of the cracked component is evaluated numerically. This method has been used by several authors [91-92] with varying degrees of success. In the crack closure work method [93] the displacement of the first node along the crack flank is calculated under the action of the required external loading system. Then a unit load is applied to this node normal to the crack face and a further set of displacements is obtained. By extrapolation the force required to close this increment of crack can be calculated and hence the strain energy release rate evaluated. This

offers an advantage over other energy approaches since only one run of the model is required with two load cases.

### **3.5 Experimental Methods**

Experimental estimates of stress intensity factors are useful in many circumstances. They can be used to confirm analytical or approximate solutions or in their own right. The stress intensity factor cannot be measured directly and must therefore be found through its relationship with other measurable quantities such as strain, displacement or compliance. Since there are always errors in experimental measurement of these quantities, particularly in complex geometries, and further since other unknowns such as residual stresses or material inhomogeneity will be unquantified experimental techniques can only give approximate solutions. Several methods exist and are widely reported in the literature. Only a brief overview is given here and the reader is referred to standard fracture mechanics texts such as Broek [94] and Knott [95] or to specific papers for more detail.

Most techniques are based on the measurement of crack tip stress and/or strain fields. One such technique commonly used is photoelasticity including the use of frozen stress techniques for three dimensional problems. In this case the cracked geometry is modelled using a transparent material, such as epoxy resin, with a machined slit to represent the crack it is impractical to produce sharp cracks in photoelastic materials. Once deformed the photoelastic material displays a fringe pattern when viewed through a polariscope. This fringe pattern can be related to the shear stress in the component and hence the stress intensity factor obtained from :

$$K_I = \tau \sqrt{(2\pi r)/f(\theta)} \quad (26)$$

As in the direct finite element techniques described above the correct solution is only obtained by extrapolating back to the crack tip,  $r=0$ . Consequently the accuracy of the resulting stress intensity factor is dependent on the extrapolation. This is further confused by the fact that the fringes close to the crack tip cannot be used since they will be influenced by

blunt notch effects. Photoelasticity has been used to examine simple cases [eg.96] with reasonable accuracy and expanded using more elaborate techniques to examine crack tip stress fields [97,98,99] but without the additional steps required to calculate K. It is also possible to use photoelasticity to study mixed mode fracture mechanics problems [100].

A more generally applicable technique makes use of conventional strain gauge technology to measure crack tip strain fields [101,102,103]. Once again the stress intensity factor is evaluated by extrapolating back to the crack tip. Care must be taken when using this technique that the strain gauges are positioned outside the plastic zone at the crack tip. In addition it should be realised that a strain gauge can only measure the average strain within the area it covers and that since steep strain gradients may exist close to the crack tip significant errors may be incurred, however reasonable results have been reported using this technique. The method has the advantage that it can readily be applied to cracked components in operational plant.

One of the most widely applied experimental techniques uses the relationship between the compliance of the specimen and the strain energy release rate, G :

$$G = \frac{P^2 dC}{2dA} \quad (27)$$

which can be combined with the relationship between  $K_I$  and G (7) to give :

$$K_I = P \sqrt{(0.5E \frac{\partial C}{\partial A})} \quad (28)$$

K can then be found from the relationship between the compliance and the crack length. Once this relationship is known for a particular specimen geometry K can be determined from the measurement of load and load point displacement. Several workers [104,105,106] have produced reasonable

results using compliance measurements on tapered cantilever beam specimens and other similar specimen geometries. However in the case of edge and centre cracked plates loaded in tension the compliance of the specimen does not change significantly with crack length and hence reliable K values cannot be expected.

A further experimental technique which can be used to estimate stress intensity factors that was utilised in this work was proposed by James and Anderson[107]. The basis of the technique is an empirical relationship of the form :

$$\frac{da}{dN} = f(\Delta K) \quad (29)$$

between the fatigue crack growth rate and  $\Delta K$ . The form of the equation can be particularised based on experimental observations using specimens with known K solutions. Having derived the relationship the stress intensity factor can be derived for a crack growing in a more complex geometry by measuring the crack growth rate and hence calculating  $\Delta K$ . Care is required in the use of the method since no account of complexities such as crack closure, residual stresses and material effects is accounted for in equation (29).

### **3.6 Other Methods for the Determination of K**

Several other approximate methods exist for the estimation of stress intensity factors. One such technique is the weight function method which will be discussed at some length here since it has been utilised in this work. Other techniques provide a means of obtaining an idea of the stress intensity factor for complex geometries subject to complex loading conditions. These methods are only discussed briefly here but are reviewed in more detail in [108].

### 3.6.1 Weight Functions

Beuckner's principle [109] allows the problem of determining stress intensity factors at a stress free crack in a loaded body to be reduced to that of a crack with pressure applied to its faces. The boundary conditions for the reduced problem are that all tractions and displacements are zero and that the pressures on the crack faces are equivalent to the stresses over the same area in the uncracked body subject to the original boundary tractions and displacements. Beuckner's principle is shown schematically in Figure 3.5. The ability to utilise the stress distribution in the uncracked body forms the basis of several methods used in the determination of stress intensity factors including Green's function, weight functions and superposition techniques.

The weight function method for the determination of stress intensity factors was proposed by Beuckner [110] and Rice [111]. A more direct derivation of the same results was later given by Paris et al [112] and the method was generalised by Labbens et al [113] to enable three dimensional crack problems to be considered in a practical manner. In a general form the weight function concept suggests that a point load  $P_Q$  acting at point Q on a crack front will produce an opening mode stress intensity factor at point Q' on the crack front, Figure 3.6. Where the stress intensity factor at Q' due to the force at point Q is given by :

$$W_{QQ'} = \frac{K_{P_{QQ'L}}}{P_Q} \quad (30)$$

Where  $W_{QQ'}$  is termed the weight function. For an opening mode pressure acting on the crack surfaces,  $q_Q$ , the stress intensity factor at point Q',  $K_{Q'}$ , is given by an integral over one crack surface area, A, given by :

$$K_{Q'} = \iint_A W_{QQ'} q_Q dA_Q \quad (31)$$

Where  $dA_Q$  is an infinitesimal area around point Q and  $q_Q$  may vary across the crack surface.  $W_{QQ'}$  is independent of the form of  $q_Q$ , the pressure

distribution over the crack faces. Further, following Beuckner's principle  $q_Q$  can be replaced by  $\sigma_{ij}$  the stress distribution at the crack location in the uncracked body. If the appropriate weight function can then be determined the stress intensity factor at any point on the crack front can be readily calculated for any given load case. The weight function  $W_{QQ'}$  can be shown to be :

$$W_{QQ'} = \frac{8\mu}{1+k} \frac{1}{K_I^*} \left( \frac{\partial v^*}{\partial x} \right)_{QQ'} \quad (32)$$

Where  $k = 3-4\nu$  for plane strain and  
 $= \frac{3-\nu}{1+\nu}$  for plane stress

$\mu$  is the shear modulus.  $K_I^*$  is a known stress intensity factor solution for the particular geometric configuration under consideration and  $v^*_{QQ'}$  is the displacement of the crack surfaces for the known condition.

Closed form solutions for  $W_{QQ'}$  are known for a limited number of problems. Tada [114] derived the solution for a circular crack in an infinite solid as :

$$W_{QQ'} = \frac{K_{P\alpha\alpha}}{P_Q} = \frac{\sqrt{(a^2 - r^2)}}{\pi \sqrt{\pi a} l_{QQ'}} \quad (33)$$

Where

- $l_{QQ'}$  = the distance from Q to Q' on the crack front
- $a$  = the radius of the crack front
- $r$  = the distance from point Q to the centre of the crack

Other closed form solutions for  $W_{QQ'}$  are known for a semi-infinite straight fronted crack in an infinite solid [115] and for a circular ligament in an infinite

body [114] as :

$$W_{QQ'} = \frac{K_{P\alpha\alpha'}}{P_Q} = \frac{\sqrt{2}\sqrt{a}}{\pi\sqrt{\pi}l_{QQ'}^2} \quad (34)$$

and

$$W_{QQ'} = \frac{K_{P\alpha\alpha'}}{P_Q} = \frac{1}{(\pi a)^{1.5}} \cos^{-1}\left(\frac{a}{r}\right) + \frac{\sqrt{(a^2 - r^2)}}{\pi\sqrt{\pi a}l_{QQ'}^2} \quad (35)$$

respectively. Where  $l_{QQ'}$ ,  $a$  and  $r$  are defined as before. From (33) and (34) it would appear that the weight function is dependent on the inverse square of the distance between points  $Q$  and  $Q'$  and the geometry (curvature) of the crack front. However for the third solution (35) these observations do not hold for the first term. If however the ligament is large compared to the distance  $l_{QQ'}$  then the first term becomes negligible and the observation is valid for the dominant second term. Oore and Burns [116] utilised this observation to formulate a generalised weight function approach. The resulting expression for the weight function was :

$$W_{QQ'} = \frac{K_{P\alpha\alpha'}}{P_Q} = \frac{\sqrt{2}}{\pi} \frac{1}{l_{QQ'}^2 \left( \int_s \frac{ds}{\rho_Q^2} \right)^{1/2}} \quad (36)$$

where  $s$  is the crack front,  $ds$  is an infinitesimal portion of the crack front and  $\rho_Q$  is the distance from  $Q$  to  $ds$ , Figure 3.7. The line integral term accounts for both the geometry of the crack front and the position of the point load within the geometry. This approach was further generalised to allow an arbitrary pressure (stress) to act over the crack face resulting in a generalised expression for  $K_{Q'}$  as :

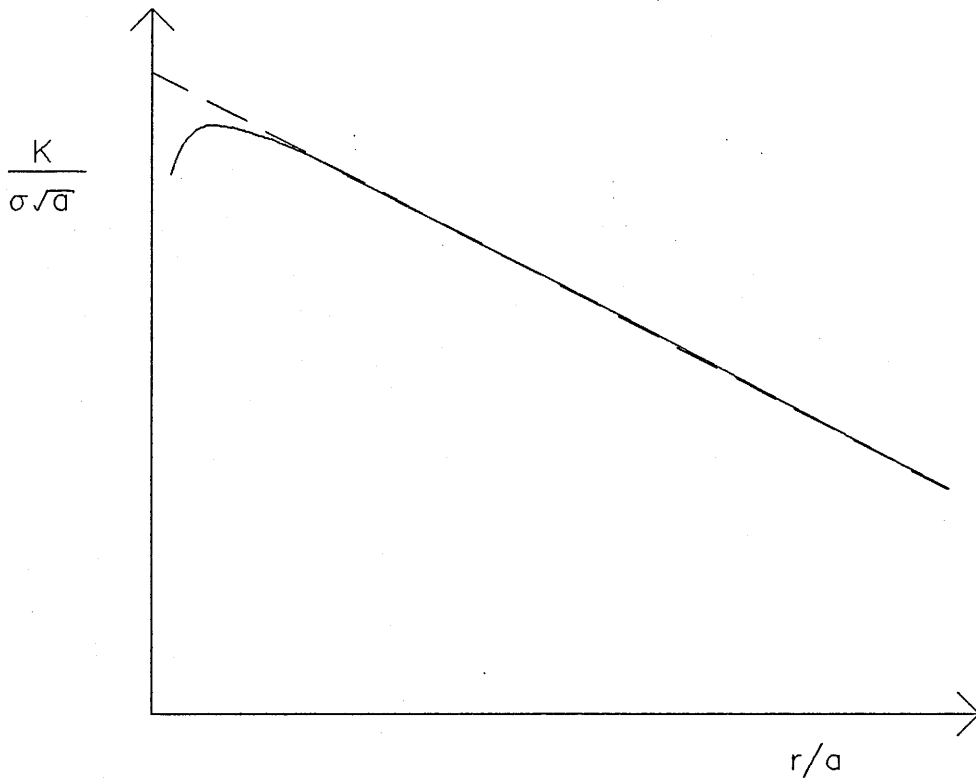
$$W_{QQ'} = \frac{K_{P_{\alpha\alpha'}}}{P_Q} = \int \int_A \frac{\sqrt{2} \sigma_Q dA_Q}{\pi l_{QQ'}^2 \left( \int_s \frac{ds}{\rho \delta} \right)^{1/2}} \quad (37)$$

Expression (37) is generally referred to as the 0-integral. The validity of the (37) was demonstrated by comparison with existing solutions for embedded crack geometries [116,117].

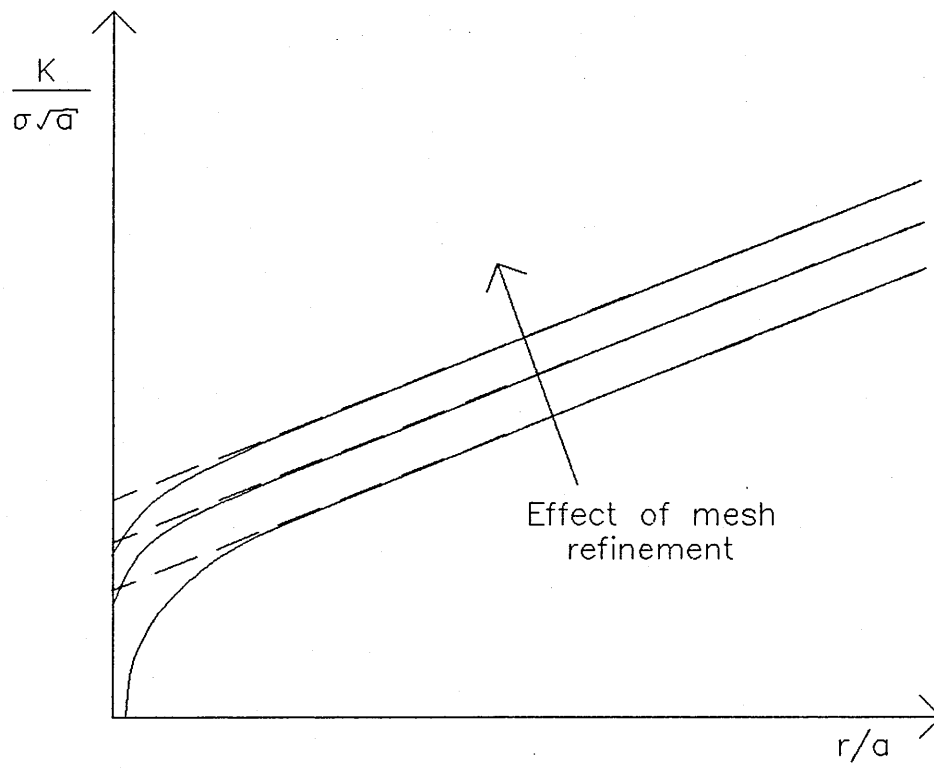
The 0-integral was further developed for application to arbitrary shaped surface cracks subject to arbitrary loading. This technique will be discussed further in the discussion of surface crack problems in a later section.

### 3.6.2 Simple Estimation Procedures

Approximate techniques may be utilised to estimate stress intensity factors for complex or 'non-standard' geometries or loadings. Generally these techniques make use of known results to either bound or estimate the unknown case. One such technique [118] uses stress concentration factor solutions to derive the stress intensity factor by extrapolating to an infinitely sharp notch. Other techniques make use of load relief factors [119] and compounding approaches [120]. A detailed review of these techniques is given elsewhere [eg. 108] and is beyond the scope of this work.

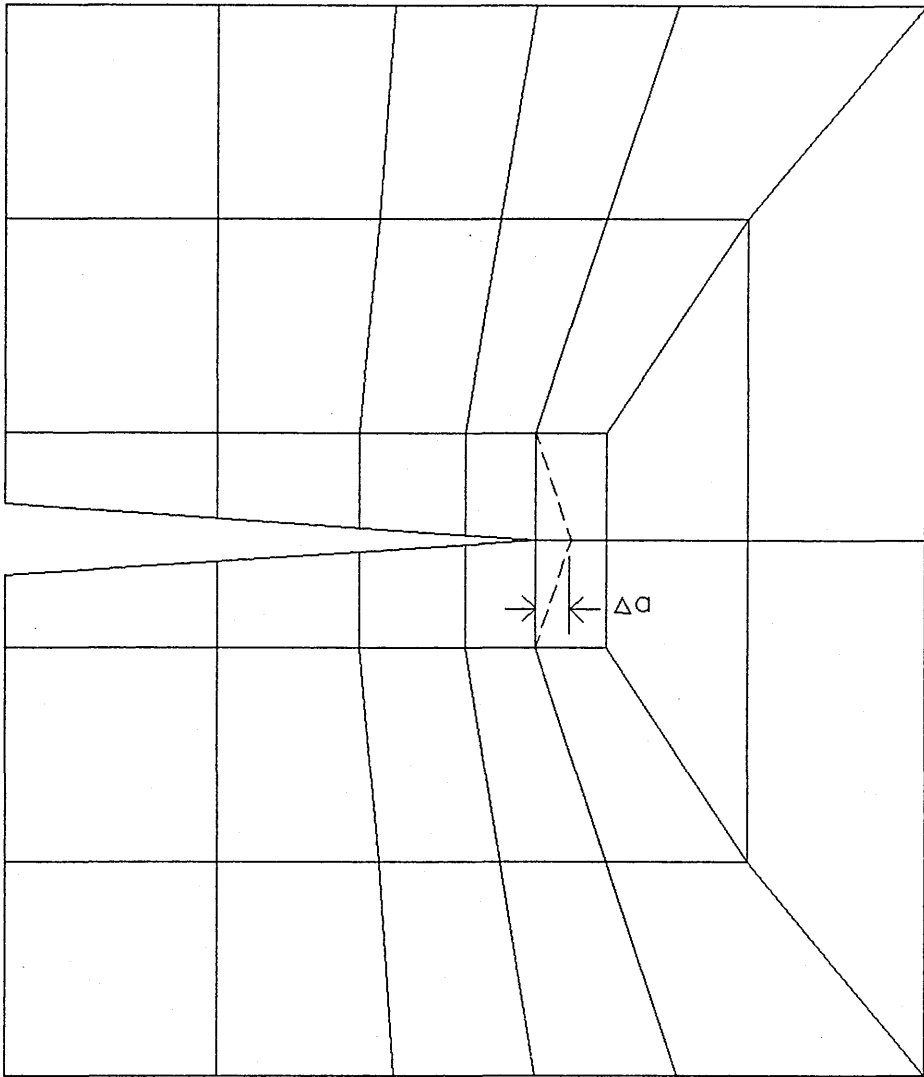


a) Stress Method



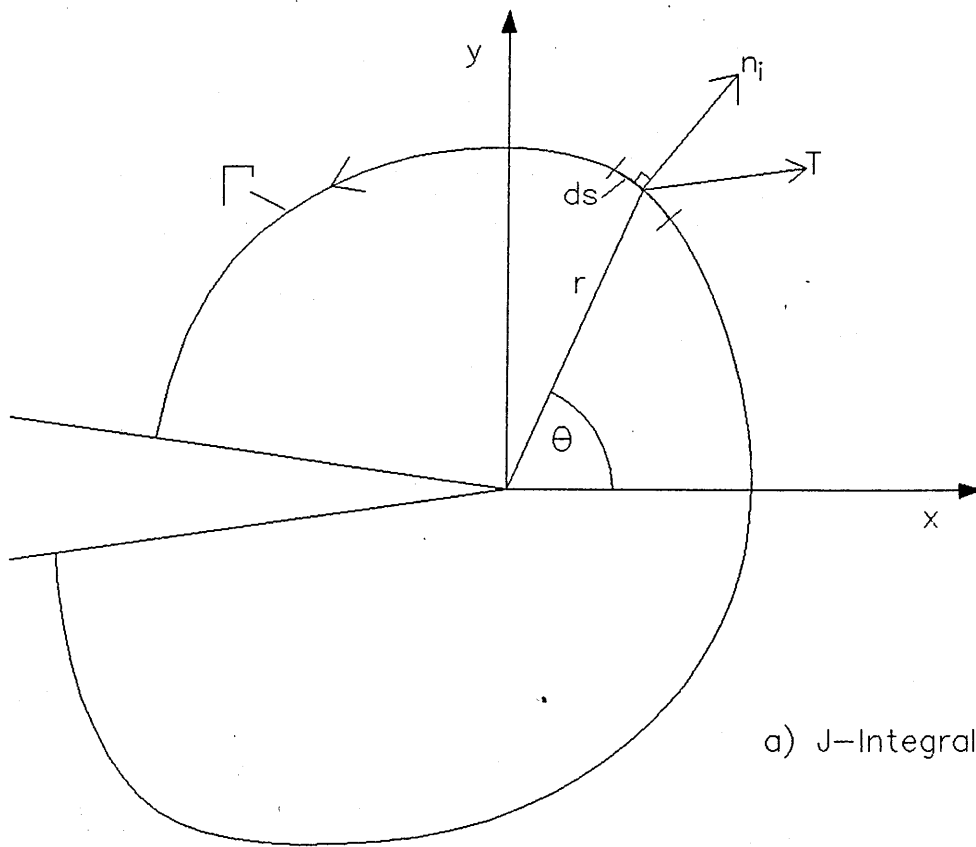
b) Displacement Method

Figure 3.1

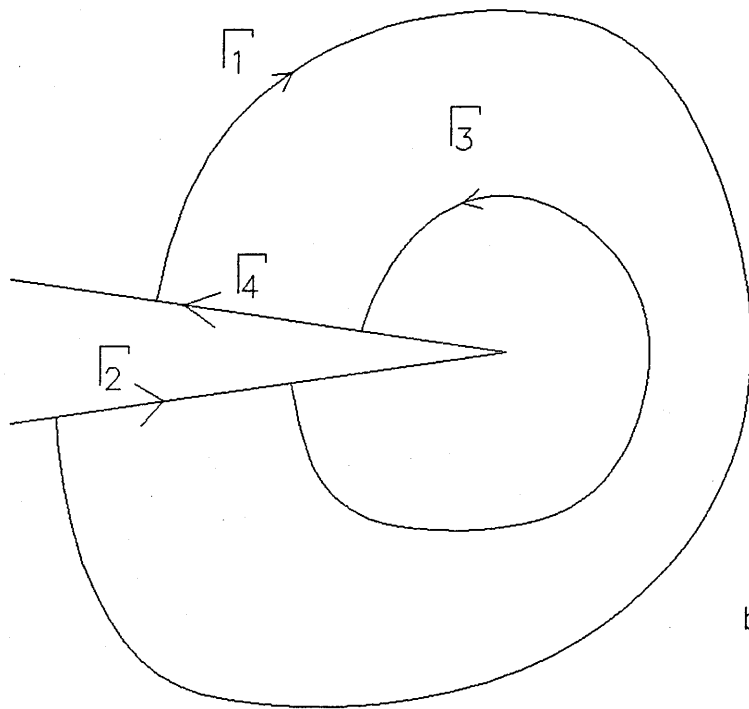


Mesh re-adjustment for Virtual Crack Extension

Figure 3.2

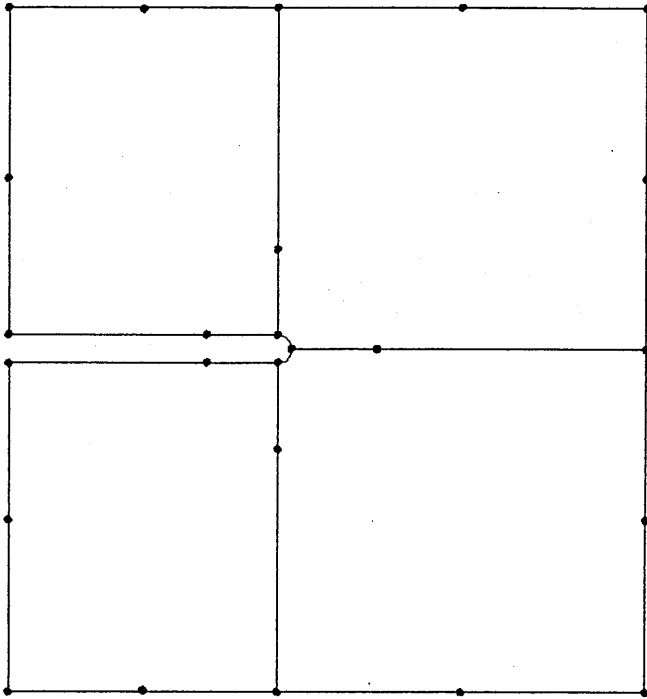


a) J-Integral Contour

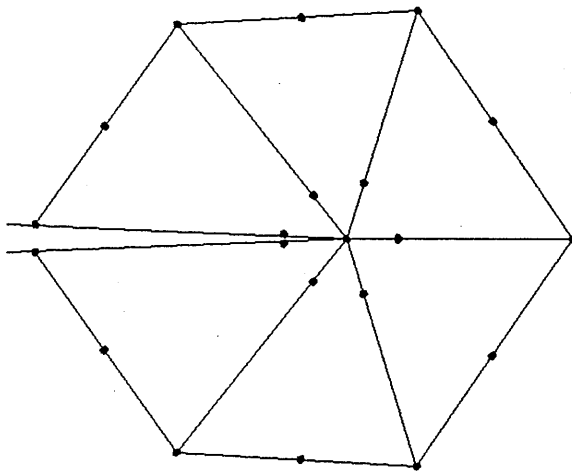


b) Path Independence

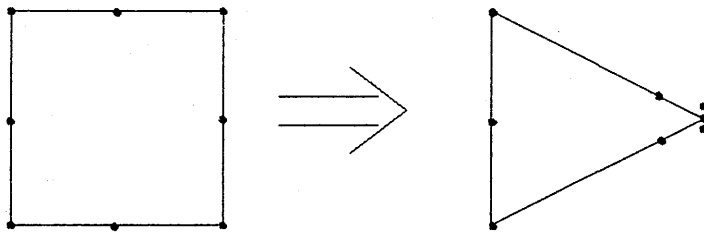
Figure 3.3



a) Eight Noded  
Quadrilaterals



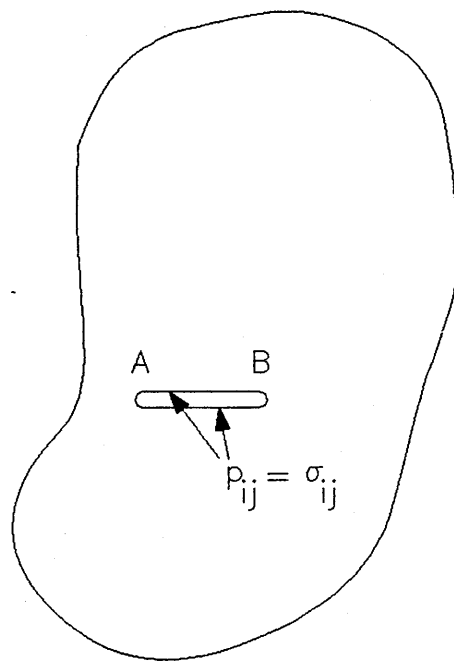
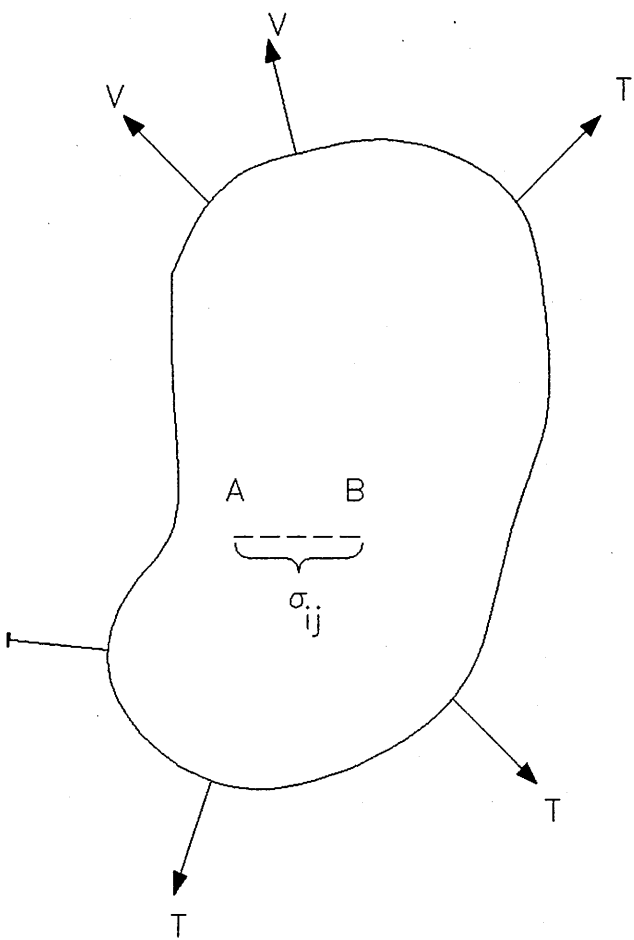
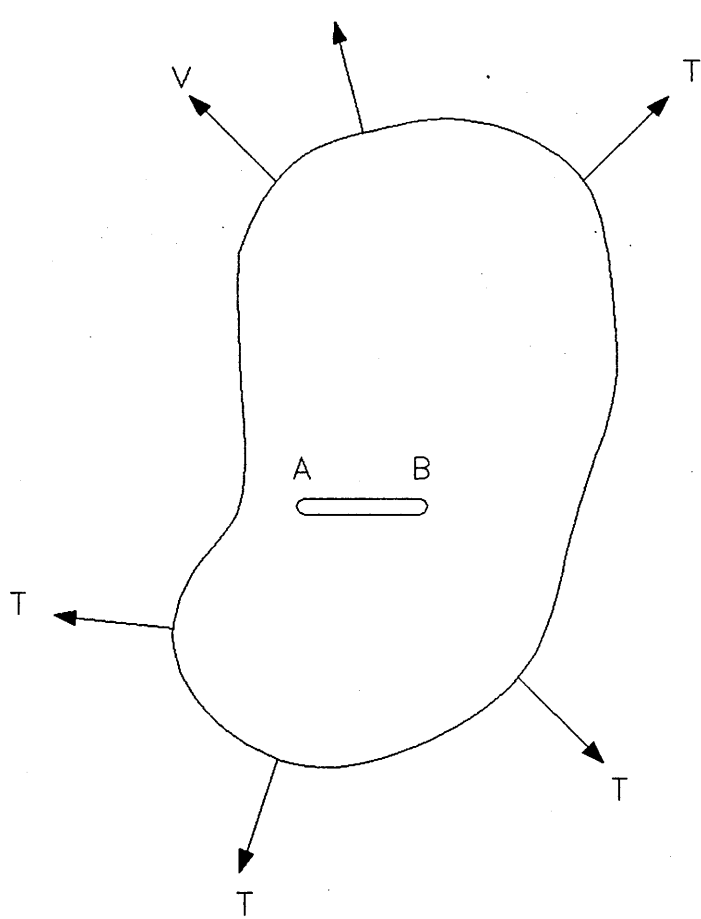
b) Triangles



c) Degenerate  
Triangles

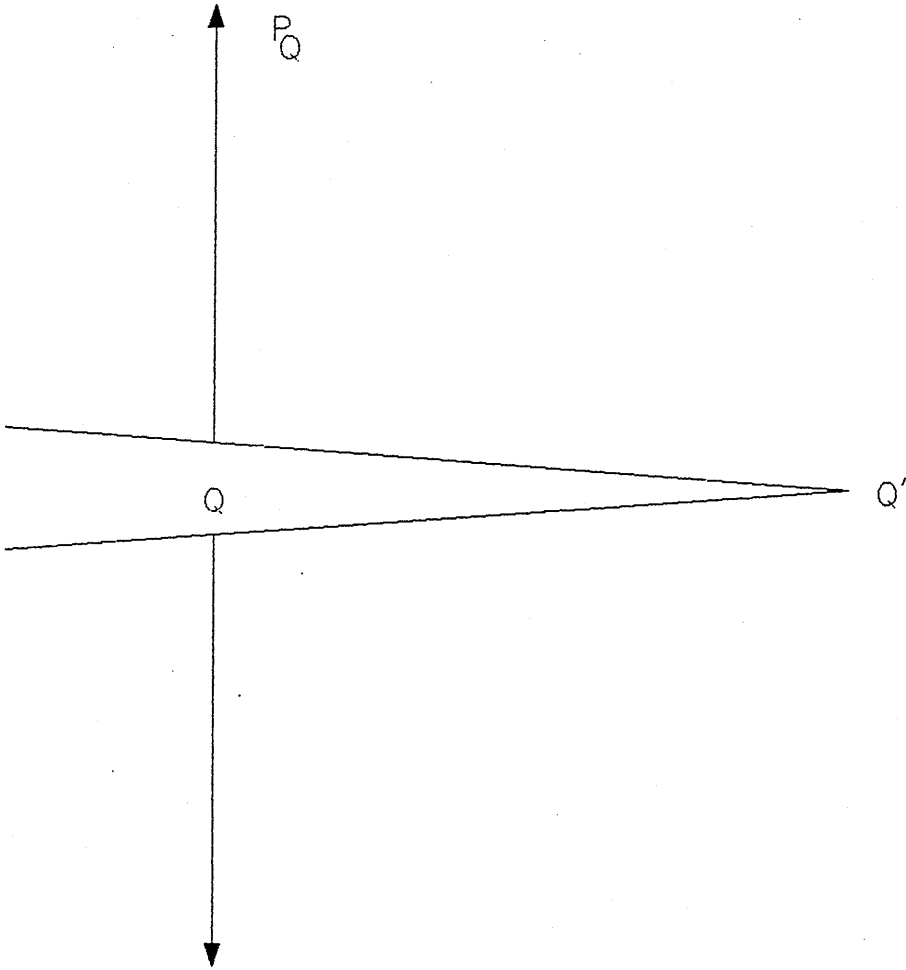
Quarter Point Elements

Figure 3.4



Buekner's Principle

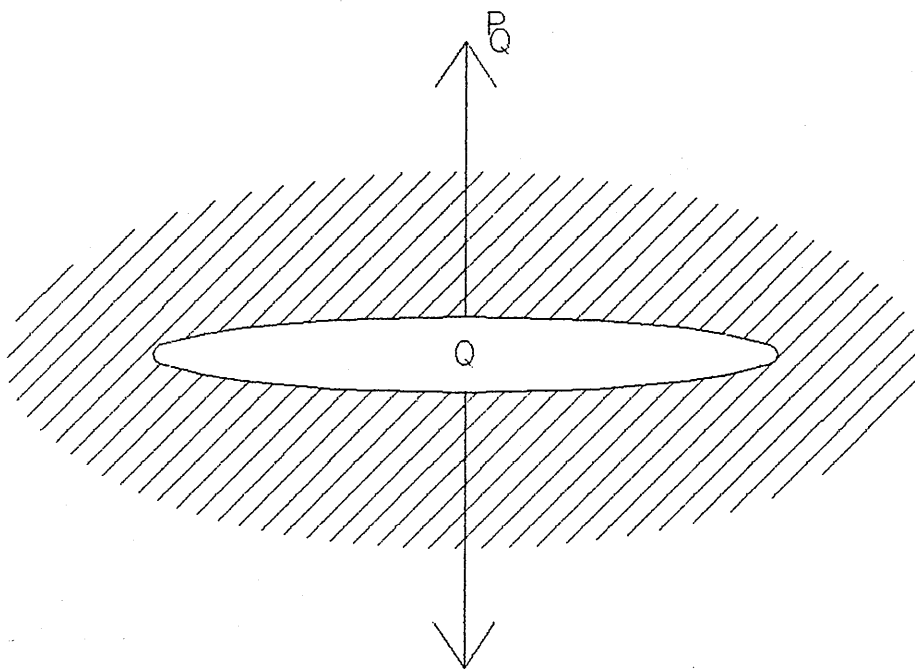
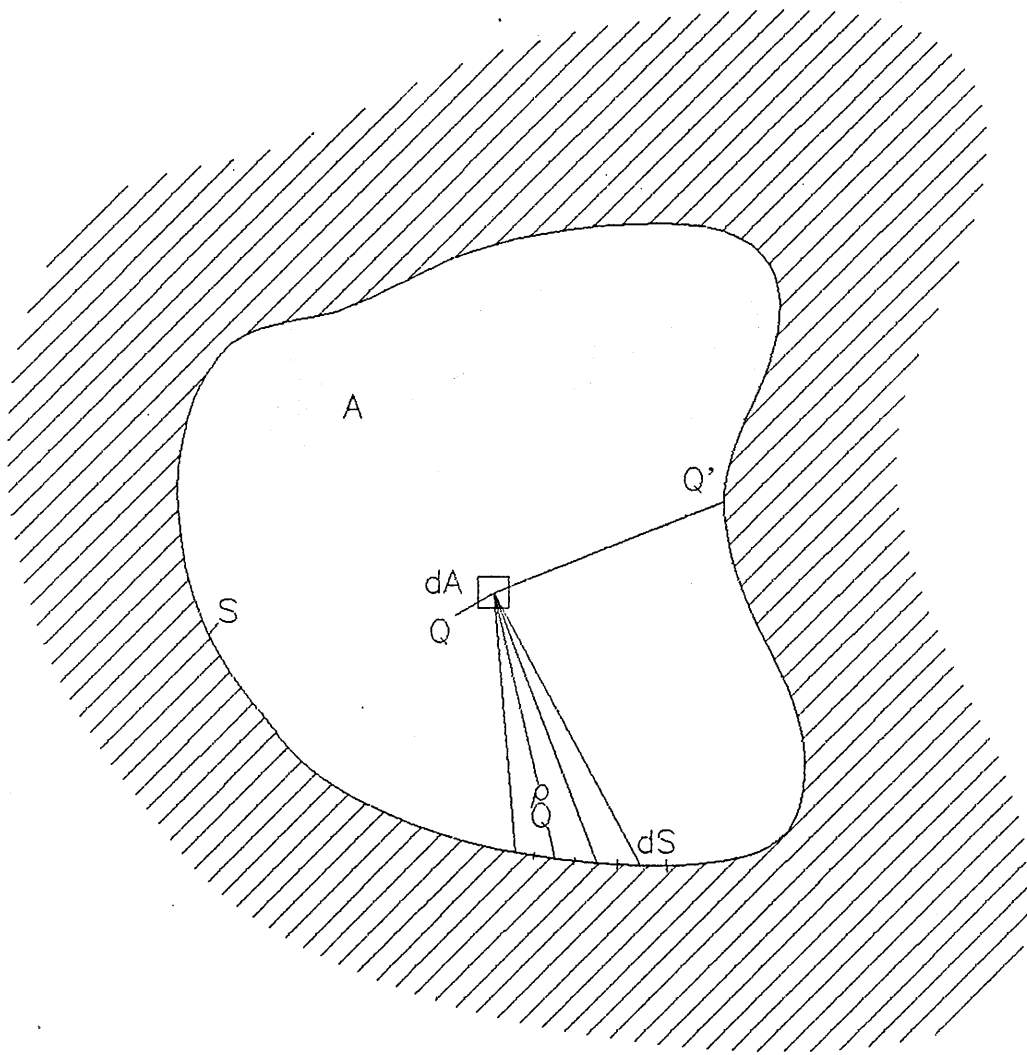
Figure 3.5



$$K_{P_{QQ'}} = P_Q \cdot W_{QQ'}$$

$W_{QQ'}$  = Weight Function

Figure 3.6



0 – Integral Terminology

Figure 3.7

## **CHAPTER 4**

### **3-D CRACK PROBLEMS**

#### **Embedded and Surface Crack Behaviour**

##### **4.1 Introduction**

The preceding sections have discussed the behaviour and analysis of 2D crack problems, in which the crack has a straight front which extends through the thickness of the structure or specimen. However in reality failures may develop from flaws which pre-exist within a structure due to inclusion clusters or welding defects such as lack of fusion, slag inclusion or porosity or from a surface imperfection such as a weld detail, arc strike site or simply as a result of the cyclic stress imposed at a local stress concentration. In these cases a complex 3D crack geometry will exist. Generally the crack front will be curved (to a closed form for submerged defects) and the crack will be sited in a non-uniform multiaxial stress system. This in turn means that the stress field, and hence the crack tip characterisation parameter such as  $K$ , will vary along the crack front. In a structure the problem may be further exacerbated by the proximity of free surfaces, other defects and geometrical complications. The complexity of the problem rapidly becomes obvious. However the application of fracture mechanics to structures demands the solution of these problems in order to guarantee the integrity of large fabricated structures such as nuclear power plant, aircraft, and offshore installations, which cannot be manufactured defect free. The challenge is then to utilise the data which can be readily generated in the laboratory on simple specimens to assess the behaviour of cracked components. To facilitate this goal it is necessary to make use of several assumptions and to utilise several of the approximate fracture mechanics analysis techniques discussed in the previous section.

The first assumption which must be made regards the defect shape. In general it is assumed that surface breaking defects will assume a semi-

elliptical form and that submerged defects will form as ellipses. Defects discovered in service which do not conform to these geometries are recharacterised into suitable forms using established rules [eg.121,122] for the purpose of assessment. This work was principally concerned with the behaviour of semi-elliptical surface defects and in particular the coalescence of multiple co-linear defects and hence this section will be focused towards analytical and numerical techniques suitable for these geometries. Embedded defects will be considered briefly prior to discussion of the surface defect problem, however a full review of this area is beyond the scope of this work.

## 4.2 Embedded Defect Solution

The basis of most modern elliptical crack solutions and indeed the extension of these to semi-elliptical crack problems is the work of Irwin [123]. A precursor to this work was the analysis of a so called 'penny-shaped' crack by Sneddon [124] and Sack [125] and the analysis of the stress field around an ellipsoidal cavity by Green and Sneddon [126]. Irwin used the calculated stresses and displacements to derive the following expression for the stress intensity factor for an embedded elliptical crack acted upon by a uniform remote tensile stress:

$$K_I = \frac{\sigma\sqrt{\pi a}}{\Phi} \left( \sin^2\theta + \frac{a^2}{c^2} \cos^2\theta \right)^{\frac{1}{4}} \quad (38)$$

Where  $\Phi$  is an elliptical integral of the second kind, given by

$$\Phi = \int_0^{\pi/2} \left[ 1 - \frac{c^2 - a^2}{c^2} \sin^2\theta \right]^{1/2} \quad (39)$$

and  $a$  and  $c$  are defined as shown in Figure 4.1. From (38) and (39) it is clear that  $K_I$  will vary round the crack front having a maximum value at the end of the minor axis and its lowest value at the end of the major axis ie.:

$$K_{I(\varnothing=\pi/2)} = \frac{\sigma\sqrt{\pi a}}{\Phi} \quad \text{and} \quad K_{I(\varnothing=0)} = \frac{\sigma\sqrt{\pi a^2/c}}{\Phi} \quad (40)$$

These expressions form the basis for most modern solutions of elliptical crack problems including semi-elliptical surface cracks and quarter elliptical corner cracks and are therefore of great practical interest. Application of the above solution to surface breaking defects is generally achieved by applying a number of correction factors to (38). Normally (38) may be modified to account for the varying plastic zone size round the crack perimeter giving:

$$K_I = \frac{\sigma\sqrt{\pi a}}{\sqrt{Q}} \left( \sin^2\varnothing + \frac{a^2}{c^2} \cos^2\varnothing \right)^{\frac{1}{4}} \quad (41)$$

Where Q is termed the 'flaw shape parameter' and includes the plasticity correction:

$$Q = \Phi^2 - 0.212 \frac{\sigma^2}{\sigma_{ys}^2} \quad (42)$$

### **4.3 Analysis of Semi-elliptical Surface Cracks**

#### **4.3.1 Overview**

A surface flaw may be considered to be comparable to an edge crack and it has been shown [127] that the stress intensity factor for an edge crack in a semi infinite body is approximately 12% greater than that for an equivalent centre crack. It then follows that to apply (38) and (41) to surface crack problems a so called 'back face correction factor' can be applied and that this will be of the order of 12% for long shallow surface flaws. In a similar manner the proximity of the free surface in front of the crack can be accounted for by addition of a front surface correction factor, as can the effects of the finite width, also referred to as the finite area, of the component

or specimen. For a surface crack loaded in tension the stress intensity factor can then be represented by the expression:

$$K_{\text{Surface}}(\varnothing) = M_{\text{F}}M_{\text{B}}M_{\text{W}}K_{\text{Embedded}} \quad (43)$$

where,

$K_{\text{Embedded}} = K$  for an embedded elliptical defect with the same aspect ratio loaded by the same remote tensile stress.

$M_{\text{F}} =$  The front face correction factor

$M_{\text{B}} =$  The back face correction factor

$M_{\text{W}} =$  A correction to account for finite area.

This can be further simplified to :

$$K_{\text{Surface}}(\varnothing) = MK_{\text{Embedded}}(\varnothing) \quad (44)$$

with,

$$M = f(a/c, a/t, c, w, \varnothing)$$

The analysis of surface crack behaviour under tensile loading is therefore reduced to the evaluation of  $M$ , a geometry dependent factor. Where the defect is loaded by a combination of bending and tensile stress, Figure 4.2,  $M$  will be dependent on both the geometry and loading such that :

$$K_{\text{Surface}}(\varnothing) = (M_{\text{b}}\sigma_{\text{b}} + M_{\text{t}}\sigma_{\text{t}})f(\varnothing)\sqrt{(\pi a)/\Phi} \quad (45)$$

where  $f(\varnothing)$  gives the variation of  $K$  around the crack front and the subscripts 'b' and 't' refer to bending and tensile components respectively.

Due to the practical importance of the surface crack problem to engineering components and structures there has been a great deal of interest in the evaluation of the magnification factors,  $M$ , in equation (45) and in the generalisation of these for application to more complex geometries and loading conditions. Since the pioneering work of Irwin, numerous stress intensity factor solutions have been proposed for the surface crack problem. These solutions have been reviewed in some detail in the open literature [128-132] and the reader is referred to these sources for a more comprehensive review of the available solutions. This section will be limited to a brief overview of some of the methods which have been utilised and will give detail only for solutions relevant to this work.

The available solutions can be categorised as those based on analytical approaches, numerical analyses and empirical approaches based on experimental observations. The first of these categories is necessarily limited by the complexity of the problem. Of the analytical procedures proposed one of the most successful is the alternating method [133]. For three dimensional crack problems the alternating method has been used in conjunction with numerical procedures to solve surface crack type problems [134-136]. More recently Nishioka and Atluri [137-139] have used the alternating method in conjunction with a finite element model to obtain stress intensity factors for more complex geometries. Experimental approaches to the problem have been attempted by correlating crack growth rates [140,141] and by photoelastic stress freezing methods [142,143]. While these techniques are extremely valuable for the verification of theoretical solutions their applicability is limited by practical difficulties and cost when attempting to analyse complex geometries and loading conditions.

It is clear from the above discussion that analytical and experimental solutions to the surface crack problem are valuable but limited, and further that the complexity of analytical approaches, such as the alternating method, often necessitates the use of numerical solution procedures. For this reason several numerical procedures have been developed for the analysis of surface crack problems. The objective of all of these methodologies is to

provide sufficient flexibility to analyse complex cracked component geometries and cracks in non-uniform stress systems. Of these approaches the finite element method is one of the most popular. The general methods used to calculate stress intensity factors within the finite element method were discussed in the previous chapter and will not be repeated here. Several authors have used the method for the analysis of surface crack geometries [144-147]. Newman [131] compared the calculated stress intensity factors at the point of maximum depth for a surface crack using fourteen different solutions. The variation between different solutions was shown to be as much as 80% for crack depths of  $a/t = 0.6$ .

### **4.3.2 Finite Element Solutions - Newman Raju**

In an effort to improve this situation Newman and Raju [148,149] produced solutions using the finite element method for a wide range of defect geometries in flat plates. As part of the analysis a sensitivity study was undertaken to study the convergence of the solutions using a range of mesh refinements from 1500 to 6900 degrees of freedom. Scott and Thorpe [132] and Newman and Raju [150] later produced empirical equations by fitting these solutions which enable stress intensity factors to be calculated for any specified surface crack subject to tension and bending loadings. The Newman and Raju equations allow the stress intensity factor to be evaluated at all points around the crack periphery whereas Scott and Thorpe only consider the deepest point and the point where the crack intersects the free surface.

The Newman - Raju solution is valid for a range of defects in flat plates bounded by :

$$\text{Aspect Ratio : } 0 < a/c \leq 1.0$$

$$\text{Depth : } 0 \leq a/t \leq 1.0$$

$$\text{and Finite Width : } c/b \leq 0.5$$

For Parametric angles :  $0 \leq \theta \leq \pi$

Where  $b$  is the half width of the plate. For a cracked plate with outer fibre bending stress,  $S_b$ , and remote tensile stress,  $S_t$ , the stress intensity factor at any point on the crack periphery is then given by :

$$K_I = (S_t + HS_b) \sqrt{(\pi a/Q)} F(a/t, a/c, c/b, \theta) \quad (46)$$

Where  $Q$  is the shape factor for an elliptical crack as described in (39). A useful approximation to this expression is :

$$Q = 1 + 1.464(a/c)^{1.65} \text{ for } (a/c \leq 1.0) \quad (47)$$

and

$$Q = 1 + 1.464(c/a)^{1.65} \text{ for } (a/c > 1.0) \quad (48)$$

Newman [131] found that the maximum error in the calculated stress intensity factor induced by using these expressions was of the order of 0.13%.  $F$  and  $H$  in equation (46) were defined such that the boundary correction factor for tension is equal to  $F$  and that for bending is equal to the product of  $H$  and  $F$ . The function  $F$  is given as :

$$F = [M_1 + M_2(a/t)^2 + M_3(a/t)^4] f_{\theta} g f_w \quad (49)$$

where

$$M_1 = 1.13 - 0.09(a/c) \quad (50)$$

$$M_2 = -0.54 + 0.89/(0.2+(a/c)) \quad (51)$$

$$M_3 = 0.5 - 1.0/(0.65+(a/c)) + 14(1.0 - (a/c))^{2.4} \quad (52)$$

$$g = 1 + [0.1 + 0.35(a/t)^2](1 - \sin \theta)^2 \quad (53)$$

$f_{\theta}$  is an angular function from the embedded elliptical crack solution [126]:

$$f_{\theta} = [(a/c)^2 \cos^2 \theta + \sin^2 \theta]^{1/4} \quad (54)$$

The function is a finite width correction factor taken from [151]:

$$f_w = [\sec((\pi/2)(c/b)\sqrt{(a/t)})]^{1/2} \quad (55)$$

For the bending component H is given by :

$$H = H_1 + (H_2 - H_1) \sin^p \theta \quad (56)$$

Where

$$p = 0.2 + (a/c) + 0.6(a/t) \quad (57)$$

$$H_1 = 1 - 0.34(a/t) - 0.11(a/c)(a/t) \quad (58)$$

$$H_2 = 1 + G_1(a/t) + G_2(a/t)^2 \quad (59)$$

and

$$G_1 = -1.22 - 0.12(a/c) \quad (60)$$

$$G_2 = 0.55 - 1.05(a/c)^{0.75} + 0.47(a/c)^{1.5} \quad (61)$$

This solution is now widely recognised and has become the standard with which alternative techniques are evaluated. The solution does however have obvious limitations. Few engineering components can be considered as flat plates under simple tension or bending loading. In reality the analyst is required to assess cracks at nozzle/vessel intersections or in tubular joints with complex weld geometries and stresses which vary along both the minor and major axis of the crack. In these cases the empirical equations

described above are of limited use. It is true that the original work of Newman and Raju [148,149] may give useful information as to how the finite element method should be applied to these problems but in practice 3D finite element modelling of cracked component geometries is prohibitively expensive in both time and computing cost. Approximate techniques have therefore been developed in order to allow the analysis of these complex problems, the alternating technique mentioned above is one such technique. Two techniques used in this study which can be applied to both complex loading conditions and geometries, but also to more complex crack shapes are the weight function method and the line spring technique. Due to their relevance to this work each of these techniques will be considered as separate sections in turn.

### **4.3.3 The Line Spring Technique**

The line spring model was introduced by Rice and Levy [152,153] as an approximate method for the analysis of surface cracks in plate and shell type geometries. In essence the method reduces a complex three dimensional crack analysis problem to a quasi two dimensional shell type analysis. If the model is incorporated within a finite element package for use in the analysis of engineering components the savings in terms of the computing resources required are clearly substantial, of the order of one order of magnitude compared to the equivalent 3-D model, and hence the method is commercially very attractive.

The line spring model, henceforth LSM, concept is demonstrated in Figure 4.3. Figure 4.3a shows the surface crack in a plate, or shell, of thickness  $t$ . The crack has a surface length of  $2c$  and has a maximum depth equal to  $a$  at  $x=0$  with  $a=a(x)$  along the crack length. Figure 4.3b shows a 2-D idealisation of the 3-D geometry where the surface crack is represented as a through crack of length  $2c$  with a series of one dimensional springs linking the crack surfaces together, the so called line springs. The plate is loaded remotely by a membrane force  $N$  and a bending moment  $M$  per unit length. Since the ligament length,  $t-a(x)$ , varies along the crack length the membrane and

bending forces which must be carried by the ligament must also vary along the crack length and may be represented as  $N^*(x)$  and  $M^*(x)$  respectively. In the 2-D idealisation  $N^*(x)$  and  $M^*(x)$  must be transmitted by the line springs. If it is then assumed that  $\delta(x)$  and  $\theta(x)$  represent the relative displacements and rotations of the crack faces at the plate mid surface respectively, then these may in turn be related to the plate mid-surface displacements  $U_x(x,y)$ ,  $U_y(x,y)$  and  $U_z(x,y)$  by :

$$\delta(x) = U_y(x,0^+) - U_y(x,0^-) \quad (62)$$

$$\theta(x) = \frac{\partial U_z(x,0^-)}{\partial y} - \frac{\partial U_z(x,0^+)}{\partial y} \quad (63)$$

The LSM relates the local  $N^*(x)$  and  $M^*(x)$  to  $\delta(x)$  and  $\theta(x)$  using :

$$\begin{bmatrix} \delta(X) \\ \theta(X) \end{bmatrix} = \begin{bmatrix} C_{11}(X) & C_{12}(X) \\ C_{21}(X) & C_{22}(X) \end{bmatrix} \begin{bmatrix} N(X) \\ M(X) \end{bmatrix} \quad (64)$$

Where  $X=x/l$ , a dimensionless coordinate, and  $\underline{C}$  and  $\underline{S} = \underline{C}^{-1}$  are the local compliance and stiffness matrices respectively.

Application of the model requires the local compliance  $\underline{C}(X)$  to be determined. It is assumed that these can be obtained at each spring location by analogy with the edge cracked strip solution, Figure 4.3c. An edge crack of depth equal to the local crack depth at the spring is considered in a strip of width  $t$  loaded by a membrane force,  $N^*(X)$ , and bending moment  $M^*(X)$ . If  $\delta_c$  and  $\theta_c$  are the load point displacement and rotations due to the crack in the edge cracked plate under elastic conditions :

$$\begin{bmatrix} \delta_c \\ \theta_c \end{bmatrix} = \begin{bmatrix} P_{11}(X) & P_{12}(X) \\ P_{21}(X) & P_{22}(X) \end{bmatrix} \begin{bmatrix} N \\ M \end{bmatrix} \quad (65)$$

$\underline{P}$  can be derived from available stress intensity factor solutions for the SECP [eg. 114]. It is then assumed that  $\underline{C} = \underline{P}$  and hence, implicitly, that  $\delta_c$  and  $\theta_c$  can be used for  $\delta$  and  $\theta$  as defined in equations (62) and (63) for the surface crack problem.

When implemented in a finite element code the method then requires the springs to be placed across a through crack in a suitable shell model of the geometry to be analysed. The resulting equations are then solved for  $\delta(x)$  and  $\theta(x)$  enabling  $N^*(x)$  and  $M^*(x)$  to be calculated using equations (64) and (65). The local stress intensity factor can then be determined from :

$$K_I(x) = (\pi a(x))^{1/2} \{ F_1(a(x)/t) N^*(x)/t + F_2(a(x)/t) 6M^*(x)/t^2 \} \quad (66)$$

Where  $F_1$  and  $F_2$  are determined from the appropriate edge cracked plate solutions.

In the analysis of Rice and Levy classical Kirchoff type plate and shell theories were utilised in the formulation of the model. More recent work has used a more general plate/shell theory allowing transverse shear deformations to be accounted for. These results have shown good agreement with full 3-D solutions [154-161]. The LSM as implemented in the commercial finite element code ABAQUS was utilised in this work. ABAQUS uses the line spring elements coupled to 'S8R' general shell elements which allow transverse shear. In general the accuracy obtainable is considered to be more than acceptable for the purposes of engineering analysis. Parks [156] has shown agreement within a few percent of the Raju Newman finite element solutions for a wide range of surface crack geometries in flat plates.

The line spring concept has been extended to consider non-linear problems by considering plastic deformations in the ligament [156,158,159,162-165].

Application to more complex geometries has been demonstrated by Hancock and co-workers [166,167] in their analysis of tubular joints. Erdogan has extended the model to enable the analysis of embedded defects [168] and to cracks in shells under mixed mode loading conditions [169]. Application to the analysis of crack growth problems was considered by Miyoshi et al [170].

The LSM model has been demonstrated to give satisfactory results in all of the above cases at a fraction of the cost of conventional analytical techniques. It was therefore an obvious technique to consider for the numerical modelling of coalescing defects.

#### 4.3.4 Weight Functions Applied to Elliptical Defects

The basis of the weight function method for the determination of stress intensity factors was discussed in section 3.6.1. Equations (30) and (31) give the general form of the weight function formulation as :

$$K_Q = \int \int_A W_{QQ'} q_Q dA_Q \quad (31)$$

where  $W_{QQ'}$  is the weight function and is given by:

$$W_{QQ'} = \frac{8\mu}{1+k} \frac{1}{K_I^*} \left( \frac{\partial v^*}{\partial x} \right)_{QQ'} \quad (32)$$

$$k = 3-4\nu \text{ for plane strain}$$

$$= \frac{3-\nu}{1+\nu} \text{ for plane stress}$$

$$\mu = \text{Shear modulus}$$

Application of this technique to surface cracks would appear, in principle, to be relatively straight forward. The problem arises in the paucity of solutions suitable for use as reference cases. Most of the solutions to surface crack problems available in the open literature are for simple geometries such as flat plates or plane cylinders and these solutions only report the calculated stress intensity factors with no information regarding crack face displacements. It is therefore necessary to determine the reference solution using an alternative method prior to application of the weight function method for most problems. An obvious candidate method for the determination of reference solutions is the finite element method. However for complex component geometries with semi-elliptical crack shapes, a detailed 3D FE analysis is required for each crack geometry. Given these results the stress intensity factors for the crack shapes modelled can be obtained for any loading condition through use of the weight function method as a post processing option. The cost of such analysis is considerable in terms of the computational resources required, the time taken to prepare the models themselves and the cost of the cpu time required to execute the analysis. Stress intensity factor solutions for surface crack type geometries are often required to calculate critical defect sizes and locations in complex components and to determine the behaviour of growing cracks. In order to analyse problems of this nature using the basic weight function technique would be impractical due to the prohibitively high cost and the time required to generate the solutions.

A significant amount of effort has been directed towards overcoming the practical limitations of the weight function technique in order to produce a more useable form. Labbens et al [113] proposed a simplification which enabled several crack geometries to be considered within one finite element run without the need for re-meshing. This is achieved by the application of closure forces to the crack faces as a series of separate load cases. The closure forces are applied to nodes close to the preceding crack tip in order to produce a smaller crack geometry and therefore to enable several crack sizes to be examined within a single FE run. The FE analysis therefore produces the reference solutions for several crack geometries under one

simple load system eg. uniform tension. Weight functions are then applied at the post processing stage for all other load cases required. The cost savings using this method could be considerable if solutions were required for several crack sizes, at the same location under a number of different load conditions eg. pressure loadings, thermal shock, residual stress etc., as may be required in practice. While the benefits to be gained from this technique are clearly attractive the requirement for 3D FE analysis, even in this reduced form, makes the weight function approach impractical for many applications. Petroski and Achenbach [171] recognized this limitation and proposed an approximation for the displacement field which would allow SIF solutions from the open literature to be utilised as the reference load case. The approximation is based on a general form of crack opening displacement  $u(a,x)$ , approximately ellipsoidal, and a specific solution determined by considering the special case of the reference and required load case being identical. Petroski and Achenbach applied the method to a number of simple 2-D crack problems in their paper and showed good agreement with analytical solutions. Application of the method is simply a matter of numerical quadrature and requires no FE or other complex analysis but does require a suitable SIF solution from the literature. The method is particularly attractive for the analysis of cracks under complex stress systems such as those caused by thermal shock or residual stresses, where although solutions for simple load cases are available they will not be available for the stress distributions for specific problems. Mattheck et al [172,173] have used the method of Petroski and Achenbach in their analyses of surface cracks in plates loaded by stress gradients and shown favourable comparison with FE results from the literature. Grebner [174] used a similar method to analyse thermal shock problems for pipes with circumferential surface cracks. Niu and Glinka [175,176] have extended the method to consider stepped plates and weldment geometries.

An alternative approach developed by Oore and Burns [116,117] was introduced in section 3.6.1. The method was based around the 0-Integral concept with a view to enable the analysis of irregular crack shapes under arbitrary normal stress fields. The 0-Integral was derived for an irregular embedded crack, Figure 3.8, based on some observations of existing closed

form solutions and is given as equation (37) and repeated here for completeness:

$$W_{QQ'} = \frac{K_{P_{\alpha\alpha}}}{P_Q} = \int \int_A \frac{\sqrt{2} \sigma_Q dA_Q}{\pi l_{QQ'}^2 \left( \int_s \frac{ds}{\rho_Q^2} \right)^{1/2}} \quad (37)$$

$\sigma_Q$  is the stress which would exist at point Q in the absence of the crack. The 0-Integral offers a very convenient method for the evaluation of stress intensity factors around the periphery of any embedded defect under a state of stress obtained from analysis of an uncracked body. Extension of this to surface crack geometries is based on the hypothesis that: .-

$$\frac{K(\theta) \text{ of surface crack subjected to any stress distribution (Figs 4.4a and 4.4b) }}{K(\theta) \text{ of embedded crack of the same half geometry with the same 'half' loading on both halves of the crack (Figs 4.4b and 4.4c) }} = C \quad (67)$$

Where C is a constant dependent on geometry but not on loading.

Hence for the particular case of a semi-elliptical surface crack in a plate we have:

$$\frac{K_{su}(\theta)}{K_{eu}(\theta)} = \frac{K_{sl}(\theta)}{K_{el}(\theta)} = \frac{K_{sl}(\theta)}{K_{el}(\theta)} \approx \text{Constant} \quad (68)$$

where the stress intensity factors  $K(\theta)$  are :

$K_{su}(\theta)$  For a semi-elliptical surface crack subjected to

uniform stress,  $\sigma_z$

$K_{eu}(\theta)$  For the equivalent embedded elliptical crack subjected to uniform stress,  $\sigma_z$ .

$K_{sl}(\theta)$  For a semi-elliptical surface crack subjected to linearly varying stress,  $\sigma_z$ , Figure 4.5a

$K_{el}(\theta)$  For the equivalent embedded elliptical crack subjected to symmetrical linear stress,  $\sigma_z$ .  
Figure 4.5b.

$K_{sv}(\theta)$  For a semi-elliptical surface crack subjected to arbitrary normal stress,  $\sigma_z$

$K_{ev}(\theta)$  For the equivalent embedded elliptical crack subjected to symmetrical arbitrary normal stress,  $\sigma_z$ . Figs 4.5c.

For the case of semi-elliptical surface cracks in plates it should then be possible to evaluate the stress intensity factor of the equivalent embedded elliptical crack using the  $\theta$ -Integral and to calculate the required surface crack solution utilising

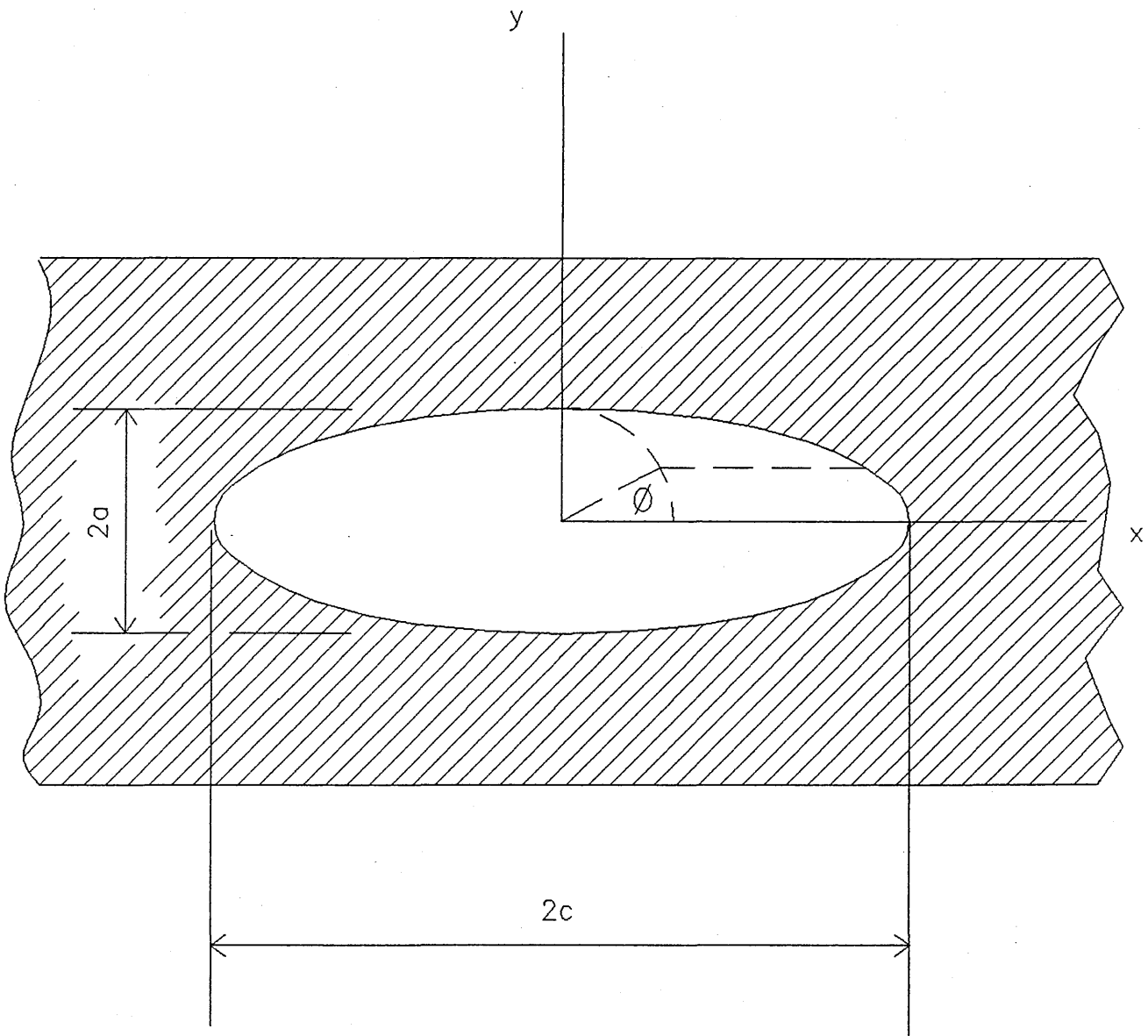
$$K_{sv} = K_{ev}(\theta) \frac{K_{su}(\theta)}{K_{eu}(\theta)} \quad (69)$$

Where  $K_{su}/K_{eu}$  can be obtained from literature solutions such as those of Raju and Newman. Extension of this to the case of irregular crack shapes under arbitrary stress assumes that the crack geometry has no effect on the magnification factors ie.:

$$K_{isv} = K_{iev}(\theta) \frac{K_{su}(\theta)}{K_{eu}(\theta)} \quad (70)$$

Where  $K_{isv}$  is the SIF at Q' for an irregular surface crack of the same half geometry and loading as the irregular embedded crack geometry used to calculate the embedded crack solution  $K_{iev}$ . The magnification factor  $K_{su}/K_{eu}$  in this case is taken for a semi-elliptical surface crack which bounds the irregular surface crack.

The method of Oore and Burns therefore has the advantage over that of Petroski and Achenbach in that it can easily allow for arbitrary stress variation both in the depth and surface length directions with respect to the crack surface and in it's ability to analyse arbitrary crack geometries.



Embedded Defect Notation

Figure 4.1

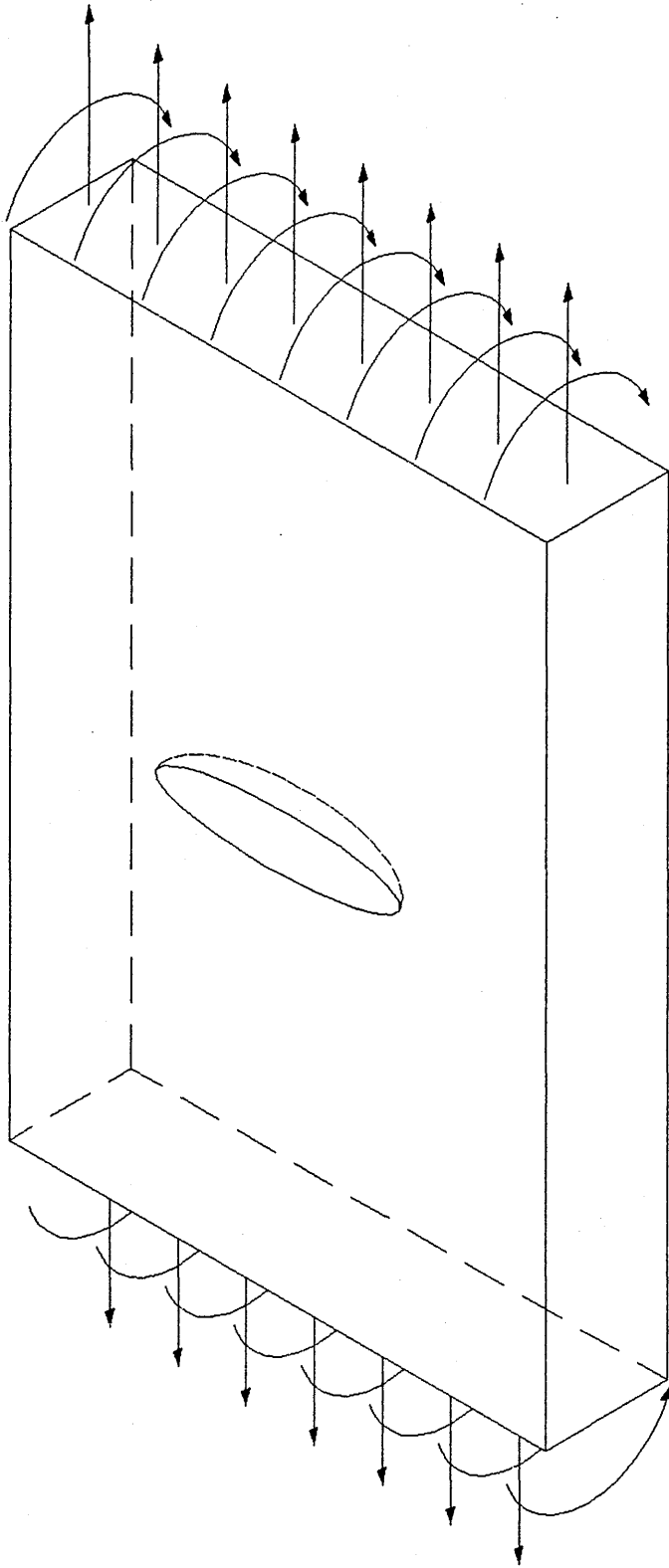
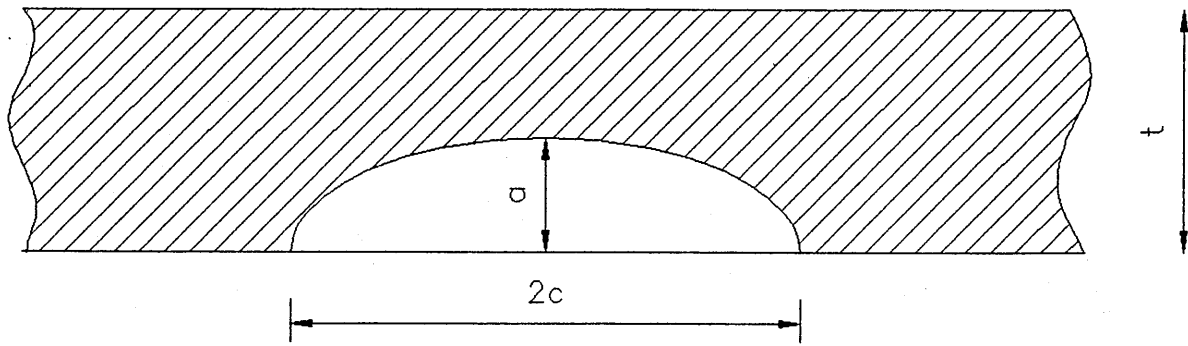
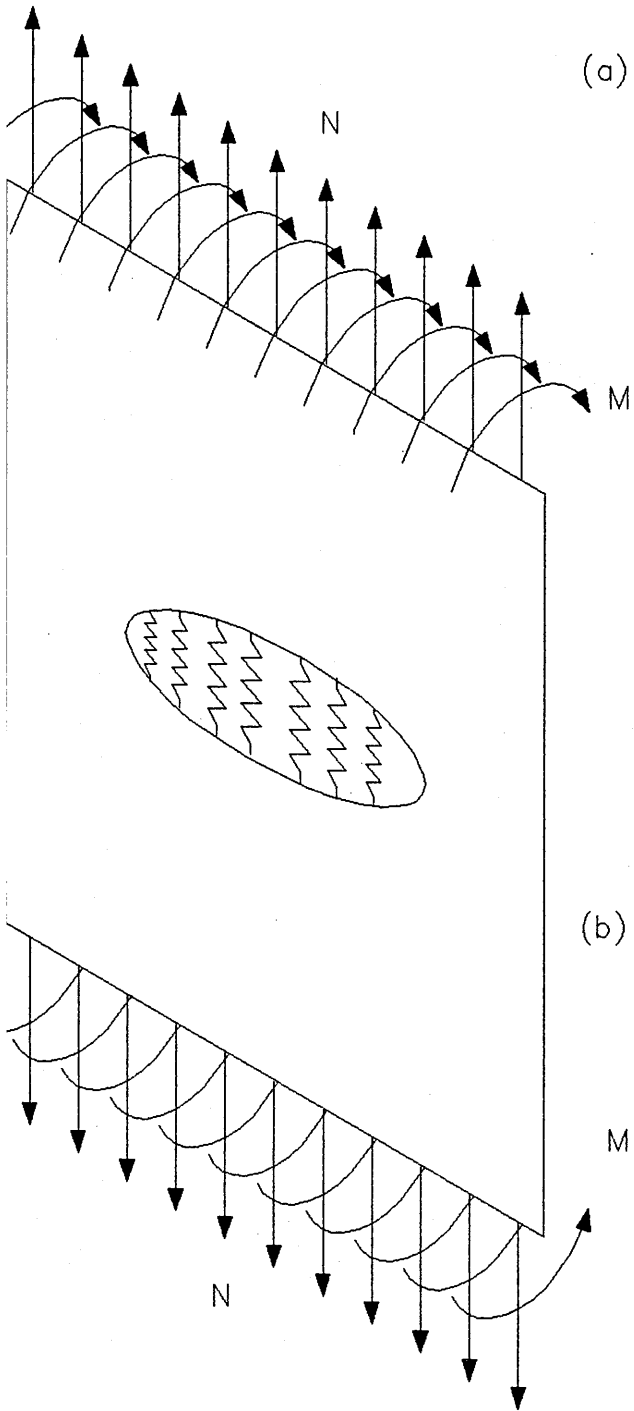


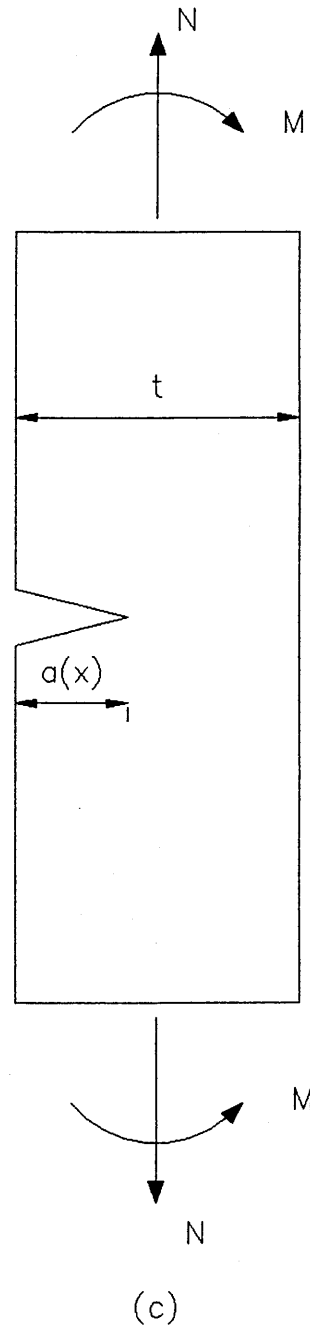
Figure 4.2



(a)

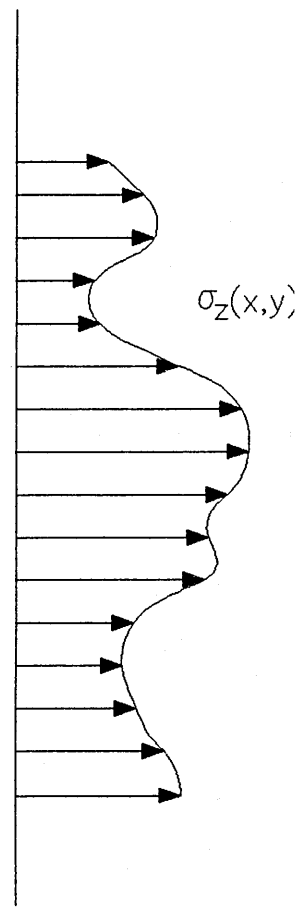
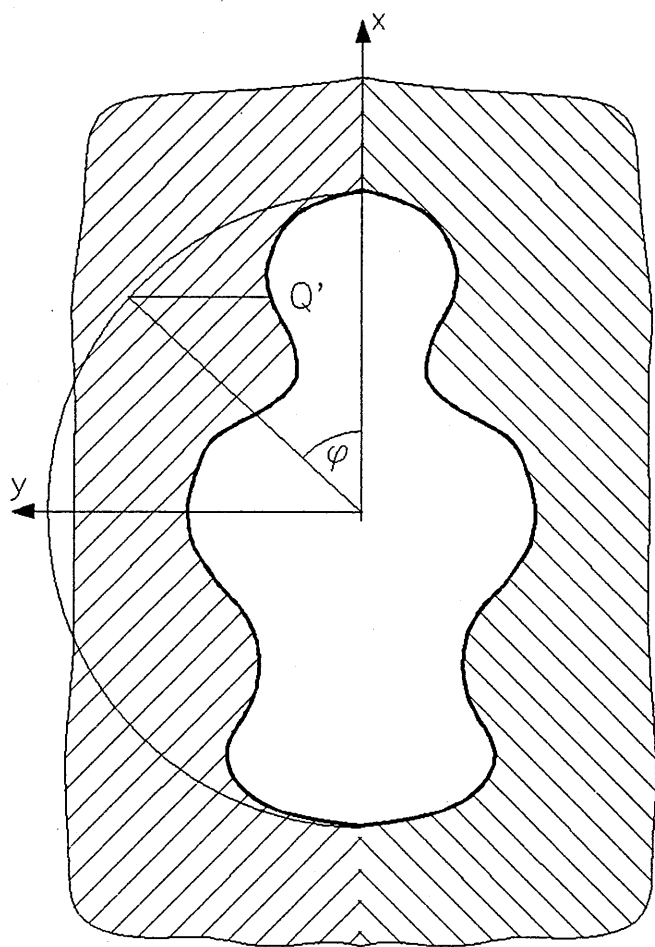
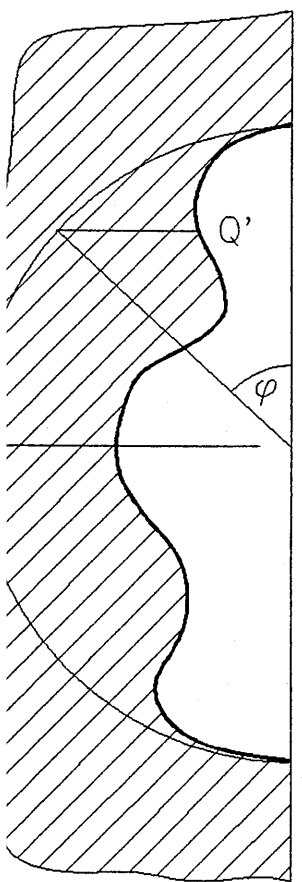
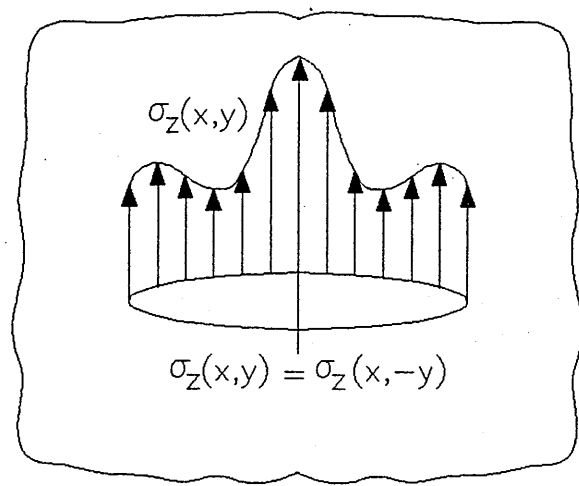
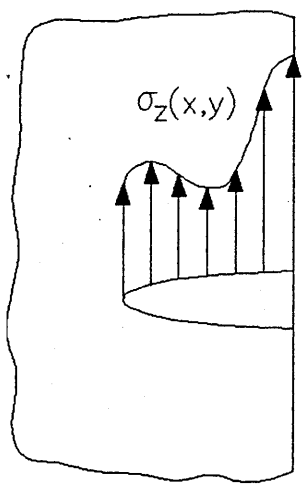


(b)



(c)

Figure 4.3

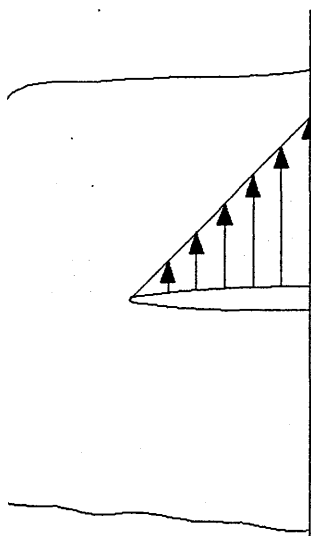


(a)  
Surface Crack

(b)  
Embedded Crack

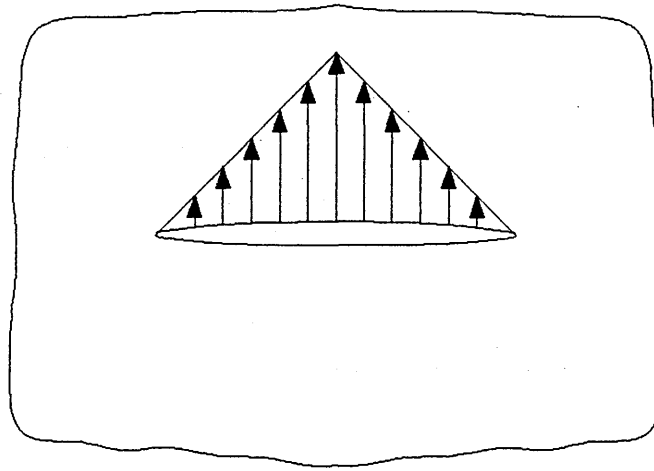
(c)  
Arbitrary Stress Field

Figure 4.4

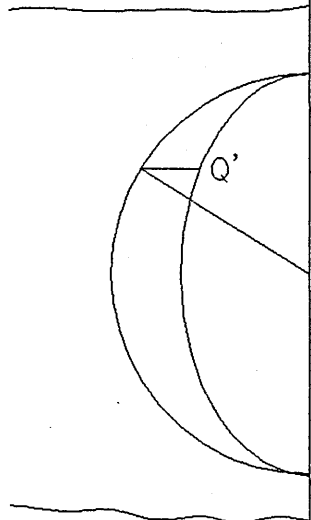


(a)

Linear Stress

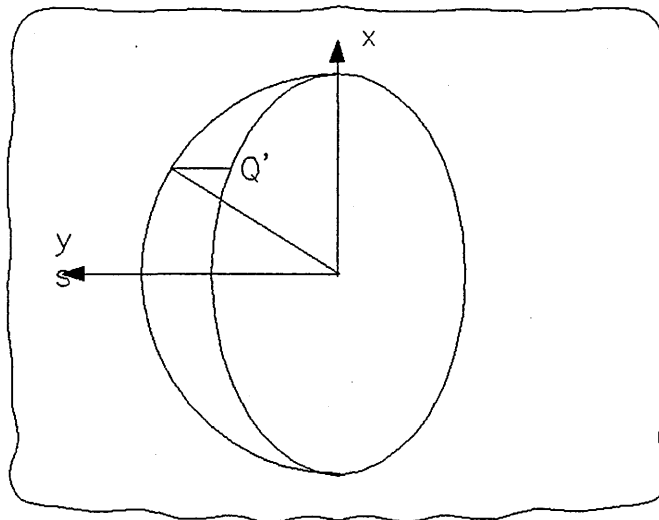


(b)



(c)

Parabolic Stress



(d)

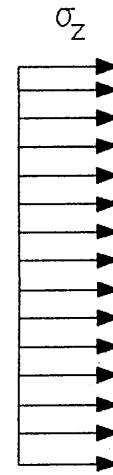


Figure 4.5

## **CHAPTER 5**

### **FATIGUE AND FATIGUE CRACK GROWTH**

#### **5.1 Introduction**

Fatigue loadings on a structure cause cyclic stress variations of either a constant or variable amplitude. Typical examples of sources of fatigue loadings on structures are vibrations from rotating machinery, wave loadings on offshore installations and thermal transient behaviour in power and petrochemical plant. These can result in sudden catastrophic failure after the structure has performed reliably over a prolonged period. Understanding the fatigue failure process is therefore essential if the integrity of critical plant is to be assured.

Fatigue failure is generally considered to be a three stage process. Initiation of small crack like defects is followed by a propagation stage where stable crack growth behaviour is observed prior to fracture. The fatigue life of a structure or component can be assessed using two types of analysis. In the S-N or Wohler approach, empirical curves are used to relate the magnitude of the alternating stress levels to the expected fatigue life. Corrections exist to account for the varying severity of the geometry and to enable variable amplitude conditions to be considered. The method is relatively simple to apply, is generally favoured by designers and has been adopted by several design codes such as BS5500. Alternatively a fracture mechanics based approach can be utilised to quantify the propagation and final fracture stages of the failure process. This requires considerably more expertise than the empirical approach but has a much better physical basis. Difficulty arises at the design stage since no known crack exists to analyse. Knowledge of the fabrication process and the resolution of the inspection techniques used during pre-service examination can allow 'maximum' initial defect sizes to be specified and analysed.

Since this work utilises a fracture mechanics approach this review of fatigue will consider only fracture mechanics based models. A brief description of fatigue mechanisms is also included. For a more comprehensive review of the topics the reader is referred to the pertinent literature [eg. 93,177]. The first section of this chapter considers fatigue in a general sense as applied to 2-D problems. Mechanisms, models and the factors which may effect fatigue life are considered. Following this general discussion the fatigue of semi- elliptical surface cracks is discussed in some detail.

## **5.2 Fatigue Mechanisms in Metals**

Under the action of cyclic stresses local plastic deformation may occur at a microstructural level, even if the nominal stress is well below yield [178,179]. Several models have been proposed to explain the fatigue crack initiation process based on this local plastic deformation [178,180, 181]. The model of Wood [178] is widely used to demonstrate the initiation process and is shown schematically in Figure 5.1. During the increasing portion of the load cycle slip occurs on a favourably oriented crystallographic plane. As the load starts to fall the slip plane changes to a parallel plane and slip occurs in the reverse direction. The model suggests that the preferential plane changes due to the effects of hardening and oxidation of the newly created surface. This cyclic slip mechanism can give rise to intrusions and extrusions at the free surface. Continued slip due to the cyclic loading may cause an intrusion to develop into a small crack.

Once initiated a fatigue crack may continue to grow by a reversed slip mechanism [182,183]. Figure 5.2 shows a schematic representation of slip at an initially sharp crack tip. Due to the large stress concentration caused by the crack tip, slip occurs along planes of maximum shear stress leading to an increase in length. Work hardening and increasing stress levels will limit the amount of slip in any given plane and activate alternative planes above and below the crack along perpendicular shear directions resulting in the blunt,

extended crack tip shown. This slip process represents localised plastic deformation at the crack tip during the opening part of the cycle. As the crack is unloaded the surrounding elastic body will compress the local plastic zone resulting in further, compressive, plastic deformation at the crack tip. This compressive deformation will tend to resharpen the crack tip and leave a ripple on the fatigue crack surface at the location of the previous crack tip. Evidence of such ripples can be observed on a fatigue fracture surface under an electron microscope, and are usually referred to as fatigue striations.

This mechanism is widely accepted as the mechanism of ductile fatigue crack growth. Fatigue cracks may also propagate under other mechanisms such as microcleavage, where striations may still result but through local brittle fractures, and microvoid coalescence. It has also been argued, [184,185], that there is no crack initiation period since pre-existing defects will be present in the slip bands. These small cracks begin propagation immediately the fatigue loading is applied and are arrested by obstructions such as grain boundaries if the fatigue loading is very small, thus explaining the fatigue limit observed in many metals. Although some experimental evidence may be used to support this it has yet to be confirmed.

### **5.3 Crack Growth Models**

For large fabricated engineering structures defects will pre-exist, probably in weldments, and the fatigue life of the structure will be largely determined by the fatigue crack growth (FCG) process. In general FCG is dominated by mode I loadings and this review will limit itself to this type of crack propagation, the effects of mixed mode loadings are discussed in some depth in [186].

In the case of high cycle fatigue, where a large number of cycles are required to cause failure of the structure, the applied stress range is relatively low and consequently the plastic zone at the crack tip is small in comparison to all other dimensions. It is therefore reasonable to assume that the stress intensity factor will give an accurate representation of the crack tip stress environment and

hence may be a suitable parameter for fatigue crack growth models. It follows that the fatigue crack growth rate per cycle,  $da/dN$ , is related to the stress intensity factor range  $K$  :

$$da/dN = f\{\Delta K\} = f\{(S_{max} - S_{min})\sqrt{(\pi a)}\} = f\{2S_a\sqrt{(\pi a)}\} \quad (71)$$

Where  $S_{max}$  and  $S_{min}$  are the maximum and minimum stress in the cycle respectively and  $S_a$  (it is conventional to represent stress as  $S$  in fatigue) is the cyclic stress amplitude, Figure 5.3. Paris [187] and Paris et al [188] were the first to point this propose this type of relationship. In constant amplitude fatigue where  $S_{min} > 0$  :

$$\Delta K = K_{max} - K_{min} \quad (72)$$

If the crack growth rate,  $da/dN$ , is plotted against  $\Delta K$  on a log-log axis, the curve generally exhibit three regions, Figure 5.4. In region I, when  $\Delta K$  is low, the crack growth rate is very low and decreases abruptly indicating a threshold below which no crack growth will occur,  $\Delta K_{th}$ . In the central region of the curve an approximately linear region is observed which can be represented by :

$$\log(da/dN) = n \log(\Delta K) + C \quad (73)$$

and hence :

$$\frac{da}{dN} = C \Delta K^n \quad (74)$$

This is the well known equation for fatigue crack growth originally proposed by Paris and Erdogan [187]. As the maximum stress intensity factor approaches the critical value  $K_c$  then the crack growth rate will accelerate rapidly as final fracture approaches and this behaviour is responsible for region III of Figure

5.4. The Paris law (74) can only describe the central region, region II, type of behaviour. To represent the whole range of crack growth rates an inverse hyperbolic tangent model has been proposed [190]:

$$\log(da/dN) = C_1 + C_2 \text{Tanh}^{-1}[f(\Delta K_{\text{eff}})] \quad (75)$$

Where  $C_1$  and  $C_2$  are material constants and  $f(K_{\text{eff}})$  is a function of the effective stress intensity factor range which can be determined by considering the crack closure stress.

If  $\log(da/dN)$  versus  $\log(\Delta K)$  is plotted for a range of materials it is found that the relationship in region II is generally linear but that different material data will lie on lines of different slopes. This may tend to imply that 'n' in equation (74) is a material property. From the ductile fatigue crack growth mechanism discussed above it would appear that the amount of growth per cycle is closely related to the crack opening. Some attempts have been made to correlate the crack growth rate with the crack opening on this basis resulting in the following types of models [191,192] :

$$\frac{da}{dN} = \frac{C(\Delta K)^2}{E\sigma_{ys}} \quad \text{or} \quad \frac{da}{dN} = C\left(\frac{\Delta K}{E}\right)^2 \quad (76)$$

Where  $E$  is Young's modulus and  $\sigma_{ys}$  is the cyclic yield stress for the material. It has been shown [193] that data for a large variety of materials fall within a reasonable scatter band when plotted on the basis of  $\Delta K/E$  v's  $da/dN$  as suggested by the second expression in (76). Conversely materials with almost identical elastic moduli have been found to exhibit substantially different crack growth rates. It would therefore appear that crack propagation is influenced by more parameters than these simple models can account for.

In general a fatigue cycle can be defined in terms of its frequency and two stress

parameters. These can be the mean stress and the stress amplitude, the maximum and minimum stress in the cycle or any other combination of this type. A further useful parameter in fatigue is the R-ratio where  $R=S_{\min}/S_{\max}$ . When R is approximately zero then it would appear to be reasonable to discuss crack propagation in terms of the range of stress intensity factor,  $\Delta K$ , since  $S_{\min}$  would be approximately zero as would  $K_{\min}$ . When R is not equal to zero there is a dilemma as to whether the crack propagation should be determined by the range of stress intensity factor in the cycle,  $\Delta K$ , or the maximum stress intensity factor in the cycle  $K_{\max}$  or both. As may be expected it has been shown that the crack propagation rate is a function of both  $\Delta K$  and  $K_{\max}$  [194,195] so that ;

$$\frac{da}{dN} = f_1(K,R) = f_2(K_{\max},R) = f_3(\Delta K, K_{\max}) \quad (77)$$

Several investigators have fitted empirical relationships which attempt to incorporate the effects of R ratio. Broek and Schijve [194] proposed the following simple equation:

$$\frac{da}{dN} = CK_{\max}^2 \Delta K \quad (78)$$

A similar equation was proposed by Erdogan [195] and Walker re-cast these in a more general form [196,197]:

$$\frac{da}{dN} = CK_{\max}^m \Delta K^n \quad (79)$$

which was then modified by introducing the concept of the effective stress intensity factor range  $\Delta K^*$  yielding:

$$\frac{da}{dN} = C\Delta K^n \quad \text{where} \quad \Delta K = S_{\max}(1-R)^m \sqrt{\pi a} \quad (80)$$

Alternatively Foreman et al [198] proposed a model which attempted to include the R-ratio effect and the effects observed in stage III of the  $da/dN$  v's  $\Delta K$  curve. Foreman argued that as  $K_{max}$  approaches  $K_{Ic}$  then the crack growth rate  $da/dN$  must approach infinity. The expression proposed was:

$$\frac{da}{dN} = \frac{C\Delta K^n}{(1-R)K_{Ic} - \Delta K} = \frac{C\Delta K^n}{(1-R)(K_{Ic} - K_{max})} \quad (81)$$

which can be re-arranged as:

$$\frac{da}{dN} = \frac{C\Delta K^n K_{max}}{K_{Ic} - K_{max}} \quad (82)$$

All of these expressions are of a similar nature and none of them are universally applicable. The user must therefore select an appropriate model for his application. For the purposes of engineering calculations the Paris- Erdogan model is often chosen for simplicity.

#### **5.4 Factors Affecting Fatigue Crack Propagation**

Many factors are known to affect fatigue crack growth rates. Among these the most prominent are the environment, mean stress, history effects (for variable amplitude fatigue), temperature, thickness, material variability and of course the particular material. Only the effects of history, environment and mean stress will be discussed here as the most significant factors affecting operating plant.

##### **5.4.1 Effect of the Environment**

Of the factors which affect the crack propagation rate, the influence of environment may be one of the most difficult to account for in predictive calculations. Fatigue tests are seldom conducted in a similar environment and

frequency to that which the component will see during service, partly due to the problem of identifying the operating environment and reproducing it in the laboratory. For example sub-sea conditions representative of those which offshore platform jackets may be exposed to, or wet steam conditions that power station boiler components will endure over a twenty year period. It would be reasonable to assume that in corrosive conditions, such as sea water, the metal surface will be degraded due to corrosion pitting and that these pits would act as stress raisers thus reducing the initiation life and hence the life of the structure. This model may be extended to the growing crack tip where newly exposed material is exposed to the corrosive environment. Interaction between the fatigue process and the corrosive action would generally be expected to enhance the crack growth rate.

The influence of environment has been the subject of a great many investigations on a number of materials [eg. 199-205]. Among these investigations it was shown that the crack growth rate in wet air can be an order of magnitude higher than in vacuum [200,203]. Hartman attributed this to the water content of the air rather than oxygen by observing equal growth rates in wet oxygen and wet argon and equal, but much lower, growth rates in dry oxygen and argon. However it was concluded that this may be material dependent. In sea water solutions the crack growth rate for steels has been shown to be up to three times greater than in air [206], although this has been shown to be frequency dependent [207]. This frequency dependence can be attributed to the time dependent nature of the corrosion process.

#### **5.4.2 Mean Stress Effects**

The effect of mean stress on the fatigue crack growth rate is normally small in region II of the  $da/dN$  v's  $\Delta K$  curve but can be significant in both region I and III [208-210]. In general terms the effect of increasing mean stress is to move the sigmoidal  $da/dN$  v's  $\Delta K$  curve to the left thus reducing the threshold stress intensity factor range in region I. In region III the crack growth rate increases

rapidly as  $K_{\max}$  approaches  $K_C$  or  $K_{IC}$  and hence since as the mean stress increases, for the same stress amplitude,  $K_{\max}$  must increase then the transition to region III behaviour will occur at lower  $\Delta K$ 's. These effects can be accounted for using the models of Foreman and Walker discussed above.

### **5.4.3 Sequence Effects**

The effect of variable amplitude cycling on fatigue crack growth is important since few structures will experience constant amplitude cycling during their lifetime. So called sequence effects can have a substantial effect on the fatigue crack growth in a structure. This can be demonstrated by applying periodic overloads during a constant amplitude fatigue test [211,212]. The effect is shown schematically in Figure 5.5. Figure 5.6 illustrates the reason for the retardation effect shown in Figure 5.5. An overload introduces a large plastic zone at the crack tip. As the load is removed the surrounding elastic body compresses this extended plastic zone resulting in compressive residual stresses at the crack tip. These residual stresses will tend to close the crack tip and hence subsequent cycling can only result in crack growth if the tensile stresses applied at the crack tip exceed the compressive residual levels. Hence the crack growth rate is retarded until the crack tip has grown through the overload plastic zone. Similar interaction effects can occur during random loading.

Several authors have presented models to predict fatigue crack growth under variable amplitude conditions [213-216] with varying degrees of success. This work considers only constant amplitude fatigue and as such a complete review of these models is beyond the scope of this thesis. The reader is referred to the relevant references for further information and to standard texts [eg. 93] for a more general coverage of the subject.

## **5.5 Fatigue of Surface Cracks**

In reality fatigue cracks initiate from discrete points along stress concentrations

such as weld toes. These cracks are not straight fronted and have a finite surface length and depth. As a first approximation these so called surface cracks are normally represented as semi-ellipses. Due to the curved crack front and the possibility that the crack front may lie in a non-uniform stress field then it will be probable that the stress intensity factor and hence the stress intensity factor range will vary around the crack front. If a simple Paris type law is assumed to describe the crack growth behaviour then it would be reasonable to assume that the crack may grow at different rates around the periphery and hence change shape as it grows. Several authors have considered this problem and 'code' type approaches offer some guidance on the analysis of surface cracks under the action of fatigue loadings. In this section a brief overview of the available guidelines is given followed by a short review of some relevant literature approaches.

### **5.5.1 Code Type Approaches**

#### **i) British Standard PD 6493.**

PD 6493 [122] provides guidance on the assessment of defects in structures under the action of different load conditions. For planar defects it is recommended that the defect is bounded by a rectangle and idealised by an ellipse inscribed within the rectangle, for embedded defects, or a semi-ellipse inscribed within the rectangle, for surface cracks, with semi-minor axis equal to the depth of the rectangle and major axis equal to the total length of the rectangle as illustrated in Figure 5.7. Under the action of fatigue loading the shape of the defect is again idealised in a simplified manner which can be discussed using the notation of PD6493:

1. If the bending component of stress,  $P_b$ , is less than 20% of the total stress acting on the area of the defect, NB. stresses are evaluated for an uncracked body, then the defect will grow in depth until the aspect ratio,  $a/c$ , reaches unity, ie. the defect becomes semi-circular. This shape will then remain constant as the defect grows until the defect depth equals 90% of the plate thickness at

which point it will become a through thickness crack.

2. If the bending component of stress,  $P_b$ , is greater 20% than of the total stress acting on the defect area then the defect will be re-characterised as an edge crack where the surface length becomes infinite and only growth in the depth will be considered.

## ii) ASME XI Appendix A

In the ASME approach [121], defects are bounded and idealised in a similar manner to that described above for PD 6493, the ASME approach is given in Figure 5.7. Article A-5200 of Appendix A describes the treatment of fatigue crack growth for the assessment of defects and is reproduced here :

1. Determine the maximum range of  $K_I$  fluctuation associated with the transient  $\Delta K_I$ .
2. Find the incremental flaw growth  $a$  corresponding to  $K_I$  from the fatigue crack growth data.
3. Update the flaw size by assuming the flaw grows to a geometrically similar, larger flaw with a minor half diameter  $a+\Delta a$ .
4. Proceed to the next transient.

In the presence of significant bending stresses the ASME approach allows for no change in crack shape in contrast to the rather drastic re-characterisation procedure in PD 6493.

## 5.6 Literature Data

Several authors have considered the behaviour of surface cracks growing by fatigue. Iida and Kawahara [217] presented an empirical model developed within a larger project by the Japan Welding Engineering Society. A large number of fatigue tests were carried out on A533B plate material under a number of different crack configurations. The model has three forms :

i) For a sufficiently small initial flaw :-

$$b/a = A - B.b/t \quad (83)$$

ii) For an initially shallow and long flaw :-

$$b/a(1 - e^{n/a^n})^{1/n} = A - B.b/t \quad (84)$$

iii) For an initially deep and short flaw :-

$$b/a = A/(1 - f^{n/b^n})^{1/n} - B.b/t \quad (85)$$

where

$$A = 0.98 + 0.07R_b \quad (86)$$

$$B = 0.06 + 0.94R_b \quad (87)$$

$$R_b = S_b/(S_m + S_b) \quad (88)$$

$S_b, S_m$  : the bending and membrane stress ranges

$n$  : an empirical constant near 2.0

$e, f$  : transient constants determined from the initial flaw shape

This model is attractive due to its simplicity in application, however its use is limited by the fact that it is empirical and was derived from flat plate data. Application of the model to surface cracks in component geometries and stress states other than those used to fit the model must therefore be considered as extrapolation. Since the model has no sound physical basis there can be little confidence in such extrapolations without experimental backup.

Scott and Thorpe considered the problem of surface crack growth in some detail [132] and observed that experimental data in the literature [218-223] demonstrated that surface cracks will tend to adopt preferred shapes under tension or bending loadings. Figure 5.8a and 5.8b show the preferred aspect ratio behaviour schematically for tension and bending load cases respectively. In general, for surface cracks in flat plates it was observed that under tension loading the preferred aspect ratio was nearly semi-circular but decreased slightly as the depth increased. For the bending case the cracks showed a rapidly decreasing aspect ratio with increasing depth. For both load cases if the initial crack shape was significantly different from the preferred (Scott and Thorpe suggest equilibrium) crack shape then a rapid change in shape occurs to achieve the preferred conditions. Following a review of available stress intensity factor solutions Scott and Thorpe proposed that adequate predictions of surface crack shape development could be obtained by evaluating the stress intensity factor range at the deepest point of the defect and at the surface of the plate and growing the crack according to the Paris law at each of these points. A similar procedure was adopted in this work and is described in more detail in a later section. Kang-Sian et al [224] found that contrary to Scott and Thorpe the Paris law type approach could predict the growth at the surface of the plate well but that the growth into the thickness was not well correlated. No reason for this is offered, however it is possible that the stress intensity factor solution which was adopted was inadequate. The discussion of SIF solutions for surface cracks by Newman [131] showed that there can be significant differences between solutions, the review conducted within Scott and Thorpe's work was designed to minimise the problem by determining the most appropriate solution. It is therefore possible that use of a better SIF solution provided adequate

results. Morgan [225] noted that there may be an anomaly in the results of Scott and Thorpe which results in adequate description of the fatigue crack shape development whilst giving inaccurate values of the SIF. To investigate this, surface fatigue crack growth data were used to determine stress intensity factors using the approach of Scott and Thorpe and the resulting data compared with the mean air line for compact tension specimen geometries. The surface crack data showed that the data for both growth into the depth of the plate and at the plate surface were well correlated by a single Paris law line, suggesting that aspect ratio development would indeed be well predicted, but that this line was displaced from the CTS line by approximately a factor of 1.5 on SIF. No explanation was given to resolve this but it was noted that other workers had observed similar phenomena. An extension of the method is proposed to determine the shape development at stress concentrations such as welded joints. Some success was demonstrated by applying the SCF to the stress range used to calculate the SIF range at the surface intersection of the crack.

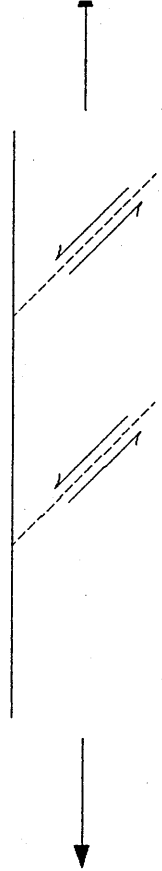
Muller et al [226] considered the effects of crack closure on the development of fatigue crack shape and compared this with predictions based on local SIF solutions as used above and the possibility that averaged SIF's should be utilised to predict the crack shape development. The closure model chosen was proposed by Jolles and Tortoriello [228] and suggests that effective  $\Delta K$ 's at points A and B, Figure 5.9 can be described by :

$$\Delta K_{A,eff} = U_A \cdot \Delta K_A; \quad \Delta K_{B,eff} = U_B \cdot \Delta K_B \quad (89)$$

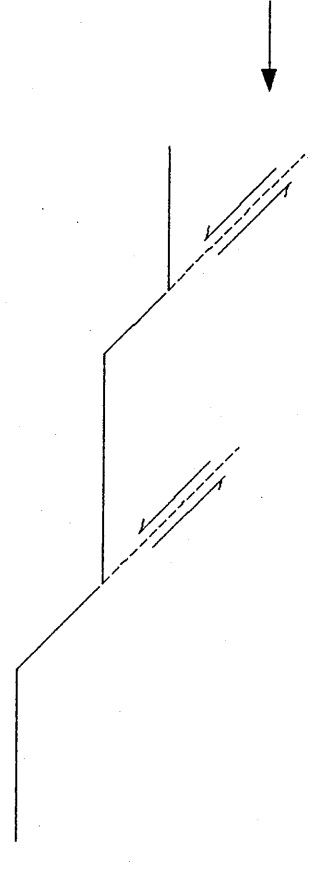
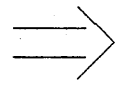
Measurements of  $U_A$  and  $U_B$  have been made by Fleck et al [229] and are given as  $U_A = 0.85$  and  $U_B = 0.75$ . The ratio of these factors  $U_B/U_A = 0.88$  is very similar to an empirical factor introduced by Newman and Raju [150] in their analysis of surface crack growth. A general application of this factor would however imply that the ratio of  $U_B/U_A$  is independent of crack shape, loading condition, crack size etc. Some improvement in the predicted crack shape development was noted in some of the results using closure and averaged

stress intensity factor ranges, however the work was inconclusive although it indicated that further study of closure effects may yield improvements. This type of study has also been extended to prediction of fatigue crack growth in more complex geometries such as weldments and tubular welded joints [230-232]. More recently statistical methods have been utilised to predict the aspect variability and crack shape development for surface cracks [233-235]. These approaches consider fatigue as a stochastic process and attempt to consider the effect of material variability and the inaccuracies in some of the solutions adopted.

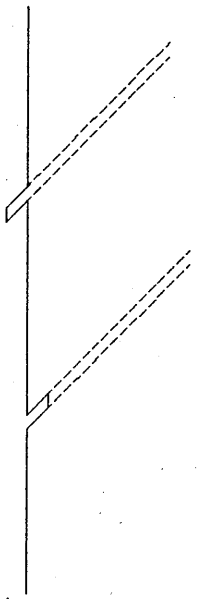
In summary, fatigue crack growth is a complex process. No definitive answer has yet been proposed to the problem of fatigue crack growth, particularly for complex crack shapes, such as surface cracks, in real component geometries under the action of complex stress fields. Several procedures have been proposed and included in codes and recommended practises to allow analysis for design and assessment purposes. The intention of these procedures has been to assure integrity at all times and to enable the analysis to be conducted by designers who have limited or no fracture mechanics expertise. To this end relatively simple models, such as the Paris equation, have been adopted in conjunction with conservative safety factors.



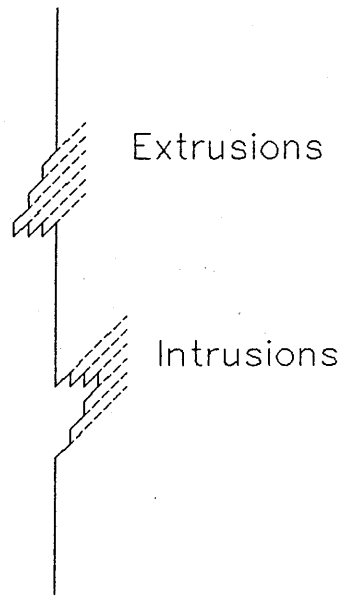
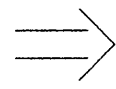
(i)



(ii)



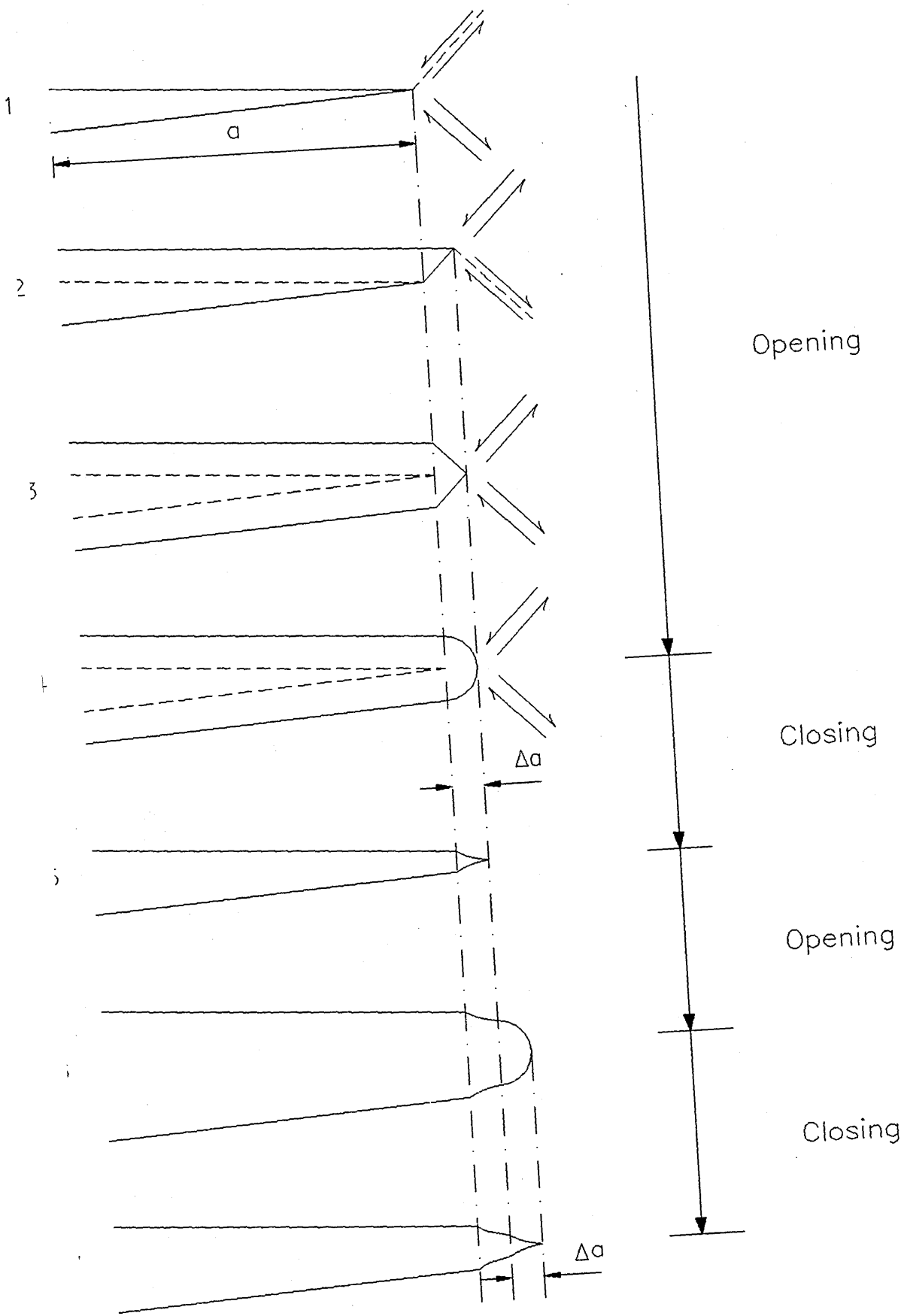
(iii)



(iv)

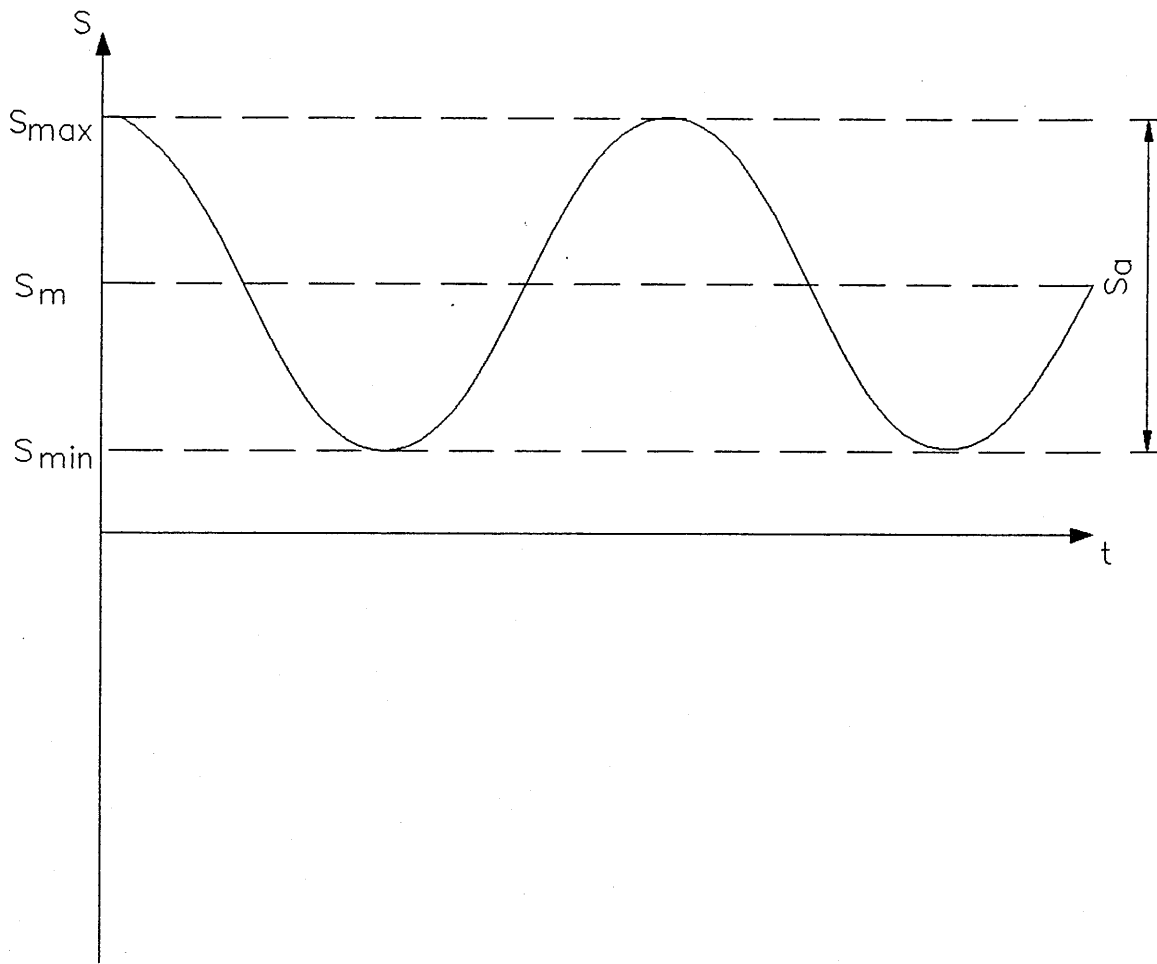
Wood's Model  
For Fatigue Crack Initiation

Figure 5.1



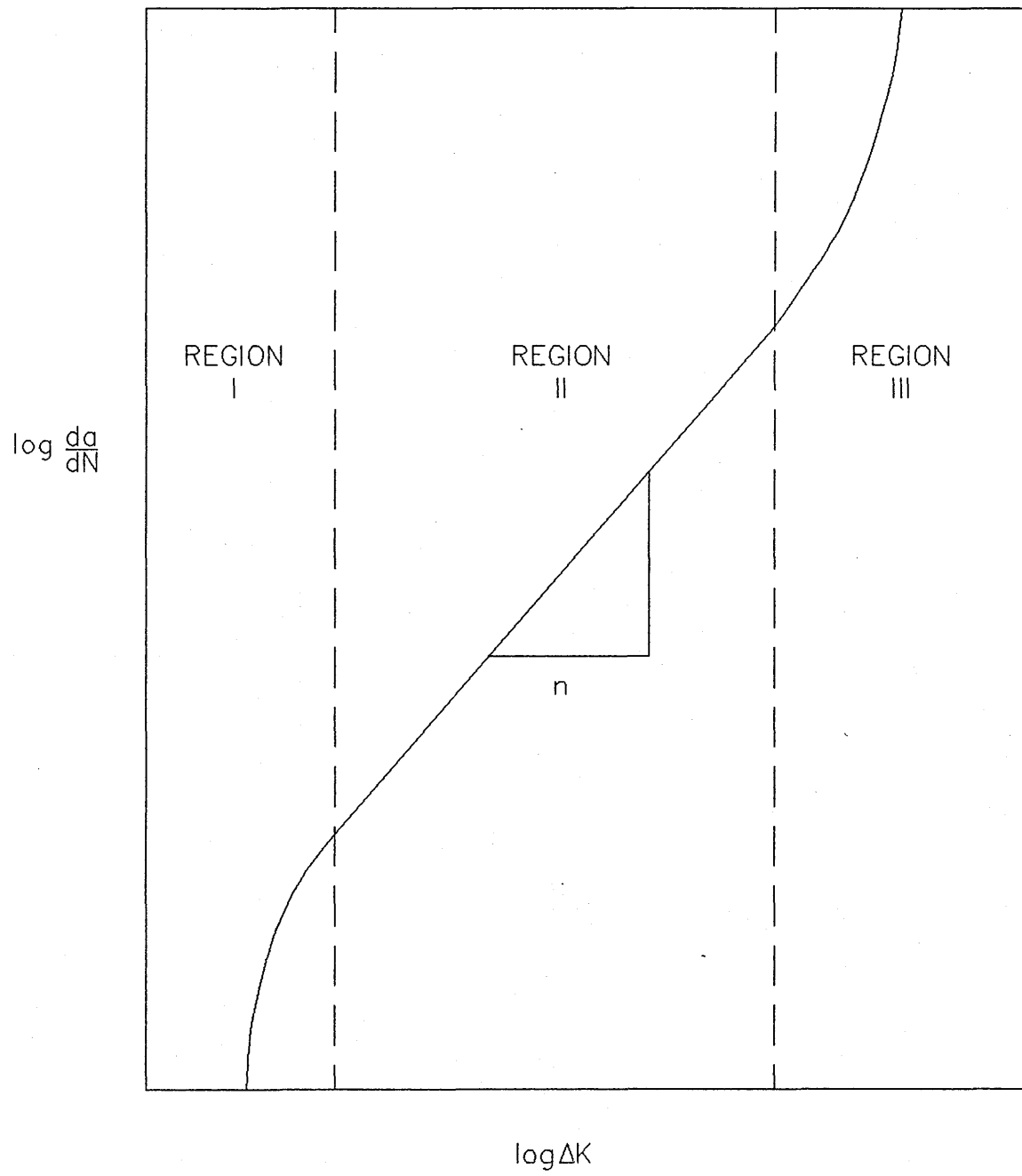
Possible Fatigue Crack Growth Mechanism

Figure 5.2



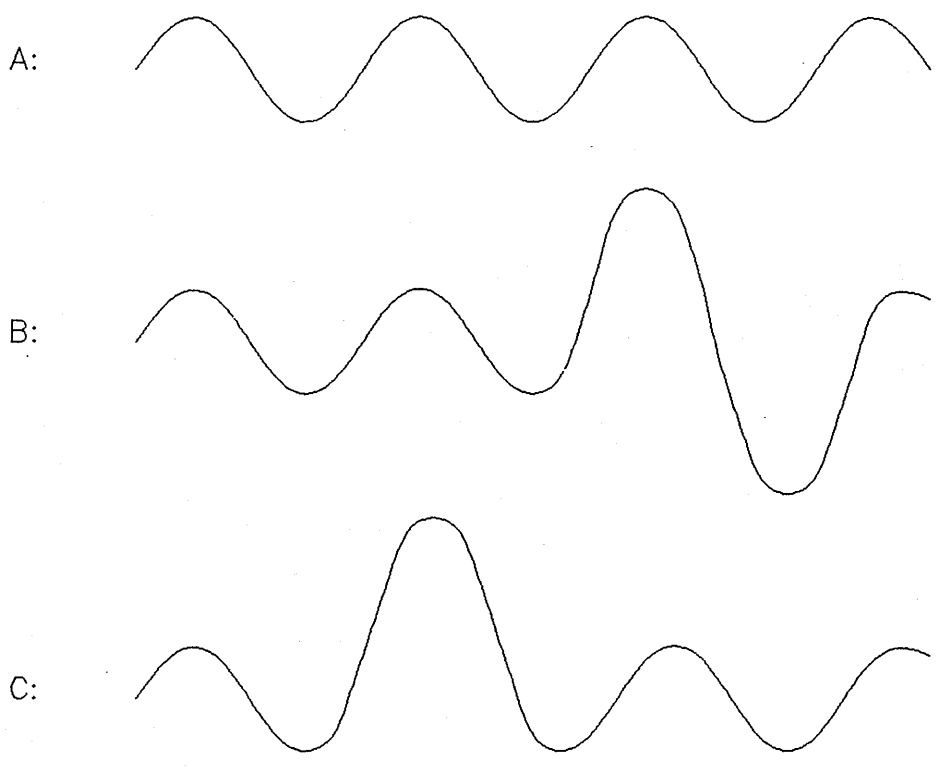
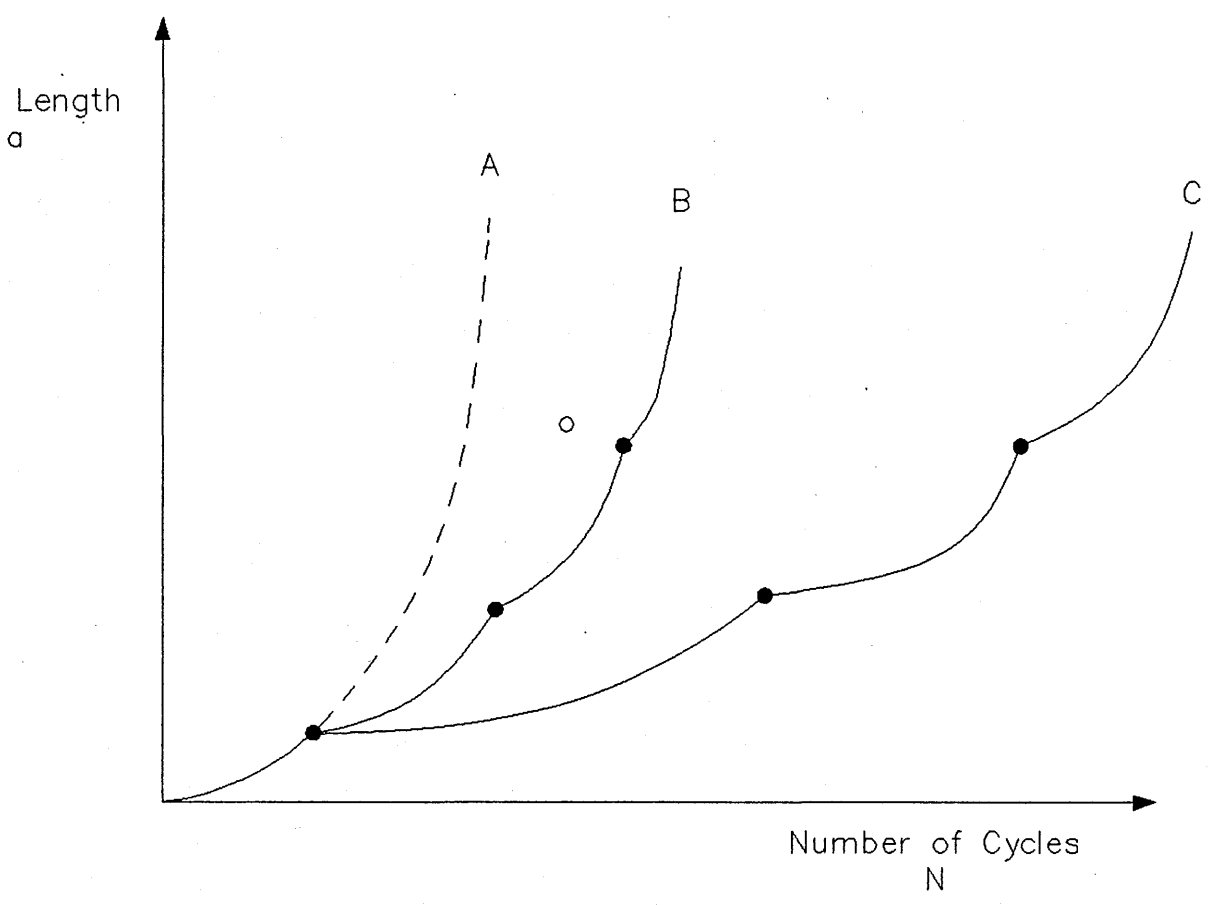
Standard Fatigue Cycle Notation

Figure 5.3



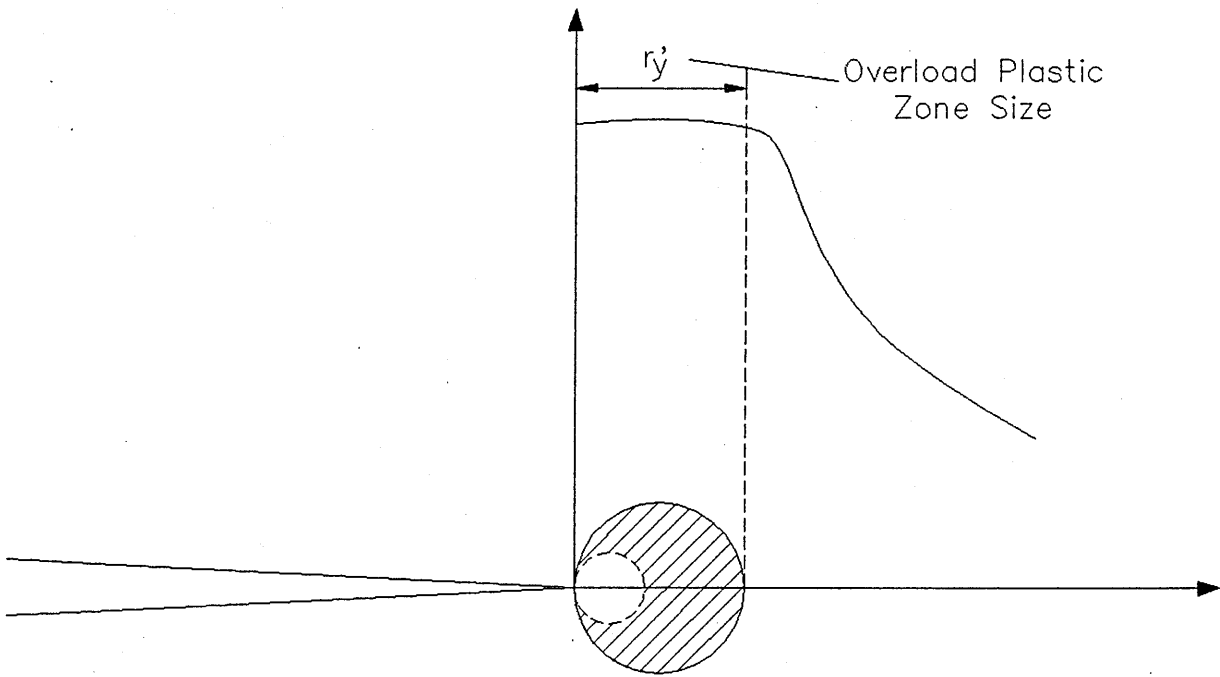
Fatigue Crack Growth Regions

Figure 5.4

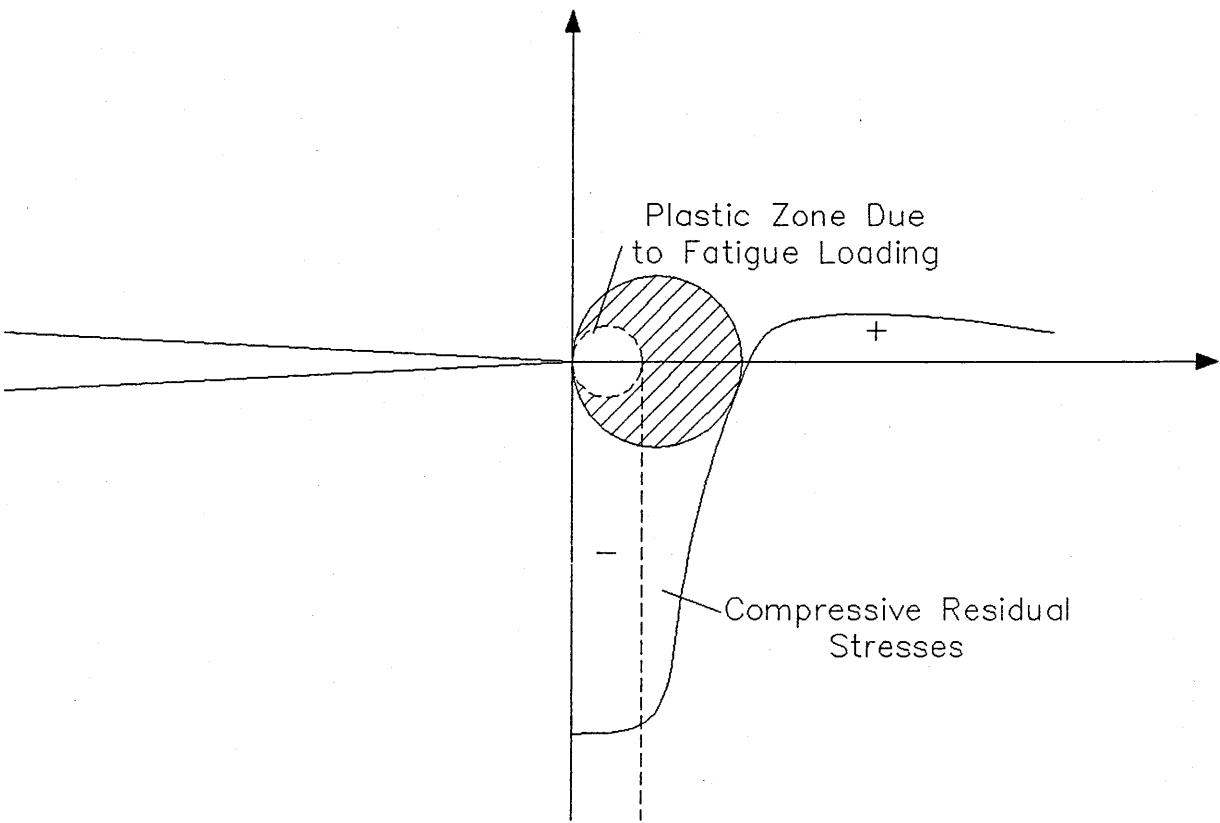


Effect of Overloads

Figure 5.5

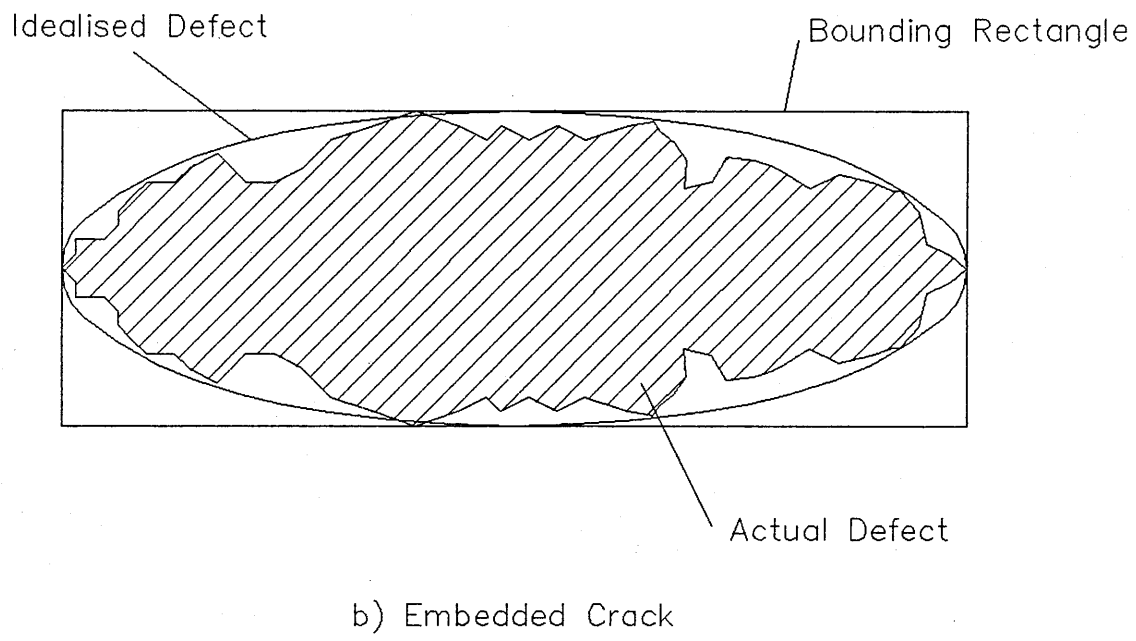
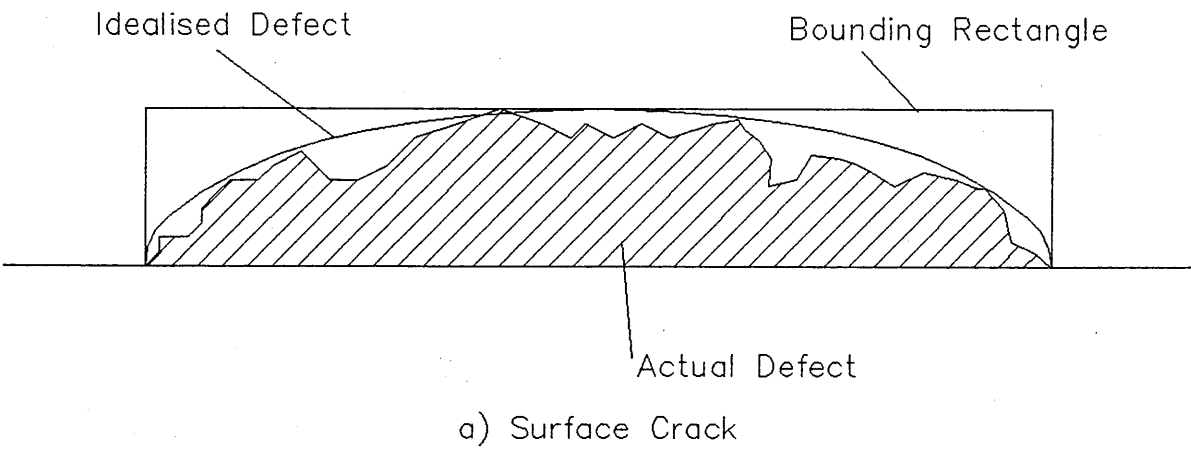


a) At Overload



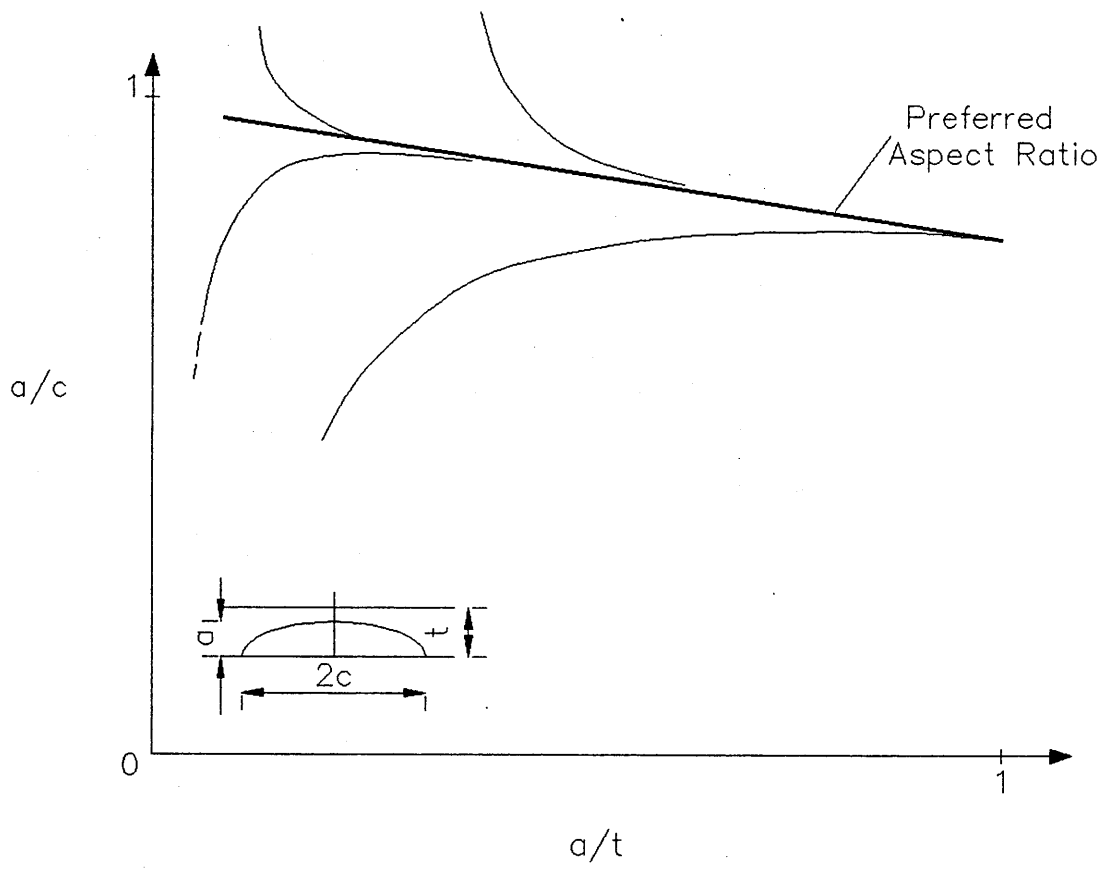
b) Following Overload

Figure 5.6

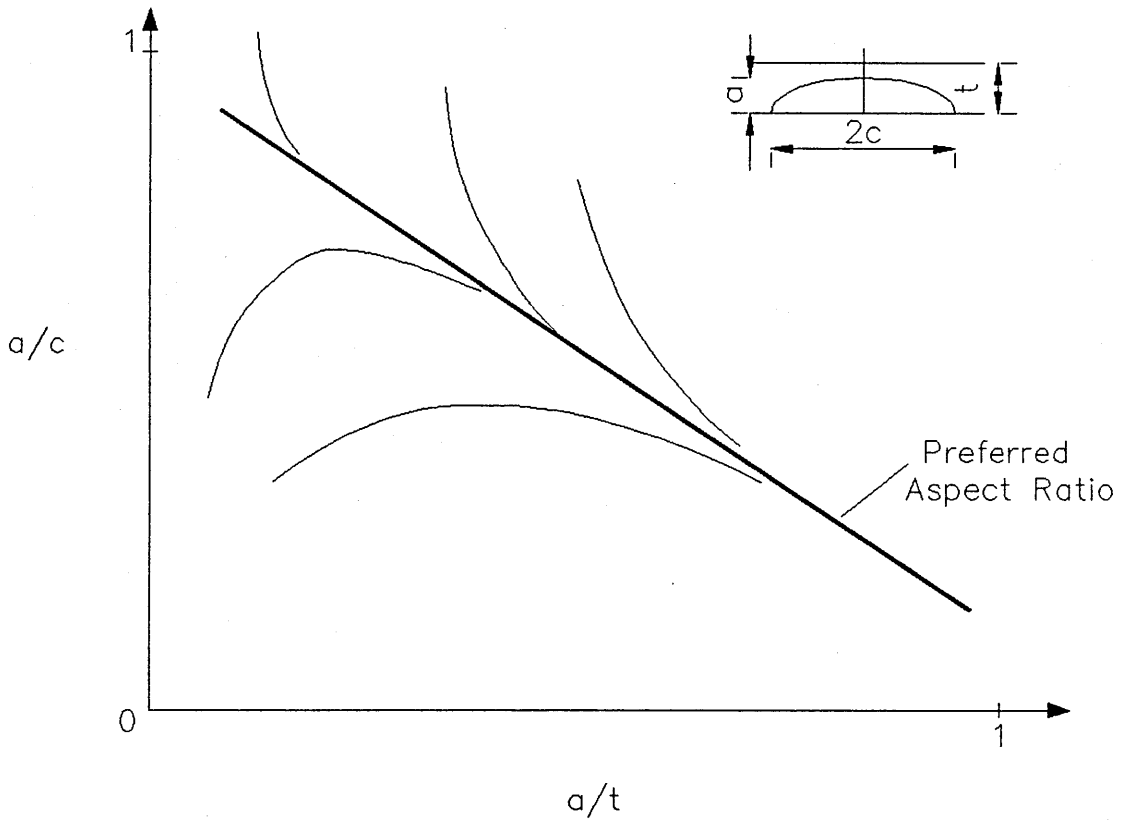


Defect Re-Characterisation

Figure 5.7



a) Tension



b) Bending

Figure 5.8

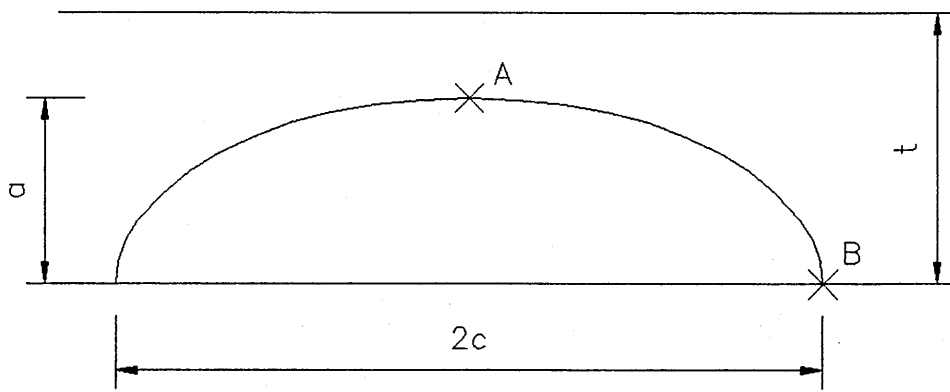


Figure 5.9

## CHAPTER 6

### MULTIPLE DEFECT BEHAVIOUR

#### 6.1 Introduction

In practice cracks will initiate in structures at regions of stress concentration or from defects pre-existing in the structure due to the fabrication process. In large welded structures there will therefore be multiple sites where fatigue crack initiation is possible, or probable, and therefore it is conceivable that several defects will initiate and grow simultaneously. It is important to gain an understanding of how multiple defects in a structure will interact if a reliable prediction of the life of the structure is to be made. This can be particularly critical in the case of part penetrating defects in structures where 'leak-before-break' arguments are utilised to justify continued service. Clearly the geometry of the crack is critical in assessing whether it will snap through the section to form a stable through thickness crack, and hence a leak condition, or become unstable and continue to propagate resulting in a catastrophic failure of the plant. The shape of the defect at the point of snap-through will be heavily influenced by the growth and coalescence of the multiple defects which lead to the dominant crack. Three distinct areas can be considered when examining such behaviour :-

1. The interaction between two adjacent defects and the resultant effect on the crack growth rate and shape development of the individual defects.
2. The coalescence of the individual defects to form a single crack.
3. The subsequent growth of the coalesced crack through the structure to cause failure.

This chapter reviews the available literature on multiple defect behaviour as a pre-cursor to the next chapter which describes a detailed numerical and experimental study of the problem. The review given here starts by considering current recommended practice as described in 'code' type procedures. A brief review of some pertinent results for two dimensional, fully penetrating defects is then given prior to a review of literature on the interaction between co-linear surface cracks and finally the fatigue and coalescence of multiple surface cracks.

## **6.2 Current Recommended Practice**

Three documents are currently widely adopted for fracture mechanics analysis in an industrial environment; British Standards PD6493, ASME XI, and the CEGB R6 Procedure [122, 121, 233]. Each of these documents contains recommendations for the 'recharacterisation' of multiple defects to single defects based on assumed interaction effects. These procedures are detailed here and will be referenced when assessing the significance of the findings of this work.

### **6.2.1 British Standards PD 6493**

PD 6493 criterion for the recharacterisation for co-linear surface cracks is shown schematically in Figure 6.1. In essence two defects are combined into one single bounding crack when the separation becomes less than or equal to the average defect surface length ie. for two similar surface defects coalescence is considered to occur by an instantaneous process when the gap between the two equals the surface length of a single defect. The recharacterised crack has a surface length equal to the sum of the two individual defects surface lengths plus the gap between them and has a depth equal to that of the deepest single defect. This resultant crack is obtained by bounding the existing separate defects by a rectangle and inscribing this rectangle with a semi-ellipse. A considerable amount of 'load carrying' material is removed in this procedure, Figure 6.1, which may result in an over-conservative life assessment if the assumed interaction is excessive.

### **6.2.2 ASME XI**

The ASME recharacterisation procedure is based on the defect depth as opposed to the surface length based procedure of PD 6493 described above. A pair of co-planar surface defects are merged when the gap between the closest points becomes less than or equal to twice the maximum defect depth as shown in Figure 6.2. As in PD 6493 the resulting single crack shape has a depth equal to the maximum depth of the individual defects and a surface length equal to the sum of the two individual defect surface lengths plus the ligament between the two.

### **6.2.3 CEGB R6 Procedure**

The R6 procedure allows three levels for the assessment of interaction effects for co-linear defects given in order of increasing complexity and decreasing pessimism of assessment. These are :-

- i) "Consider all ligaments between defects or between defects and surfaces to be part of the defect region." That is bound all existing defects by one single large crack without considering the range of any interaction effects. This type of approach is obviously conservative and could be adopted as a 'first estimate' type calculation to determine the severity of the problem and therefore to establish whether a more sophisticated analysis will be required.
- ii) "Use the interaction criteria of British Standards Institution, PD 6493 or ASME Boiler and Pressure Vessel Code, Section XI." As described above.
- iii) "Estimate K-solutions with the ligaments present". That is perform an analysis of the problem 'as is'. This will naturally be the most realistic approach but will also be the most expensive and complex and will probably require sophisticated techniques such as the finite element

method.

The R6 procedure offers the most flexible approach and by virtue of option (iii) allows the possibility of adopting new technologies as they become available thereby allowing some scope for the reduction of the conservatism often inherent in fracture mechanics analysis. It may be unsuitable for use by analysts who are not experienced in fracture mechanics methods since it gives no clear guidance on the most appropriate procedure for any specific problem. Both PD 6493 and ASME XI, conversely, offer a very simple approach. There is no indication, however, as to the level of conservatism inherent in the assumptions or how over conservatism could be reduced.

### **6.3 Interaction of Fully Penetrating Cracks**

The interaction between fully penetrating cracks was studied by Westergaard [5], Irwin [8] and Koiter [234]. In these studies an analyses of a periodic array of co-linear cracks in an infinite plate was considered, Figure 6.3. The resulting expression for the stress intensity factors at the 'interacting' crack tips was given as :

$$K_I = \sigma \sqrt{\pi a} \sqrt{\left( \frac{W}{\pi a} \tan \left( \frac{\pi a}{W} \right) \right)} \quad (90)$$

This solution was then utilised as the basis for the derivation of solutions for a central crack in a finite plate by considering the non-zero stress components along lines AB and CD in Figure 6.4. Isida [61] developed mapping functions to derive appropriate stress concentrations for this geometry which were subsequently used to determine stress intensity factors [127]. Feddersen [235] showed that these results could be closely approximated by :

$$K_I = \sigma \sqrt{\pi a} \sqrt{\sec \left( \frac{\pi a}{W} \right)} \quad (91)$$

If these solutions are normalised using the SIF for a central crack in an infinite plate ( $= \sigma\sqrt{\pi a}$ ) and compared, some preliminary indications of the effect of defect interaction become apparent. Figure 6.3 shows a plot of the two solutions from which the following observations were made :-

i) For  $2a/W \leq 0.3$  there is very little increase in SIF due to either defect interaction or finite width, the increase in SIF over the infinite plate solution ( $= 1$  on the plot) is less than 10%.

ii) The effect of finite width and crack-crack interaction are comparable. ie. the two solutions lie close to each other.

iii) As  $2a/W$  increases beyond 0.5, the effect of defect interaction and finite width are substantial. That is the SIF is magnified by more than 20% compared to the infinite plate solution with the magnification tending towards infinity as  $2a/w$  approaches 1.

Observation (iii) indicates that when the gap between two co-linear crack tips is of the order of the total crack size interaction effects become significant. This is consistent with the recharacterisation procedures given in PD 6493 as discussed above.

#### **6.4 Interaction Between co-linear Surface Cracks**

The results for two dimensional crack problems discussed above give rise to some concern when considering the behaviour of surface cracks. If the stress intensity factor at a crack tip can be magnified by more than twenty percent due to the presence of another crack then it would follow from a simple Paris law with an exponent of approximately three, typical for steels, that the fatigue crack growth rate would be enhanced by approximately 80%. Based on Figure 6.3 the two cracks growing towards each other in a co-linear manner would be expected to accelerate rapidly once the gap between them was less than the crack size. An effect of this magnitude would have a considerable implications for life prediction calculations.

The problem becomes more complex for surface cracks. It has been shown that the stress intensity factor can generally be expected to vary around the crack periphery according to the component geometry and loading conditions. It may therefore be expected that defect interaction will influence the stress intensity factor distribution around the crack periphery which will alter the fatigue crack growth rates around the periphery and consequently the crack shape development characteristics will deviate from the preferred shape observed for single cracks. As discussed in the introduction to this chapter any effect on the crack shape development may be particularly critical where leak-before-break arguments may be utilised to justify continued plant operation.

Murakami [236] and Isida [237] considered this problem using the body force method. Their results are reproduced from the Japanese Publications [238,239] in [7]. The results were considered at three points; A, B and C, Figure 6.5, and for aspect ratios ranging from 0.25 to infinity (the 2-D solution). For all the points considered it was shown that the interaction would increase as the aspect ratio increased ie. the solutions tend towards the 2-D results for higher aspect ratios. As would be expected point A shows the most significant effect with SIF's magnified by up to 45% for the 2-D case as the defects approached each other. Some magnification due to interaction was shown at point B reaching a maximum of 11.7% for the 2-D case, point C showed very little effects. It is notable that the results considered only the case where  $a/t$  is approximately zero ie. a half space. Given that the indication would appear to be that the interaction effects increase towards the 2-D solution as the aspect ratio increases, it may be that finite thickness and hence finite area effects will be significant. The work of Murakami was extended to consider the case of the interaction between dissimilar defects [238] ( also presented in [7]). For dissimilar defects it was shown that  $K$  around the periphery was significantly enhanced due to the presence of a larger defect while the larger defect SIF's were relatively unaffected. For more detail of these results the relevant literature should be consulted as the results were not directly relevant to this work.

O'Donoghue et al [239,240] investigated the interaction between axial co-

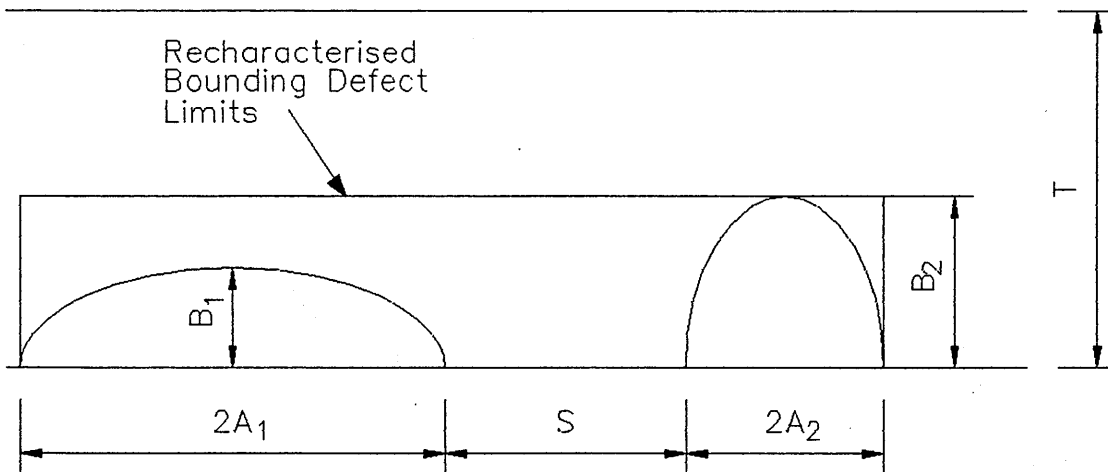
linear surface cracks in cylindrical pressure vessels using the finite element alternating method. The defects considered had an aspect ratio of 0.67 and the defects separation was equal to 0.75 times the surface length. Two depths were considered;  $a/t = 0.5$  and  $0.667$ . It was demonstrated that the SIF was increased by interaction. From the results presented in the paper it would appear that the interaction was larger for the deeper defects as would be expected. It is not possible to draw positive conclusions from these results since only two specific cases were considered. The maximum enhancement to  $K$  was of the order of 15% at point A for the deepest defect case. This would be expected to result in an increase in fatigue crack growth rate of approximately 52%. Miyoshi et al [241] utilised the line spring model to evaluate the SIF distribution around single surface cracks, twin co-linear cracks and some simple 'irregular' shaped cracks represented by triangles and rectangles. The paper only presents results for defects with an aspect ratio of 0.6 and  $a/t$  of 0.8 with varying degrees of separation. Interaction was shown to become significant as the gap between the defect tips decreased. A maximum magnification due to interaction of around 25% was presented graphically for the case of defects separated by an eighth of the total surface length ( $2c$ ) of one crack. The validity of the line spring model for the defects considered is not clear.

## **6.5 Fatigue of Multiple Surface Cracks**

The most comprehensive study of surface crack coalescence by fatigue crack growth was conducted by the AFC sub-committee of the Japanese Welding Society to determine the applicability of the ASME XI fracture mechanics guidelines. A large experimental programme was used to generate a database and a predictive method was proposed. The work was reported in a series of publications by Iida et al [217, 242, 243]. In the predictions no interaction between defects was considered, crack shape development was governed by the empirical model described for single defects in section 5.2. The stress intensity factor at the deepest point was evaluated using a suitable solution and this point was then propagated using a Paris law type equation. The surface length was altered according to

the shape change model. Coalescence was assumed to occur when the crack tips touched. At this moment the defect was recharacterised by a single bounding semi-ellipse. ie. it was assumed that no cycles are required to form the single crack shape following coalescence. The model is empirical and no justification was given for the assumptions, however the results appear impressive. Whether the model could be extrapolated from the tension and bending of flat plates considered in its derivation to complex component geometries is not clear.

Grandt et al [244, 245] considered the coalescence of defects along the bore of a hole. Surface and corner crack geometries were considered, a similar philosophy to that of Iida was adopted in that defects were assumed to coalesce when they touched. The cracks were propagated by evaluating  $K$  at the surface and deepest point and growing them using a Paris law. Interaction was included via 'interaction factors' evaluated in [246] for two symmetrical corner cracks at the bore of a hole in a flat plate. Soboyejo et al [247, 248] considered the fatigue and coalescence of semi-elliptical surface cracks using 3-D finite element methods and experimental investigations. Twaddle and Hancock [249] studied the interaction and coalescence of co-linear surface cracks using a line spring model.

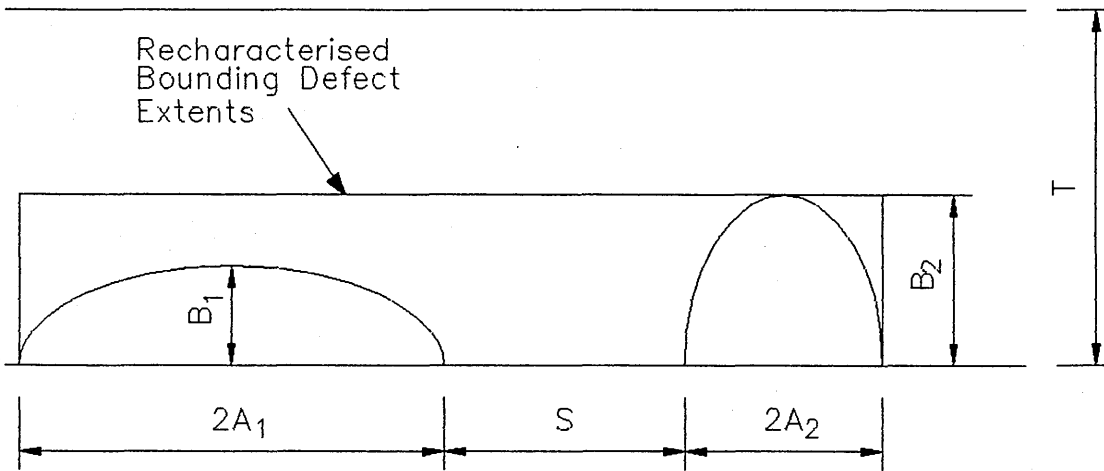


Defects Recharacterised When :

$$S \leq (2A_1 + 2A_2)/2$$

PD6493 Defect Recharacterisation

Figure 6.1

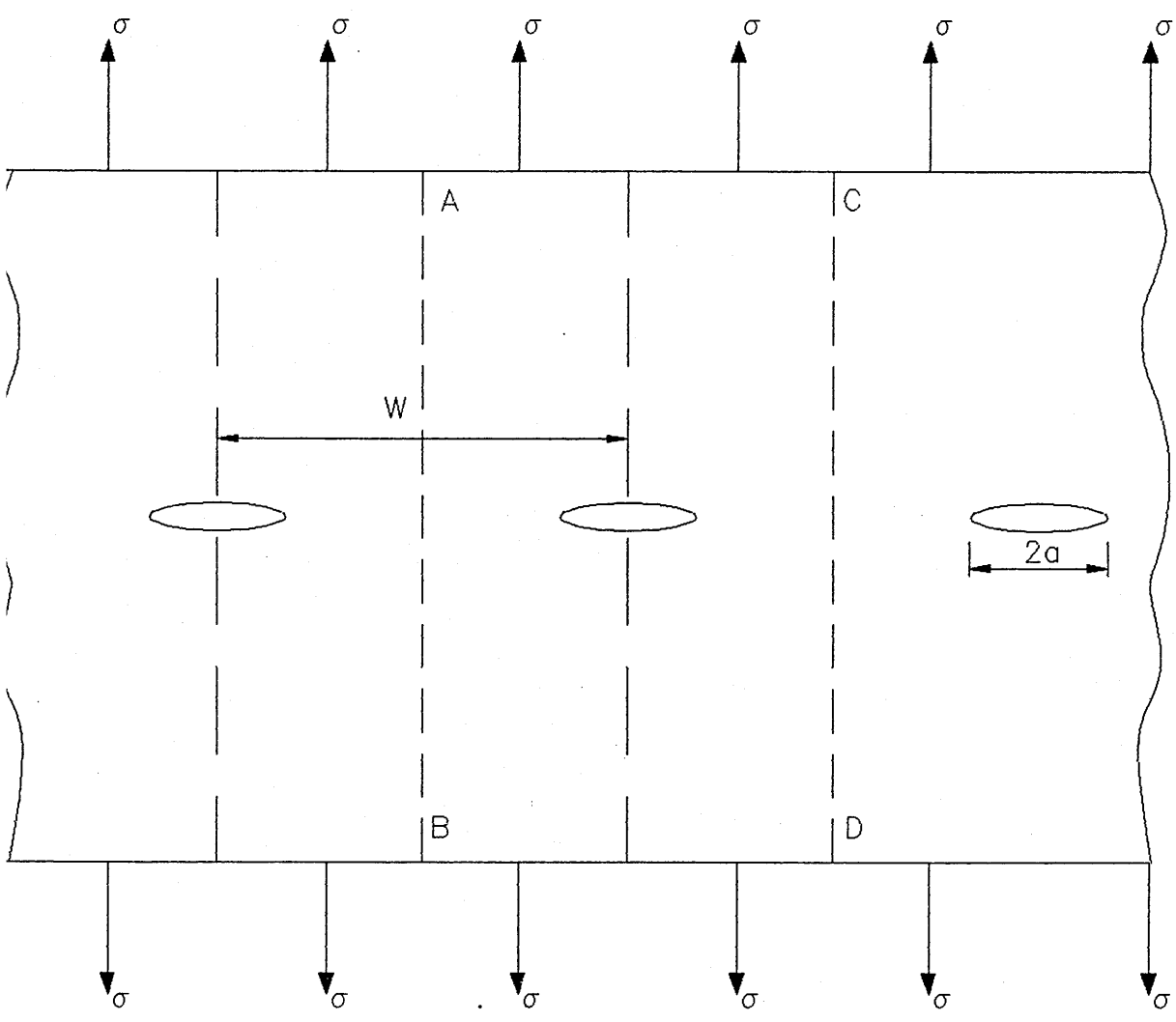


Defects Recharacterised When :

$$S \leq 2B_{\max}$$

ASME XI Defect Recharacterisation

Figure 6.2



Infinite Array of Collinear Cracks

Figure 6.3

# Finite Width Correction for Centre Cracked Plate

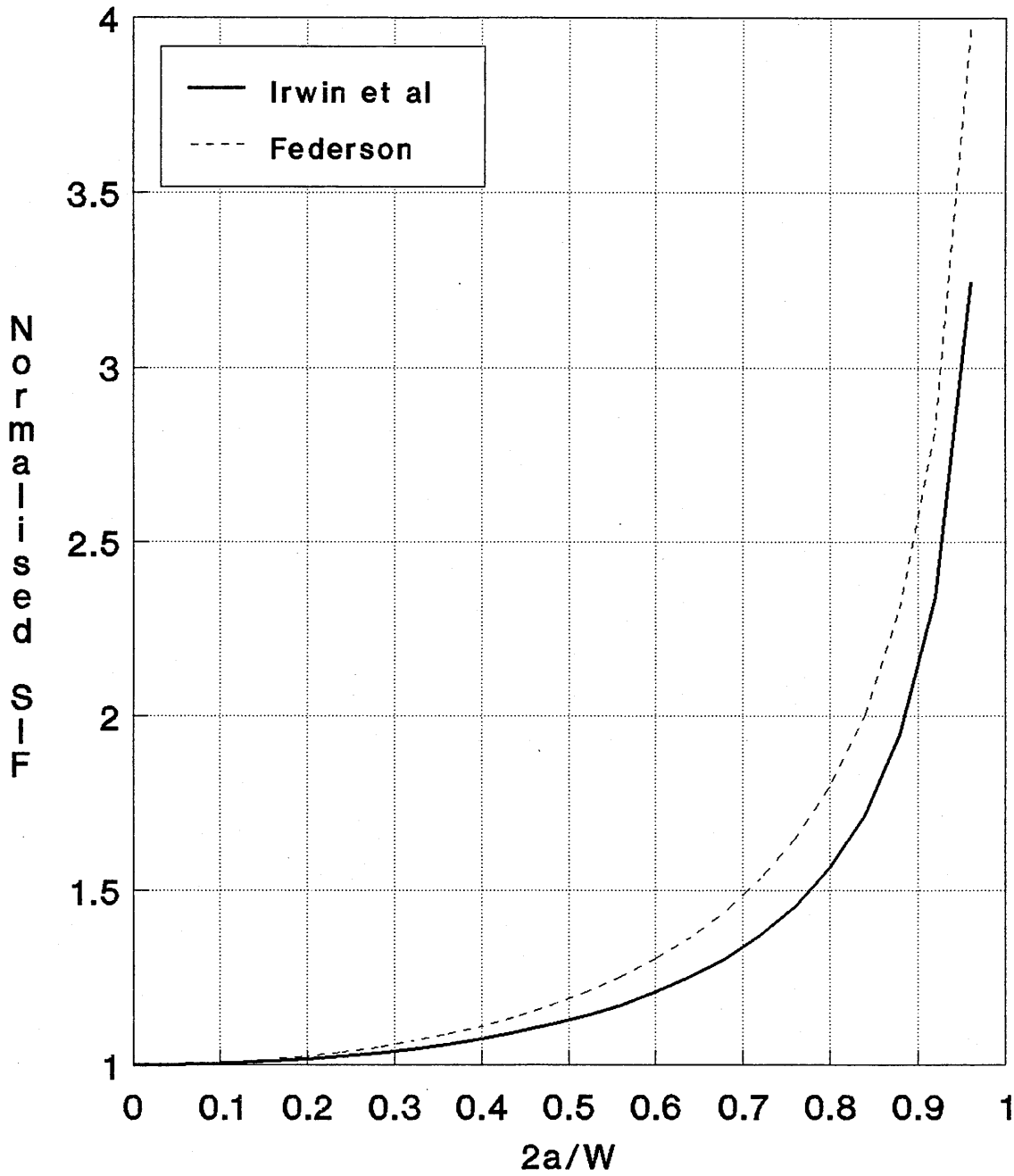
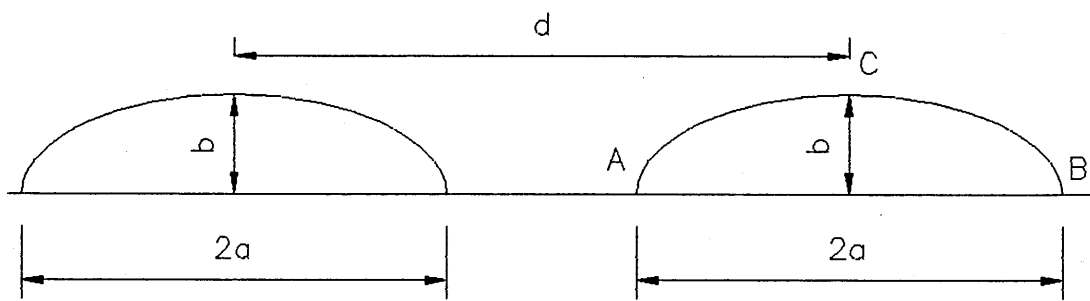


Figure 6.4



Notation Used by Murakami et al

Figure 6.5

## **CHAPTER 7**

### **A NUMERICAL STUDY OF THE INTERACTION BETWEEN CO-LINEAR SEMI-ELLIPTICAL DEFECTS**

#### **7.1 Introduction**

The primary objective of this work as set out in the introduction was to investigate the process whereby surface cracks develop through the coalescence of small surface defects.

As the first step towards understanding the coalescence of co-linear surface cracks a numerical study was undertaken to determine the influence that adjacent defects have on each other. Any interactive effects between adjacent defects would be expected to significantly influence the local fatigue crack growth rate. This would in turn affect the individual defect shape development and hence the development of the final coalesced crack shape. It was shown in section 5.6 that surface fatigue cracks tend to adopt preferential shapes according to the applied loading. Initial crack shapes which significantly deviate from the so called preferred shape were shown to grow rapidly towards it by propagating preferentially at either the plate surface or into the thickness. On this basis the shape of the crack developed by coalescence of small defects could be expected to play a significant part in the determination of the useful life of the component or structure.

This chapter describes a finite element study of the interaction between adjacent co-linear surface defects. The flexibility, simplicity and computational efficiency of the line spring method coupled with the quality of the results available in the open literature, as discussed above, made it the obvious choice for this analysis. The present work utilised the line spring model as implemented in the ABAQUS commercial finite element package [70].

A brief description of the models utilised in this work has been given prior to presentation of the results. The results were then reviewed with regard to their significance in respect of existing design methodologies and defect assessment procedures. Finally pertinent conclusions were drawn.

## **7.2 Geometries Considered**

The notation utilised to describe and discuss the geometries utilised in this work is given in Figure 7.1.

A total of twelve defect geometries were utilised for this analysis. Due to the flexibility of the line spring method this required only one basic finite element mesh, Figure 7.2. The ABAQUS finite element package was chosen for this analysis and the mesh consisted of two hundred and twenty five 'S8R' eight noded generalised shell elements and ten 'LS3S' symmetrical line spring elements. Each defect geometry was created by simply changing the depth information for the line spring elements, Three defect aspect ratios,  $a/c$ , were considered, 0.2, 0.4 and 0.6. Four defect depths,  $a/t$ , were considered for each aspect ratio, 0.2, 0.4, 0.6, and 0.8. The different defect shapes were obtained by modifying the specified depths at each line spring element.

A  $c/L$  ratio of two was utilised for all defect geometries considered in this study ( $c/b=0.667$ ). For the case of multiple defects this represents a defect separation equal to  $c$ , that is half of the total surface length of one defect. Clearly this defect spacing would result in immediate coalescence utilising the methodology outlined in BS PD6493 as described in section 6.2.1 and possibly that of ASME XI, depending on the defect depth, and it must therefore be assumed that current design approaches consider that significant interaction should be expected.

## **7.3 Assumptions and Boundary Conditions**

Due to symmetry only one quarter of the plate was modelled, Figure 7.2. Symmetrical boundary conditions were imposed along the plate edge at

X=0 and along the ligament length of the plate at Y=0. No symmetrical boundary conditions were required along the defect plane as the LS3S line spring element has built in symmetry. In order to consider the case of multiple defects a periodic boundary condition was considered to act along the plate edge at Y=c+L (=2b). This was achieved by specifying constraint equations using the ABAQUS '\*EQUATION' option, which forces the edge to remain plane while allowing it to displace in X. In effect the solver calculates the X displacement for the first node on the edge and imposes this on the remainder. By applying this periodic boundary condition the resultant model effectively considered an infinite array of self similar defects. The separation, defined as the distance between the crack tips, of these defects was equal to twice the ligament length, L, for the single defect model ie. equal to c, half the defect surface length.

The plate material was assumed to be linear elastic for the purpose of this analysis and an elastic modulus of  $2 \times 10^5$  MPa and a Poisson's ratio of 0.3 were specified for all geometries considered.

#### **7.4 Load Cases**

Two options were considered for applying the load to the plate models; either a uniform stress, bending or tensile as appropriate. Alternatively a fixed displacement (tension) or rotation (bending) could be applied. For the case of uniform stress being applied at the free boundary it would be reasonable to expect a non-uniform displacement and, similarly, for a fixed displacement a non-uniform stress distribution may be expected along the free surface.

Displacement controlled load conditions were selected for the purpose of this analysis. Justification for this decision was based on consideration of the possible application of the results. The objective was to consider the development of cracks through defect coalescence on the basis that this may be a possible mechanism for defect development and hence failure in large fabricated structures. Compatibility considerations would therefore imply that the constraint of the surrounding structure would prevent the non-

uniform displacement which would result from the uniform stress boundary condition. In such a structure the loading would be more consistent with the displacement controlled boundary conditions.

Two load steps were run for each defect geometry, one with an imposed displacement in the Y direction along the top surface and a second with an imposed rotation. Both load steps were included in both the single defect and periodic defect models resulting in a total of forty eight cases.

## **7.5 Results**

### **7.5.1 $a/c = 0.2$**

Figures 7.3 to 7.6 and Figures 7.7 to 7.10 present the results for the analysis of the lowest aspect ratio defect under tension and bending conditions respectively. For each case the results have been presented as plots of normalised stress intensity factor versus  $\theta$ , the parametric angle. The stress intensity factors were normalised by  $\sigma_{av}\sqrt{\pi a}$  for all cases. Where  $\sigma_{av}$  was the average stress applied along the top edge of the plate and  $a$  was the defect depth. For the bending load cases  $\sigma_{av}$  was the average outer fibre stress. Superimposed on each plot is the appropriate Newman and Raju solution [150] for the geometry and loading. Two variations on the Newman Raju solution have been shown on each plot, the first is the complete solution as described in section 4.3.2, the second omits the correction for finite area,  $f_w$ . The results were presented in this manner to demonstrate the magnitude of the finite area correction for comparison with the magnitude of any interaction effects which were observed.

Figures 7.3 and 7.7 also show the normalised stress intensity factor for an edge crack of equivalent depth as determined from solutions 1.1.20 and 1.1.21 of [6]. The edge crack solution utilised was the equivalent solution for the recharacterised defect assuming the methodology of British Standards PD6493 were adopted. Due to the required compression of the y-axis it was not feasible to include the edge cracked plate solution on the other figures.

The effect of recharacterisation has been considered further in the discussion of these results.

### **7.5.2 $a/c = 0.4$**

Figures 7.11 to 7.13 and 7.14 to 7.16 present the results for the analysis of the intermediate aspect ratio defect under tension and bending load cases respectively. As above the Newman Raju solutions, with and without the finite area correction  $f_w$ , were superimposed on each plot. Similarly the recharacterised edge crack solutions were also presented for the shallowest defect cases, Figures 7.11 and 7.14.

### **7.5.3 $a/c = 0.6$**

Figures 7.17 to 7.20 and 7.21 to 7.24 present the results for the case where the defect aspect ratios were 0.6 for the tension and bending load cases respectively. As above the Newman Raju solutions both with and without the finite area correction  $f_w$  were superimposed on each plot and the recharacterised edge crack solutions have been included presented for the shallowest defect cases only.

## **7.6 Discussion**

### **7.6.1 Validation of the Line Spring Solution**

Before considering the effects of interaction based on the results of this analysis the suitability of the methodology was checked by comparison with the Newman Raju solution.

In general the results were more than acceptable, particularly for the shallowest defect for each case. As the defect depth,  $a/t$ , increased the discrepancy between the Newman Raju solution and the line spring results also increased. In particular it was noted that as the defect depth increased the line spring solution tended to underestimate the stress intensity factor at the deepest point,  $\theta = 90$  degrees although the magnitude of this effect was

never greater than that of the finite width correction. This was apparent for both the tension and bending load cases.

There are two possible explanations for this effect. First the validity of the line spring solution must be in doubt for deep defects and particularly where the aspect ratio is high due to its basis on the plane strain edge crack solution. The validity of the line spring solution is limited by the validity of the edge crack plate solution itself as the crack gets deeper, eg. the Gross and Strawley solution [45] as utilised by Rice and Levy [152] quoted a range of applicability of  $0.1 < a/t < 0.7$ , and further by the fact that as the surface length of the crack reduces relative to the plate thickness then the plane strain assumptions of the edge crack plate model and the shell model formulation may become less accurate. It may therefore be possible that the deviation between the two solutions was simply due to problems with the line spring solution. An alternative explanation may be the form of the loading. Newman and Raju used a uniform stress loading condition in their finite element analysis and consequently the empirical equations utilised here are based on an applied uniform stress. Conversely in this analysis a uniform displacement or rotation was applied along the top edge of the plate. For shallow defects both types of loading condition would be expected to produce the same results and this was clearly demonstrated in the figures for the shallowest defect cases. However for deeper defects the loading conditions become slightly different. It is therefore feasible that for the deeper defects the applied conditions in this analysis were less severe than those of Newman and Raju due to the effects of load shedding at the minimum ligament resulting in lower stress intensity factors at the deepest point of the defects.

It should also be noted that the geometry considered in this work was marginally outside the applicability of the Newman Raju solution. The defined range of suitability for the empirical solution is limited by  $c/b < 0.5$  whereas the geometries considered in this analysis all had  $c/b = 0.667$ . On the basis that the purpose of the Newman and Raju solutions was simply to determine the suitability of the line spring models it was thought that this relatively small extrapolation was acceptable.

### 7.6.2 Defect Interaction Effects

Figures 7.3 to 7.24 show that there was very little interaction effects between adjacent defects. The single and periodic defect results are closely similar. If anything the periodic defect stress intensity factor distribution always lies below that for the single defect. However the maximum difference observed was of the order of a few percent. On the basis that the line spring model itself and the finite element method in general are approximations then errors of this magnitude may be expected from the solution itself. Hence, accounting for the limitations of the method the results must be taken to demonstrate that there was no difference between the two solutions.

The resulting deduction was that the interaction effect between defects in a periodic array acted upon by a remotely applied displacement was of a similar order to the finite width correction,  $f_w$ , for a single defect in a plate of width  $2(c+L)$  where  $2L$  is the gap between periodic defects. Qualitatively this would seem reasonable since the so called 'finite width' correction of Newman and Raju can be considered more generally as a finite area correction. Given that a periodic array of defects reduces the load bearing material area by an identical amount as a single defect in a plate then the effect may be expected to be of the same magnitude. For defects with higher aspect ratios this may not hold as, locally the conditions approach the penetrating crack. This would be consistent with the results of Murakami et al [236,238] who considered interaction between semi-elliptical cracks in a half space and found negligible interaction for aspect ratios of less than unity but some interaction for higher aspect ratio defects. As the finite area correction must be zero for a half space no interaction effects would be expected for defects with low aspect ratios on the basis of the above discussion.

In engineering applications defects may not be expected to exist in periodic self similar arrays, however the magnitude of the interaction between the adjacent tips of co-linear defects would be expected to be of the same order as that evaluated for the periodic array ie. the finite area correction described above would still apply. The magnitude of this effect, and hence

the implications for component life prediction, for specific defects may be judged by the difference between the Newman Raju solutions with and without  $f_w$  as presented on Figures 7.3 to 7.24. The indication would appear to be that the effect for shallow defects,  $a/t = 0.2$ , would be small, less than 10%, for all of the aspect ratios considered and would increase for deeper defects. For the problem addressed by this work of small defects coalescing to form the more dominant single cracks the shallow defect results are the most relevant. On this basis it would appear that the errors would be small if such defect behaviour was modelled by consideration of single defects only, with no interaction effects.

The consequence of this finding for defect assessment and sentencing in engineering components for the purposes of fatigue crack development are therefore fairly simple. Rather than recharacterising defects as at present adjacent defects can simply be assessed as single defects with a finite area correction applied as a function of half the ligament length between the two defects. Such a methodology would allow the defect shape development and the fatigue crack growth rate to be predicted using simple algorithms. The significance of these results for current practice is discussed further in the following section.

### **7.6.3 Comparison with Existing Procedures**

Ultimately the significance of the results of this work must be assessed by whether they may present any possibility for improvement of defect assessment methodologies. To determine this it was therefore necessary to review the results against the practice dictated by the code type methodologies described in section 6.2.

Three methodologies were presented, British Standards PD 6493, ASME XI and the CEGB R6 method. The R6 approach offered a three level solution varying from the assumption that all ligaments were part of the crack up to performing a finite element analysis of the individual situation. PD 6493 would recharacterise all defects as edge cracks since the gap between the defects was less than the total surface length,  $2c$ , of the single crack. ASME

XI is more complex to apply since it is based on the ligament between the defects being less than the depth of the largest defect, in fact only the defects with an aspect ratio of 0.6 would be recharacterised by the ASME XI approach. Clearly any recharacterisation which was deemed necessary by these methodologies would result in an edge crack replacing the periodic array. Figures 7.3, 7.7, 7.11, 7.14, 7.17 and 7.21 show the edge cracked plate stress intensity factor superimposed for the shallowest defect cases. Table 7.1 summarises the results for the remaining geometries.

Table 7.1 shows that the recharacterisation procedure is extremely severe. In all cases the recharacterised SIF, the edge cracked plate solution, is significantly greater than the maximum calculated value. Even for the least severe condition,  $a/c=a/t=0.2$  under tension, the recharacterised defect has a normalised stress intensity factor of approximately 18% greater than the peak calculated value. If this was utilised as input to a fatigue crack growth calculation using a Paris law with exponent three, the calculated fatigue crack growth rate could be over estimated by approximately 64%.

The consequences of excessive conservatism for plant operation could be considerable. If the remaining life of a defective structure was evaluated using such a procedure then unnecessary repairs or even shutdown may be deemed necessary. In addition to the excess conservatism in the calculated stress intensity factors and the resulting propagation rate, defects recharacterised as edge cracks or very long surface cracks provide a considerably more severe condition if leak-before-break approaches could be adopted. It is unlikely that very long surface cracks would pass such an assessment and it is not possible for edge cracks to be treated in this way.

This argument suggests that shallow surface defects are currently treated in an extremely conservative manner. A simple evaluation procedure based on single defect analysis would appear to offer a more realistic solution since the interaction between shallow, co-linear semi-elliptical defects has been shown to be small. For the assessment of deeper defects, single defect solutions have been shown to be appropriate if a finite area correction is applied.

## **7.7 Conclusions for Chapter 7**

1. The line spring model was shown to offer a very effective and inexpensive tool for the analysis of complex surface crack problems.
2. The interaction between a periodic array of co-linear semi-elliptical defects was shown to be of the same magnitude as the finite area correction for the case of a single defect in a plate of the repeated cell size for the array.
3. Current methodologies were shown to be over conservative for the cases considered. Improved procedures could be developed by considering the defects individually and applying finite area type corrections.

### TENSION

a/c	a/t	<u>K<sub>max</sub></u>	$\varnothing$	ECP
		$\sigma\sqrt{\pi a}$	(Deg)	NSIF
0.2	0.2	1.16	90	1.370
	0.4	1.41	90	2.113
	0.6	1.76	90	4.05
	0.8	2.08	90	9.06*
0.4	0.2	1.06	90	1.37
	0.4	1.18	90	2.113
	0.8	1.42	49	9.06*
0.6	0.2	0.98	90	1.37
	0.4	1.04	90	2.113
	0.6	1.10	90	4.05
	0.8	1.56	41	9.06*

### BENDING

a/c	a/t	<u>K<sub>max</sub></u>	$\varnothing$	ECP
		$\sigma\sqrt{\pi a}$	(Deg)	NSIF
0.2	0.2	0.852	90	1.052
	0.4	0.749	60	1.255
	0.6	0.808	30	1.906
0.4	0.2	0.757	90	1.052
	0.4	0.661	20	1.255
	0.8	0.598	16	3.72*
0.6	0.2	0.695	45	1.052
	0.4	0.620	16	1.255
	0.6	0.560	16	1.906
	0.8	0.495	16	3.72*

\* Beyond validity of ECP solution

Table 7.1

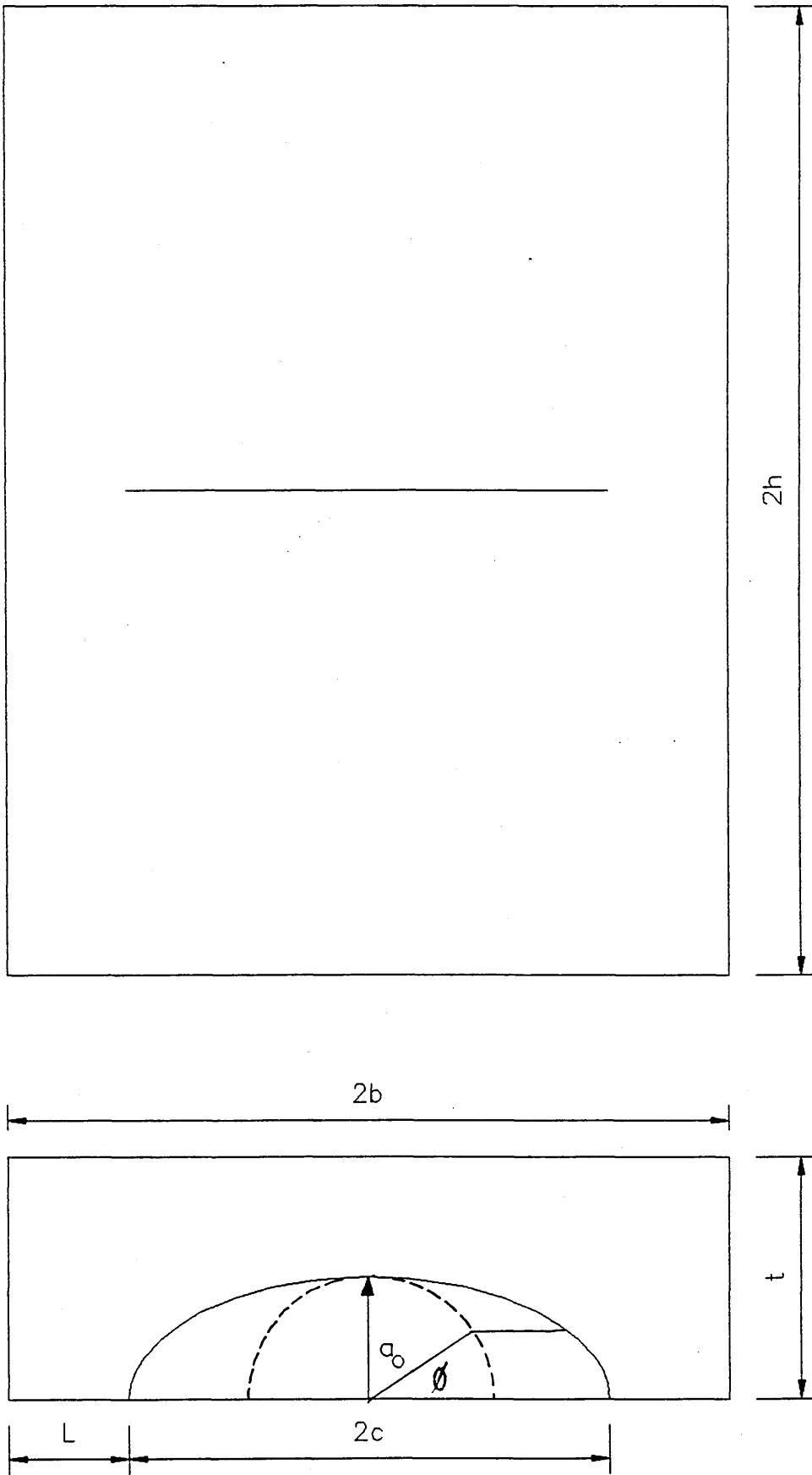


Figure 7.1

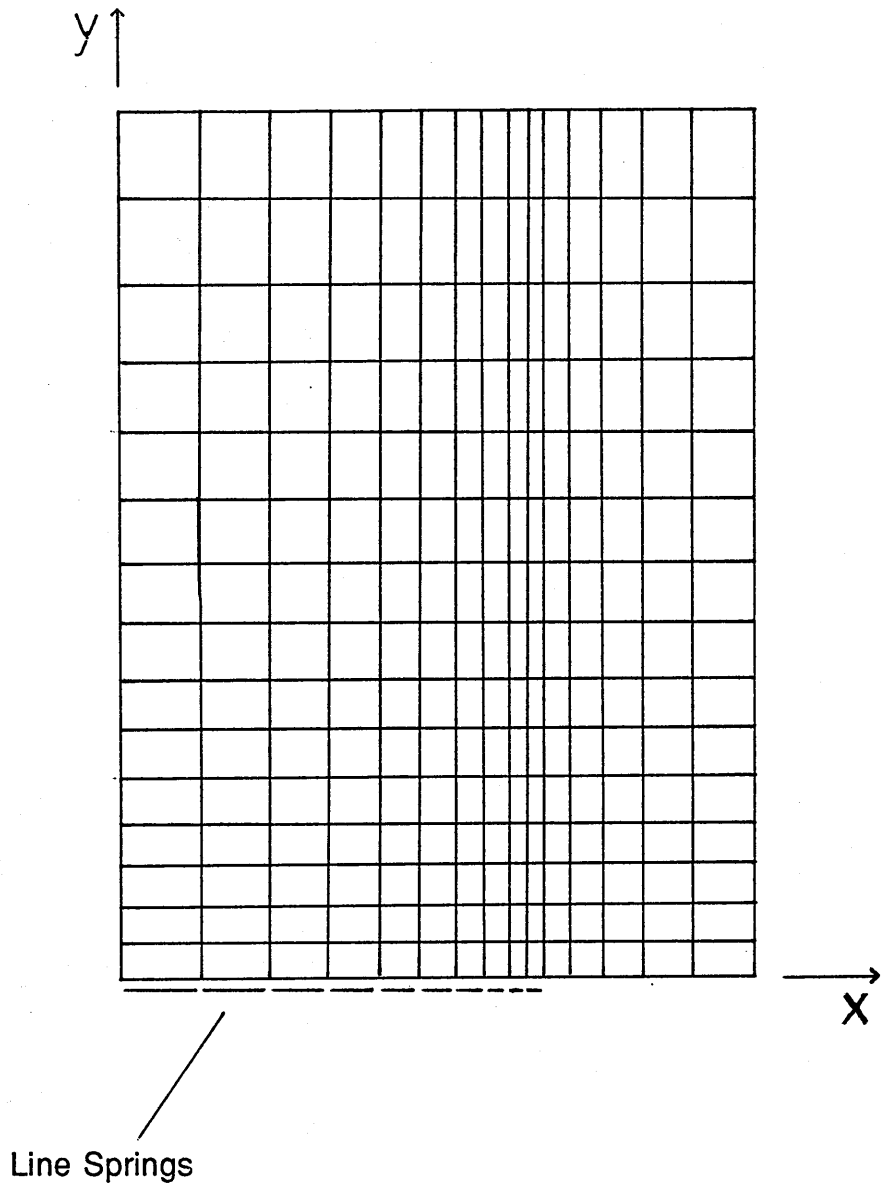
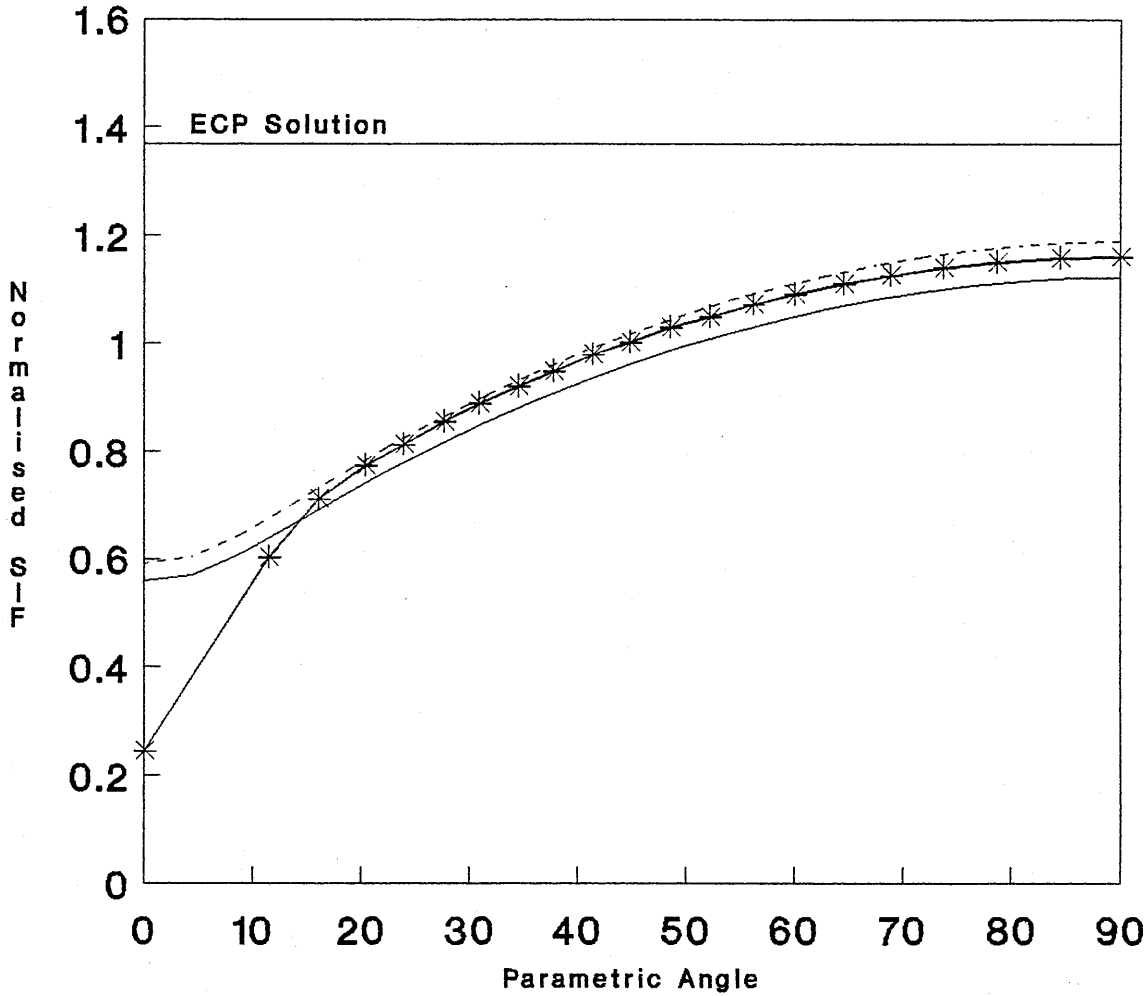


Figure 7.2

$a/c=0.2, a/t=0.2, c/b=0.667$   
 Tension Load Case  
 Newman Raju and ECP Solution Also Shown



**Legend**

<p>+ Single Defect LS</p> <p>— Raju &amp; Newman no Fw</p>	<p>* Periodic LS</p> <p>- - - Raju &amp; Newman + Fw</p>
--	--

**Figure 7.3**

$a/c=0.2, a/t=0.4, c/b=0.667$   
Tension Load Case  
Newman Raju Solution Superimposed

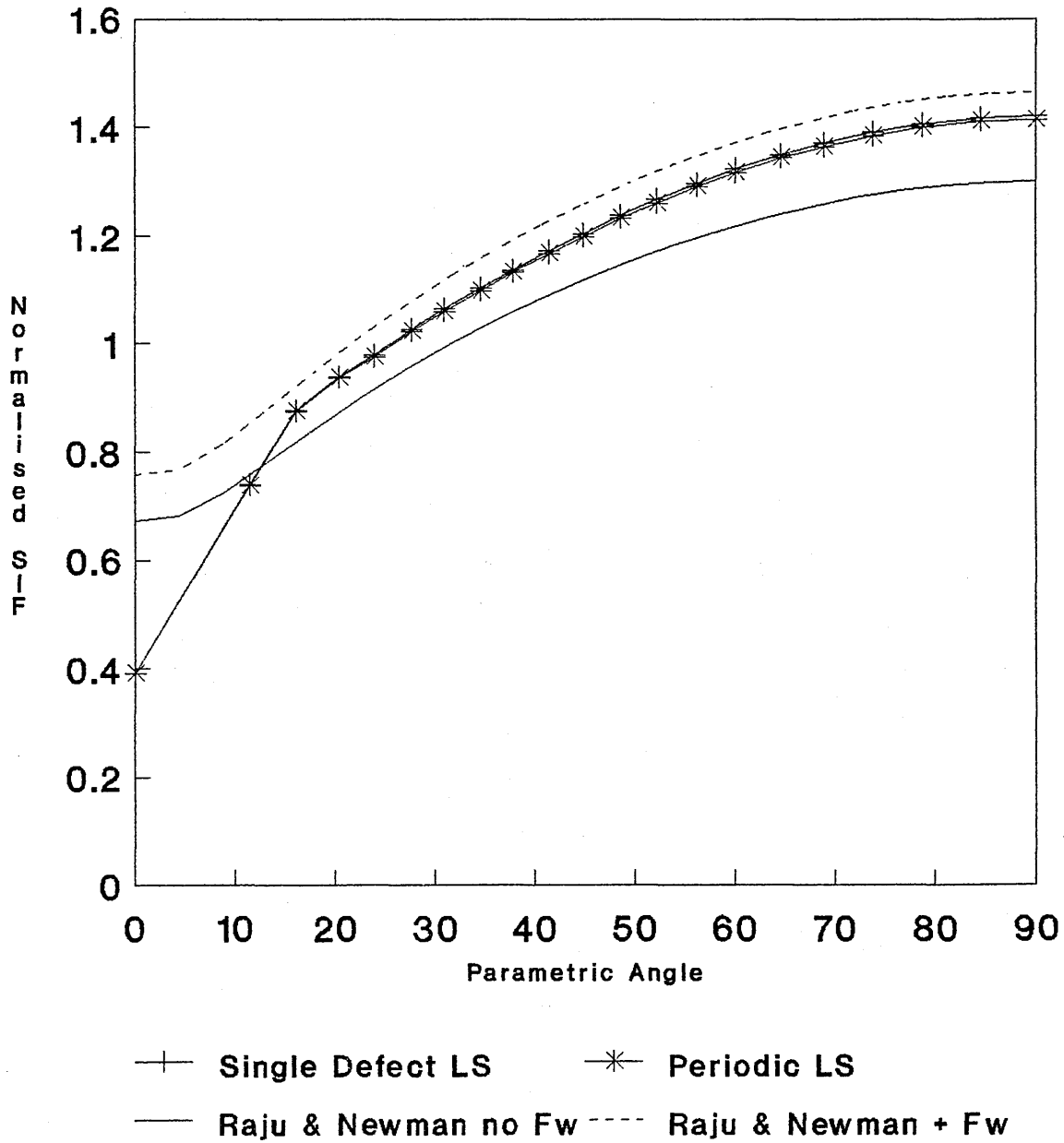


Figure 7.4

$a/c=0.2, a/t=0.6, c/b=0.667$   
Tension Load Case  
Newman Raju Solution Superimposed

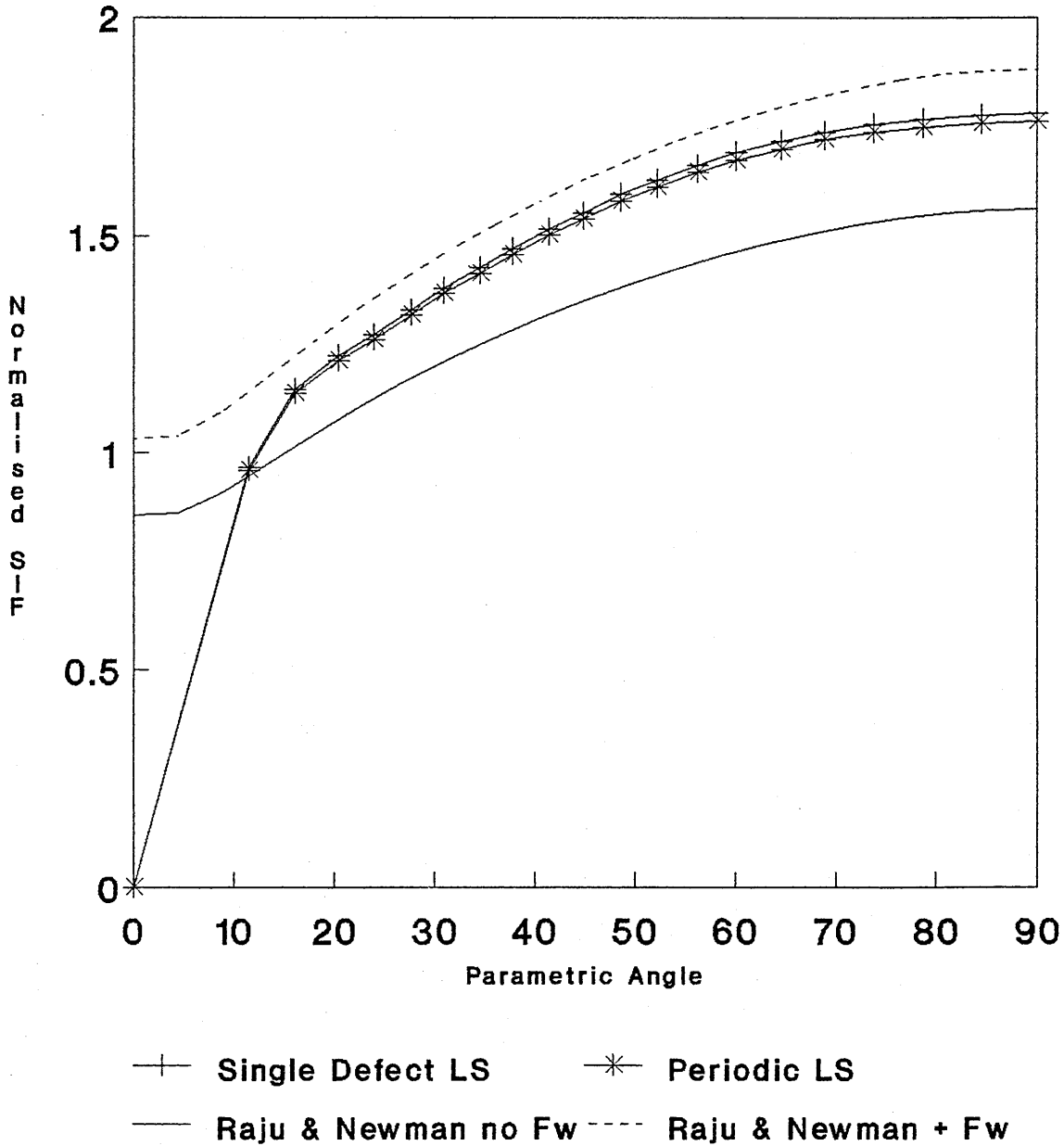


Figure 7.5

$a/c=0.2, a/t=0.8, c/b=0.667$   
 Tension Load Case  
 Newman Raju Solution Superimposed

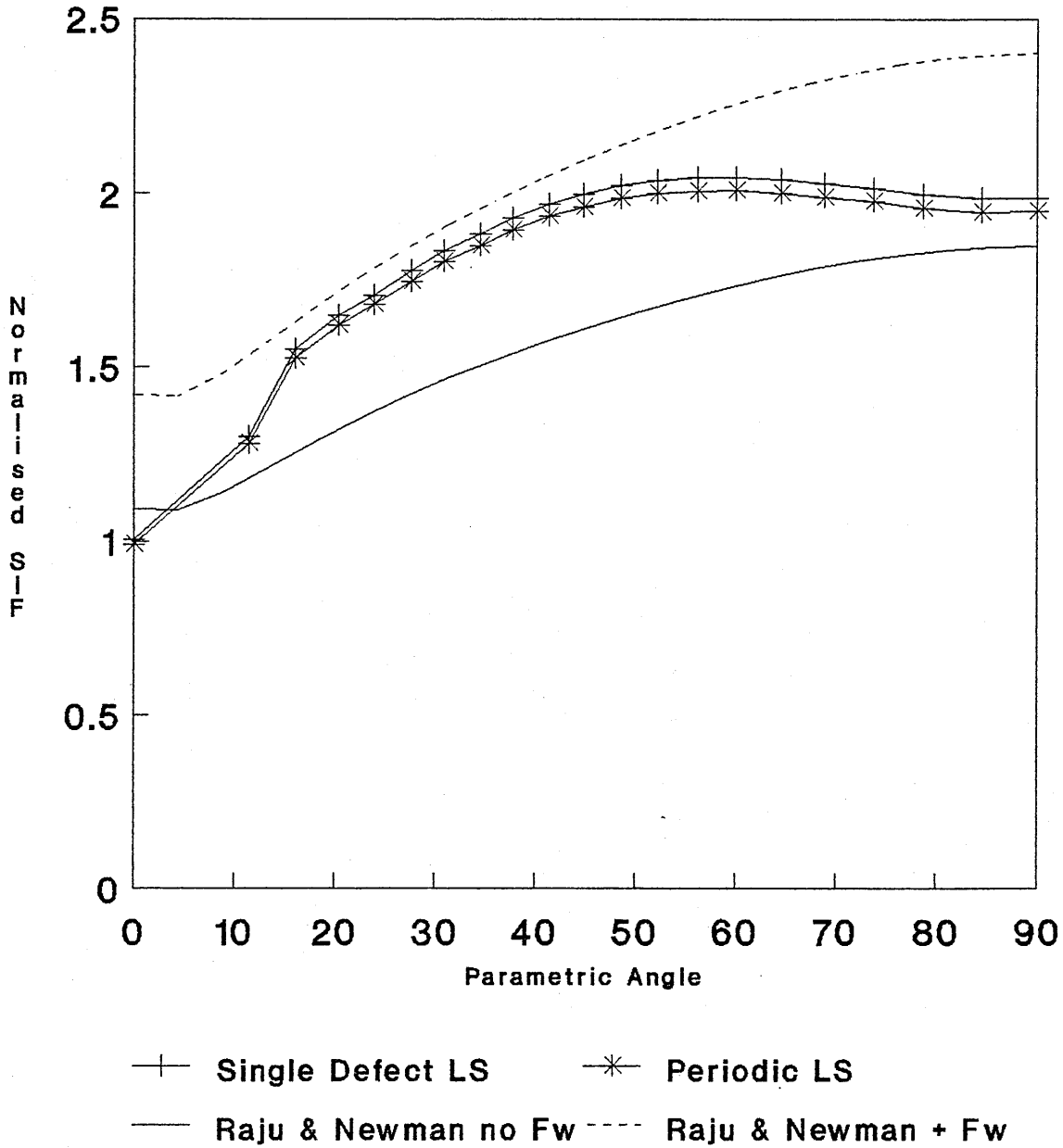


Figure 7.6

**a/c=0.2, a/t=0.2, c/b=0.667**  
**Bending Load Case**  
**Newman Raju and ECP Solutions Also Shown**

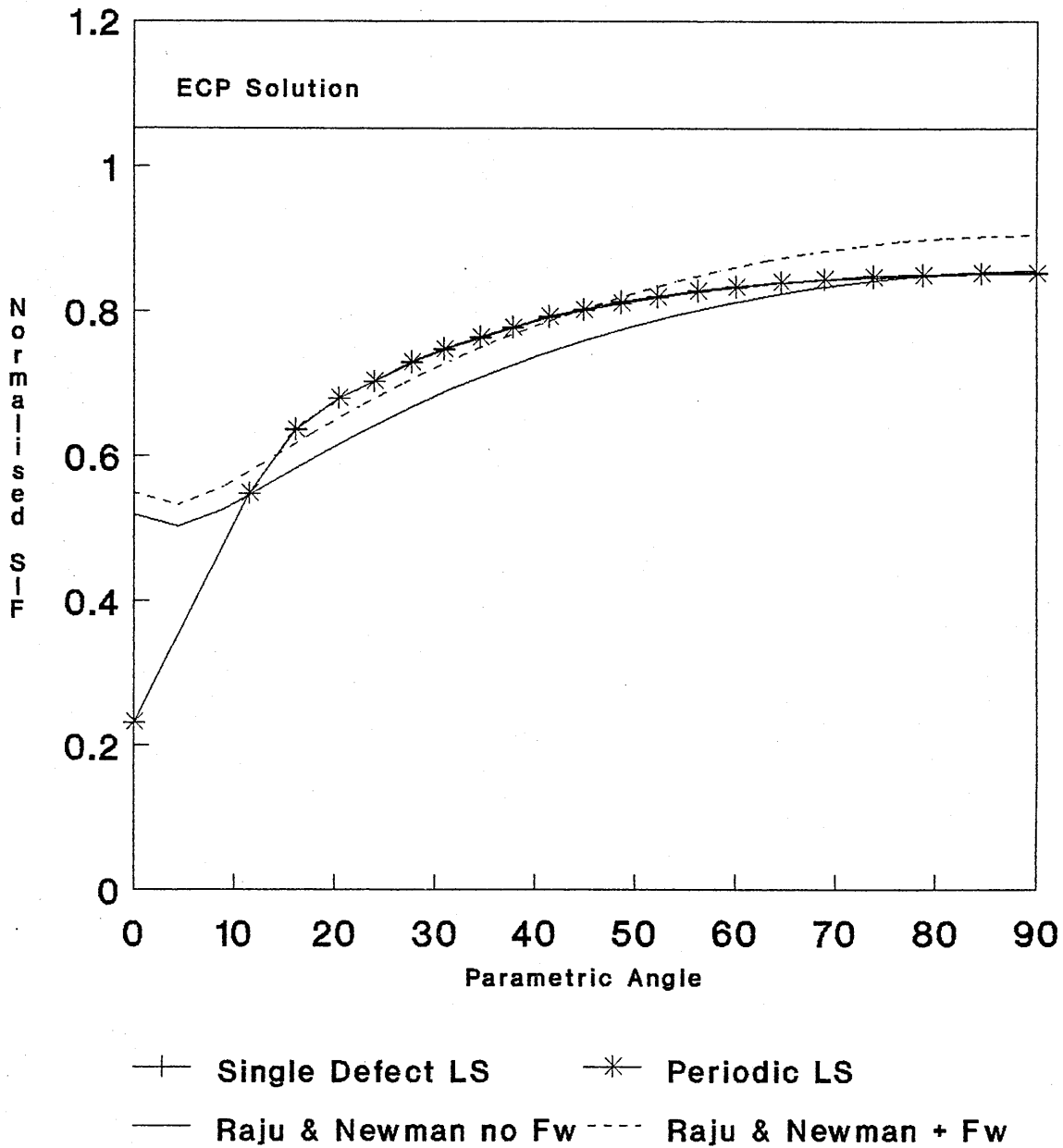


Figure 7.7

$a/c=0.2, a/t=0.4, c/b=0.667$   
Bending Load Case  
Newman Raju Solution Superimposed

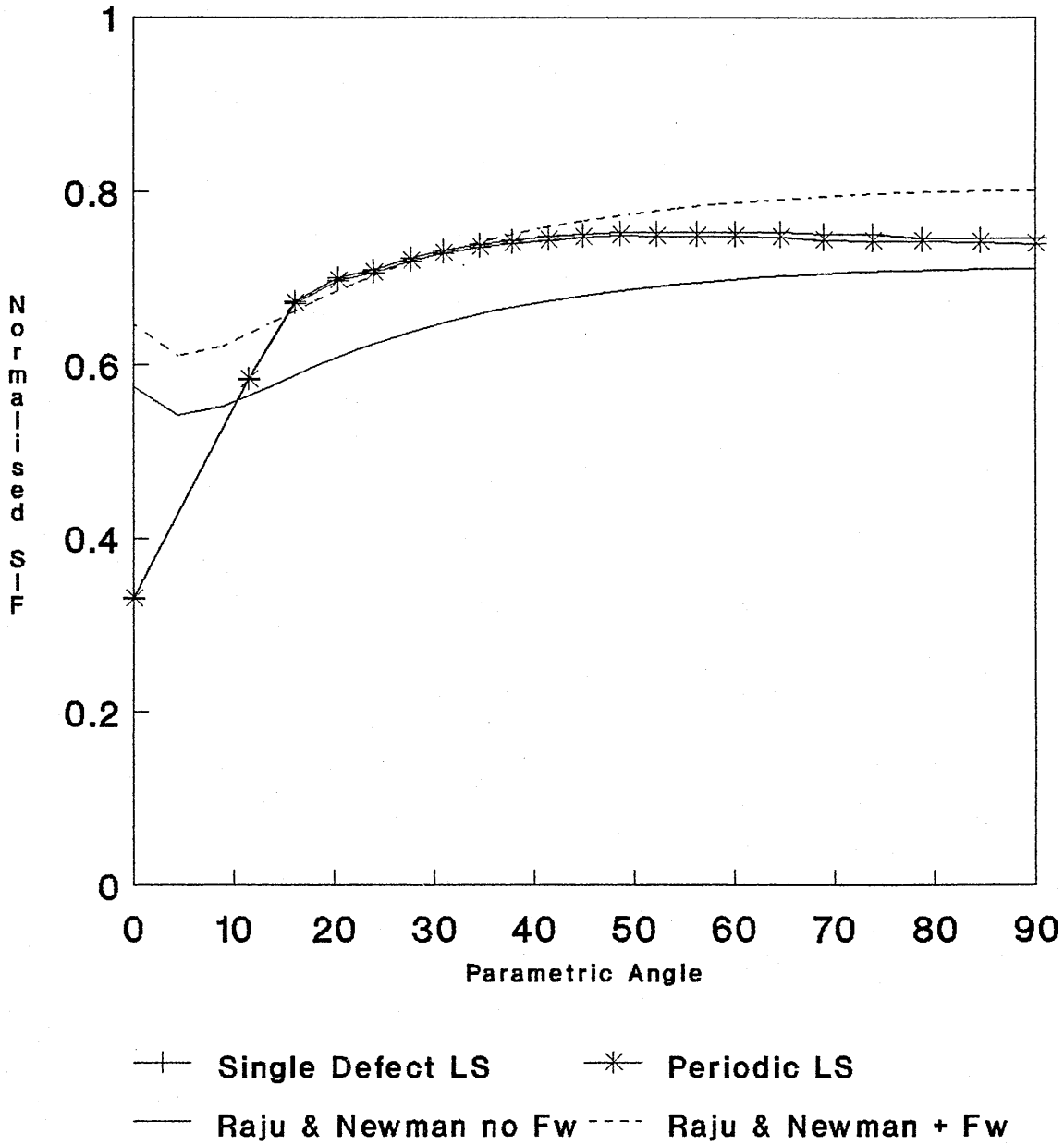


Figure 7.8

$a/c=0.2, a/t=0.6, c/b=0.667$   
Bending Load Case  
Newman Raju Solution Superimposed

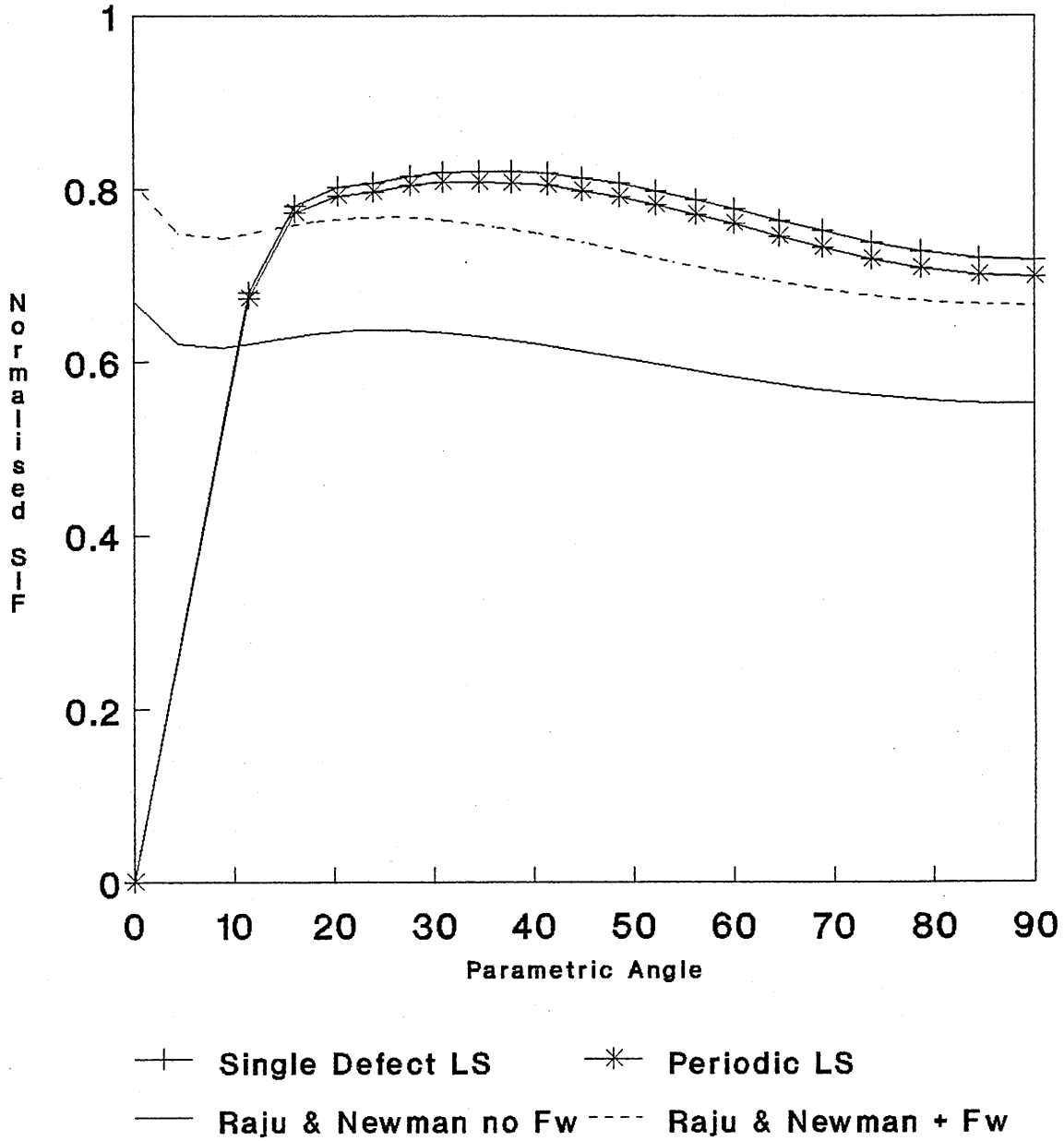


Figure 7.9

$a/c=0.2, a/t=0.8, c/b=0.667$   
 Bending Load Case  
 Newman Raju Solution Superimposed

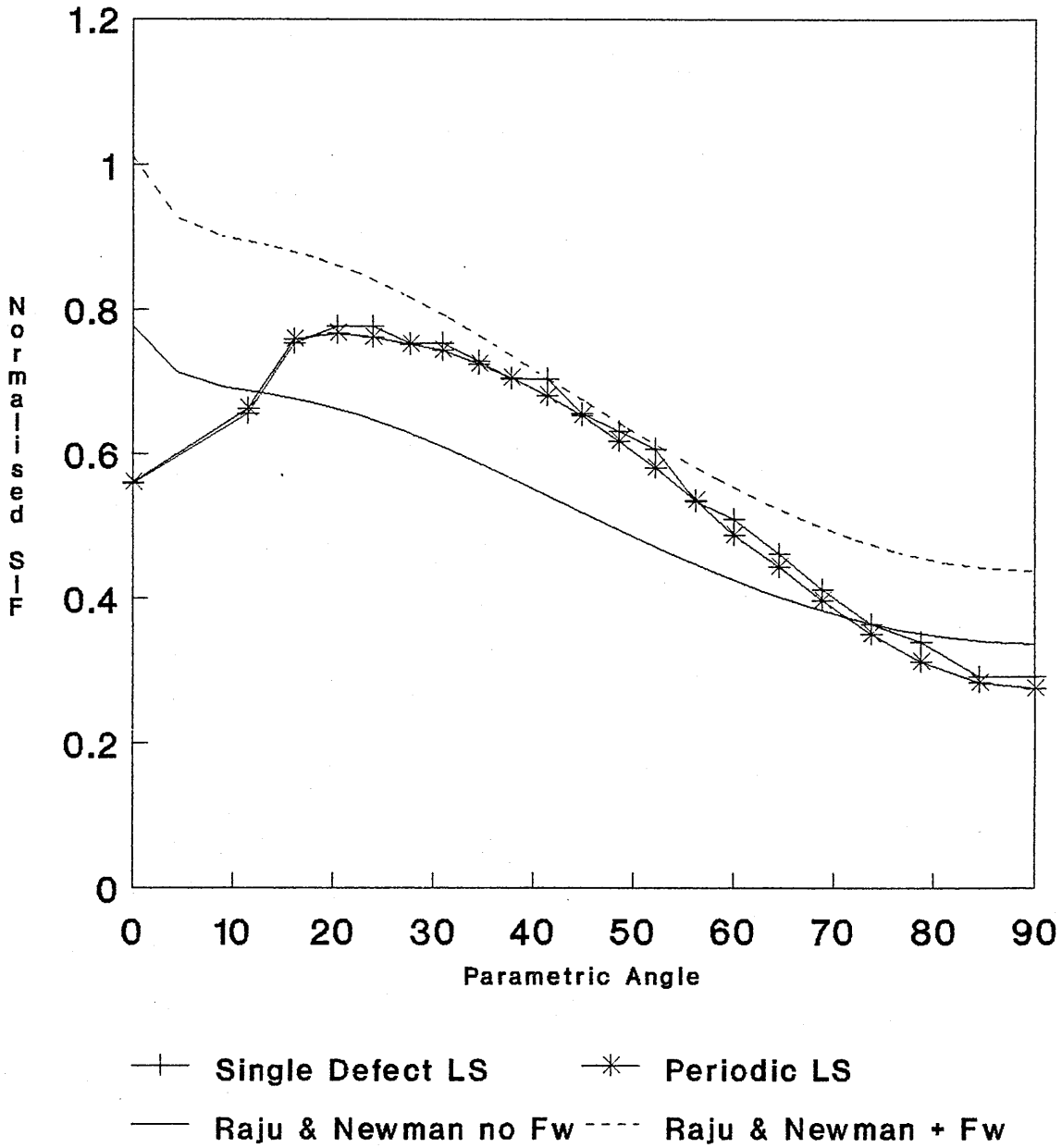


Figure 7.10

$a/c=0.4, a/t=0.2, c/b=0.667$   
 Tension Load Case  
 Newman Raju and ECP Solutions Also Shown

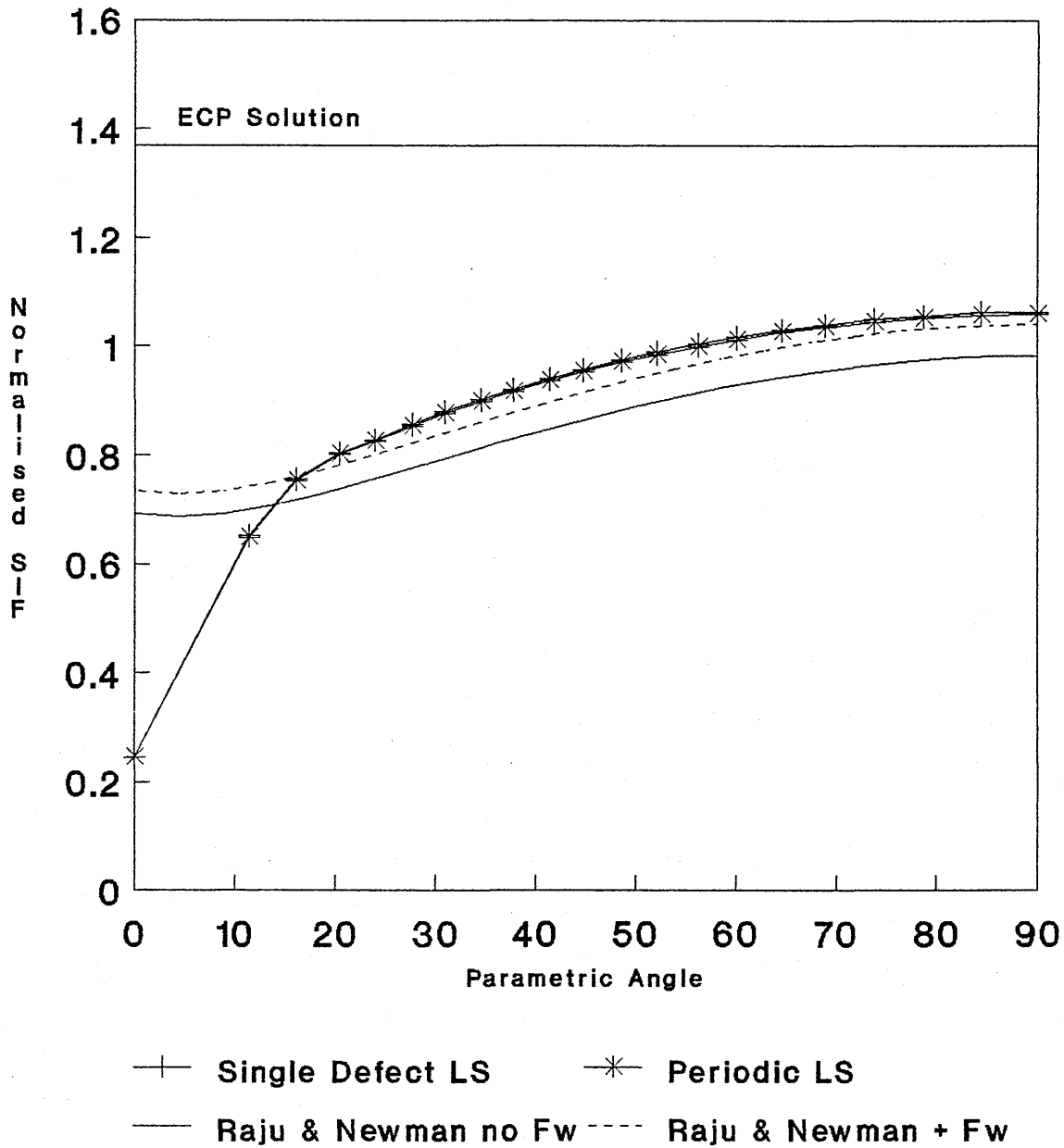


Figure 7.11

$a/c=0.4, a/t=0.4, c/b=0.667$   
Tension Load Case  
Newman Raju Solution Superimposed

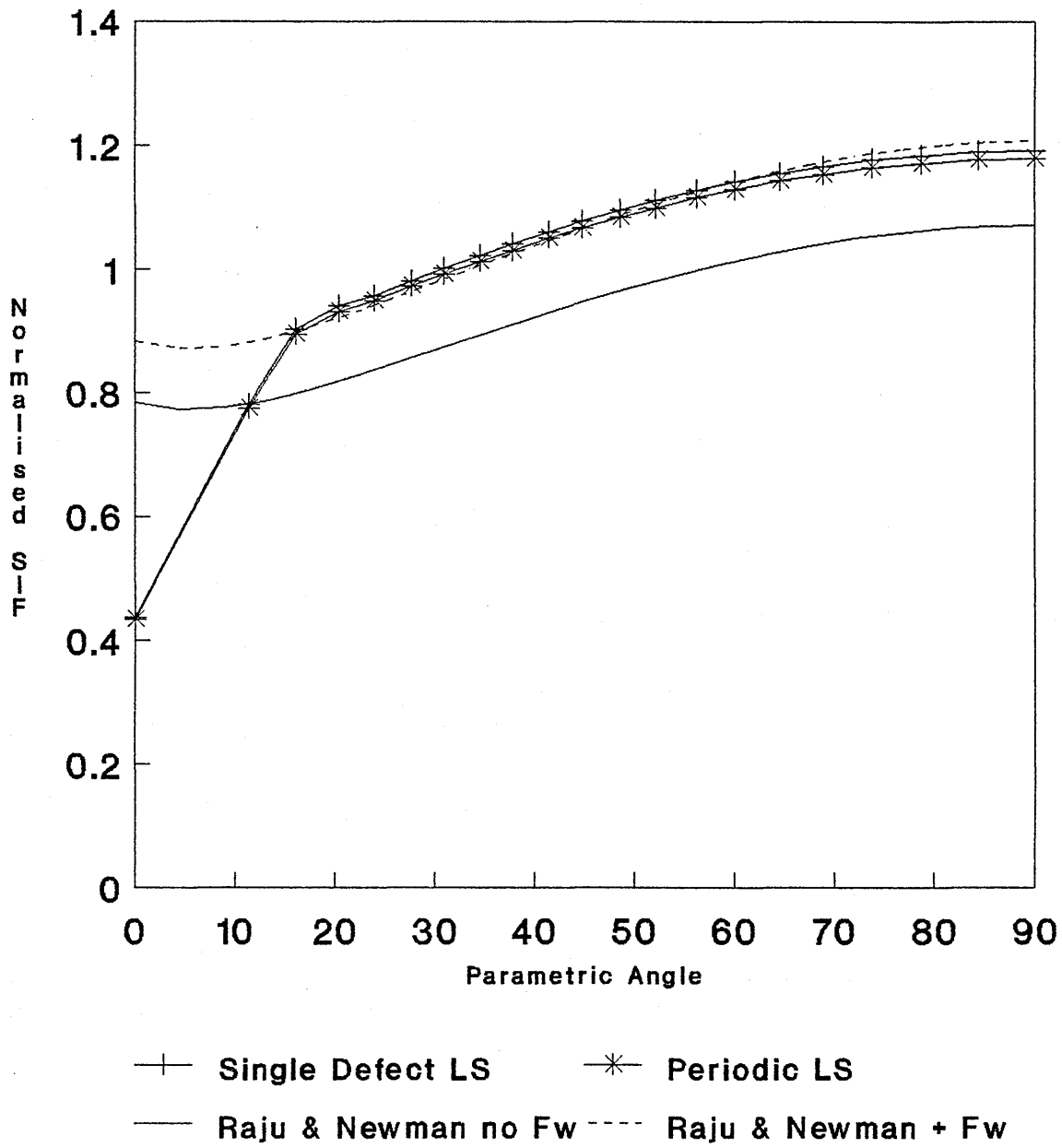


Figure 7.12

$a/c=0.4, a/t=0.8, c/b=0.667$   
Tension Load Case  
Newman Raju Solution Superimposed

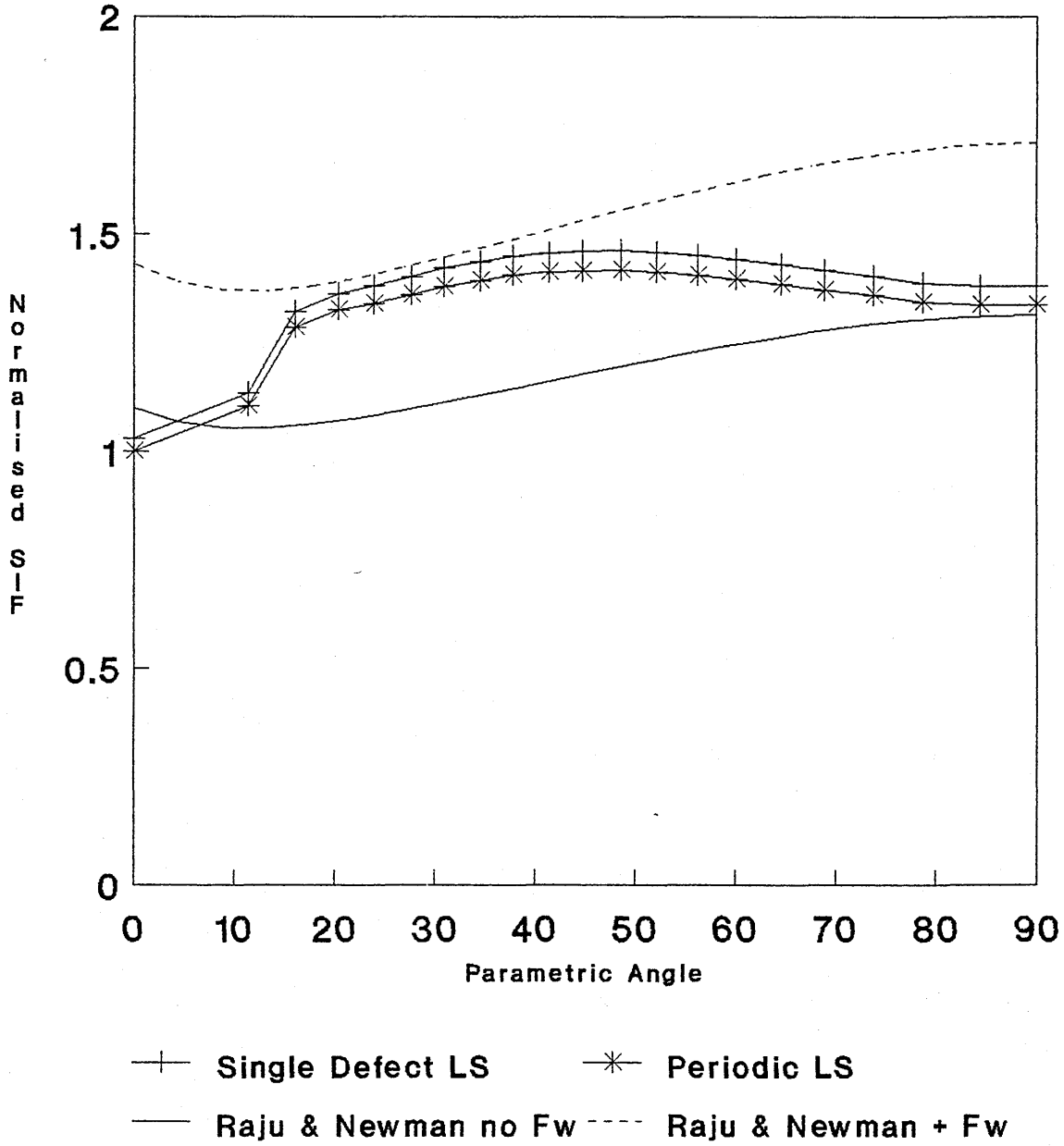


Figure 7.13

$a/c=0.4, a/t=0.2, c/b=0.667$   
 Bending Load Case  
 Newman Raju and ECP Solutions Also Shown

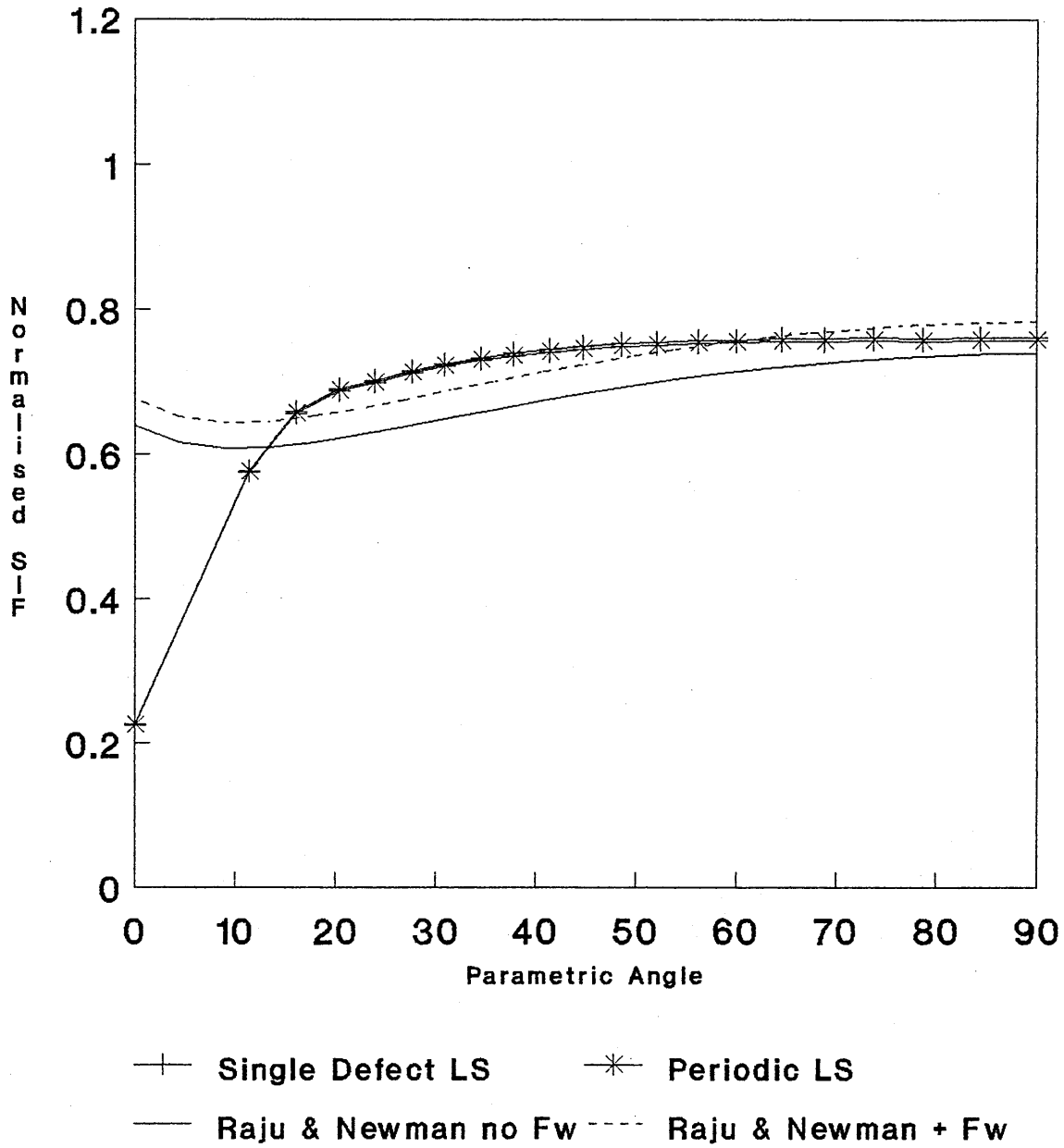


Figure 7.14

$a/c=0.4, a/t=0.4, c/b=0.667$   
 Bending Load Case  
 Newman Raju Solution Superimposed

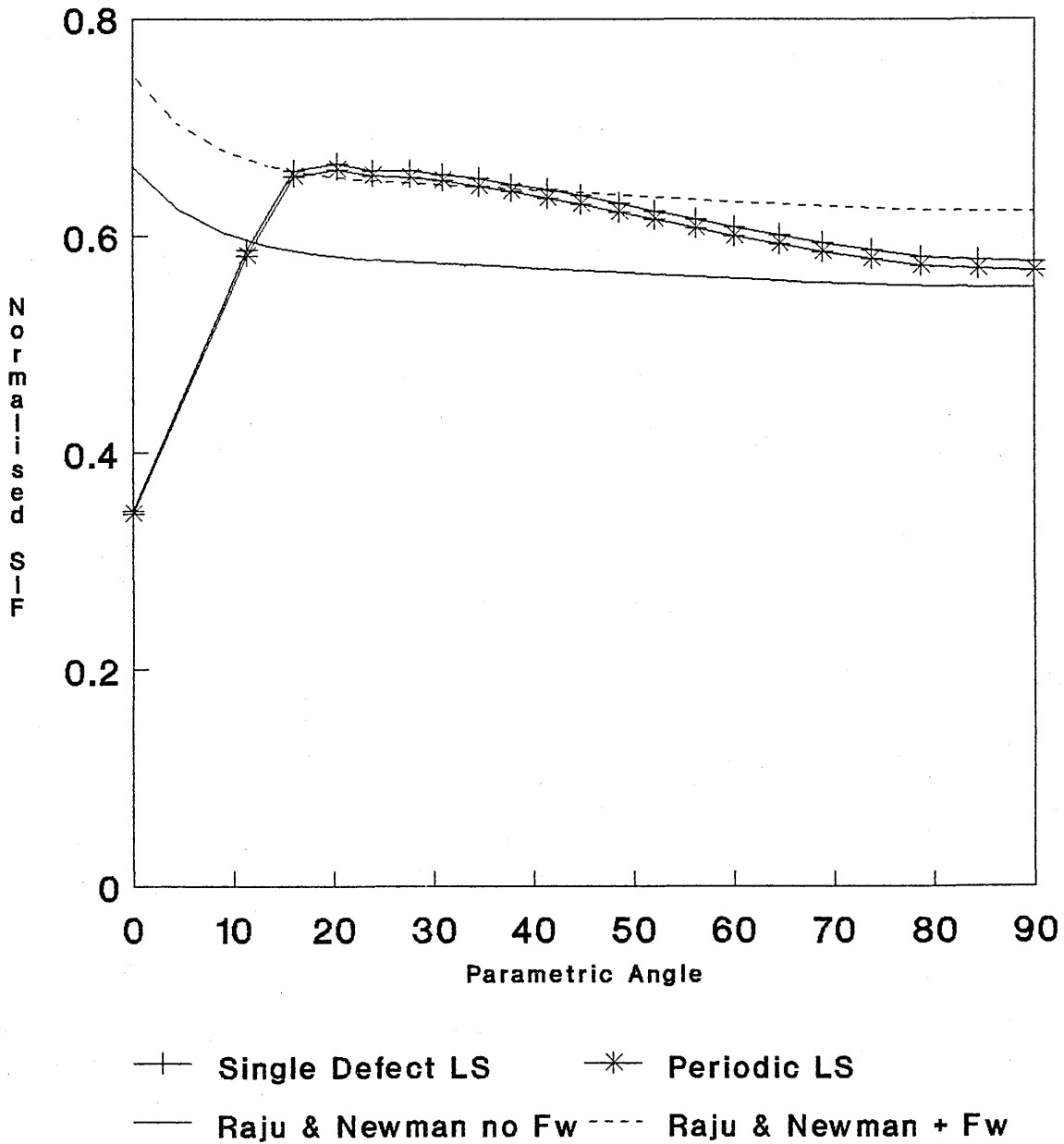


Figure 7.15

$a/c=0.4, a/t=0.8, c/b=0.667$   
 Bending Load Case  
 Newman Raju Solution Superimposed

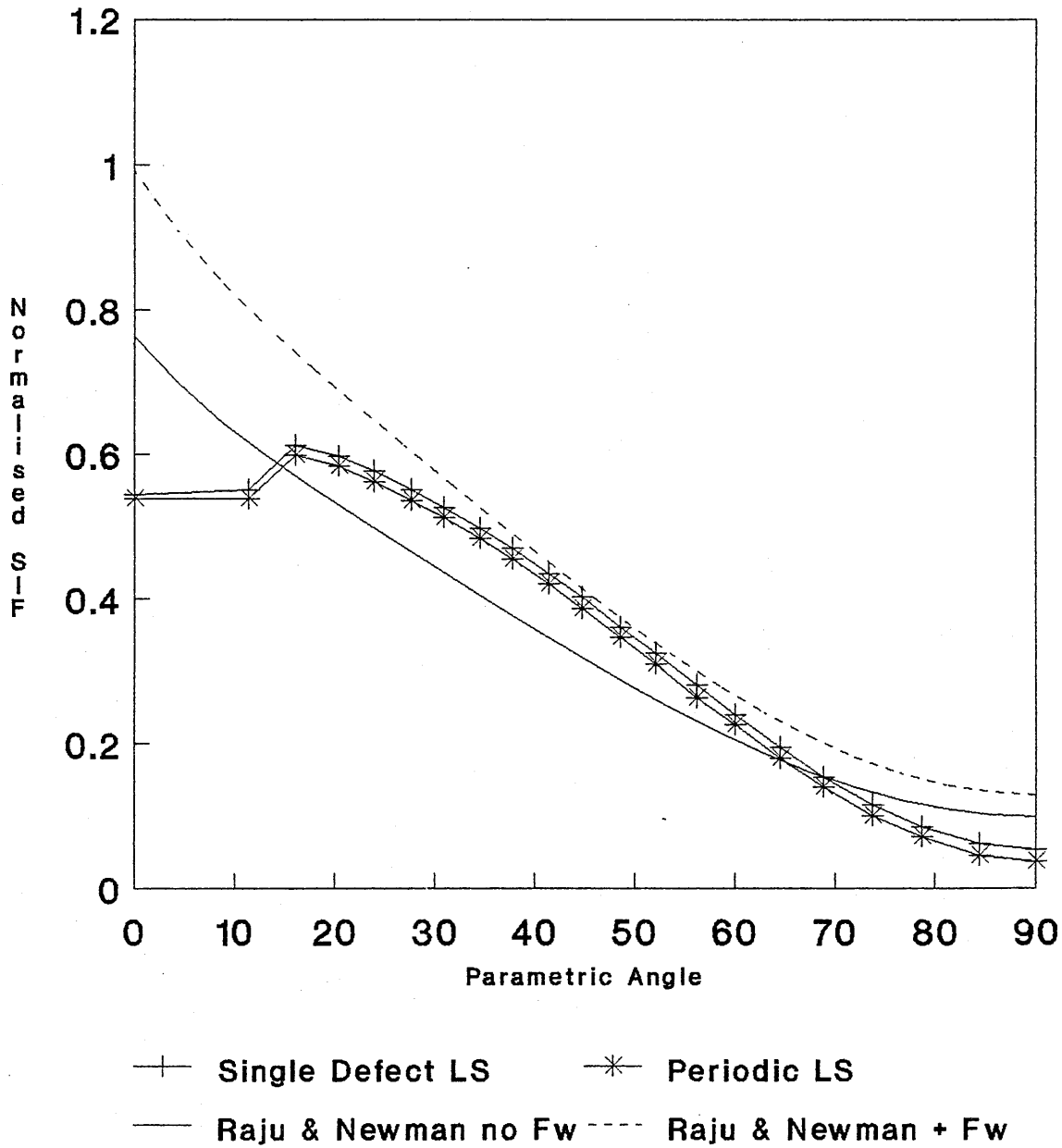


Figure 7.16

$a/c=0.6, a/t=0.2, c/b=0.667$   
 Tension Load Case  
 Newman Raju and ECP Solutions Also Shown

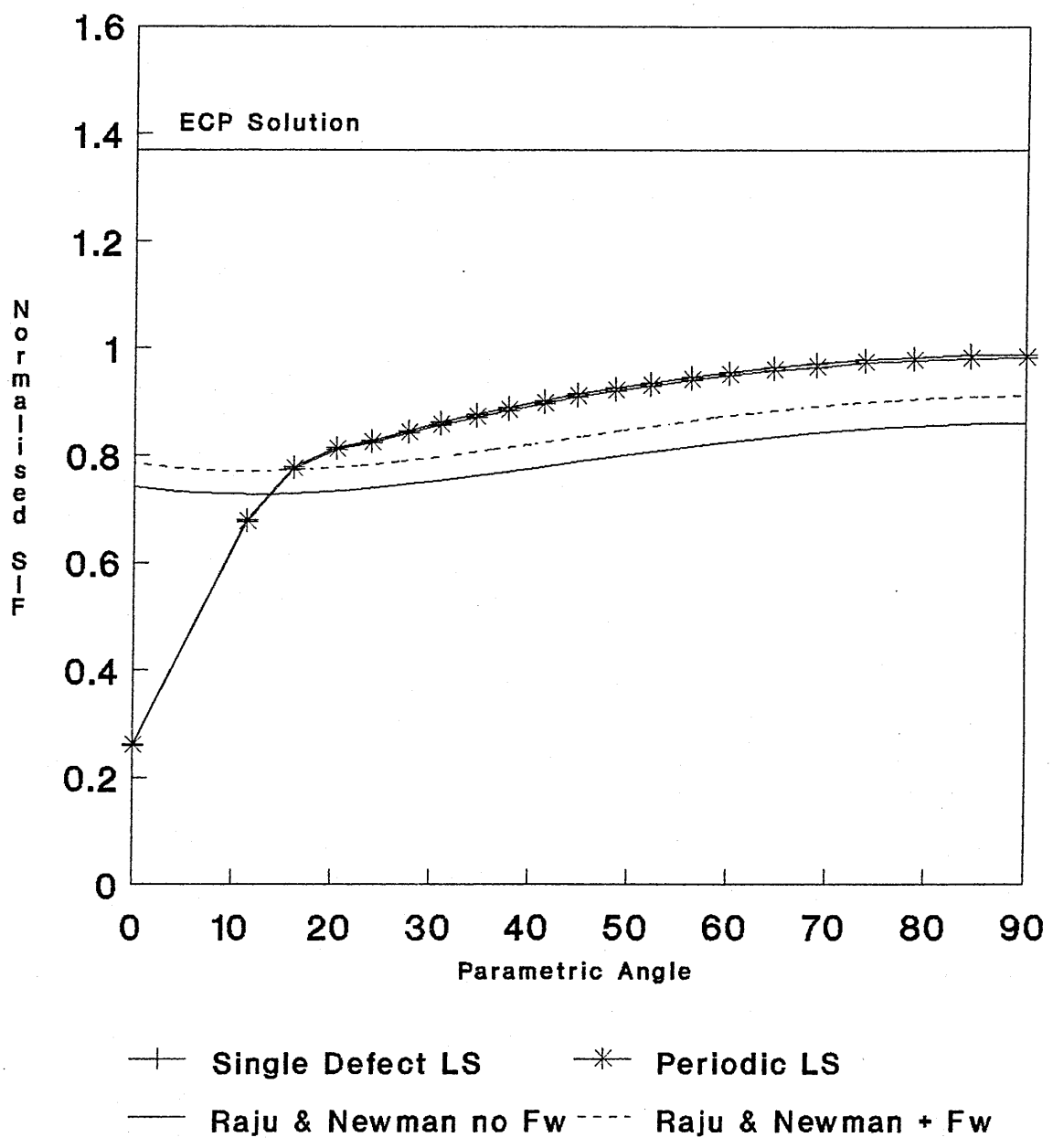


Figure 7.17

$a/c=0.6, a/t=0.4, c/b=0.667$   
Tension Load Case  
Newman Raju Solution Superimposed

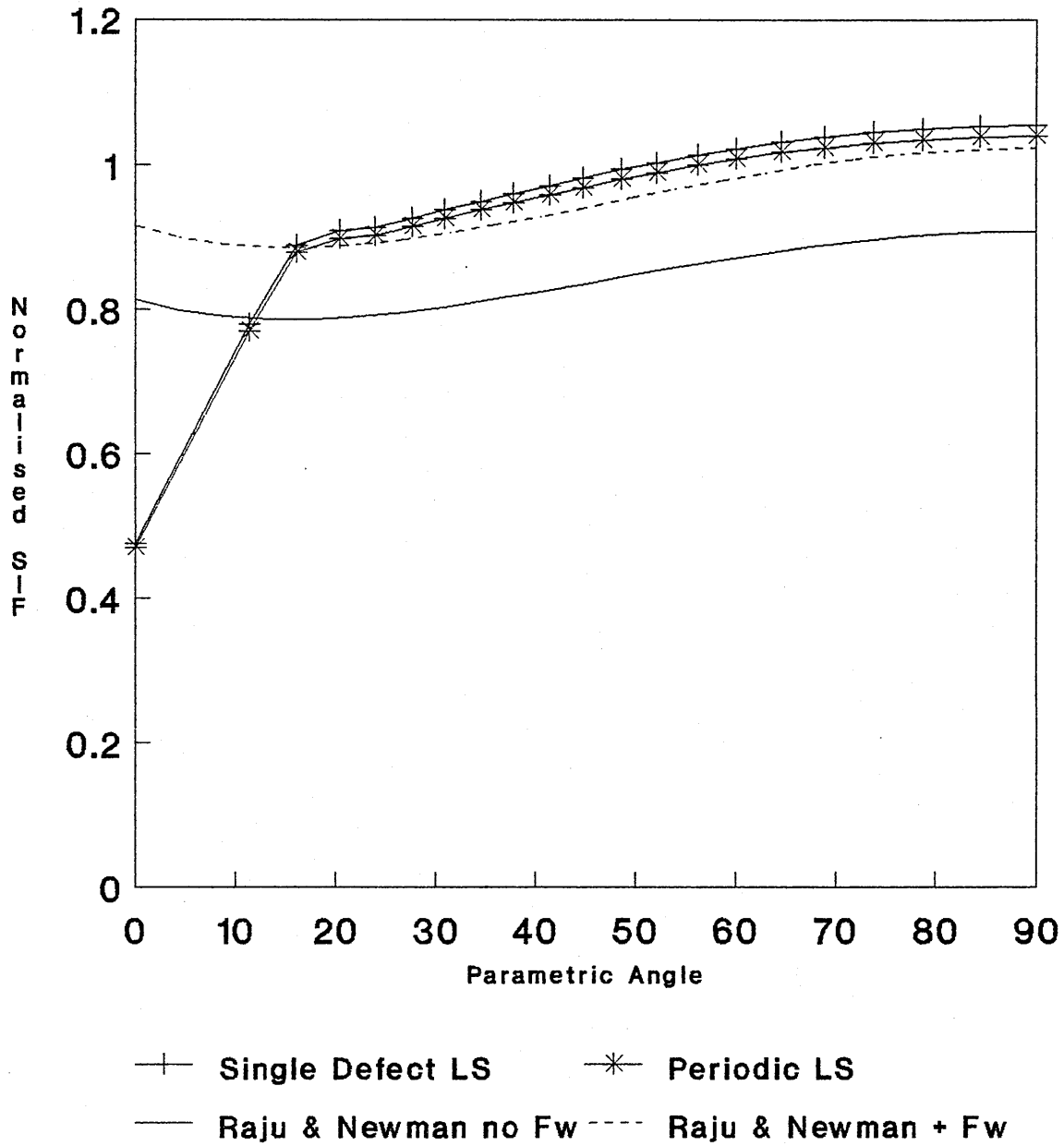


Figure 7.18

$a/c=0.6, a/t=0.6, c/b=0.667$   
 Tension Load Case  
 Newman Raju Solution Superimposed

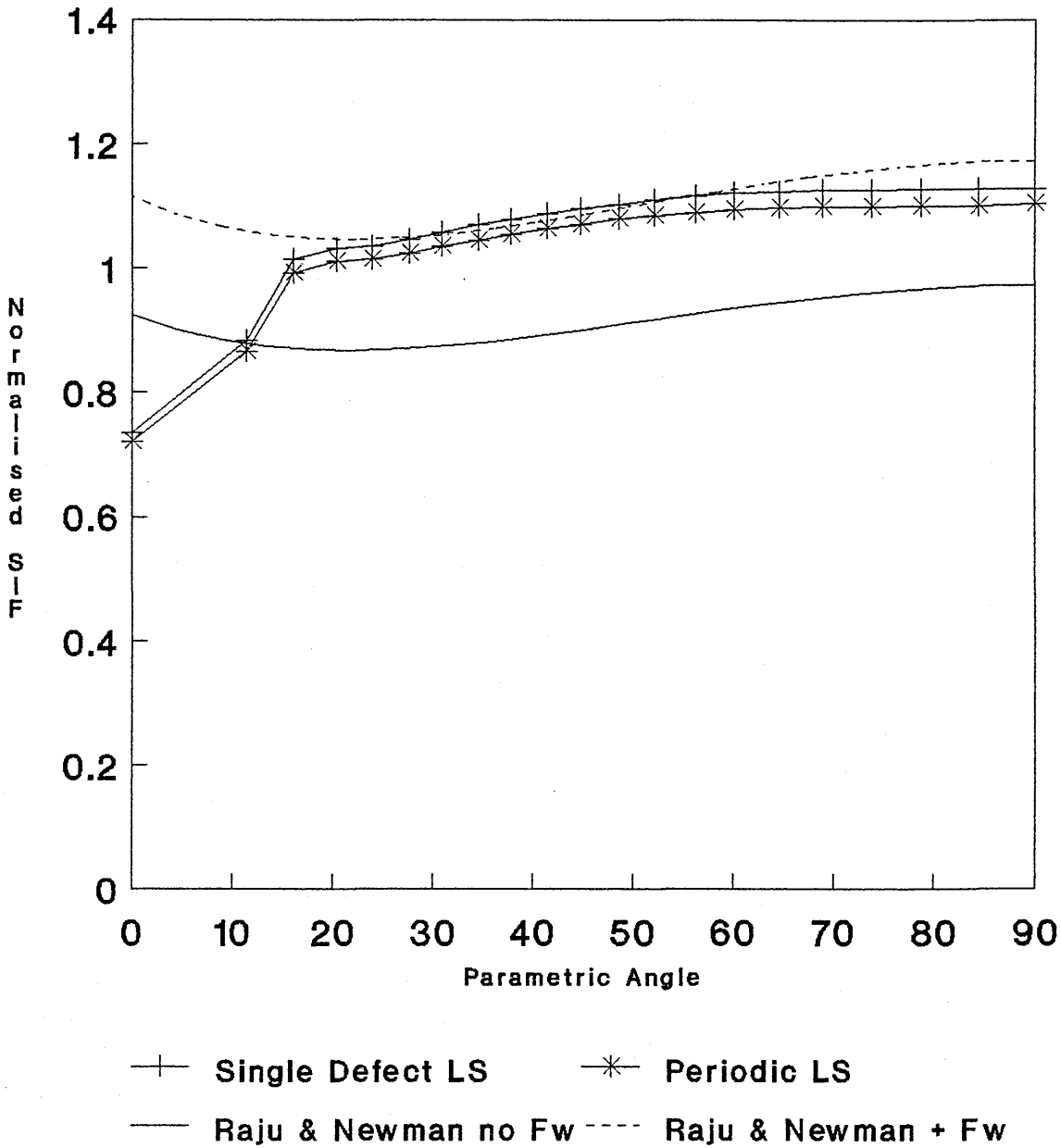


Figure 7.19

$a/c=0.6, a/t=0.8, c/b=0.667$   
 Tension Load Case  
 Newman Raju Solution Superimposed

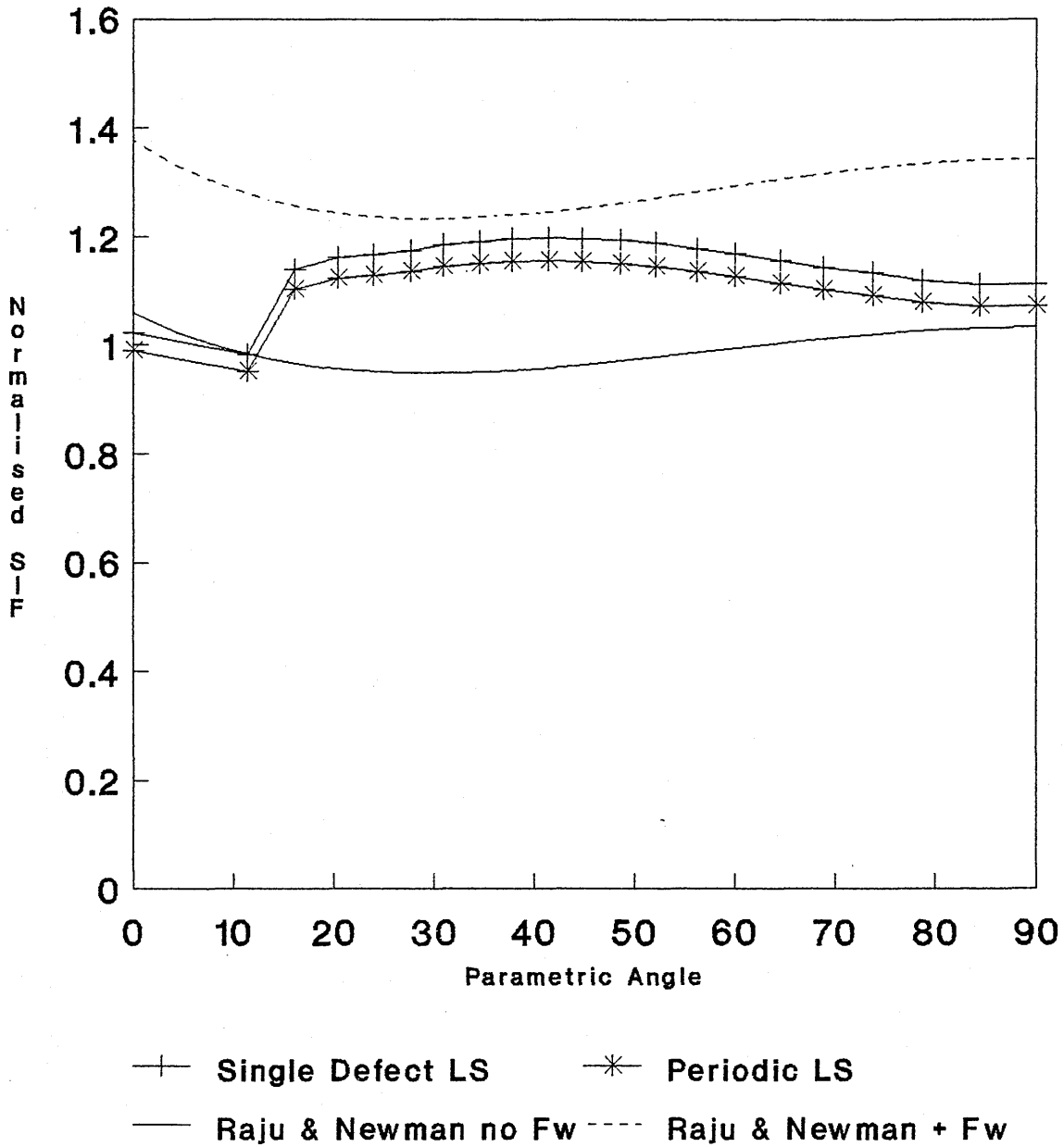


Figure 7.20

$a/c=0.6, a/t=0.2, c/b=0.667$   
 Bending Load Case  
 Newman Raju and ECP Solutions Also Shown

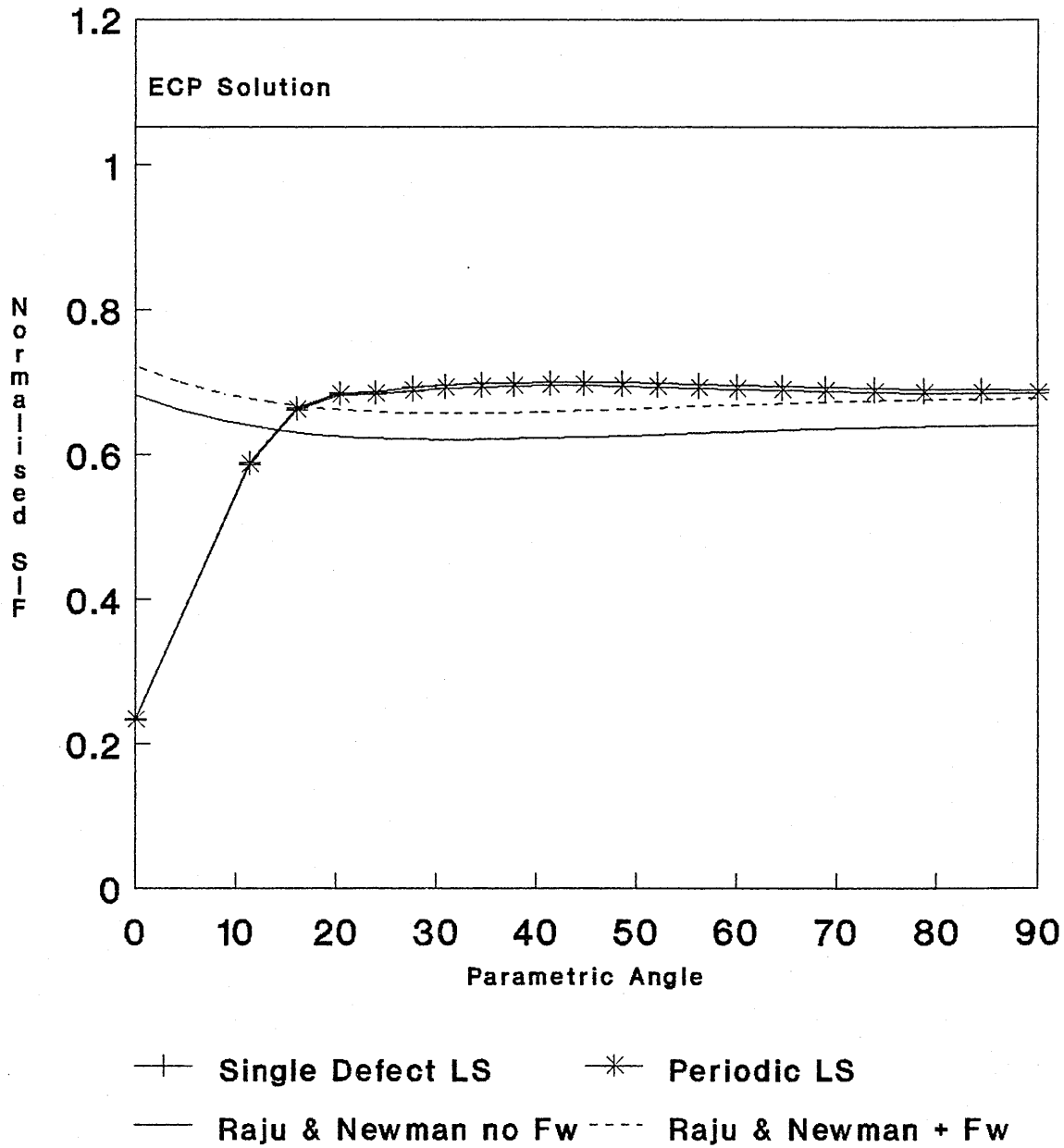


Figure 7.21

$a/c=0.6, a/t=0.4, c/b=0.667$   
Bending Load Case  
Newman Raju Solutions Superimposed

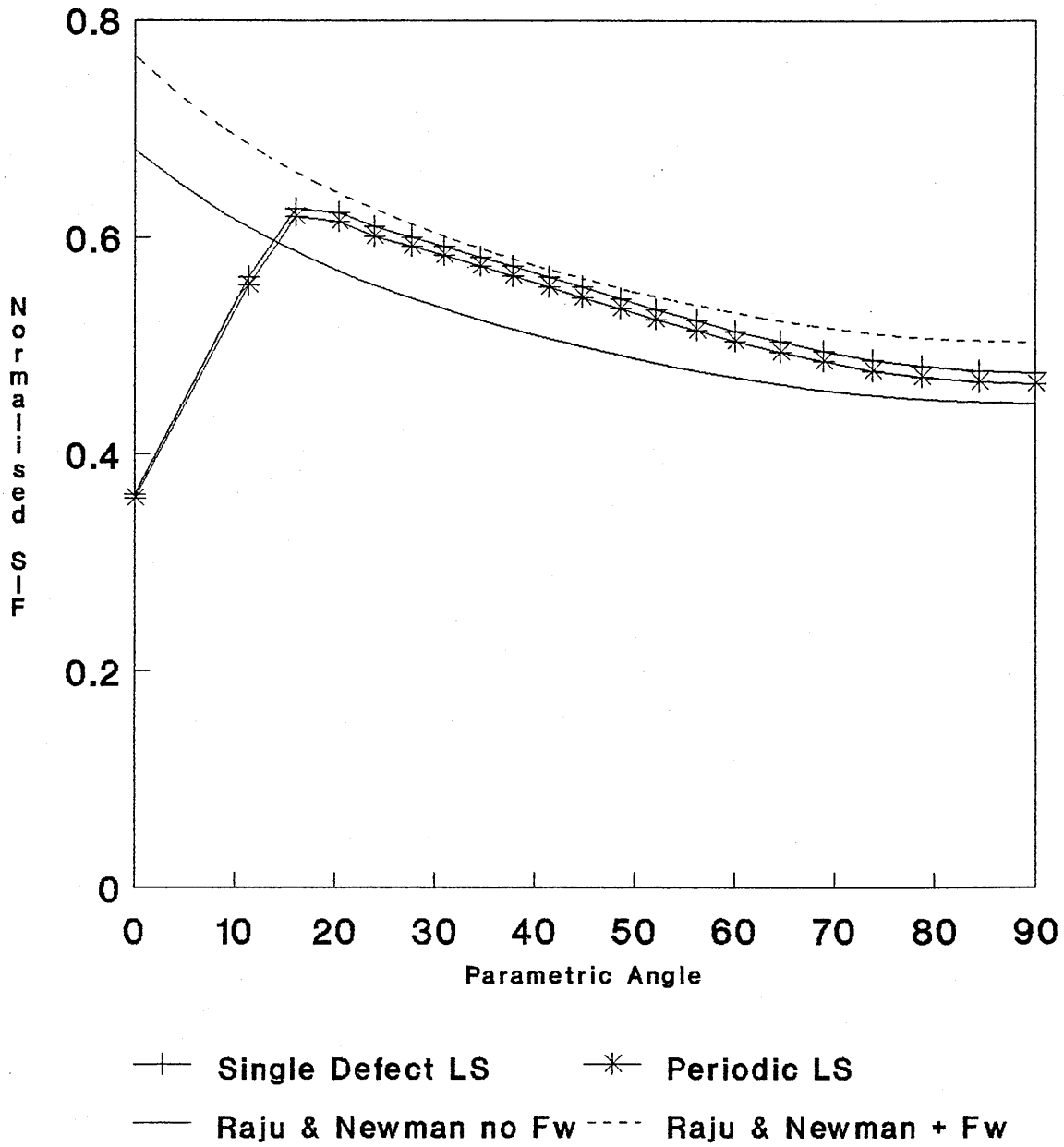


Figure 7.22

$a/c=0.6, a/t=0.6, c/b=0.667$   
 Bending Load Case  
 Newman Raju Solution Superimposed

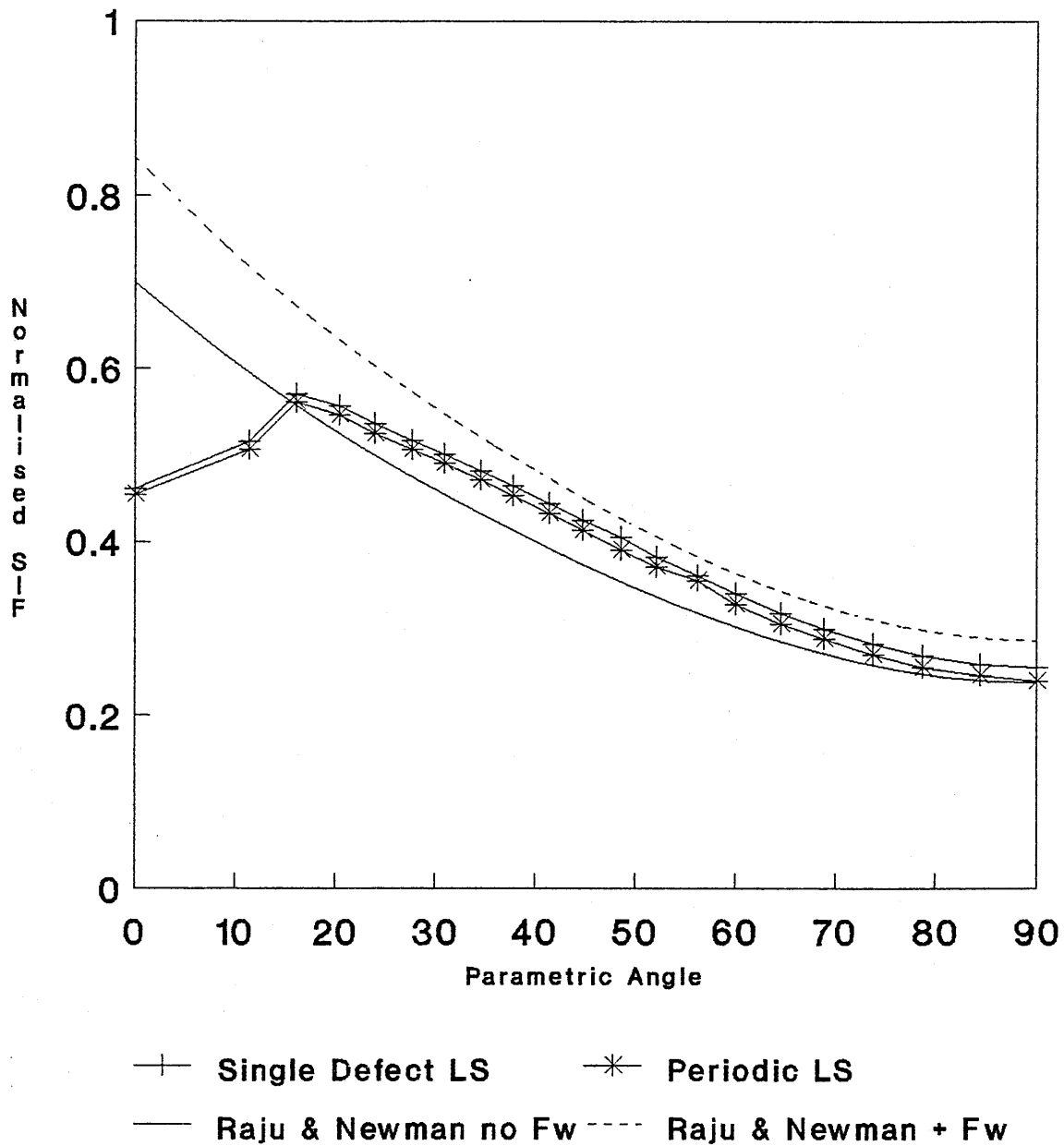


Figure 7.23

$a/c=0.6, a/t=0.8, c/b=0.667$   
 Bending Load Case  
 Newman Raju Solutions Superimposed

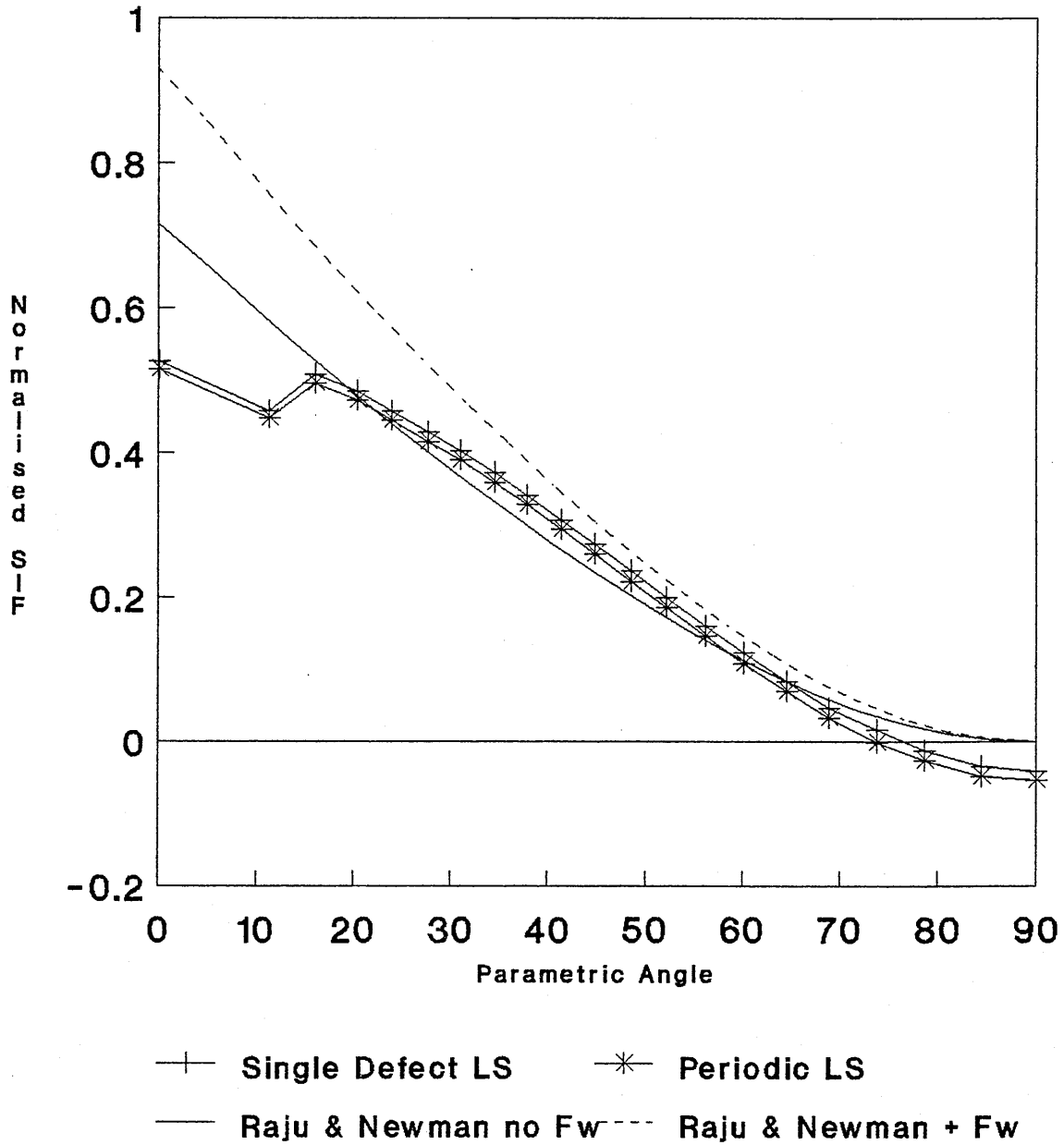


Figure 7.24

## **CHAPTER 8**

### **AN EXPERIMENTAL STUDY OF DEFECT COALESCENCE**

#### **8.1 Introduction**

In order to support the numerical study presented in the previous chapter and to demonstrate the coalescence process, a series of experiments were conducted. This chapter gives details of the procedures utilised before presenting the results. The results have then been discussed in some detail with relevant information from the literature and other pertinent sources used for comparison where possible. Finally conclusions based on the result of the experimental observations and subsequent analysis have been presented.

#### **8.2 Experimental Procedure**

The material chosen for the experimental investigation was a plain carbon manganese steel described as grade 50D under British Standard specification 4360. This material is typical of that used in the fabrication of tubular welded joints for offshore structures operating in the North Sea.

In Chapter 5 evidence from the open literature was presented that indicated that surface cracks growing under bending appear to grow towards relatively low stable aspect ratios, Figure 5.8. On this basis it would be expected that, after an initial transient period, the crack growth at the surface of the plate would be greater than at the deepest point and hence the defects would tend to coalesce more quickly. If any defect interaction effects were to occur it was thought that they may be demonstrated more clearly under bending conditions. For this reason three point bending tests were chosen for the purpose of this work.

Two test plates were manufactured to the geometry shown in Figure 8.1. The starter notches were machined perpendicular to the rolling direction using a fine diamond slitting wheel 70mm diameter and 0.15mm thick, producing two initial defects nominally 2mm deep with a surface length of 25mm and a part circular cross section. The initial defect separation was 25mm ie. equal to the surface length of one defect.

A beach marking technique was chosen to monitor the defect development during the tests. The procedure utilised was similar to that presented in [141], briefly this was :-

1. Utilising the Newman Raju solution [150] the stress intensity factor at the surface and the deepest point the defect was evaluated..
2. The number of cycles required to grow the crack into the plate thickness by a specified amount, normally 1-2mm, was then calculated utilising a suitable fatigue crack growth law. In this case Paris law constants were taken from [250] which had been determined for the same batch of material. The law utilised was:

$$\frac{da}{dN} = 8.02 \times 10^{-12} \Delta K^{2.92} \quad \text{m/cycle} \quad (92)$$

This was the mean line for the specimens tested.

3. The crack growth at the plate surface was then calculated using the stress intensity factor from (1) and the number of cycles from (2) in equation (92). At the end of this step the crack shape was re-defined.
4. The applied stress range was then modified for the beach marking cycle block by increasing the minimum stress to what had previously been the mean while the peak stress was maintained constant.
5. The applied stress intensity factors at the deepest point and at the

plate surface were then calculated for the defect shape at the start of the beach marking block and the number of cycles required to propagate the crack by 0.1mm calculated. 0.1mm was thought to be sufficient crack growth to produce a visible beach mark.

6. The stress range was then re-defined for the main crack growth cycle block.

7. The defect shape was then updated prior to the start of the next increment of crack growth, that is return to step (1).

Figure 8.2 shows the stress history for the beach marking process schematically.

The test on the plate was then conducted according to the cycle limits defined from the above algorithm. A stress ratio of 0.1 was utilised throughout the tests and care was taken to maintain a peak stress intensity factor of less than  $30 \text{ MPa}\sqrt{\text{m}}$  in order to maintain linear elastic conditions. Both tests were conducted using an ESH servo hydraulic testing machine using a standard three point bending rig and a loading frequency of 20 Hz.

After the defects had grown past coalescence, observed by the meeting of the crack tips at the plate surface, and the final single crack shape had been given time to develop the test was stopped. The specimens were then cooled in liquid nitrogen and fractured to reveal the fatigue crack surface. Fractographs were made using a medium format camera to allow accurate measurement of the beach mark separation.

### **8.3 Results**

The beach marks on the first specimen were extremely faint, particularly during the early part of the crack growth. Why this occurred was not clear, however the test was paused over night and it may have been possible that the crack surface was either damaged when the specimen was unloaded or that the beach marks were lost due to corrosion effects on the new surface.

For this reason there were only limited data which could be extracted from the first specimen. The available results have been presented where possible.

Figure 8.3 shows the two specimen surfaces and identifies the starter notches, the point at which the defects coalesced and the final, coalesced crack.

Three regions of interest were identified for analysis and presentation of results, Figure 8.4. These were the growth of the initial defects through the thickness of the plate, the growth of the initial defects at the plate surface both towards each other and towards the plate edge and finally the development of the final crack shape after the two defects coalesce.

Figure 8.5 shows the defect growth into the plate thickness. The crack length axis has been normalised by the plate thickness and the cycles by the total number of cycles in the test, in order to present the data from both tests on a single graph. As mentioned above only limited data was available for test 1. Data has been presented for both individual defect deepest points and the 'line of coalescence', ie. the growth from the point at which the defects coalesced into the plate thickness. The line of coalescence growth becomes the deepest point growth of the final coalesced crack after coalescence.

Figure 8.6 presents the defect growth along the plate surface before, during and after coalescence, no data was available from the first test for the surface growth.

## **8.4 Analysis and Discussion**

### **8.4.1 General Observations from Fracture Surfaces**

Some general observations were possible from simple examination of the fracture surfaces. These have been shown in Figures 8.3, 8.7 and 8.8. Qualitatively Figure 8.3 shows no indication of distortion of the semi-elliptical shape of the individual defects as may have been expected if significant

interaction had occurred. Figures 8.7 and 8.8 show indications of shear lips on the fracture surface. It was observed that on both specimens coalescence appeared to occur by a final shear process, seen as a line on the fractographs where coalescence occurred. Several of these shear areas were also observed along the starter notches as demonstrated in Figure 8.8. In both specimens the defects apparently grew co-linearly until the last few millimetres before coalescence at which point they turned to grow past each other and coalesced by a shear process as they overlapped. This behaviour has been shown schematically in Figure 8.9. No obvious explanation for this was apparent other than that coalescence by shear may be energetically more favourable and that this may cause the observed behaviour. Similar shear lines along the starter notch fronts, Figure 8.8, were attributed to coalescence of several smaller defects which initiated along the notch prior to formation of the single defect. In fact, the same coalescence behaviour as at the centre of the plate.

The first beach mark after the coalescence, Figure 8.7, showed that the crack had a re-entrant shape at this stage as would be expected. Propagation of this re-entrant corner into the plate thickness would appear to have been extremely rapid in comparison with the growth at the individual defect fronts such that the final, single crack shape formed very rapidly after the defects first coalesced.

#### **8.4.2 Analysis of Crack Growth Behaviour**

Observations regarding the crack growth rate through the thickness were substantiated by the crack growth behaviour shown in Figure 8.5 for both tests where the 'line of coalescence' growth merges with the individual defects almost immediately.

Figure 8.6 shows that there was apparently no interaction at the surface of the plate. The growth of the defects towards the free edges of the plate overlays the growth of the defects towards coalescence. Defect 1 showed a marginally slower growth rate towards the free surface than defect 2, this was attributed to uneven initiation around the notch periphery which resulted

in defect 1 lagging a little in this direction. No dramatic acceleration of the adjacent tips was observed as may have been expected from the guidelines of PD6493.

Figure 8.10 shows the variation of the stress intensity factor at the deepest point of the individual defects and at the line of coalescence as the defects propagated into the plate before, during and after coalescence. Superimposed on the figure is the stress intensity factors calculated utilising the Newman Raju solution for single defects of the same aspect ratio and depth as those measured. Although there was some discrepancy between the experimental and calculated stress intensity factors during the early stages of growth, the agreement is generally good. The discrepancy during the early stages can be explained by the irregular initiation behaviour indicated by the shear marks along the notch front.

On this basis it would appear that reasonable agreement was obtained after stable defect geometries had formed. The stress intensity factor at the deepest point of the two defects decreased as coalescence approached, coalescence occurred when both defects had an aspect ratio of approximately 0.4. Following coalescence the stress intensity factor at each crack tip rose with increasing crack depth. At the point of coalescence the stress intensity at the re-entrant sector of the crack was extremely high. A rapid reduction in the stress intensity factor at this point was then observed as the depth at this point increased rapidly towards that at the centre lines of the starter notches, Figure 8.5. As the three points approached the same depth the stress intensity factors merged towards similar levels. The point where these three lines merge on Figure 8.10 effectively defines the completion of the coalescence process as the stress intensity factor distribution around the crack front returns to that for a single crack. As before the agreement between the calculations and the experimental data for the stress intensity factor was shown to be satisfactory even though no attempt was made to model defect interaction indicating that any interaction effects were at best second order.

In order to assess the possibility of predicting the coalescence behaviour

using simple procedures based on existing knowledge, the crack shape development was predicted and compared to that observed in the experiments. Two predictive techniques were utilised for this study.

The first prediction utilised the solution of Newman and Raju in conjunction with the fatigue crack growth law given in (92). For the purpose of the prediction it was assumed that there was no interaction between the adjacent defects. The stress intensity factors were evaluated at the deepest point and at the intersection with the plate surface for the individual defects and the defect depths were then extended by a small increment into the plate thickness. Equation 8.1 was then utilised to determine the required number of cycles to produce the increment of crack growth at the deepest point and subsequently to re-calculate the crack surface length based on the evaluated stress intensity factor and the determined number of cycles. This procedure was repeated until the defects were predicted to touch at the adjacent crack tips. At this point the defects were recharacterised as a single semi-elliptical crack of the same depth as the individual defects and with a surface length equal to the combined length of the two.

In addition a prediction of the defect shape development was made using the empirical model presented by Iida [217, 242, 243], and described in section 5.6 for single defects. Briefly the model describes the developing aspect ratio for defects with initially low aspect ratios by :

$$a/c = (A - B.a/t)(1 - (e/c)^n)^{1/n} \quad (93)$$

Where

$$\begin{aligned} A &= 0.92 + 0.03R_b \\ B &= 0.10 + 0.80R_b \\ R_b &= \Delta S_b / (\Delta S_m + \Delta S_b) \end{aligned}$$

$\Delta S_b$  and  $\Delta S_m$  are the bending and membrane stress components respectively,  $n$  is an empirical constant given as 2.8 and  $e$  is a constant

determined from the initial conditions.

Figure 8.11 shows the resulting predictions superimposed on the experimental data. The data from the two individual defects deviate slightly as they propagate into the thickness of the plate. This behaviour may be explained by the initiation procedure for each defect along the notch fronts resulting in marginally different aspect ratios developing in the early stages of growth. The prediction based on the Newman Raju stress intensity factor solution lies between the two experimental data sets and was therefore considered to provide an excellent prediction. The Iida model predicted the early stages of growth well but slightly overestimated the aspect ratio as the crack depth increased and consequently predicted coalescence at a slightly greater defect depth. Coalescence of the two defects appears as a step change on the figure as the aspect ratio of the final coalesced crack in the tests was determined by bounding the entire crack in a similar way to that used to coalesce the cracks in the predictions. Both of the predictions essentially coincided for the coalesced crack shape and lay very close to the experimental data.

Both the predictions and the data presented in Figure 8.11 appear to show the initial defects and the final crack growing towards a similar preferred aspect ratio of the type presented in section 5.6 and observed in [132]. This behaviour has been discussed further with respect to the ASME guidelines below.

The success of the predictions would again indicate that the interaction between the adjacent defects was a minor effect since neither model included any allowance for interaction.

#### **8.4.3 Comparison with Existing Procedures**

In order to determine the significance of the results reported above they were evaluated with respect to existing practices. Section 6 outlined the main approaches to be considered. Only PD6493 and ASME XI have been utilised for this comparison, the R6 offers more scope for variation, including

full analysis of the actual situation and was not utilised here.

The methodology given in British Standards PD 6493 directs that if the bending stress component is greater than twenty percent of the total stress then the defect should be recharacterised as an edge crack. Hence for the experimental work considered here there was no coalescence to consider and both defects were enveloped by a single edge crack. Solution 1.1.21 from [6] was utilised to determine the stress intensity factor for the recharacterised defect geometry. The defect was then propagated incrementally by assuming 0.1mm growth, calculating the number of cycles required to produce this growth using (92), re-calculating the stress intensity factor and repeating until the edge crack reached the same depth as the final crack shape.

Figure 8.12 shows the resulting crack growth prediction superimposed on the experimental data for growth into the depth of the plate. Using this procedure the recharacterised crack was predicted to reach the same depth as the experimental defects in approximately two hundred and thirty thousand cycles. By comparison the test was halted after approximately seven hundred and sixty five thousand cycles.

ASME XI assumes that the aspect ratio of semi-elliptical cracks will stay constant as they propagate and that coalescence will occur when the gap between the two defects is equal to twice the depth of the deepest. The procedure indicates that the maximum stress intensity factor around the crack front should be evaluated and that this should then be utilised to calculate the fatigue crack growth rate. Using these guidelines as a basis and a crack growth procedure similar to that described above, a prediction of the crack propagation rate into the plate thickness was made. The Newman Raju solution was utilised to calculate the stress intensity factor around the crack periphery for the purposes of the prediction.

The ASME XI prediction has also been superimposed on to Figure 8.12. Coalescence was predicted to occur after approximately eighty thousand cycles and at a crack depth of 3.8mm. Failure occurred, defined by  $c/b = 0.85$

ie. when the surface length of the crack was equal to 85% of the plate width, after approximately one hundred and twenty four thousand cycles and at a crack depth of 5.8mm. In the experiment coalescence of the defects occurred after approximately six hundred and sixty five thousand cycles and when the individual defect depths were approximately 10mm and the test was stopped after seven hundred and sixty five thousand cycles.

Clearly both of the predictions based on existing methodologies significantly under-estimated the duration of the test, PD 6493 by a factor of 3.3 and ASME XI by a factor of 6.2. The possible consequences of such over conservatism could be considerable when applied to high integrity plant. For example if an assessment was done on a power station component which was required to last for twenty years then on the basis of ASME it would have to actually be suitable for one hundred and twenty four years in order to be considered fit for purpose. Such an example is extremely crude but it does demonstrate a valid point. A more realistic consideration would be the sentencing of defects found during in-service inspection. Often defects are found during the routine inspection of plant and critical decisions must be made as to whether the plant must be shut down immediately or whether it is acceptable to continue operation until the next scheduled shutdown when repairs can be undertaken. The commercial implications of these decisions are important. If an offshore platform had to close down production outwith a scheduled programme the loss in production alone could amount to many millions of pounds per day. It is perhaps in this circumstance that the limitations of current procedures must be viewed as unacceptable.

Both methodologies significantly under estimated the aspect ratio of the growing defects and coalesced crack shape. PD 6493 was the most dramatic in that no consideration for finite defect surface length was given due to the recharacterisation procedure. ASME XI also significantly underestimated the aspect ratio due to the fixed aspect ratio growth stipulation. It was however noted that if the initial defects had been of a higher aspect ratio the ASME prediction would have resulted in a much shorter final crack size, although the defects would have been coalesced earlier. This poor prediction of aspect ratio could also have significant

implications for defect assessment. By over estimating the defect surface lengths leak-before-break conditions would be unlikely to be met. That is where a defect may have been sentenced as acceptable, at least until a convenient repair opportunity, due to the fact that it would not result in catastrophic failure of a component but only a leak condition would be deemed as critical. Conversely for defects of higher aspect ratios a leak condition may be predicted due to the under estimate of crack surface length when in fact fracture would occur.

#### **8.4.4 An Alternative Prediction**

Due to the apparent inadequacy of the above methodologies for the prediction of coalescing behaviour an attempt was made to predict the experimental results utilising the Newman Raju stress intensity factor solution and the fatigue crack growth law given as equation (92) above. In making the crack growth predictions the finite width correction was determined from each of three methods :

i)  $f_w$  was calculated by specifying the plate width for the single defect as the distance from the notch centre line to the edge of the plate.

ii)  $f_w$  was calculated by specifying the plate width as the distance from the notch centre line to the middle of the ligament between the two defects ie.  $b=c+L$ .

iii) To determine the significance of the finite width correction on the single defect growth  $f_w$  was determined based on a single defect in the centre of the plate.

In all cases the defects were assumed to coalesce when they touched. Coalescence was assumed to occur instantly such that the coalesced defect could be considered as a single semi-elliptical crack with depth,  $a$ , equal to that of the single defects at the point of coalescence and surface length,  $2c$ , equal to the combined length of the single defects.

All three predictions have been superimposed on Figure 8.12. All three predicted a significantly shorter life than that observed in the test, a maximum of six hundred and ten thousand cycles compared to seven hundred and sixty five thousand in the test. Evaluation of  $f_w$  based on methods (i) and (iii) produced very similar results with only a small deviation during the later stages of growth, the prediction based on (ii) was similar during the early stages but deviated after approximately 50% of the predicted life.

The developing aspect ratio predicted by all three methods was identical. It is important to recognise that an accurate prediction of the developing aspect ratio, Figure 8.11, does not mean that the predicted life will also be accurate. Due to the aspect ratio prediction, all three methods predicted identical defect depths at coalescence and identical behaviour following coalescence. The defect depth at coalescence was predicted as 11.9mm compared with approximately 10 and 11mm for the two defects in test 2 and approximately 11.6mm in the first test.

It was not expected that the life would be under estimated by these predictions. No interaction effect was assumed other than the finite width correction utilised in (ii) which produced an under estimate of life of approximately 36%. Even the prediction which assumed a single defect in the centre of the plate for the calculation of  $f_w$ , (iii), under estimated the life by approximately 20%. The reason for this apparent conservatism in the predictions was not clear. The predictions and the experimental data deviated from very early in the life. In particular the experimental crack growth into the thickness appears to slow between 230-350 thousand cycles. It may be possible that the specimen was inadvertently overloaded at this point leading to retardation of the crack growth, however no overload was observed during the test. A beach marking cycle block was included at 230000 cycles and the problem could have occurred there although great care was taken. An alternative explanation can be found in the form of the crack initiation around the notch fronts. The shear lines around the notch periphery, Figure 8.8, were thought to represent the coalescence of several small defects which initiated at different points along the notch front. This

behaviour had not been fully resolved by three hundred thousand cycles as can be determined by counting the beach marks with respect to the data points of Figure 8.12. The decrease in crack growth rate and consequently the surprisingly long test duration may have been a result of this initial defect formation.

Qualitatively the predicted curve shapes were of the same form as the experimental data. The sharp increase in crack growth rate at coalescence was accurately predicted and the defect depth at coalescence and aspect ratio was well predicted. In any case the predictions represented a considerable improvement over those based on the methodologies of PD 6493 or ASME XI. Prediction of the aspect ratio may provide some significant advantage when assessing leak before break type problems as discussed above. Further work would be required to verify the life prediction, although on the basis of this data assuming an individual defect in a plate with a free surface at the middle of the ligament between defects would appear promising.

## **8.5 Conclusions**

1. Experimental evidence has been presented which supports the finding of the previous chapter that defect interaction is a second order effect.
2. A considerable magnification of the stress intensity factor at the re-entrant crack sector immediately after coalescence results in rapid propagation and formation of the final stable crack shape. The rate at which the final crack shape is formed is rapid enough that this stage can be ignored for predictive purposes.
3. BS PD 6493 and ASME XI procedures for assessing and propagating co-linear cracks have been demonstrated to be unrealistic and extremely conservative.
4. A prediction based on the Newman Raju stress intensity factor results was shown to provide improved predictions.

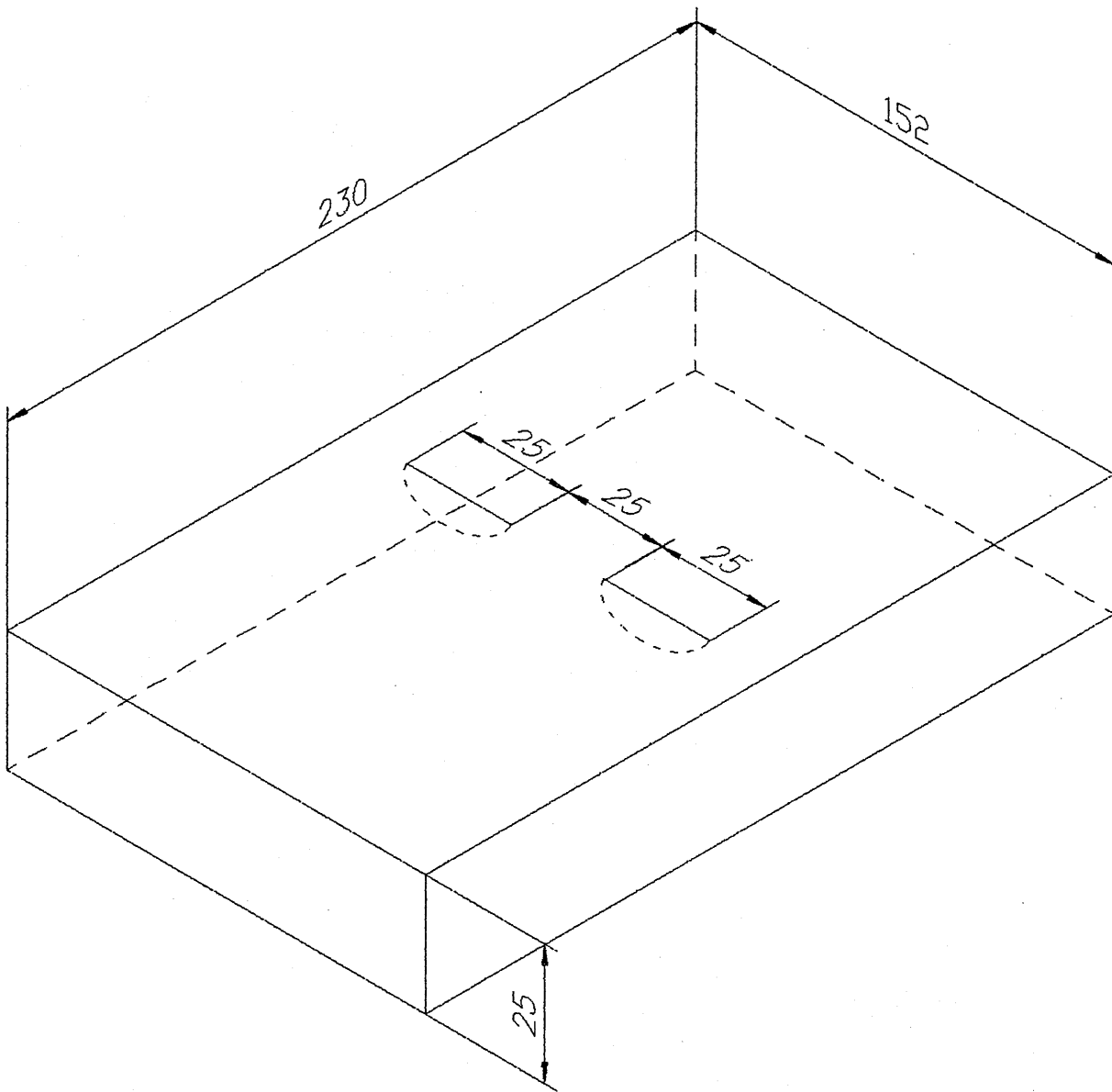
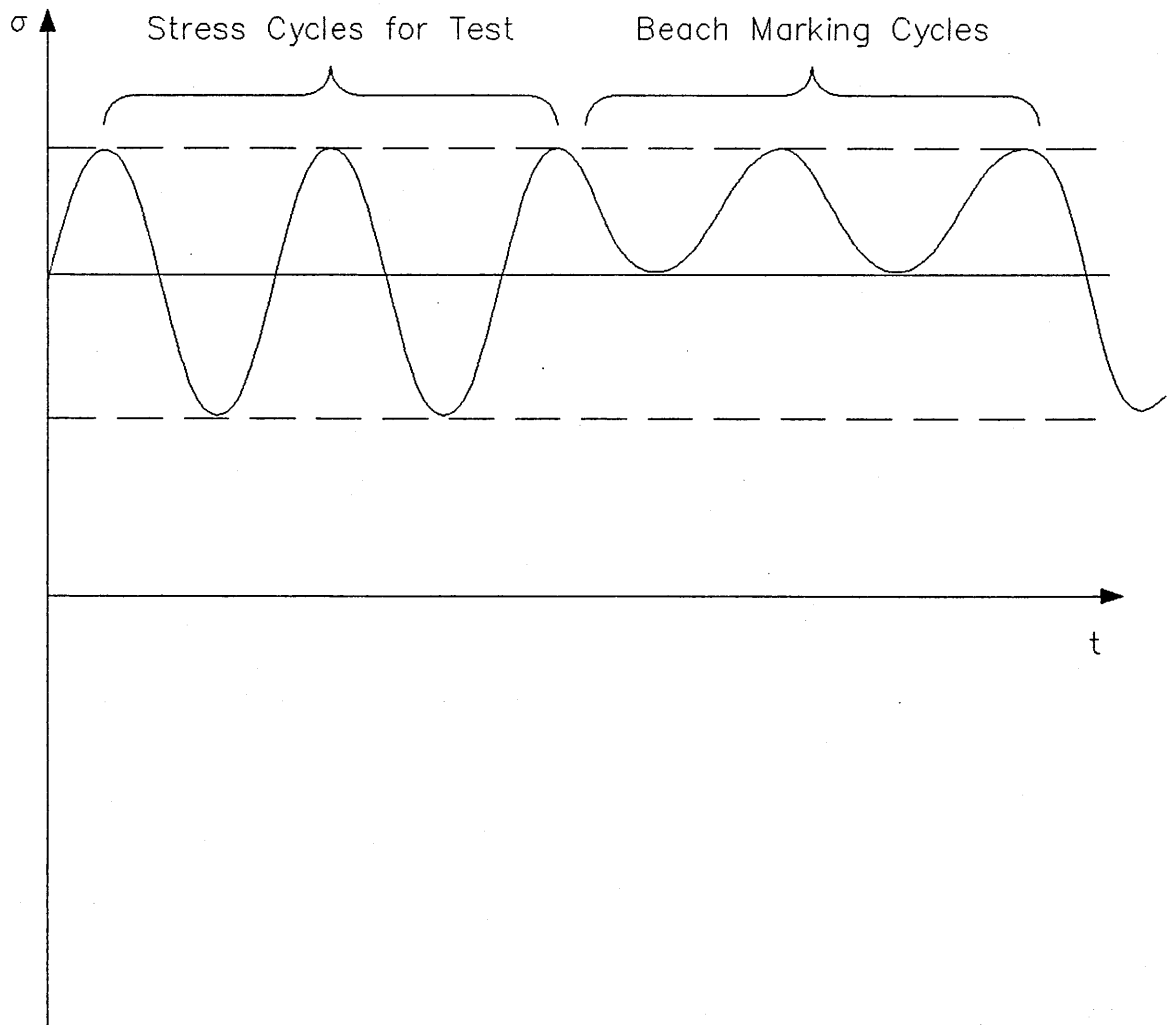


Figure 8.1



Beach Marking Method

Figure 8.2

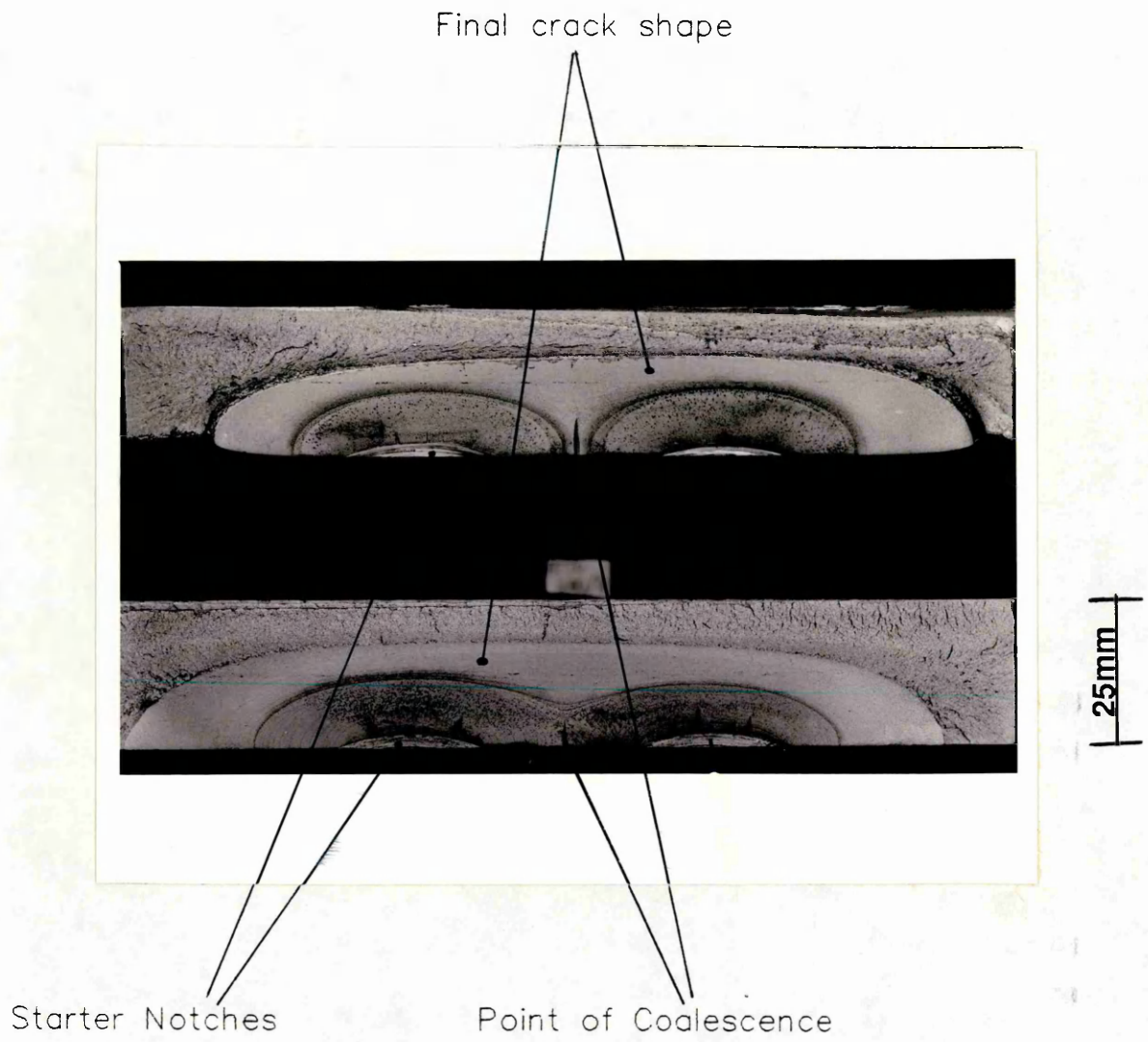
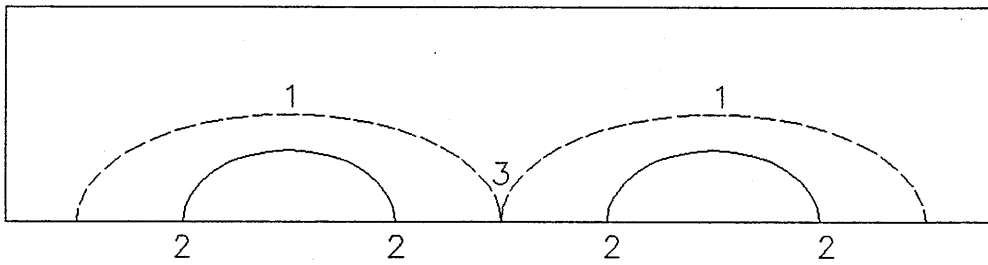


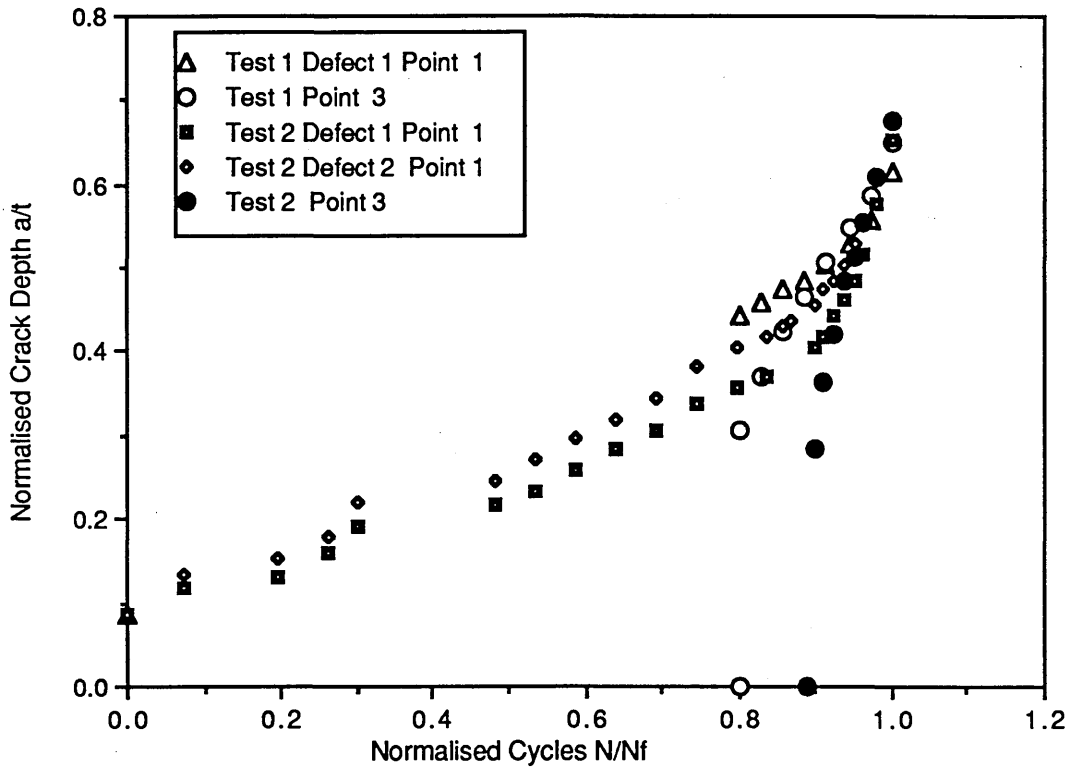
Figure 8.3



1. Individual Defect Growth Into Plate
2. Growth at Plate Surface
3. Growth at the Point of Coalescence .

Regions of Interest on Fracture Surface

Figure 8.4



**Defect Through Thickness Growth**

**Figure 8.5**

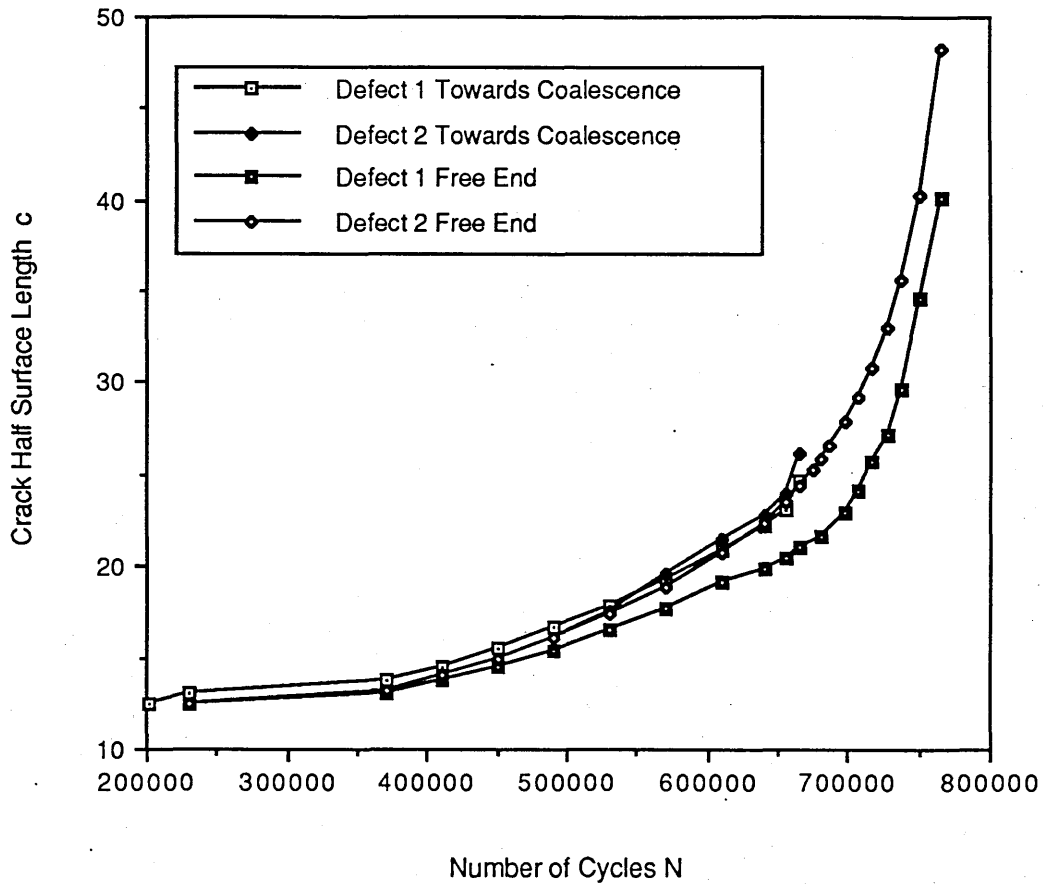
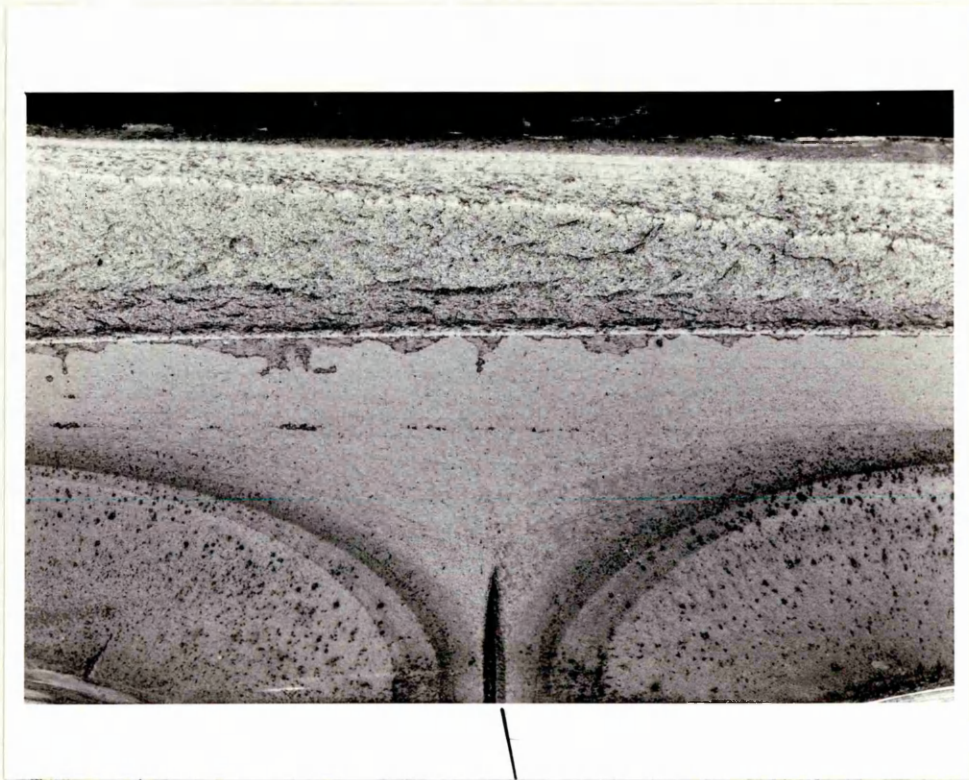


Figure 8.6

25mm



Shear lip at point  
of coalescence

Figure 8.7

25mm



**Indications of Multiple Initiation Around Notch**

Figure 8.8

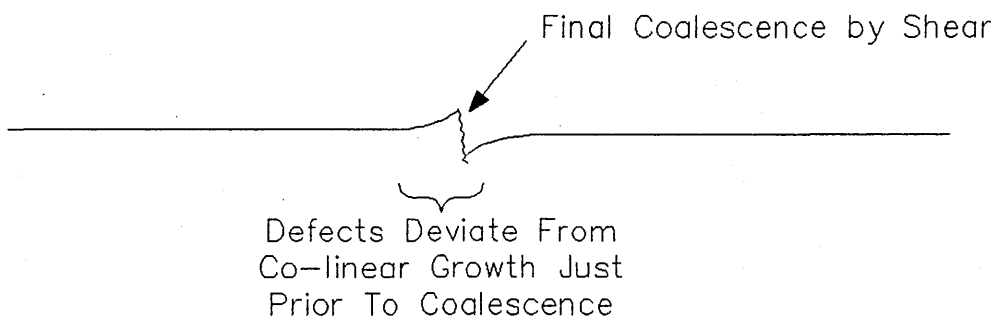
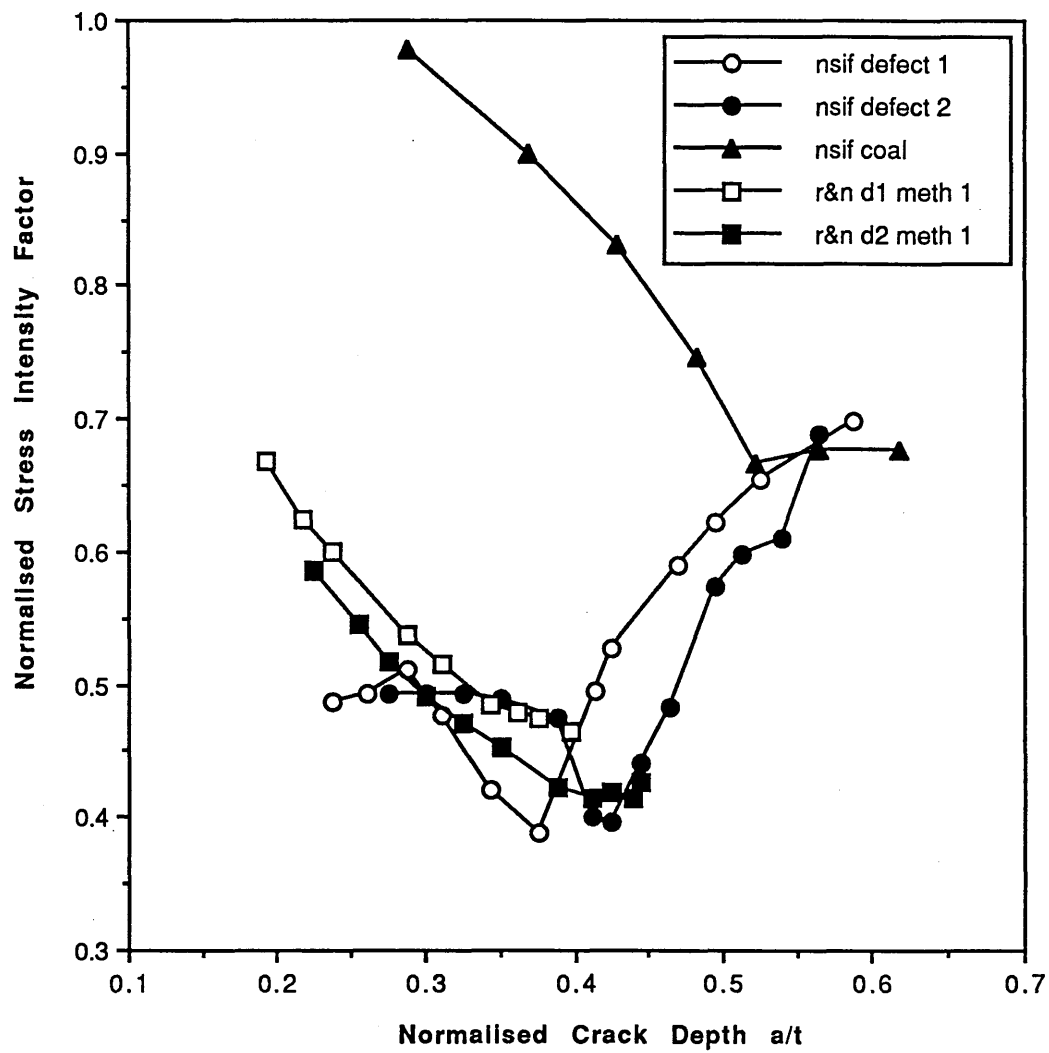
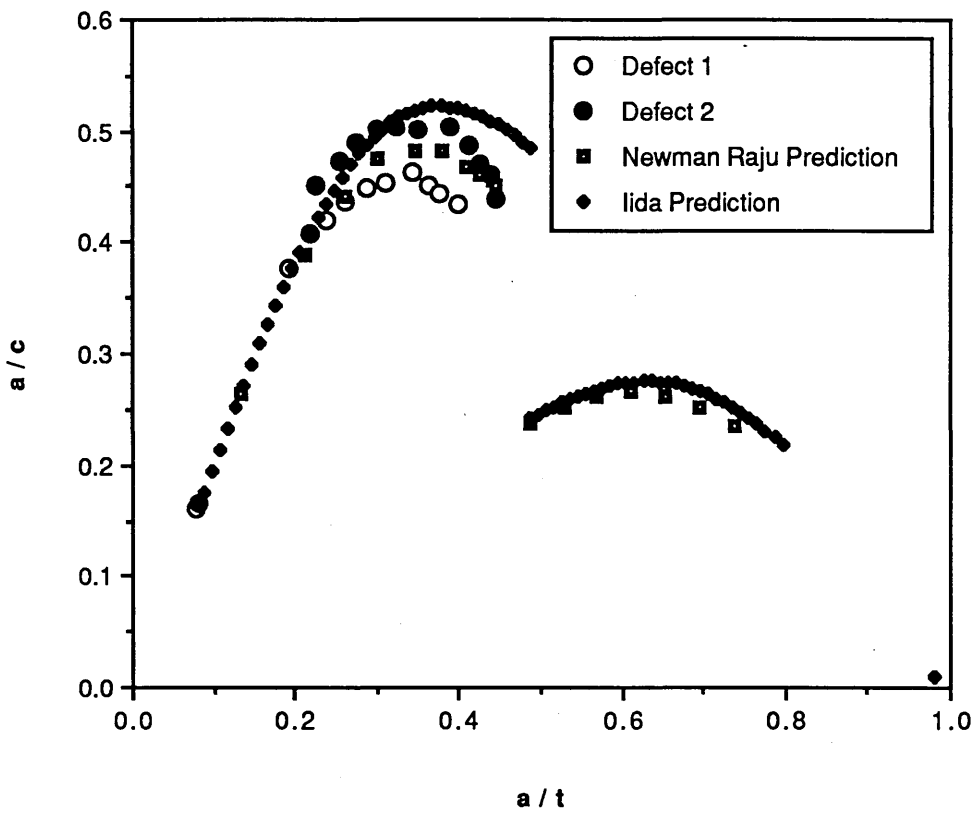


Figure 8.9



**Stress Intensity Factor Development  
at Defect Deepest Points**

**Figure 8.10**



**Aspect Ratio Development**

**Figure 8.11**

# Crack Growth Into Thickness Comparison With PD6493 and ASME XI Defect Geometries

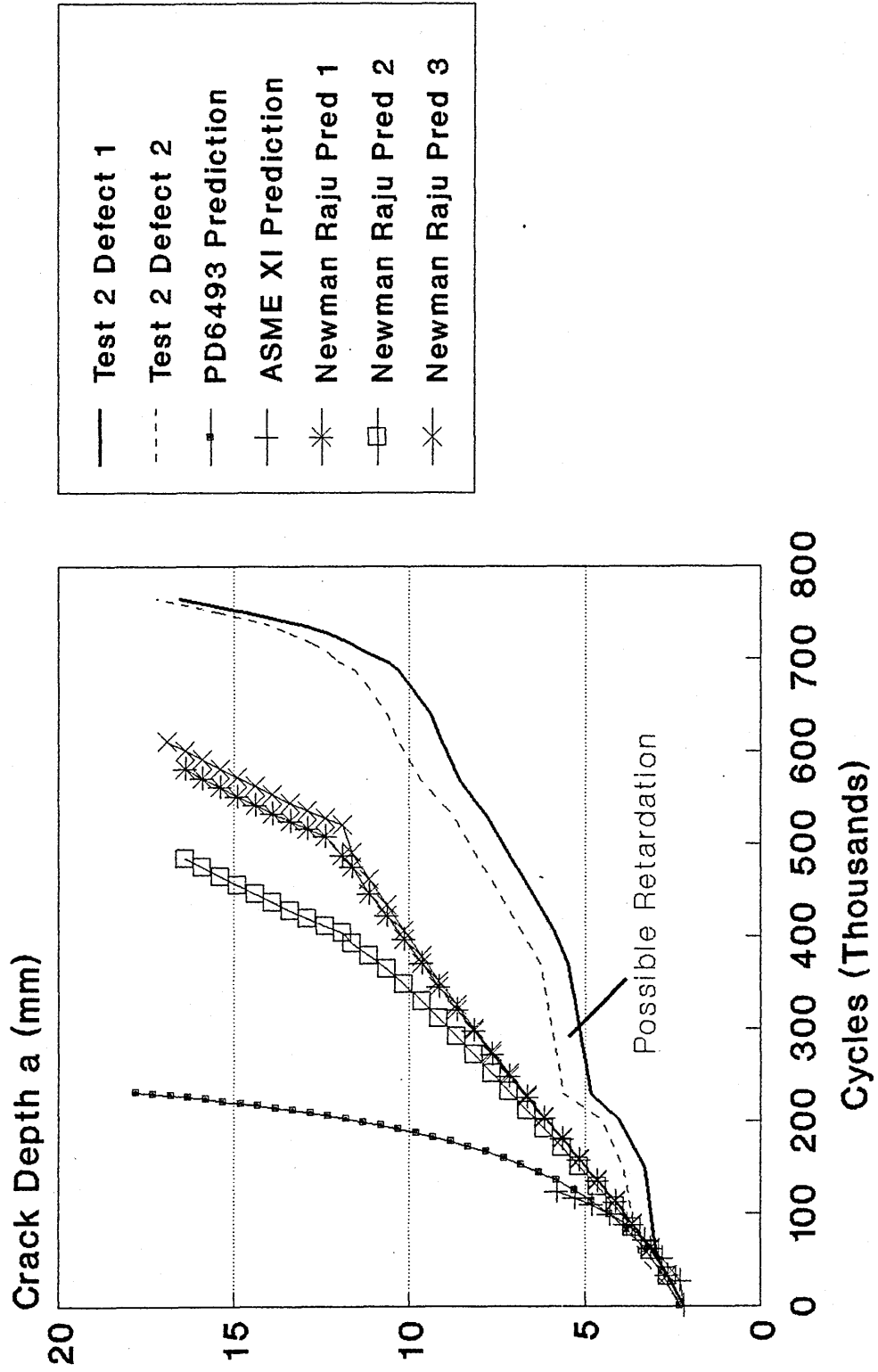


Figure 8.12

## **CHAPTER 9**

### **A NUMERICAL STUDY OF THE STRESS INTENSITY FACTOR DISTRIBUTION AROUND A CRACK IMMEDIATELY AFTER COALESCENCE**

#### **9.1 Introduction**

During the experimental investigation of defect coalescence a considerable magnification effect on the stress intensity factor at the re-entrant sector of the newly coalesced crack was observed. This sector then propagated rapidly into the plate thickness to produce a single semi-elliptical crack geometry. As the semi-elliptical crack shape was approached the stress intensity factor at the re-entrant sector reduced to a magnitude consistent with the rest of the crack front. This behaviour was of some interest as it provided the basis for the assumption that a predictive technique may be developed in which defects are combined to form a single semi-ellipse as soon as the adjacent tips meet. In order to gain further insight into this behaviour a numerical study was undertaken to determine the stress intensity factor distribution around the crack front immediately after coalescence.

Two numerical methods were chosen for this investigation. Firstly the line spring method was selected due to the ease with which the crack shape could be defined within the model. In addition the universal weight function or  $O$ -integral technique of Oore and Burns [116,117] was utilised. Two independent techniques were chosen due to the irregular defect shape to be analysed in the hope that some consistency between the two solutions would validate the results. Although the line spring methods applicability to surface crack problems has been widely confirmed for elliptical cracks there are very few solutions for irregular defects. Similarly, although irregular defects were analysed by Oore and Burns in their original papers [116,117]

little validation of this solution is available.

The crack geometry analysed was taken from the first beach mark after coalescence for the second test specimen as described in Chapter 8. By adopting this defect shape, comparison with the experimental results for the bending load case was possible and provided a further source of validation.

This Chapter describes the methodologies adopted and the assumptions made, particularly with respect to the weight functions method. Results have been presented for the re-entrant crack geometry under both tension and bending. Where relevant, comparisons have been made between these results and the experimental data presented in Chapter 8.

## **9.2 Numerical Models**

### **9.2.1 Line Spring Model**

The line spring model was formulated using the philosophy described in Chapter 7 for the defect interaction study, with the exception that in this case the depth specified at each line spring element was determined from the beach marked specimen. As before a quarter plate model was possible through the use of symmetrical boundary conditions and the ABAQUS symmetrical line spring elements. A total of one hundred and twenty two generalised eight noded second order shell elements were utilised in the mesh. As in the defect interaction study loading was applied along the top edge of the plate. Both fixed displacement and uniform stress boundary conditions were applied in both tension and bending cases.

### **9.2.2 Universal Weight Function Model**

The generalised weight function concept was introduced in section 3.6.1 as a methodology formulated for use in the analysis of irregular defect problems. In order to utilise this methodology a numerical procedure must be developed to solve the so called 0-Integral equation given as equation (37) and repeated here :

$$W_{QQ'} = \frac{K_{P\alpha\alpha'}}{P_Q} = \int \int_A \frac{\sqrt{2} \sigma_Q dA_Q}{\pi l_{QQ'}^2 \left( \int_s \frac{ds}{\rho_Q^2} \right)^{1/2}} \quad (37)$$

In this work (37) was solved in two stages. Initially a model of the crack geometry to be analysed was created utilising the FEMGEN finite element pre-processor. It should be noted that the 0-integral is only applicable to embedded defects and for surface cracks a full geometry was created by reflection about the free surface as shown in Figure 9.1. A mesh of quadrilateral elements was then created over the crack surface with the elements getting progressively smaller towards the crack periphery. Refinement towards the crack periphery was included to account for the sensitivity of the solution to the evaluation of the  $1/l_{QQ'}^2$  term. Figure 9.2 shows the quantities from equation (37) which must be evaluated in the solution. For the purposes of this analysis the stress intensity factor was evaluated at every node on the crack perimeter. The first step in the solution procedure was to evaluate the area of each element as  $dA_Q$ , with point Q assumed to be the centre of the element, and the line integral term associated with that particular area segment. This information was then stored along with the coordinates of the element centroid.

In the second stage of the analysis the required stress distribution was specified and  $\sigma_Q$  evaluated to determine  $K_Q$  for each node around the crack periphery. Splitting the procedure into two steps in this manner allowed a number of stress distributions to be considered without the need for re-evaluation of the area parameters for the crack geometry. Several magnification factors could also be utilised in the second stage by specifying different plate thicknesses or widths for use in the solution..

In order to apply the universal weight function technique to surface crack problems corrections must be applied to account for the proximity of free surfaces and finite areas as discussed in section 4.3.4. The hypothesis presented by Oore and Burns was that the ratio of the stress intensity factor

for an embedded crack to that of a surface crack of the same half geometry and loading was a constant independent of crack shape. Hence :

$$\frac{K_{su}(\theta)}{K_{eu}(\theta)} = \frac{K_{isu}(\theta)}{K_{ieu}(\theta)} = \frac{K_{isv}(\theta)}{K_{iev}(\theta)} \approx \text{Constant}$$

where subscript 's' represents a surface crack, 'i' an irregular crack, 'e' an embedded crack, 'u' uniform loading and 'v' arbitrary loading. To apply the solution of the 0-Integral to the case of a surface crack it was necessary to determine the above correction. On the basis that the correction is the same irrespective of crack geometry the Newman Raju solution was utilised to determine the correction using the following method.

Newman Raju present the solution for the stress intensity factor for a surface crack under uniform loading as :

$$K = \sigma\sqrt{(\pi a/Q)}.F(a/t, a/c, c/b, \theta)$$

within the expansion of F there is a function  $f_{\theta}$  which determines the angular variation of K around the crack front.

$$F = (M_1 + M_2(a/t)^2 + M_3(a/t)^4)f_{\theta}g f_w$$

$$f_{\theta} = ((a/c)^2 \cos^2 \theta + \sin^2 \theta)^{1/2}$$

The Irwin solution for an embedded elliptical crack under uniform tension is :

$$K = \sigma\sqrt{(\pi a/Q)}((a/c)^2 \cos^2 \theta + \sin^2 \theta)^{1/2}$$

An alternative representation of the Newman Raju solution would then be :

$$K_{su} = (M_1 + M_2(a/t)^2 + M_3(a/t)^4)g f_w \cdot K_{eu}$$

with subscripts as before. This formulation allows the correction required for the 0-Integral solution to be determined and was adopted in this work.

This correction procedure was included in the second stage of the evaluation procedure described above. Hence once the area parameters had been evaluated for any crack geometry a solution could be determined for any number of surface crack depths under any stress distribution. It was felt that the flexibility offered by this procedure justified the two step method.

In order to validate the numerical procedure developed the stress intensity factor variation around an embedded elliptical crack under uniform loading was evaluated. An ellipse of aspect ratio 0.5 was chosen for this benchmark study. Figure 9.3 shows the comparison between the 0-integral solution and the Irwin solution. In general the solution was acceptable although some oscillation was observed towards the end of the major axis,  $\theta=0$ , this was thought to be due to the relative coarseness of the mesh in this region. The quality of this solution gave confidence in the general methodology for use in the analysis of the re-entrant crack geometry.

In order to analyse the re-entrant crack geometry a model of the crack surface was created and meshed as described above. A total of almost fifteen hundred elements were used to evaluate the 0-Integral. The corrections required to determine the equivalent surface crack solution were obtained using the methodology described above for an elliptical crack of semi-minor axis equal to the maximum depth of the re-entrant crack and semi-major axis equal to half the entire surface length. The surface crack depth,  $a/t$ , was specified as the maximum crack depth along the front,  $c/b$  was determined on the basis of the experimental plate width.

### **9.3 Results**

Figures 9.4 and 9.5 present the results of the numerical analysis of the re-entrant crack shape for tension and bending respectively. The normalised stress intensity factors have been plotted against  $x/c$ , where  $x$  is the distance from the line of coalescence. This axis was chosen in preference to the

parametric angle,  $\phi$ , to avoid ambiguity in its definition for the irregular crack shape. The Newman Raju solution for an equivalent semi-elliptical crack of the same maximum depth and surface length has been superimposed on each graph and the experimental data has been included in Figure 9.5 at the appropriate locations.

#### **9.4 Discussion**

Figures 9.4 and 9.5 show good agreement between the line spring and universal weight function solutions. Both exhibit a peak stress intensity factor at the re-entrant sector as observed from the experimental data. The two solutions apparently diverge slightly towards the point where the crack intersects the free surface for the bending load case. It was thought that this may have been due to some distortion of the grid used for the numerical integration in the 0-Integral evaluation in this region.

The agreement between the experimental data and the numerical results, particularly the line springs, at the re-entrant sector and at the surface intersection was excellent. Some discrepancy was noted at the deepest point of the crack with both analyses apparently over-estimating the stress intensity factor at this point. It is possible that this discrepancy was a function of the analysis of the experimental data at this point. In order to follow the development of the re-entrant sector it was necessary to beach mark the specimen frequently just after coalescence. As a result of this the beach marks at the deepest point of the individual defects became very closely spaced and difficult to resolve accurately. A typical separation was less than 1mm. Errors in measuring the beach mark separation at this point may have resulted in errors in the calculated fatigue crack growth rate and consequently in the estimation of the stress intensity factor. Alternatively part of the discrepancy may have been due to the fatigue crack growth law utilised to evaluate the stress intensity factors from the experimental data being incorrect for the specimen utilised. This explanation was thought to be less probable due to the accuracy of the solution at the re-entrant sector and the surface intersection.

The Newman Raju solutions for the bounding semi-elliptical crack show very good agreement with the line spring solutions along most of the crack length. The re-entrant crack solution deviates from the semi-elliptical solution only over a small region local to the re-entrant crack sector. This observation gave further confidence in the numerical solution and indicated that the misgivings concerning the accuracy of the experimental results at the deepest point as discussed above may be correct.

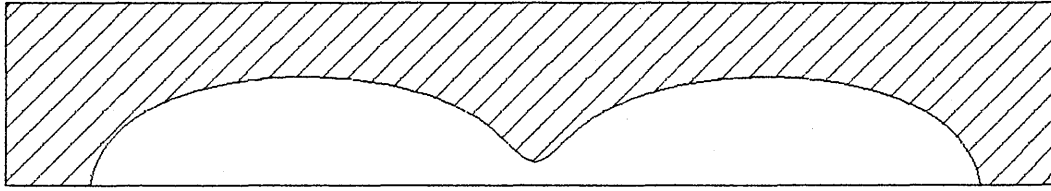
Both numerical techniques clearly predicted the magnification of the stress intensity factor at the re-entrant sector as observed from the experimental data. From this the rapid crack propagation at this region to form a single semi-elliptical crack shape in a relatively small number of cycles could have been accurately predicted from the numerical analysis alone. This result has relevance to two particular areas. Firstly it confirms the proposal presented in the preceding chapter that fatigue life prediction calculations need not consider the coalescence process explicitly due to its short duration. Secondly it may indicate some consequence for defect assessment procedures for brittle materials. If two such cracks coalesced it may be possible that the magnification of the stress intensity factor at the point of coalescence would result in local brittle crack propagation. This problem was beyond the scope of this work but may merit some attention.

A possible explanation for the severity of the magnification of the stress intensity factor at the re-entrant sector may be derived by consideration of the crack face displacements. It was shown in section 4.2 that an embedded elliptical defect under uniform tension will have the maximum stress intensity factor at the end of the minor axis and the minimum stress intensity factor at the end of the major axis. This behaviour is due to the crack face displacements. Given that the displacement at the centre of the crack must be the same on both the minor and major axis the displacement local to the crack tip itself must be more on the minor axis than the major. Since the crack tip opening displacement can be related to the stress intensity factor directly it then follows that the stress intensity factor must be largest on the minor axis. If this argument is then transferred to the re-entrant crack considered in this work then it may be postulated that as soon as the two

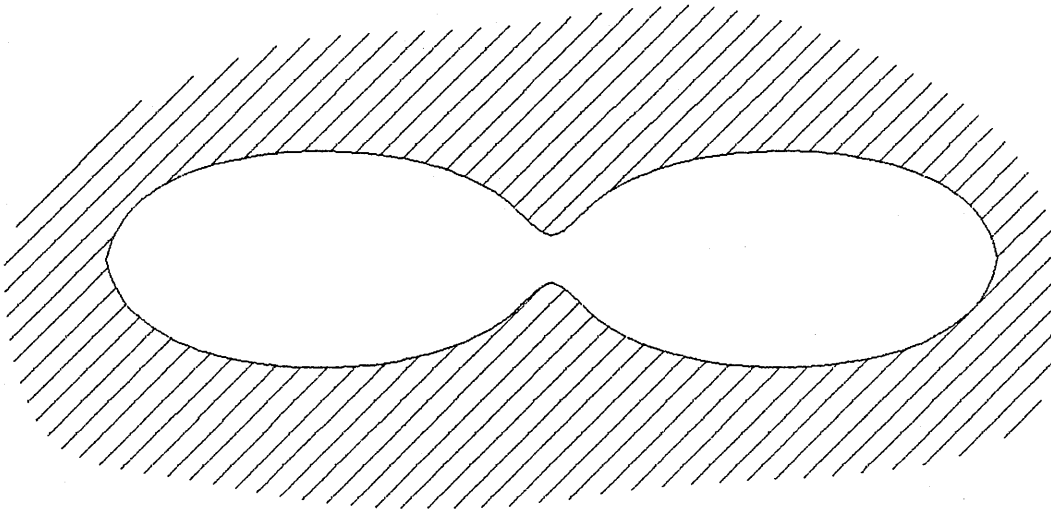
defects coalesce the crack faces along the major axis would attempt to displace in an elliptical form. This displacement would however be restrained due to the short re-entrant sector which, if considered as an edge crack, would adopt a much smaller displacement under the same loading. The resulting displacement would therefore be a compromise between these two and would result in a significant amplification of the local stress intensity factor at the re-entrant sector as observed. A more detailed study would be required to demonstrate this behaviour utilising more involved procedures such as three dimensional finite element modelling. Such models are complex and expensive computationally and were not attempted as part of this work.

## **9.5 Conclusions**

1. A numerical procedure was presented to enable the universal weight function technique to be utilised for the analysis of irregular crack geometries.
2. A numerical study utilising universal weight functions and line spring models was used to predict the magnification of the stress intensity factor at the re-entrant crack sector observed in the experimental investigation.
3. The numerical solutions were verified utilising both the experimental data and the Newman Raju solution for a bounding semi-elliptical crack.

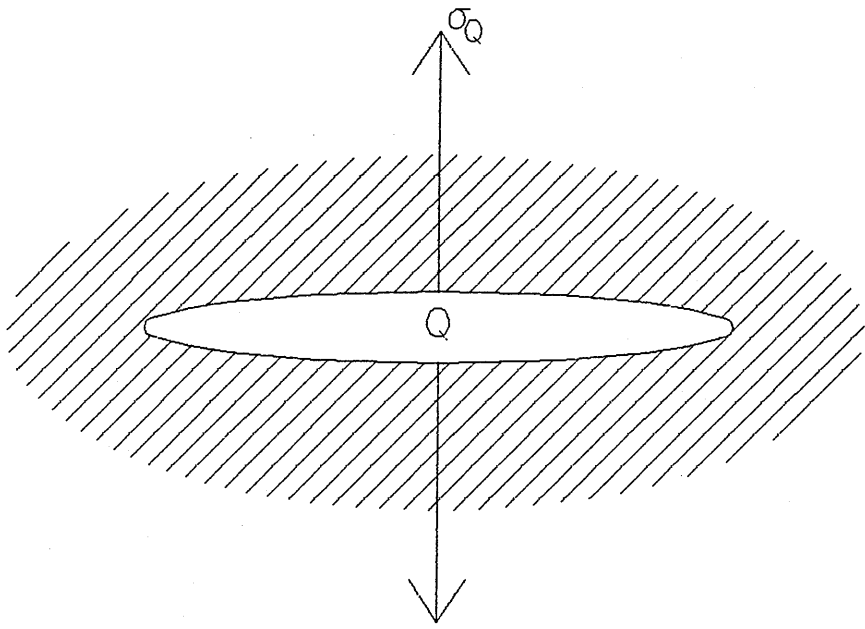
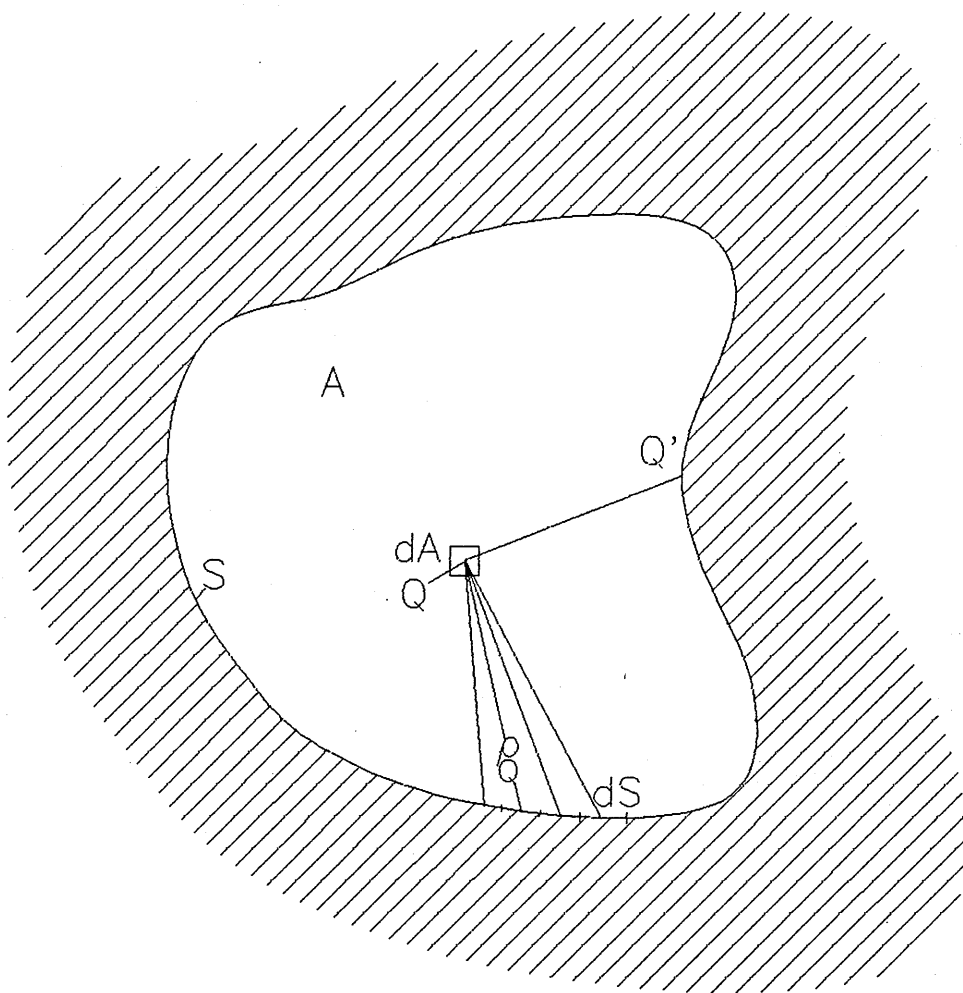


Crack Geometry to be Analysed



Geometry Modelled

Figure 9.1



0 - Integral Terminology

Figure 9.2

# Validation of 0-Integral Elliptical Crack : Tension

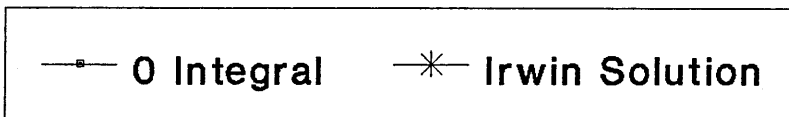
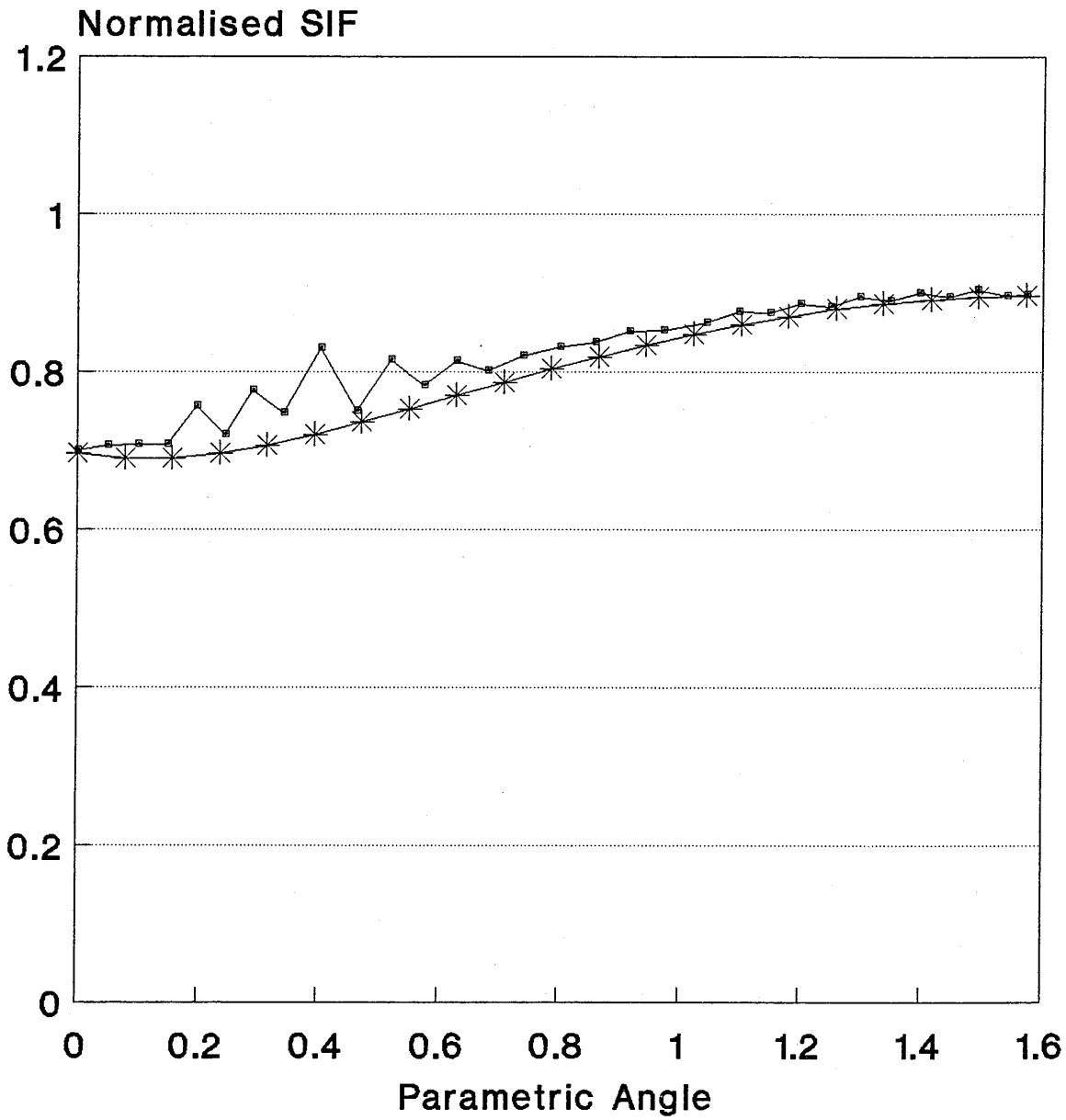


Figure 9.3

### Tension Load Case Results

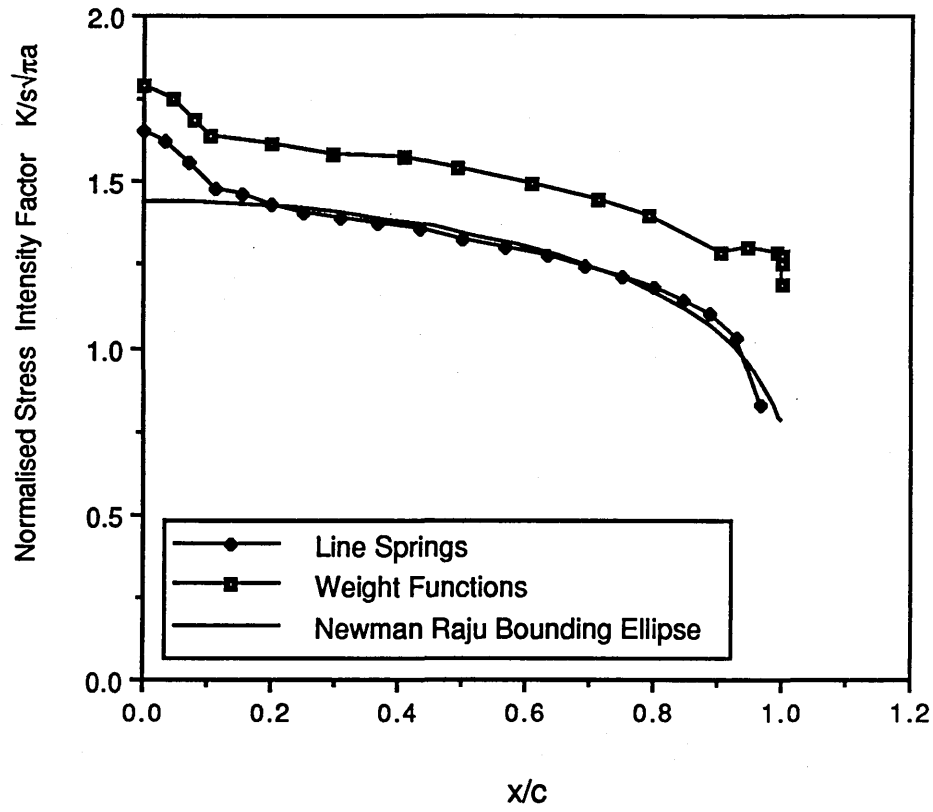


Figure 9.4

### Bending Load Case Results

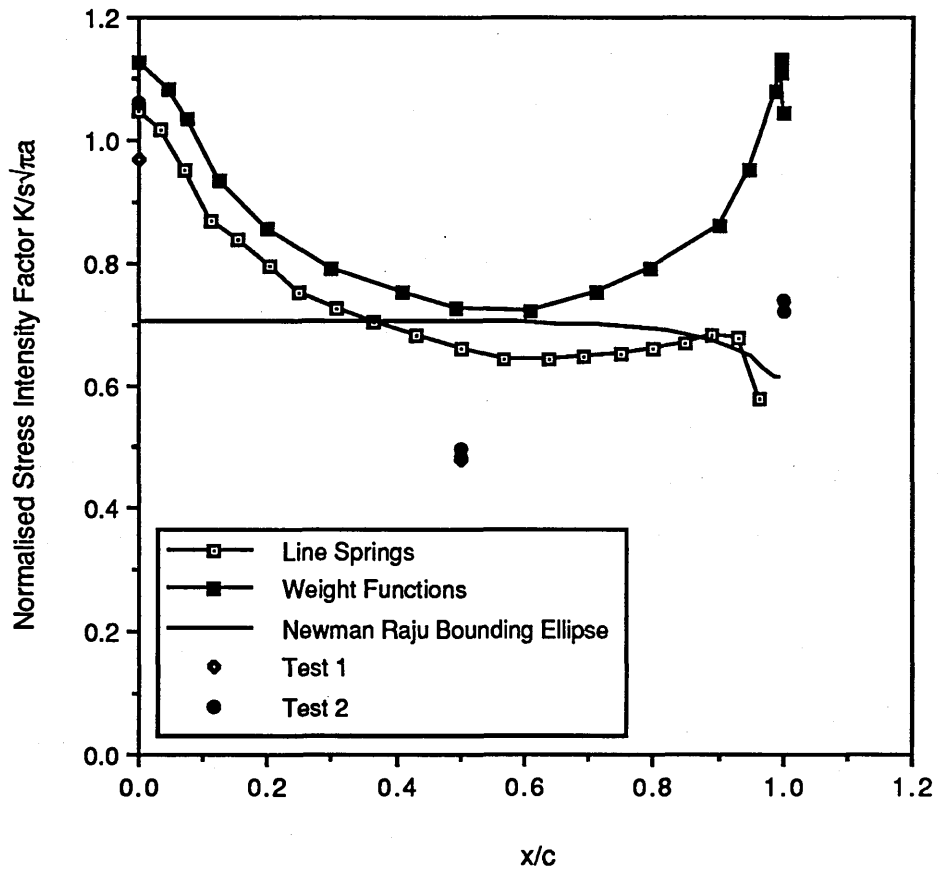


Figure 9.5

## **CHAPTER 10**

### **DISCUSSION AND CONCLUSIONS**

Chapters 7,8 and 9 presented the results of a numerical and experimental investigation of the coalescence of co-linear semi-elliptical defects by fatigue. In this chapter the significance of these results has been discussed prior to drawing the overall conclusions.

The results have been reviewed in three sections. Initially the interaction between defects has been discussed by reference to the numerical and experimental results. A brief discussion of the coalescence process itself has then been presented. Finally, the implications of the results have been discussed in terms of current recommended practice. Possible improvements to these procedures have been indicated where relevant.

#### **10.1 Defect Interaction**

A numerical study of defect interaction was presented in Chapter 7. The line spring model was shown to be an efficient methodology for the analysis of complex surface crack problems. The suitability of the model was demonstrated for aspect ratios ranging from 0.2 to 0.6, and for normalised defect depths,  $a/t$ , ranging from 0.2 to 0.8. It was shown that the interaction between two co-linear defects under tension or bending loads was of the same order as the finite area correction,  $f_w$ . This was supported by the observations from the experimental investigation described in Chapter 8. No enhancement to the fatigue crack growth rate at the adjacent crack tips was observed during the tests indicating that no significant magnification to the local stress intensity factor occurred due to defect interaction. Further, it was found that the developing aspect ratio could be accurately predicted using models which did not consider interaction between the defects. That is, there

was apparently no deviation from the shape development which would have been expected for a single a defect growing under the same loading. The test durations predicted by models which did not consider interaction between the adjacent defects were found to be less than the observed test lives. If significant interaction had occurred between the defects these predictions would have over estimated the test durations. This further supported the finding that the interaction between defects is simply due to the finite area of the test plate.

The combined experimental and numerical results demonstrated that the growth of co-linear defects could be adequately predicted using isolated defect solutions, such as those of Newman and Raju, with an appropriate finite area correction. It was also noted that the ability of any given model to predict the developing aspect ratio did not imply that an accurate prediction of life could be produced. Test durations were predicted in Chapter 8 using three different methods to determine the finite area correction. The results showed variations in the predicted life but identical aspect ratio development predictions.

## **10.2 The Coalescence Process**

The results of the numerical study of the stress intensity factor distribution around the crack periphery immediately after coalescence showed a significant magnification of the stress intensity factor at the re-entrant sector. This was consistent with the observations from the experimental results. It was found that the re-entrant sector propagated rapidly into the plate resulting in the final crack shape developing in relatively few cycles. The stress intensity factors calculated from the beach marks were consistent with those determined from the numerical analysis.

During the coalescence process itself, the two adjacent crack tips were observed to deviate from their co-linear growth during the final few millimeters of growth before combining by a shear process. Similar shear lips were observed around the notch peripheries indicating that the initiation along the notches had occurred at several discrete points resulting in several

small defects which coalesced to form the semi-elliptical defect which grew from the notch.

The high stress intensity factor produced at the re-entrant sector of the crack resulted in rapid propagation of this sector to form the final crack shape. The duration of this process was extremely short when compared to the total test duration. It would therefore be reasonable to consider the coalescence process as instantaneous for the purpose of any predictive model. Both the life predictions and the aspect ratio predictions presented in Chapter 8 would support this proposal. If the coalescence process need not be considered then relatively simple prediction procedures could be developed on the basis of single defect solutions as indicated in 10.1. That is, co-linear defects could be analysed separately and assumed to coalesce to form a bounding elliptical crack as soon as the adjacent tips meet.

The implications of the magnification to the stress intensity factor at the re-entrant sector of the coalescing crack for brittle material may merit some investigation. If the local stress intensity factor was greater than the material fracture toughness then local brittle crack extension could occur. Consequently unstable crack advance may occur along a larger area of the crack front before arresting. Clearly this problem would need to be addressed in the formulation of new models for fatigue life prediction designed to assess multiple crack problems.

### **10.3 Significance With Respect to Existing Procedures**

The relevance of this work must ultimately be assessed against whether it offers any indication towards possible improvements to current procedures. Three current procedures were presented during the discussion of multiple defects in Chapter 6, ASME XI, British Standard PD6493 and the CEGB R6 approach. The R6 approach was the most flexible and included the option of conducting a detailed analysis of the specific problem. Conversely the two 'code' type approaches proposed more rigid rules for the assessment of multiple defects. Since the R6 approach offered no detailed guidance it was not suitable for comparison with the results of this analysis and has not been considered further.

Both PD6493 and ASME XI provide guidance as to how the defect aspect ratio should be controlled as it grows. ASME XI suggests that the aspect ratio should be kept constant irrespective of the loading condition. PD6493 differentiated between applied stress distributions with less than 20% of the total as bending stress, and those with larger bending components. Where the bending stress is less than 20% of the total, the defect surface length is assumed to remain constant and the depth increased until an aspect ratio of unity is reached. A constant aspect ratio is then assumed for the remaining growth. If however the bending stress component is greater than twenty percent of the total, the defect is recharacterised as an edge crack. Both of these procedures were found to be unrealistic. ASME XI significantly underestimated the developing aspect ratio for the test plates. PD6493 did not recognise that the defects would grow as surface cracks at all since the tests were conducted under bending and hence PD6493 recharacterised the defects as a single edge crack. It was found that the developing aspect ratio could be accurately predicted using either the empirical model of Iida or using a simple numerical procedure based on single defect stress intensity factor solutions. The simplistic approach of both ASME and British Standards procedures would not be suitable for the assessment of cracked components where leak-before-break arguments could be utilised to justify continued service due to the inadequate predictions of the crack shape development.

The recharacterised edge crack was shown to considerably over estimate the stress intensity factor at the crack tips even for shallow, low aspect ratio co-linear defects. It was shown in Chapter 7 that the conservatism due to the recharacterisation increased for deeper defects and higher aspect ratios. Since the analysis presented in Chapter 7 included the effects of defect interaction then the assumptions of PD 6493 were shown to be excessively conservative.

ASME XI and PD6493 also give guidance as to how adjacent defects should be taken to coalesce. The ASME XI rules are based on a comparison between the defect maximum depth and the separation between the

adjacent tips. PD6493 compares the largest defect surface length with the separation. Specific recommendations were presented in Chapter 6 and discussed in Chapters 7 and 8. It was found that the codified procedures did not accurately reflect the observed behaviour. The numerical results for both tension and bending load cases, presented in Chapter 7 showed that there was no significant interaction between the defects and hence no requirement to coalesce the defects at some level of separation was indicated. This was supported by the experimental observations where no interaction between the coalescing crack tips was observed and coalescence was found to occur only after the crack tips overlapped. Consequently when the code guidelines were utilised to predict the crack growth behaviour for the test conditions they were both found to be extremely conservative. Further the defect shape at coalescence and the final 'failed' crack shape was poorly predicted. The PD6493 prediction was based on a growing edge crack due to the recharacterisation. The ASME guidelines also resulted in the crack surface length being grossly over-estimated. PD6493 under-estimated the test duration by a factor of 3.3 while ASME under-estimated by a factor of 6.2. The commercial implications of these inadequacies in terms of the assessment of operating plant could be considerable due to over conservative predictions resulting in premature shut down or unscheduled outages.

If the findings from the defect interaction study and the experimental observations were utilised to develop a predictive model using single defect solutions with finite area corrections then more realistic assessments could be produced. It may also be possible to develop the method for use at the design stage by considering statistical distributions of initial defects and therefore predicting the size and locations of cracks which could develop in the structure. The initial defect size would be specified based on experience of the fabrication process. That is through prior knowledge of the type of defects which may be introduced through specific welding processes or production techniques. A possible application for this type of analysis would be the reliability assessments of high integrity plant such as offshore jacket structures or nuclear power station components. The benefit of the statistical approach would be that there would be no requirement to specify the initial

crack for analysis during the design stage thus making the use of fracture mechanics technology at the design stage more practicable. It would be possible to update these calculations using the results of conventional in service inspection routinely carried out on high integrity plant.

## **10.4 Overall Conclusions**

1. The line spring model was shown to offer an efficient and inexpensive tool for the analysis of complex surface crack problems.
2. It was demonstrated that the interaction between a periodic array of co-linear semi-elliptical defects was of the same magnitude as the finite area correction for the case of a single defect in a plate of the repeated cell size for the array. This was supported by the experimental observations.
3. A numerical procedure was presented to enable the universal weight function technique to be utilised for the analysis of irregular crack geometries.
4. A numerical study utilising universal weight functions and line spring models was used to predict the magnification of the stress intensity factor at the re-entrant crack sector observed in the experimental investigation.
5. A considerable magnification of the stress intensity factor at the re-entrant crack sector immediately after coalescence, resulted in rapid propagation and formation of the final stable crack shape. The rate at which the final crack shape is formed was found to be rapid enough that this stage can be ignored for predictive purposes. The enhanced stress intensity factor was predicted by both the line spring and weight function models.
6. BS PD 6493 and ASME XI procedures for assessing and propagating co-linear cracks have been demonstrated to be unrealistic and extremely conservative.
7. A prediction based on the Newman Raju stress intensity factor solution for single defects was shown to provide improved predictions.

## **Acknowledgements**

I would like to thank Professor John W Hancock for his support, guidance and encouragement throughout this work. Thanks are also due to Hibbitt, Karlsson and Sorensen for access to ABAQUS and to the computing staff of Glasgow University. The support of Babcock Energy Limited is also acknowledged.

Special thanks are due to Julie for showing the patience of a saint and for her continued support and encouragement during this ordeal. Without it I would never have completed this thesis.

## 11. References

1. Griffith, A.A. 'The Phenomena of rupture and flow in solids', Phil. Trans. R. Soc. Vol. 221, pp. 163-198, 1921.
2. Griffith, A. A. 'The Theory of Rupture'. Proc. 1st International Congress on Applied Mechanics, Ed. Biezeno and Burgers, Waltman, pp. 55-63, 1924.
3. Irwin, G.R. and Keis, J. 'Fracture and Fracture Dynamics', Welding J. Res. Suppl. Feb. 1952.
4. Orowan, E. 'Fundamentals of brittle behaviour of metals', Fatigue and Fracture of Metals, Wiley, New York 1952, pp. 139-167.
5. Westergaard, H.M. 'Bearing Pressures and Cracks', Journal of Applied Mechanics, Volume 61, pp. A49-A53, 1939.
6. Rooke, D. P. and Cartwright, D. J., 'Compendium of Stress Intensity Factors', HMSO 1976.
7. Murakami, Y., 'Stress Intensity Factors Handbook' Pergammon Press 1987.
8. Irwin, G.R., Fracture, 'Handbuch der Physik VI, pp. 551- 590, Flugge Ed., Springer (1958)
9. Irwin, G.R., 'Plastic Zone Near a Crack and Fracture Toughness', Proc. 7th Sagamore Conf., p. IV-63 (1960)
10. Dugdale, D.S., 'Yielding of Steel Sheets Containing Slits', J. Mech. Phys. Solids, 8, pp.100-108, (1960)
11. Barenblatt, G.I, 'The Mathematical Theory of Equilibrium of Cracks in Brittle Fracture', Advances in Applied Mechanics, 7, pp. 55-129, 1962
12. Duffy, A.R. et al 'Fracture Design For Pressure Piping', Fracture I, pp. 159-232, ed. Leibowitz, Academic Press, 1969.
13. Simpson, L. D. and Eaton, D.M. 'The extent of elastic- plastic yielding at the crack point of an externally notched plane stress tensile specimen.' Aer. Res. Lab. Australia, Rept. ARL 24, 1961.
14. Hult, J.A. and McIntock, F.A., 'Elastic-Plastic stress and strain distribution around sharp notches under repeated shear,' IXth Int. Congr. Appl. Mech., 8, pp. 51-62, 1956.
15. Tuba, I.S. 'A method of elastic-plastic plane stress and strain analysis' J.

Strain Analysis,1, pp. 115-122, 1966.

16. Rice,J.R. and Rosengren,G.F. 'Plane strain deformation near a crack tip in a power law hardening material', J. Mech. Phys. Sol., 16, p.1, 1968.

17. Bateman et al, 'Some observations on surface deformation round cracks in cracked sheets', Roy. Aircr. Est. Farnborough TN-CPM 63, 1963.

18. Underwood, J.H. and Kendall, D.P. 'Measurement of plastic strain in the region of a crack tip.',Experimental Mechanics, pp. 296-304, 1969.

19. Hahn, G.T. and Rosenfield, A.R. 'Local yielding and extension of a crack under plane stress,' Acta Met., 13, pp. 293-306, 1965.

20. Hahn,G.T., Hoagland,R.G. and Rosenfield, A.R. 'Local yielding attending fatigue crack growth', Met. Trans., 3, pp. 1189-1196, 1972.

21. Hahn,G.T. and Rosenfield, A.R. 'Plastic flow in the locale on notches and cracks in Fe-3Si steel under conditions approaching plane strain' Rept. to ship structure committee, 1968.

22. Broek,D.A. 'A study on ductile fracture', National Aerospace Inst. Amsterdam, Rept. TR 71021, 1971.

23. Broek,D.A. 'Fail safe design procedures', Agard Fracture Mechanics survey, Chapter II, 1974

24. Tada,H. Paris,P.C. and Irwin,G.R. 'The stress analysis of cracks handbook', Del Research Corporation, 1973.

25. Sih, G.C. 'Handbook of stress intensity factors', Inst. of Fracture and Solid Mechanics, Lehigh University, 1973.

26. Cartwright, D.J. and Rooke, D.P. 'Methods of determining stress intensity factors', RAE Technical report 73031, 1973.

27. Sih, G.C. 'Methods of analysis and solution of crack problems', Mechanics of fracture vol. 1, Noordhoff, 1973.

28. Sih, G.C. 'On the Westergaard method of crack analysis', International Journal of Fracture Mechanics, vol. 2, pp.628-631, 1966.

29. Eftis, J. and Liebowitz, H. 'On the modified Westergaard equations for certain plane crack problems', International Journal of Fracture Mechanics, vol. 8, pp. 383-392, 1972.

30. Irwin, G.R. 'Fracture Handbuch der Physik VI', pp.551- 590, Springer-

verlag, Berlin, 1958.

31. Irwin, G.R. Structural Mechanics, pp.557-594, Permagon, NY. 1960.

32. Tada, H. Engineering Fracture Mechanics, vol. 2, 177, 1970.

33. Muskhelishvili, N.I. 'Some basic problems of the mathematical theory of elasticity', 1938, english translation, Noordhoff, 1953.

34. Sih, G.C. 'Application of Muskhelishvili's method to fracture mechanics' Trans. Chin. Ass. Adv. Studies, 1962.

35. Erdogan, F. 'On the stress distribution in plates with colinear cuts under arbitrary loads', Proc. 4th U.S. National Congress Appl. Mech 1962.

36. Bilby, B.A., Cottrell, A.H., Smith, E. and Swinden, K.H., 'Plastic yielding from sharp notches', Proc. Royal Society, A 279, pp.1-9, 1964.

37. Bilby, B.A. and Eshelby, J.D. 'Dislocations and the theory of fracture' Fracture vol 1. Liebowitz, Ed. Academic press, 1969.

38. Irwin, G.R. 'The crack extension force for a crack at a free surface boundary', Report No. 5120, Naval Research Lab., 1958.

39. Irwin, G.R. 'Analytical aspects of crack stress field problems', T&AM Report No. 213, University of Illinois, March, 1962.

40. Sneddon, I.N. and Lowengrub, M. 'Crack problems in the classical theory of elasticity', Wiley, N.Y. 1969.

41. Neuber, H. 'Theory of Notch stresses', Springer, Berlin, 1958.

42. Irwin, G.R. 'Fracture Mechanics', Structural Mechanics, pp.557-594, 1960.

43. Williams, M.L. 'On the stress distribution at the base of a stationary crack', Transactions of ASME., Journal of Applied Mechanics, Vol 24., p. 109, 1957.

44. Gross, B. Strawley, J.E. and Brown, W.F., 'Stress intensity factors for a single edge notch tensile specimen by boundary collocation of a stress function', NASA TN D- 2395, 1964.

45. Strawley, J.E. and Gross, B., 'Stress intensity factors for crack-line loaded edge crack specimens', NASA TN D-3820, 1967.

46. Isida, M., 'On th determination of stress intensity factors for some

common structural problems', Engineering fracture mechanics, vol. 2, pp. 61-79, 1970.

47. Bowie, O.L. 'Analysis of an infinite plate containing radial cracks originating at the boundary of an internal circular hole', Journal Math. and Phys., 25, pp. 60-71, 1956.

48. Bowie, O.L. and Neal, D.M. 'Modified mapping collocation technique for accurate calculation of stress intensity factors', International Journal of fracture mechanics, 6, pp. 199-206., 1970.

49. Cruse, T.A. 'Lateral constraint in a cracked three dimensional Elastic body', International Journal of fracture mechanics, 6, pp. 326-328, 1970.

50. Nisitani, H. Bull. JSME., 11, 14, 1968.

51. Zienkiewicz, O.C., 'The Finite Element Method', McGraw-Hill, 1977.

52. Gallagher, 'Survey and evaluation of the finite element method in linear elastic fracture mechanics analysis', Conf. Struct. Mech. in reactor technology', Berlin, 1971.

53. Hellen, T.K. 'Jerram, K. and Hellen, T.K., 'Finite element techniques in fracture mechanics', Int. Conf. on welding research related to power plant', 1972.

54. Rice, J.R. and Tracey, D.M., 'Computational fracture mechanics', Numerical and computer methods in structural mechanics, Academic press, N.Y., 1973.

55. Chan, S.K., Tuba, I.S. and Wilson, W.K. 'On the finite element method in linear fracture mechanics', Engineering fracture mechanics, 2, pp. 1-17, 1970.

56. Wilson, W.K. and Thompson, D.G. 'On the finite element method for Calculating stress intensity factors for cracked plates in bending', Engineering fracture mechanics, 3, pp.97- 108, 1971.

57. Watwood, V.B., 'The finite element method for prediction of crack behaviour', Nuclear engineering design, 11, pp. 323-332, 1969.

58. Kfourri, A.P. and Miller, K., 'Stress, displacement, line integral and closure energy determination of crack tip stress intensity factors', International journal of pressure vessels and piping, 2, pp. 179-191, 1974.

59. Anderson, G.P., Ruggles, V.L. and Stibor, G.S., 'Use of finite element computer programs in fracture mechanics', International journal of Fracture mechanics, 7, pp. 63-76, 1971.

60. Watwood Jr., V. B. 'The finite element method for prediction of crack behaviour', Nuclear Engineering and Design, vol. 11, pp. 323-332, 1969.
61. Isida, M. 'On the tension of a strip with a central elliptical hole', Trans. Jap. Soc. Mech. Eng., vol. 21, 1955.
62. Swanson, S. R. 'Finite element solutions for a cracked two layered elastic cylinder', Engineering fracture mechanics, Vol. 3, pp. 283-289, 1971.
63. Anderson, G.P., Ruggles, V.L. and Stibor, G.S. 'Use of finite element computer programs in fracture mechanics', Int. Journal of Fracture Mechanics, vol. 7, pp. 63-76, 1971.
64. Dixon, J.R. and Strannigan, J.S. 'Determination of energy release rates and stress intensity factors by the finite element method', Journal of strain analysis, vol. 7, pp. 125-131, 1972.
65. Dixon, J.R. and Pook, L.P. 'Stress intensity factors calculated generally by the finite element method', Nature, vol. 224, p. 166, 1969.
66. Parks, D.M., 'A stiffness derivative finite element technique for determination of elastic crack tip stress intensity factors', International Journal of Fracture, vol. 10., No. 4, pp. 487-502, December 1974.
67. Hellen, T.K. 'On the method of virtual crack extensions', International of numerical methods in engineering, vol. 9, pp. 187-208, 1975.
68. Hellen, T.K. 'Finite element energy methods in fracture mechanics', Ph.D. Thesis, University of London, March 1976.
69. Irons, B. M. R., 'A front solution program for finite element analysis International Journal of Numerical Methods in Engineering, vol. 2, pp. 5-32, 1970.
70. Hibbit, Karlsson and Sorensen, 'ABAQUS Users Manual' (1984)
71. CEGB BNL BERSAFE Users Manual
72. Eshelby, J.R., 'The continuum theory of lattice defects', Solid state physics 3., 1956.
73. Rice, J.R., 'A path independent integral and the approximate analysis of strain concentration by notches and cracks', Journal of Applied mechanics, vol. 35, pp. 379-386, 1968.
74. Cherepanov, G.L., 'Cracks in solids', Prikl. Math. Mekh. vol. 25, pp. 476-488, 1967.

75. Hayes, D.J., Ph.D. thesis, imperial college, London, 1970.
76. Blackburn, W.S. 'Path independent integrals to predict the onset of crack instability in elastic plastic materials', International of Fracture Mechanics, vol. 8, pp. 343-346., 1972.
77. Stern, M., Becker, E. and Dunham, R.S., 'A contour integration computation of mixed mode stress intensity factors', International journal of Fracture, vol. 12, pp. 359-368, 1976.
78. Stern, M. and Soni, M., 'The calculation of stress intensity factors in anisotropic materials bu a contour integral method', in 'Computational fracture mechanics', eds. E. Rybicki and S. Benzley, ASME spec. publication, 1975.
79. Bergvist, H. and Guex-le Lan Huong, 'J-integral related quantities in axisymmetric cases', International journal of fracture, vol. 13, pp. 556-558, 1977.
80. Knowles, J.K. and Sternberg, E. 'On a class of conservation laws in linearised and finite elastostatics', Arch. Rat. Mech. Analysis, vol. 44, pp. 187-211, 1972.
81. Wilson, W.K. 'On combined mode fracture mechanics', Westinghouse report 69-LE7-F.Mech-RL, 1969.
82. Byskov, E. 'The calculation of Stress Intensity Factors Using the Finite Element Method With Cracked Elements', Int. J. Fract. Mech. Vol. 6, pp. 159-167, 1970.
83. Walsh, P.F. 'The computation of Stress Intensity Factors by a Special Finite Element Technique', Int. J. of Solids and Structures, vol. 7, pp. 1332-1342, 1971.
84. Tracey, D.M. 'Finite Element Methods for Determination of Elastic Stress Intensity Factors', Engineering Fracture Mechanics, Volume 3. pp. 255-265, 1971.
85. Blackburn, W.S. 'Calculation of Stress Intensity Factors at Crack Tips Using Special Finite Elements', Conf. on Maths of Finite Els. and Appls., Brunel University, April 1972.
86. Gallagher, R.H. 'A review of finite element techniques in fracture Mechanics', Proc. Conf. on 'Numerical Methods in Fracture Mechanics', University college Swansea, Jan. 1978.
87. Fawkes, A.J., Owen, D.R.J. and Luxmore, A.R. 'An assessment of crack

tip singularity models for use with isoparametric elements', Eng. Frac. Mech. vol. 11, pp. 143- 159, 1979.

88. Henshell, R.D. and Shaw, K.G. 'Crack Tip Finite Elements are Unnecessary', Int. J. of Num. Methods in Engineering, vol. 9, pp. 495-507, 1975.

89. Barsoum, R. S. 'Application of Quadratic Isoparametric Finite Elements in Linear Fracture Mechanics', Int. J. Fract. Mech., vol. 10, pp. 603-605, 1974.

90. HK&S Inc. ABAQUS users manual, version 4.7.

91. Adams, N. J. I. 'The effect of Curvature on stress Intensity and and crack growth in shells', Ph.D. Thesis, University of Southampton 1969.

92. Dixon, J.R. and Pook, L.P. 'Stress Intensity Factors calculated generally by the finite element technique', Nature, vol. 224, p. 166, 1969.

93. Jerram, K. Discussion to paper by Smith and Alavi, Int. Conf. on Press. Vess. Tech. Pt. III Discussion, ASME, New York 1970.

94. Broeke, D. 'Elementary Engineering Fracture Mechanics', Martinus Nijhoff Publishers, Dordrecht. 1986.

95. Knott, J. F., 'Fundamentals of Fracture Mechanics', Butterworths, London, 1973.

96. Smith, D.G. and Smith, C.W. 'A Photoelastic evaluation of the influence of closure and other effects upon the local stresses in cracked plates', Int. J. Fract. Mech., vol. 6, pp. 305-318, 1970.

97. Gerberich, W.W. 'Stress distribution around a slowly growing crack determined by photoelastic coating method', Proc. SESA, 19, pp. 359-365, 1962.

98. Kobayashi, A.S. 'Photoelastic studies of fracture', Fracture III, pp. 311-369, Leibowitz, ed., Academic Press, 1969.

99. Dixon, J.R., 'Stress distribution around edge slits in tension', National Eng. Lab., Glasgow, Report 13, 1961.

100. Smith, D.G. and Smith, D.W. 'Photoelastic determination of mixed mode stress intensity factors', Eng. Fract. Mech., vol. 4, pp.357-366, 1972.

101. Monthulet, A., Bhandari, S.K. and Riviere, C., 'Méthodiques pratiques de détermination du facteur d'intensité des contraintes pour la propagation des fissures', La Recherche Aérospatiale, pp.297-303, 1971.

102. Barrois, W., 'Manual on fatigue of structures', AGARD- Man-8-70, 1970.
103. Bhandari, S.K., 'étude expérimentale du facteur d'intensité des contraintes au voisinage de la pointe d'une fissure de fatigue centrale dans une tôle mince au moyen des mesures extensométriques', Thèse, école Nat. Supérieure de L'Aéronautique, Paris 1969.
104. Gallagher, J.P., 'Experimentally determined stress intensity factors for several contoured DCB specimens', Eng. Fract. Mech., vol. 3, pp. 27-43, 1971.
105. Schra, L. Boerema, P.J. and Van Leeuwen, H.P., 'Experimental determination of the dependence of compliance on crack tip configuration of a DCB specimen', Nat. Aerospace inst. Amsterdam, Rept. TR 73025, 1973.
106. Ottens, H.H. and Lof, C.J., 'Finite element calculations of the compliance of a tapered DCB specimen for different crack configurations', Nat. Aerospace Lab. report TR 72083, 1972.
107. James, L.A. and Anderson, W.E., 'A simple experimental procedure for stress intensity factor calibration', Eng. Fract. Mech., vol. 1, pp. 565-568, 1969.
108. Rooke, D.P., Baratta, F.L. and Cartwright, D.J., 'Simple methods of determining stress intensity factors', AGARDograph 257, 1980.
109. Beuckner, H. F. 'The propagation of cracks and the energy of elastic deformation', Trans. ASME, 80E, pp.1225- 30, 1958.
110. Beuckner, H. F. 'A novel principle for the computation of stress intensity factors.' Z. Angew. Math. Mech., vol. 50, pp. 529-546, 1970.
111. Rice, J. R. 'Some remarks on elastic crack tip stress fields', Int. J. Solids and Structures, vol. 8, pp. 751- 758, 1972.
112. Paris, P.C, McMeeking, R.M. and Tada, H. 'The weight function method for determining stress intensity factors', In Cracks and Fracture STP 601, pp. 471-489, 1976.
113. Labbens, R.C., Heliot, J. and Pellissier-Tanon, A., 'Weight Functions for three dimensional crack problems', In Cracks and Fracture, STP 601, pp. 448-470, 1976.
114. Tada, H., Paris, P.C. and Irwin, G.R. 'The stress analysis of cracks Handbook', Del. Research Corporation, Hellertown, Pa., pp. 5.4, 24.2, 25.1.
115. Kassir, M.K., and Sih, G.C., 'Three dimensional crack problems', pp. 67-

68, 137-142, Noordhoff, 1975.

116. Oore, M. and Burns, D.J., 'Estimate of stress intensity factors for embedded irregular cracks subjected to arbitrary normal stress fields', Transactions of ASME, Journal of Pressure Vessel Technology, Vol. 102, pp. 202- 211, 1980.

117. Oore, M. and Burns, D.J., 'Estimation of stress intensity factors for irregular cracks subjected to arbitrary normal stress fields'. 4th international conference on pressure vessel technology, I.Mech.E. London, 1980.

118. Irwin, G.R. 'Fracture', In Handbuch der Physik VI, pp.551-590, Springer-Verlag, Berlin (1958).

119. Baratta, F.I., 'Stress Intensity factors for internal multiple cracks in thick walled cylinders stressed by internal pressure using load relief factors', AMMRC TN 77- 3, 1977.

120. Cartwright, D.J. and Rooke, D.P., 'Approximate stress intensity factors compounded from known solutions', Eng. Frac. mech., Vol. 6, pp.563-571, 1974.

121. ASME, Boiler and pressure vessel design code, section XI, Division I, Appendix A, 'Analysis of flaw indications', 1980.

122. British Standards Institution, 'Guidance on some methods for the derivation of acceptance levels for defects in fusion welded joints', BS PD 6493, 1980.

123. Irwin, G.R. 'Crack Extension Force for a Part-Through Crack in a Plate', Trans. ASME. Journal of Applied Mechanics, vol. E29, p. 651, 1962

124. Sneddon, I.N., 'The distribution of stress in the neighborhood of a Crack in an Elastic Solid', Proc. of the Royal Society, London, vol. A-187, pp.229-260, 1946.

125. Sack, R.A., 'Extension of Griffith's Theory to rupture in three dimensions', Proc. of the Physical Society, London, vol. 58, pp. 729-736, 1946.

126. Green, A.E. and Sneddon, I.N., 'The distribution of stress in the neighborhood of a flat elliptical crack in an elastic solid', Proc. of the Philisophical Society, vol. 46, 1950, pp. 159-163.

127. Paris, P.C. and Sih, G.C. 'Stress Analysis of Cracks,' ASTM STP 391, pp. 30-81, 1965.

128. 'The Surface Crack: Physical Problems and Computational Solutions.'

American Society of Mechanical Engineers, J. L. Swedlow, Ed., 1972.

129. Merkle, J. G., 'A Review of Some of the Existing Stress Intensity Factor Solutions for Part-Through Surface Cracks', ORNL-TM-3983, Oak Ridge National Laboratory, January, 1973.

130. Keays, R. H., 'A Review of Stress Intensity Factors for Surface and Internal Cracks,' Report ARL/SM 343, Australia Aeronautics Research Laboratory, April 1973.

131. Newman, J. C. Jr., 'A Review and Assessment of the Stress Intensity Factors for Surface Cracks', in "Part- Through Crack Fatigue Life Prediction", ASTM STP 687, J. B. Chang, Ed., American Society fo Testing and Materials, 1979, pp. 16-42.

132. Scott, P. M. and Thorpe, T. W., 'Prediction of Semi- elliptic Crack Shape Development during Fatigue Crack Growth', Report R-10104, Atomic Energy Research Establishment, Harwell, United Kingdom, 1981.

133. Kantorovich, L. V. and Krylov, V. I., Approximate Methods of Higher Analysis, Interscience, New York, 1964.

134. Hartranft, R. J. and Sih, G. C., 'Alternating Method Applied to Edge and Surface Crack Problems', Technical Report NASA-TR-72-1, April 1972.

135. Shah, R. C. and Kobayashi, A. S. 'On the Surface Flaw Problem', in "The Surface Crack: Physical Problems and Computational Solutions", J. L. Swedlow Ed. ASME New York, 1973.

136. Smith, F. W. and Sorensen, D. R., 'The Semi-elliptical Surface Crack: A Solution by the Alternating Method', Int. J. of Fracture, vol. 12, p. 77, 1976.

137. Nishioka, T. and Atluri, S. N., 'A Major Development Towards a Cost Effective Alternating Method for Fracture Analysis of Steel Reactor Pressure Vessels', Transaction of the 6th International Conference on Structural Mechanicsin Reactor Technology, Paper G1/2, Paris, France, 1981.

138. Nishioka, T. and Atluri, S. N., 'Analytical Solution for Embedded Elliptical Cracks, and finite Element Alternating Method for Elliptical surface Cracks, Subjected to Arbitrary Loadings', Engineering Fracture Mechanics, vol. 17, 1982

139. Nishioka, T. and Atluri, S. N., 'Analysis of Surface Flaw in Pressure Vessels by a New 3-Dimensional Alternating Method', J. Press. Vess. Technology, vol. 104, pp. 299-307, November 1982.

140. Holbrook, S. J. and Dover, W. D., 'The Stress Intensity Factor For A Deep Surface Crack in a Finite Plate', Eng. Fract. Mechanics, Vol. 12, pp.

347-364, 1979.

141. Aboutorabi, A. A. and Cowling, M. J. 'Determination of Stress Intensity Factors for Surface Cracks Using Fatigue Crack Growth Data', Int. J. of Fracture, Vol. 31, pp. 67- 79, 1986.

142. Smith, C. W., in "Mechanics of Fracture 7: Experimental Evaluation of Stress Concentration and Intensity Factors", G. C. Sih Ed., 1981.

143. Ruiz, C. and Epstein, J., 'On the Variation of the Stress Intensity Factor Along the Front of A Surface Flaw', Int. J. of Fracture, Vol. 28, pp. 231-238, 1985.

144. Tracey, D. M., 'Three Dimensional Elastic Singularity Element for Evaluation of K along an Arbitrary Crack Front', Int. J. of Fracture, Vol. 9., p. 340, 1973.

145. Tracey, D. M., 'Finite Elements for Three Dimensional Elastic Crack Analysis', J. Nuclear Energy and Design, Vol. 26, pp. 282-290, 1974.

146. Hellen, T. K. and Blackburn, W. S. 'The Calculation of Stress Intensity Factors in Two and Three Dimensions Using Finite Elements', in Computational Fracture Mechanics, ASME, New York, 1975.

147. Atluri, S. and Kathiresan, K., 'An Assumed Displacement Hybrid Finite Element Model for Three Dimensional Linear Fracture Mechanics Analysis', Proc. 12th Annual Meeting of the Soc. Engr. Science, University of Texas, Austin, Texas 1975.

148. Raju, I. S. and Newman, J. C. Jr., 'Stress Intensity Factors for a Wide range of Semi-Elliptical surface Crcks in Finite Thickness Plates', Engineering Fracture Mechanics, Vol. 11 No. 4, pp. 817-829, 1979.

149. Newman, J. C. Jr. and Raju, I. S., 'Analyses of Surface Cracks in Finite Plates Under Tension or Bending Loads', NASA TP-1578, 1979.

150. Newman, J. C. Jr. and Raju, I. S., 'An Empirical Stress Intensity Factor Equation for The Surface Crack', Engineering Fracture Mechanics, Vol. 15 No. 1-2, pp. 185- 192, 1981.

151. Newman, J.C. Jr., 'Predicting failure of Specimens with Either Surface Cracks or Corner Cracks at Holes', NASA TN D-8244, 1976.

152. Rice, J. R. and Levy, N., 'The Part Through Surface Crack in an Elastic Plate', ASME J. of Applied Mechanics, Vol. 39, pp. 185-194, 1972.

153. Rice, J. R., 'The Line Spring Model for Surface Flaws', in "The Surface Crack: Physical Problems and Computational Solutions", J. L. Swedlow Ed.

ASME New York, 1973.

154. Delale, F. and Erdogan, F., 'Application of the Line Spring Model to a Cylindrical Shell Containing a Circumferential or Axial Part Through Crack', Lehigh University Report for DOT contract No. DOT-RC-82007, Apr. 1981.

155. Delale, F. and Erdogan, F., 'Line Spring Model for surface Cracks in a Reissner Plate', Int. J. of Engineering Science, Vol. 19, pp. 1331-1340, 1981.

156. Parks, D. M., 'The Inelastic Line Spring Estimates of Elastic Plastic Fracture Mechanics Parameters for Surface Cracked Plates and Shells', ASME J. of Pressure Vessel Tech., Vol. 103, pp. 246-254, 1981.

157. Parks, D. M., Lockett, R. R. and Brockenbrough, J. R., 'Stress Intensity Factors for Surface Cracked Plates and Cylindrical Shells Using Line Spring Finite Elements', in "1981 Advances in Aerospace Structures and Materials", AD- 01, ed. S. S. Wang and W. J. Renton, ASME, N.Y., pp. 279-285, 1981.

158. Parks, D. M. and White, E. S., 'Elastic Plastic Line Spring Finite Elements for Surface Cracked Plates and Shells', in Aspects of Fracture Mechanics in Pressure Vessels and Piping, ASME Publication No. PVP Vol. 58, pp. 37-48, pp. 159-174, 1982.

159. Kumar, V. et al., ' Estimation Technique for the Prediction of Elastic Plastic Fracture of Structural Components of Nuclear Systems', Combined Fifth and Sixth Semiannual Report to EPRI, Contract No. RP1237-1, General Electric Company, Schenectady, N.Y., Feb. 1981-Jan. 1982.

160. German, M. D., Kumar, V. and deLorenzi, H. G., 'Analysis of Surface Cracks in Plates and Shells Using the Line Spring Model and ADINA', in "Nonlinear Finite Element Analysis and ADINA", ed. K. J. Bathe, Proc. of the 4th ADINA Conference, MIT, Cambridge, Mass., pp. 881-890, June 15-17, 1983.

161. Shiratori, M. and Miyoshi, Y., 'Evaluation of J- Integral for Surface Cracks', presented at ASTM 2nd International Symposium on Elastic Plastic Fracture Mechanics, Philadelphia, Pa., October 6-9, 1981.

162. Parks, D.M., 'The Inelastic Line Spring: Estimates of Elastic-Plastic Fracture Parameters for Surface Cracked Plates and Shells', Paper 80-C2/PVP-109, ASME, New York, 1980.

163. Parks, D. M., 'Inelastic Analysis of Surface Flaws Using the Line Spring Model', Proc. 5th Int. Conf. on Fracture, Cannes, France, 1981.

164. Kumar, V. and German, M. D., 'Studies of the Line- Spring Model for

Nonlinear Crack Problems', J. Pressure Vessel Technology, Vol. 107, pp. 412-420, ASME, Nov. 1985.

165. King, R. B., 'Elastic-Plastic Analysis of Surface Flaws Using a Simplified Line-Spring Model', Eng. Fract. Mechanics, Vol. 18, No. 1, pp. 217-231, 1983.

166. Du, Z. Z. and Hancock, J. W., 'The Stress Intensity Factors of Semi-elliptical Cracks in a Tubular Welded T- Joint Under Axial Loading', J. Eng. fract. Mech. Volume 30, pp. 25-36, 1988.

167. Huang, X. and Hancock, J. W., 'The Stress Intensity Factors of Semi-Elliptical Cracks in a Tubular Welded T- Joint Under Axial Loading', J. eng. fracture Mech. Volume 30, pp. 25-36, 1988.

168. Erdogan, F., 'The Line Spring Model', in "Computational Methods in the Mechanics of Fracture", Ch. 8, Ed. S. N. Atluri, Elsevier, 1986

169. Joseph, P. F. and Erdogan, F., 'A Surface Crack in shells Under Mixed Mode Loading Conditions', Trans. ASME J. of Applied Mechanics, Vol. 55, pp. 795-805, Dec. 1988.

170. Miyoshi, T., Shiratori, M. and Yoshida, Y., 'Analysis of J-Integral and Crack Growth for Surface Cracks by Line Spring Method', Trans. ASME J. Press. Vessel Tech., Vol. 108, pp. 305-311, 1986.

171. Petroski, H. J. and Achenbach, J. D., 'Computation of the Weight Function from a Stress Intensity Factor', Engineering Fracture Mechanics, Vol. 10, pp. 257-266, 1978.

172. Mattheck, C., Munz, D. and Stamm, H., 'Stress Intensity Factor For Semi-Elliptical Surface Cracks Loaded by Stress Gradients', Engineering Fracture Mechanics, Vol. 18, No. 3, pp. 633-641, 1983.

173. Mattheck, C., Morawietz, P., and Munz, D., 'Stress Intensity Factor at the Surface and at the Deepest Point of a Semi-Elliptical Surface Crack in Plates Under Stress Gradients', International Journal of Fracture, Vol. 23, pp. 201-212, 1983.

174. Grebner, H., 'Thermal Shock of a Pipe with a Partly Circumferential Surface Crack', Engineering Fracture Mechanics, Vol. 28, No. 3, pp. 309-317, 1987.

175. Niu, X. and Glinka, G., 'Stress Intensity Factors for Semi-Elliptical Surface Cracks in Welded Joints', International Journal of Fracture, to be published.

176. Niu, X. and Glinka, G., 'Weight Functions for Edge and Surface Semi-

Elliptical Cracks in Flat Plates and Plates with Corners', Engineering Fracture Mechanics, Vol. 36, No. 3, pp. 459-475, 1990.

177. Pook, L. 'The Role of Crack Growth in Metal Fatigue', Printed by J. W. Arrowsmith Ltd., Bristol, 1983.

178. Wood, W. A., 'Recent Observations on Fatigue Fracture in Metals', ASTM STP 237, pp. 110-121, 1958.

179. Tetelman, A. S. and McEvily, A. J., 'Fracture of Structural Materials', Published by John Wiley, 1967.

180. Cottrell, A. H. and Hull, D., 'Extrusion and Intrusion by Cyclic Slip in Copper', Proc. Royal Society A 242, pp. 211-217, 1957.

181. Mott, J.N. F., 'A Theory of the Origin of Fatigue Cracks', Acta Met., vol. 6, pp. 195-197, 1958.

182. Pelloux, R. M. N., 'Mechanism of Formation of Fatigue Striations', Int. J. Fracture Mechanics, Vol. 8, pp. 75-85, 1969.

183. Neumann, P., 'On the Mechanism of Crack Advance in Ductile Materials', 3rd ICF Conference, III, p233, 1973.

184. Miller, K. J., in 'Fundamentals of Deformation and Fracture', Eshelby Memorial Symposium, Sheffield, 1985.

185. Miller, K. J. and Zachariah, K. P., J. Strain Analysis, Vol. 12, p262, 1977.

186. Pook, L. and Greenan, A. F., in 'Fracture Mechanics', ASTM 677, p. 23, 1979.

187. Paris, P. C. 'The growth of fatigue cracks due to variations in load', Ph.D. Thesis, Lehigh University, 1962.

188. Paris, P. C., Gomez, M. P. and Anderson, W. E., 'A Rational Analytic Theory of Fatigue', in "The Trend in Engineering", Vol. 13, pp. 9-14, 1961.

189. Paris, P. C. and Erdogan, F., 'A Critical Analysis of Crack Propagation Laws', Trans. ASME(D), Vol. 85, pp. 528- 534, 1963.

190. Davies, K. B. and Feddersen, C. E.: J. Aircraft, Vol. 12, p. 943, 1975.

191. McClintock, F. A., Discussion, ASTM STP 415, pp. 170 - 174, 1967.

192. Hahn, G. T., Sarrat, H. and Rosenfield, A. R., 'The Nature of the Fatigue Crack Plastic Zone', Air Force Conference on Fatigue and Fracture, AFFDL, TR-70-144, pp. 425-450, 1970.

193. Bates, R. C. and Clark, W. G., 'Fractography and Fracture Mechanics', ASM Trans. 62, pp. 380-388, 1969.
194. Broek, D. and Shijve, J., 'The Influence of the Mean Stress on the Propagation of fatigue Cracks in Aluminium Alloy Sheets', Nat. Aerospace Inst. Amsterdam TR-M-2111, 1963.
195. Erdogan, F., 'Crack Propagation Theories', NASA-CR-901, 1967.
196. Walker, E. K., 'Effects of Environment and Complex Load History on Fatigue Life', ASTM STP 462, pp. 1-14, 1970.
197. Walker, E. K., 'An Effective Strain Concept for Crack Propagation and Fatigue with Specific Application to Biaxial Stress Fatigue', Air Force Conf. on Fracture and Fatigue, AFFDL-TR-70-144, pp. 225-233, 1970.
198. Foreman, R. G., Kearney, v. E. and Engle, R. M., 'Numerical Analysis of Crack Propagation in a Cyclic Loaded Structure', ASME Trans. J. Basic Eng. 89D, p. 459, 1967.
199. Hartman, A., 'On the Effect of Oxygen and Water Vapour on the Propagation of Fatigue Cracks in an Al Alloy', Int. J. Fracture Mech., Vol. 1, pp. 167-188, 1965.
200. Bradshaw, F. J. and Wheeler, C., 'Effect of Environment and Frequency on Fatigue Cracks in Al Alloys', Int. J. Fracture Mech., Vol. 5, pp. 255-268, 1969.
201. Frost, N. E., 'The Effect of Environment on the Propagation of Fatigue Cracks in Mild Steel', Applied Mat. Res., Vol. 3, p. 131, 1964.
202. Meyn, D. A., 'Frequency and Amplitude Effects on Corrosion Fatigue Cracks in a Titanium Alloy', Met. Trans. Vol. 2, pp. 853-865, 1971.
203. Meyn, D. A., 'The Nature of Fatigue Crack Propagation in Air and Vacuum for 2024 Aluminium', ASM Trans., Vol. 61, pp. 52-61, 1968.
204. Achter, M. R., 'Effect of Environment on Fatigue Cracks', ASTM STP 415, pp. 181-204, 1967.
205. Wei, R. P., 'Some Aspects of Environment Enhanced Fatigue Crack Growth', Eng. Fracture Mech., Vol. 1, pp. 633-651, 1970.
206. Frost, N. E., Marsh, K. J. and Pook, L. P., 'Metal Fatigue', Oxford University Press, London, 1974.
207. Crooker, T. W., Bogar, F. D. and Cares, W. R., in 'Corrosion

- Fatigue Technology', ASTM STP 642, p. 189, 1978.
208. Vosikovsky, O., Engineering Fracture Mechanics, Vol. 11, p595, 1979.
209. Cooke, R. J. and Beevers, C. J., Engineering Fracture Mechanics, Vol. 5, p. 1061, 1973.
210. Moutz, J. and Weiss, V., in 'Cracks and Fracture', ASTM STP 601, p. 154, 1976.
211. Schijve, J. and Broek, D., 'Crack Propagation Tests Based on a Gust Spectrum with Variable Amplitude Loading', Aircraft Engineering, Vol. 34, pp. 314-316, 1962.
212. Hudson, C. M. and Hardrath, H. F., 'Investigation of the Effects of Variable Amplitude Loadings on Fatigue Crack Propagation Pattern', NASA-TN-D-1803, 1963.
213. Wheeler, O. E., 'Spectrum Loading and Crack Growth', J. Basic Engineering, Vol. 94, p. 181, 1972.
214. Willenborg, J., Engle, R. M. and Wood, H. A., 'A Crack Growth Retardation Model Using an Effective Stress Concept', AFFDL-TM-71-1-FBR, 1971.
215. Bell, P. D. and Wolfeman, A., 'Mathematical Modeling of Crack Growth Interaction Effects', ASTM STP 595, pp. 157-171, 1967.
216. Newman, J. C. (Jr.), in 'Methods and Models for Prediction Fatigue Crack Growth Under Random Loading', ASTM STP 748, p. 53, 1981.
217. Iida, K. and Kawahara, M., 'Propagation and Coalescence of Fatigue Cracks Initiated From Collinear or Parallel Adjacent Surface Flaws', 4th international conference on pressure vessel technology, I.Mech.E. London, 1980.
218. Corn, D. L., Engineering Fracture Mechanics, Vol. 3, pp. 45-52, 1971.
219. Cruse, T. A., Meyers, G. J. and Wilson, R. B., ASTM, Special Technical Publication 631, pp. 174-189, 1977.
220. Hodulak, L., Kordisch, H., Kunzelmann, S. and Sommer, E., ASTM, Special Technical publication 677, pp. 399-410, 1979.
221. Portch, D. J., CEEGB Report No. CEEGB/RD/B/N4645, 1979.
222. Lloyd, G. J. and Walls, J. D., Engineering Fracture Mechanics, Vol. 13, pp. 897-911, 1980.

223. Kawahara, M. and Kurihara, M. in Proceedings "International Conference on Fracture - 4", Vol. 2, pp. 1361-1373, 1978.
224. Kang-Sian Lee, Len-Ji Yu, Zi-Hong Jin and Kai-Zuo Liang, 'Experimental Research on Surface Crack Propagation Laws for Low Alloy Steels,' Eng. Fracture Mechanics, Vol. 16, No. 1, 1982..
225. Morgan, H. G., 'Fatigue Crack Shape Development in Cracked Plates and Welded Joints', Fatigue of Offshore Structures , Paper C142/86, Inst. Mechanical Engineers, 1986.
226. MÅller, H. M., MÅller, S., Munz, D. and Neumann, J., 'Extension of Surface Cracks During Cyclic Loading', in "Fracture Mechanics : Seventeenth Volume", J. H. Underwood, et al Eds., ASTM STP 905, American Society for Testing and Materials, Philadelphia, pp. 625-643, 1986.
227. Cruse, T. A. and Besuner, P. M., Journal of Aircraft, Vol. 12, pp. 369-375, 1975.
228. Jolles, M. and Tortoriello, V., in "Fracture Mechanics : Fourteenth Symposium - Volume I: Theory and Analysis", ASTM STP 791, American Society for Testing and Materials, Philadelphia, pp. 300-311, 1984.
229. Fleck, N. A., Smith, I. F. C. and Smith, R. A., Fatigue of Engineering Materials and Structures, Vol. 6, pp. 225-239, 1983.
230. Dover, W. D. and Connolly, M. P., 'Fatigue Fracture Mechanics Assessment of Tubular Welded Y and K Joints', Fatigue of Offshore Structures , Paper C141/86, Inst. Mechanical Engineers, 1986.
231. , Connolly, M. P. and Collins, R., 'The Measurement and Analysis of Semi-Elliptical Surface Fatigue Crack Growth', Engineering Fracture Mechanics, Vol. 26, pp. 897- 911, 1987.
232. Glinka, G. and Niu, X., 'Theoretical and Experimental Analyses of Surface Fatigue Cracks in Weldments', in "Surface Crack Growth: Models, Experiments and Structures", ASTM STP 1060, W. G. Reuter et al Eds., American Society for Testing and Materials, Philadelphia, pp. 9-33, 1990.
233. Milne, I., Ainsworht, R. A., Dowling, A. R. and Stewart, A. T., 'Assessment of the Integrity of Structures Containing Defects', CEGB Report No. R/H/R6 - Rev. 3, May 1986.
234. Koiter, W. T., 'An Infinite Row of Colinear Cracks in an Infinite Elastic Sheet', Ingenieur Archiv. Vol. 28, pp. 168-172, 1959.

235. Feddersen, C. E., Discussion, ASTM STP 410, pp. 77-79, 1967.
236. Murakami, Y. and Nisitani, 'Stress Intensity Factors for Interacting Two Semi-Elliptical Surface Cracks in Tension', Trans. Japan Soc. Mechanical Engineers, Ser. A, Vol. 47, No. 415, pp.295-303, 1981.
237. Isida, M., Yoshida, T. and Noguchi, H., Prelim. Proc. Japan Soc. Mechanical Engineers and Japan Soc. Precision Engineering, Mie District, No. 823-3, pp. 15-17, 1982.
238. Murakami, Y. and Nemat-Nasser, S., 'Interacting Dissimilar Semi-Elliptical Surface Flaws Under Tension and Bending', Engineering Fracture Mechanics, Vol. 16, No. 3, pp. 373-386, 1982.
239. O'Donoghue, P. E., Nishioka, T. and Atluri, S. N., 'Multiple Surface Cracks in Pressure Vessels', Engineering Fracture Mechanics, Vol. 20, No. 3, pp. 545-560, 1984.
240. O'Donoghue, P. E., Nishioka, T. and Atluri, S. N., 'Analysis of Interaction Behaviour of Surface Flaws in Pressure Vessels', Trans. of the ASME J. Press. Vess. Technology, Vol. 108, no. 1, pp.24-32, 1986.
241. Miyoshi, T., Sinatori, M. and Tanabe, O., 'Stress Intensity Factors for Surface Cracks with Arbitrary Shapes in Plates and Shells', in "Fracture Mechanics : Sixteenth Symposium", ASTM STP 868, M. F. Kanninen and A. T. Hopper Eds., American Society for Testing and Materials, Philadelphia, pp. 521-534, 1985.
242. Iida, K., 'Shapes and Coalescence of Surface Fatigue Cracks', Proc. ICF International Symposium on Fracture Mechanics, pp. 679-693, Beijing, China. IIW Document XIII- 1126-84, 1984.
243. Iida, K., Ando, K. and Hirata, T., 'An Evaluation Technique for Fatigue Life of Multiple Surface Cracks', Naval Arch. and Ocean Engineering, Vol. 22. pp177-199, 1984.
244. Grandt, A. F., Thakker, A. B. and Tritsch, D. E., 'An Experimental and Numerical Investigation of the Growth and Coalescence of Multiple Fatigue Cracks at Notches', in "Fracture Mechanics : Seventeenth Volume", J. H. Underwood, et al Eds., ASTM STP 905, American Society for Testing and Materials, Philadelphia, pp. 239-252, 1986.
245. Grandt, A. F., Perez, R. and Tritsch, D. E., 'Cyclic Growth and Coalescence of Multiple Fatigue Cracks', Proc. 6th Int. Conf. Fracture., Vol. 3, pp. 1571-1578, 1984.
246. Heath, B. J. and Grandt, A. F., 'Stress Intensity Factors for Coalescing and Single Corner Flaws Along a Hole Bore in a Plate', Engineering

Fracture Mechanics, Vol. 19, No. 4, pp. 665-673, 1984.

247. Soboyejo, W. O., Kishimoto, K., Smith, R. A. and Knott, J. F., 'A Study of the Interaction and Coalescence of Two Coplanar Fatigue Cracks in Bending', Fatigue Fract. Engineering Materials and Structures, Vol. 12, No. 3, pp. 167-174, 1989.

248. Kishimoto, K., Soboyejo, W. O. and Smith, R. A. and Knott, J. F., 'A Numerical Investigation of the Interaction and Coalescence of Twin Coplanar Semi-Elliptical Fatigue Cracks', Int. J. Fatigue, Vol. 11, No. 2, pp. 91-96, 1989.

249. Twaddle, B. R. and Hancock, J. W., 'The Development of Cracks By Defect Coalescence', Fatigue of Offshore Structures, EMAS, 1986.

